



**HAL**  
open science

# Impact behaviour of sandwich structures with nanoparticle reinforced composite face sheets

Karthik Ram Ramakrishnan

► **To cite this version:**

Karthik Ram Ramakrishnan. Impact behaviour of sandwich structures with nanoparticle reinforced composite face sheets. Mechanics of materials [physics.class-ph]. Ecole nationale supérieure d'arts et métiers - ENSAM; University of New South Wales, 2014. English. NNT : 2014ENAM0042 . tel-01132472

**HAL Id: tel-01132472**

**<https://pastel.hal.science/tel-01132472>**

Submitted on 17 Mar 2015

**HAL** is a multi-disciplinary open access archive for the deposit and dissemination of scientific research documents, whether they are published or not. The documents may come from teaching and research institutions in France or abroad, or from public or private research centers.

L'archive ouverte pluridisciplinaire **HAL**, est destinée au dépôt et à la diffusion de documents scientifiques de niveau recherche, publiés ou non, émanant des établissements d'enseignement et de recherche français ou étrangers, des laboratoires publics ou privés.

École Doctorale n° 432: Science des Métiers de l'ingénieur

**Doctorat ParisTech**

**T H È S E**

pour obtenir le grade de docteur délivré par

**l'École Nationale Supérieure d'Arts et Métiers**

**Spécialité: Mécanique - Matériaux**

Présentée et soutenue publiquement par

**Karthik Ram RAMAKRISHNAN**

le – 6 novembre 2014

**Impact behaviour of sandwich composites with  
nanoparticle modified facesheets**

Directeur de thèse: **Philippe Viot**

Co-encadrement de la thèse: **Krishna Shankar, Sandra Guérard**

**Jury**

<b>M. Gérard Bernhart</b> , Professeur, Institut Clément Ader	Président
<b>M. Frank Lauro</b> , Professeur, LAMIH, Université de Valenciennes	Rapporteur
<b>Mme. Nadia Bahlouli</b> , Professeur, ICube, Strasbourg	Rapporteur
<b>M. Pierre Gerard</b> , Docteur, Arkema, Lacq	Invité
<b>M. Philippe Viot</b> , Directeur, Arts et Métiers ParisTech	Examineur
<b>Mme. Sandra Guérard</b> , Maître de Conférences, I2M, Arts et Métiers ParisTech	Examineur
<b>M. Krishna Shankar</b> , Sr. Lecturer, University of New South Wales, Canberra	Examineur



# Acknowledgements

I am grateful for the support of my supervisors, Dr. Krishna Shankar, Prof. Philippe Viot, and Dr. Sandra Guérard, without whose encouragement and guidance, this thesis would not be possible. It was a remarkable concurrence of events that gave me this incredible opportunity to do part of my thesis in France. I am thankful for such fortuities.

I express my sincere gratitude to my thesis examiners Prof. Frank Lauro and Prof. Nadia Bahlouli for their excellent feedback. I'd also like to thank the other members of the jury: Prof. Gérard Bernhart and Dr. Pierre Gerard. Special thanks are due to Sebastián Denneulin and Jean-Luc Barou whose contributions to my thesis are invaluable. I would also like to express my appreciation to Frederic Leonardi, Rodrigue, Naoufel and all the engineers, technicians and support staff who helped me in conducting experiments. I am beholden to Mme. Annie Artal and Mme. Valerie Pernot for their help in jumping through the administrative hoops.

Friends, too many to name here, made this journey a blast. I thank Nicolas (Huchon and Guillaud), Jojo, Momo, Jebahi, Sondes for being awesome colleagues and helping me with my French; and Kevin, Jeremy, Tony and Christophe for petanque. I also cherish all the time spent huddled in the office with my labmates in Canberra. Julia, I thank for, among numerous things, Penguin Waffles.

I don't know what I'd do without: the good Doctor with his two hearts and Blue box, Tina Fey who as Liz Lemon was a comfort blanket in times of stress, Jon Stewart and Colbert, Jorge Cham of PhD comics, the Green brothers (John and Hank) for reminding me to DFTBA - you guys are lifesavers.

I am eternally indebted to my parents and my sister who have been a pillar of support through my years in the wilderness. Their love and encouragement made me the person that I am. And finally Vanti, for being.



# Abstract

Sandwich composites are lightweight structures with widespread applications in aerospace, offshore and marine industries. The sandwich construction is based on strong, stiff skins, for instance Fibre Reinforced Polymers (FRPs), bonded to either side of a low density core material, such as polymeric foams. However, sandwich structures are susceptible to impact damage. Researchers have tried to improve the impact resistance of sandwich composites by various methods including toughening the matrix. However toughening the epoxy matrix with micro-rubber particles compromised other favourable properties. Recently, nano-reinforcements such as carbon nanotubes, nanoclay and  $SiO_2$  nanoparticles have been used to toughen the resin. However, one of the challenges with these nanoparticles is obtaining uniform dispersion. Current research has shown that acrylate triblock copolymers which self-assemble in the nano-scale do not agglomerate and are therefore a promising candidate for improving the impact performance of composites. The objective of this thesis is to investigate the effectiveness of these block copolymers in improving the impact resistance of sandwich structures with FRP facesheets. Normal impact tests are conducted using drop tower on sandwich composites made of Kevlar and Glass fibre reinforced epoxy facesheets and Rohacell<sup>®</sup> foam core. The macroscopic behaviour and the microscopic phenomena involved in dissipating impact energy are identified and compared for sandwich plates with and without the nanoparticles. The results from drop tower impact tests show that the addition of 10% M52N Nanostrength<sup>®</sup> substantially improves the impact resistance of the Kevlar- Rohacell sandwich plates. Numerical simulation of the low velocity impact of sandwich plate is conducted using Finite Element Analysis (FEA) software LS-Dyna. Laminated Composite Fabric model (MAT58), a material model based on Continuum Damage Mechanics (CDM) and Hashin failure criteria is used for the facesheets and a Crushable foam model (MAT63) is used for the foam core. The FE models show good correlation with the experimental results. In order to establish that the nano block copolymers are effective in loading conditions other than normal impact, a new method to conduct low velocity tri-dimensional impact tests on sandwich panels using a modified Stewart platform (Hexapod) was developed. This setup was used to test Kevlar Rohacell sandwich panels for parabolic impact and the results compared with numerical simulation.



# Résumé substantiel

## Comportement de matériaux sandwich sous sollicitations dynamiques de chocs : Effet de l'ajout de nanoparticules à la matrice thermodurcissable

### Introduction

L'objectif de ce travail est l'étude du comportement à l'impact à faible vitesse de panneaux sandwich. Les structures sandwich sont des structures légères composées de deux peaux superficielles minces, relativement denses, à haute résistance qui sont collées de part et d'autre d'une âme, épaisse, de faible densité telle que les mousses ou nids d'abeilles. Les peaux sont conçues pour résister à des chargements de flexion et sont généralement en aluminium, en polymères ou en polymères renforcés de fibres. L'âme ou cœur sépare et stabilise les peaux externes pour reprendre les sollicitations de compression, torsion ou de flexion et est généralement fait de bois, de mousses de polymères, ou plus largement de nids d'abeilles métalliques ou polymères. Un collage entre les peaux externes et l'âme du sandwich assure le transfert des sollicitations. Le concept de sandwich existe à l'état naturel dans des structures telles que les os (animaux ou humains) ; une représentation schématique de structure sandwich est présentée sur la figure 1.

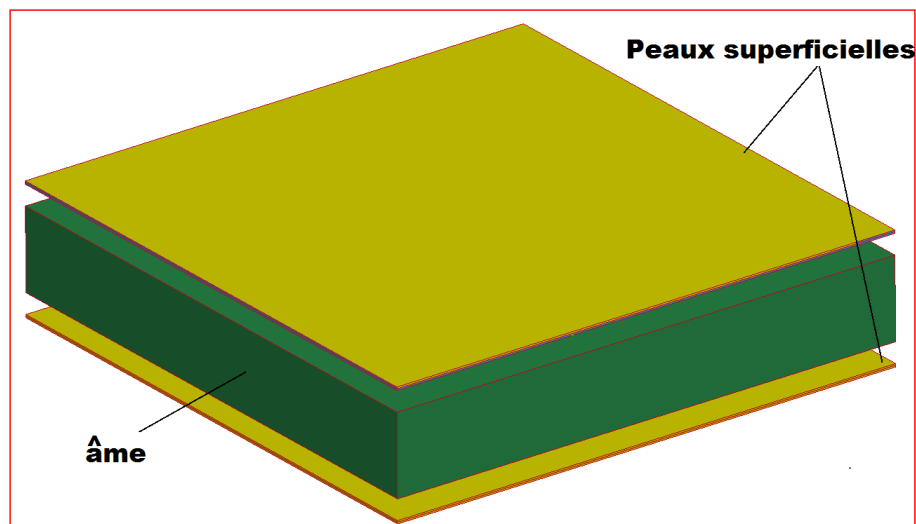


Figure 0.1. Schéma du panneau sandwich

Les structures sandwich ont un ratio rigidité de flexion / poids élevé ce qui leur confère une résistance élevée au flambage, des déformations latérales minimisées et de haute capacité d'absorption d'énergie. Ils possèdent également de bonnes propriétés thermiques et acoustiques, des fréquences propres élevées et une bonne flottabilité. Les matériaux sandwich sont largement utilisés pour l'optimisation de structures pour lesquelles le poids est une variable critique telles que les pièces d'avions, les structures spatiales, les pales d'éoliennes, les structures navales et les articles de sport [1]. Ils sont également utilisés pour la protection de biens et de personnes (casques de protection notamment pour les pilotes, motards ou pour les sports tels que le hockey ou le football américain).

Les matériaux sandwich à peau composite renforcée de fibres plastiques et des cœurs en matériaux polymère représentent aujourd'hui une classe importante des matériaux structuraux légers dans de nombreux domaines de l'ingénierie tels que l'aéronautique et l'aérospatiale, l'automobile et les structures marines. Toutefois, certaines de ces structures sandwich ont des capacités d'absorption d'énergie très limitées dans le cas d'un choc normal à la surface du sandwich. Cette limitation devient critique lorsque ces structures sont susceptibles d'être soumises à un impact[2]. L'endommagement par impact dans le cas de structures sandwich peut être d, notamment, à des chutes d'outils, des vols de débris sur piste d'atterrissage, des chocs à oiseaux, des averses de grêles ou des impacts balistiques.

L'endommagement par impact basse vitesse est particulièrement préoccupant dans les applications aérospatiales : l'impact peut ne créer à la surface de la structure qu'une légère indentation au niveau du lieu de l'impact, mais correspondre à des endommagements plus importants dans l'épaisseur du panneau sandwich. Ce genre d'impact peut alors compromettre gravement l'intégrité structurelle du panneau sandwich. Les modes de rupture communément associés à l'impact basse vitesse dans les structures sandwich sont les ruptures de fibres, la fissuration de la matrice, le délaminage et un effondrement du cœur. Richardson et al. [3] ont noté que l'endommagement de la matrice est le premier type de défaillance généré par un impact à faible vitesse transversale et qu'il correspond à une fissuration de la matrice mais aussi à une décohésion entre fibre et matrice. Le délaminage a également été observé associé à une fissuration matricielle.

Les résines utilisées en tant que matrice dans le cas des sandwiches à peaux en composites stratifiés sont généralement des résines thermodurcissables comme les résines époxy dont le comportement est relativement fragile. En raison de la nature fragile de la matrice, même la présence d'un léger délaminage interne se propage essentiellement à angle droit par rapport à la contrainte de compression appliquée ayant alors des résultats désastreux pour la structure sandwich. Le renforcement au choc par l'ajout de particules élastomériques s'est avéré efficace et est largement utilisé, mais l'inconvénient de cette approche est que ce

renforcement se fait au détriment de propriétés telles qu'une rigidité ou une température de transition vitreuse de la résine époxy élevées . Une des solutions proposées est alors la modification des résines thermodurcissables avec l'ajout de particules organiques et inorganiques de taille nanométrique. Les nanotubes de carbone (CNT) ou nanoparticules argileuses et les nanocomposites de silicate ont été étudiés par plusieurs chercheurs [4], mais une nouvelle méthode de synthèse de copolymères par blocs qui s'auto-assemblent à l'échelle nanométrique permettrait de réduire sensiblement les problèmes liés à la dispersion des nanoparticules.

Barsotti et al. [5] ont montré que l'utilisation de résine époxy modifiée par l'ajout de blocs de copolymères augmente la ténacité et les performances à l'impact sans dégrader les propriétés thermiques. Denneulin et al. [6] ont rapporté que, alors que l'ajout de nanotubes de carbone n'a pas eu d'effet considérable, l'utilisation de copolymères tribloc (Nanostrengths) dans la matrice du composite Kevlar/Epoxy augmente significativement les performances à l'impact du composite. L'effet de ces nano-renforts sur les performances mécaniques de panneaux sandwich fabriqués à l'aide de ces résines nanomodifiées n'a pas encore été étudié, en particulier dans le cas de chargement de type impact. L'objectif de cette thèse est donc d'étudier l'effet d'une matrice renforcée par des copolymères tribloc sur les performances à l'impact basse vitesse de panneaux sandwich composites.

L'effet de l'ajout de nano-particules sur les performances à l'impact de panneaux sandwich à peaux en composites stratifiés Fibres/Epoxy a été étudié expérimentalement et numériquement. Le comportement au choc faible vitesse de plaques sandwich est étudié en imposant une vitesse initiale à un impacteur infiniment rigide par rapport à la plaque et qui entre en contact avec la peau supérieure du spécimen. La réponse macroscopique du composite en sandwich à l'impact et les mécanismes par lesquels microscopiques amélioration de la ténacité à la rupture de la résine se traduit par une meilleure résistance du panneau sandwich d'impact sera étudié.

Ce travail portera sur deux types de chargement d'impact différents ; des impacts à faible vitesse dont l'angle d'incidence est normal à la surface de l'échantillon et des impacts à faible vitesse et à trajectoire parabolique. Dans les situations réelles, les structures sont le plus souvent impactées selon un angle oblique voire un angle qui évolue au cours de l'impact. La mise en œuvre de tests d'impact normal à la surface de l'échantillon est largement répandue grâce à des dispositifs de type tour de chute, mais les tests à trajectoire fonction du temps sont difficile à réaliser. Un dispositif d'impact tridimensionnel adossé à un hexapode de mouvement a été développé pour étudier la réponse mécanique d'un panneau sandwich soumis à une trajectoire parabolique.

Cette thèse fait l'objet d'un accord de Cotutelle signé entre Arts et Métiers ParisTech, campus de Bordeaux-Talence et l' Université de New South Wales (USNW), en Australie. Par conséquent, ce travail a été réalisé en partie à l'Ecole d'ingénierie et de technologie de l'information (SEIT) du campus Australian Defence Force Academy (ADFA) et le département Durabilité des Matériaux, des Assemblages et des Structures (DuMAS) de l'Institut de Mécanique et d'Ingénierie de Bordeaux (I2M). Cette thèse a été effectuée sous la direction du Dr Krishna Shankar à l'UNSW et sous le co-encadrement du Pr. Philippe Viot et du Dr Sandra Guérard à l'I2M. Les échantillons de panneaux sandwich nécessaires aux essais expérimentaux ont été fabriqués au sein de l'équipe Physico-Chimie des Polymères de l'Institut Pluridisciplinaire Recherche Environnement Matériaux (IPREM) à l'Université de Pau et des Pays de l'Adour avec le soutien du Dr Frédéric Léonardi.

## Objectifs

L'objectif de ce travail est d'étudier et de mieux comprendre l'amélioration de la résistance à l'impact des panneaux sandwich à peau en stratifiés composites grâce à l'ajout de copolymère tribloc (Nanostrengths) dans la matrice Epoxy du composite Fibres/Epoxy. L'effet des nanoparticules sur les performances mécaniques des panneaux sandwich à peau Kevlar/Epoxy ou Verre/Epoxy et âme en mousse Rohacell<sup>®</sup> sera investigué : pour cela une comparaison entre les résultats entre résine pure et résine modifiée par l'ajout de 10% de Nanostrength sera effectuée en utilisant des essais expérimentaux et une modélisation numérique.

## Déroulement de la thèse

L'effet de l'ajout de particules nano-élastomériques sur les performances à l'impact des panneaux sandwich sera étudié en utilisant des méthodes expérimentales (premier volet du travail présenté) ainsi qu'une modélisation numérique à l'aide de la méthode des éléments finis (deuxième volet de ce travail).

1. La première partie expérimentale de ce travail correspond à des essais d'impact à faible vitesse et d'incidence normale en utilisant un dispositif de type tour de chute.
2. La deuxième partie du volet expérimental s'articulera autour de la mise en place d'essais d'impact à trajectoire parabolique utilisant un hexapode de mouvement. Ce dispositif ouvre le champ des études d'impact aujourd'hui limitées à des impacts normaux et/ou obliques. L'hexapode ou encore plateforme de Stewart permet de définir une trajectoire d'impact imposée sur la surface du panneau sandwich.

3. La troisième partie du volet expérimental traite de l'analyse des endommagements générés par impact à l'aide d'un microscope optique.
4. La modélisation numérique de la réponse à l'impact des panneaux sandwich avec et sans ajout de nano-particules sera effectuée pour identifier l'effet de ces nano-additifs dans différentes conditions de chargement (énergie, vitesse, direction). En amont de cette modélisation des essais de caractérisation seront mis en place pour identifier les paramètres des matériaux constitutifs de la structure sandwich notamment ceux la mousse polymère Rohacell<sup>®</sup> dépendant de la vitesse de chargement. Les paramètres des plaques sandwich seront issus des travaux de Denneulin [6]. Des essais de délaminages seront également effectués pour caractériser l'interface fibres/matrice des plaques du composite.
5. Les résultats des tests d'impact sur tour de chute seront utilisés pour valider les modèles numériques mis en place. Le modèle numérique validé sera ensuite utilisé pour la simulation des impacts paraboliques ; les résultats numériques et expérimentaux seront finalement confrontés.

Les principaux apports de la thèse seront (a) d'étudier pourquoi l'augmentation de la ténacité de la matrice grâce à l'ajout de copolymère tribloc améliore la résistance à l'impact des panneaux sandwich, (b) de développer un modèle EF phénoménologique pour les panneaux sandwich et (c) de mettre en place de nouveaux essais à trajectoires tridimensionnelles en utilisant un hexapode de mouvement.

## **Essais de choc normal sur panneaux sandwich avec et sans nano-renfort**

Deux types composites tissés ont été utilisées pour constituer les peaux des panneaux sandwich : Kevlar/Epoxy et Verre/Epoxy. Les panneaux sandwich ont été fabriqués en utilisant un processus de drapage humide. Pour les stratifiés Kevlar/Epoxy, trois couches de tissu taffetas [0-90] ont été utilisées, et pour les stratifiés Verre/Epoxy, cinq plis de tissu taffetas [0-90] ont été nécessaires afin d'obtenir des peaux de même épaisseur quel que soit le type de fibres (environ 0.8mm). Denneulin et al. [7] ont testé trois formulations différentes du copolymère bloc (M22, M42, et M52N) sur des composites Kevlar/Epoxy et ont montré que le M52N Nanostrength<sup>®</sup> ajouté à une résine Epoxy augmentait le plus significativement les propriétés de résistances à l'impact. 10% de M52N Nanostrength<sup>®</sup> a été choisi parmi différents pourcentages de renfort, étant donné qu'il a été montré par Denneulin et al. [7] que ce pourcentage représentait le pourcentage optimal permettant d'améliorer la résistance à l'impact sans dégrader de manière trop importante les autres

propriétés utiles telles que la rigidité. Les Nanostrength, sous forme de poudre, sont ajoutées à la résine tout en mélangeant à l'aide d'un agitateur mécanique à 290 trs/min à 110C pendant une durée de deux heures. Les deux couches de tissus de Kevlar [0-90]<sub>3</sub> ont ensuite été positionnées de part et d'autre du cœur du sandwich et le panneau sandwich est co-durci dans une presse à chaud, à 90C, pendant 90 minutes à une pression de 1.5 bars. Aucun adhésif supplémentaire n'est utilisé entre les peaux et le cœur du sandwich. Enfin, le panneau sandwich est post-durci dans un four à 80C pendant deux heures.

Les dispositifs de type tour de chute sont largement utilisés pour les essais d'impact et permettent de mener facilement des essais à faible vitesse. Les plaques sandwich constitués de mousse Rohacell<sup>®</sup> et de peaux composite à résine Epoxy pure (sans Nanostrength) seront référencées KR (Kevlar-Rohacell) et les plaques avec résine chargée KNR (Kevlar-Nanostrength-Rohacell). Les plaques sandwich ont été impactées à l'aide d'un impacteur hémisphérique de 16 mm de diamètre pour trois hauteurs de chute (0.5 m, 0.75 m et 1m) correspondant à des énergies d'impact de 8J, 12J et 16J respectivement. L'effet des nano-renforts sur la réponse des plaques sandwich impactées sous incidence normale a été tout d'abord étudié au niveau macroscopique sur la base des courbes force-déplacement et de l'examen visuel des échantillons après impact. La figure 2 présente, par exemple, les résultats obtenus pour un impact de 16J. Tandis que la plaque sandwich KR est rompue par rupture de fibres et perforation, la peau supérieure du sandwich KNR ne présente aucune perforation à même niveau d'énergie d'impact. La perforation des plaques sandwich KR est intervenue sur la peau supérieure dès 12J d'énergie d'impact alors que les plaques KNR restent non perforées après des impacts de 16J.

Une comparaison des plaques sandwich Kevlar a été effectuée en termes d'énergie absorbée. Les plaques sandwich KNR demandent des niveaux d'énergie plus élevés que les plaques KR pour arriver à rupture. La zone de mousse polymère endommagée sous la peau supérieure de l'échantillon était également plus répartie autour du lieu d'impact dans le cas de plaque KNR que pour les plaques KR pour l'endommagement de la mousse est localisée sous l'impacteur. Plusieurs paramètres d'endommagement ont été introduits pour comparer les éprouvettes post-mortem. La microscopie optique a été utilisée pour observer les mécanismes d'endommagement mis en jeu lors de l'impact au niveau de la peau supérieure en composite et de la mousse polymère au cœur de la structure. Les mécanismes d'endommagement activés identifiés pour la plaque KNR ont principalement été de la fissuration de matrice, ce qui peut expliquer pourquoi l'ajout de Nanostrength améliore la résistance à l'impact. On peut en conclure que les nanoparticules élastomériques M52N améliorent significativement la résistance à l'impact faible vitesse de plaque sandwich Kevlar/Epoxy.

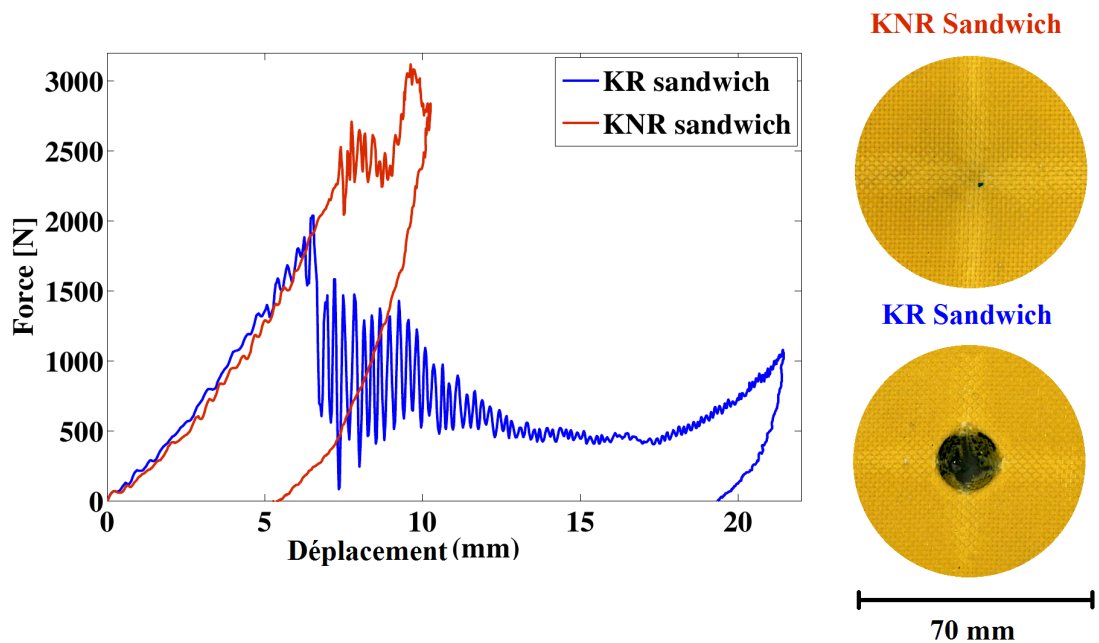


**Figure 0.2.** Courbe force-déplacement (à gauche) et vue de dessus de l'échantillon après impact (à droite) pour un impact normal de KR et KNR sandwich à l'énergie de 16 J

Une approche similaire a été utilisée pour caractériser l'influence des nanoparticules dans le cas d'un stratifié Verre/Epoxy : aucune amélioration significative n'a été obtenue sur les résultats à l'impact basse vitesse. De potentielles explications de ce résultat ont été avancées mais n'ont pas été investiguées, cette étude faisant l'objet d'un travail ultérieur. La suite de ce travail de thèse a été focalisée sur les sandwichs composites Kevlar/Epoxy.

## Modélisation par éléments finis de l'impact normal sur stratifiés et panneaux sandwich composites

La mise en œuvre d'expérimentation est souvent longue, couteuse et nécessite une instrumentation spécifique telle que des caméras rapides par exemple pour mesurer l'état de déformation et de chargement de la structure. Par ailleurs les larges campagnes expérimentales, au-delà d'être difficile de mise en œuvre, ne fournissent qu'une réponse discrète par rapport à la possibilité de variables à prendre en compte. La méthode des éléments finis est donc un moyen largement usité pour étudier l'impact sur les structures et notamment les structures sandwich. La modélisation numérique représente un outil approprié pour multiplier les cas de chargement, les conditions aux limites et étudier des structures plus complexe. Cette approche permet par ailleurs d'accéder à des paramètres tels que les contraintes ou l'évolution de l'endommagement.

Un modèle LS-Dyna a été développé pour la simulation de l'impact normal sur plaque de composites stratifiés et sur plaques sandwich Kevlar/Epoxy mousse Rohacell. Une loi de comportement basée sur la mécanique de l'endommagement, disponible dans la bibliothèque de modèles matériaux proposés par LS-Dyna et dénommé Laminated Composite Fabric (MAT58) et a été utilisée pour représenter le comportement des plaques composite. Les paramètres d'entrée du modèle MAT58 ont été obtenus par combinaison d'essais et études paramétriques. Le modèle CRUSHABLE FOAM (MAT63) a été utilisé pour le cœur du sandwich en mousse Rohacell. Les propriétés matériaux des plaques Kevlar/Epoxy avec copolymère tribloc ont aussi été étudiées pour mettre en place le modèle EF correspondant. L'effort de contact, le déplacement de l'impacteur et les modes de ruptures obtenus numériquement ont montré une bonne correspondance avec les résultats expérimentaux obtenus par tour de chute.

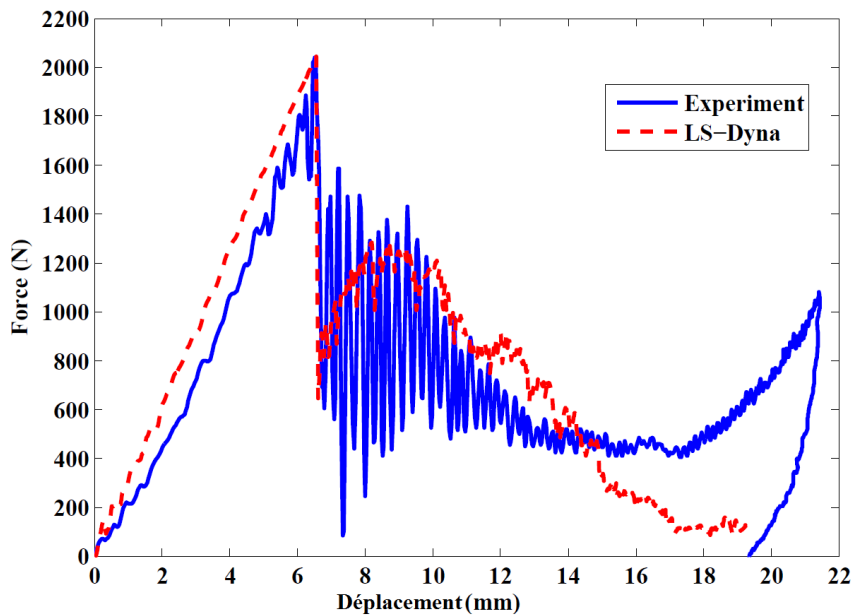


**Figure 0.3.** Comparaison entre un essai tour de chute et la simulation LS-Dyna correspondante pour une plaque sandwich KR et un impact de 16 J

Le modèle LS-DYNA développé a fourni une réponse macroscopique proche de celle observée expérimentalement (voir figure 3 pour un impact de 16 J sur une plaque sandwich KR) mais quelques limites dans la représentation des modes d'endommagement de la matrice ainsi que le rebond élastique observé sur les plaques sandwich chargées en nanorenforts. Toutefois, le modèle FE peut être validé et donc être utilisé pour étudier la réponse de plaques sandwich dans d'autres conditions d'impact. La mise en place de ce modèle permettra une réduction des coûts liés aux essais expérimentaux et au temps associé.

## Étude de l'impact parabolique sur panneaux sandwich

Sur les structures réelles, le chargement dynamique est souvent tridimensionnel et les trajectoires des impacteurs sont complexes. Guérard et al. [8] ont donc développé un module d'essais tridimensionnels qui s'appuie sur un hexapode de mouvement et permet de réaliser des essais à trajectoires complexes en vitesse lente. Ce dispositif, représenté figure 4, permet notamment d'étudier expérimentalement le chargement de plaque sandwich en utilisant une trajectoire parabolique. Des essais d'impact à trajectoire parabolique et à faible vitesse ont donc été réalisés sur des plaques sandwich Kevlar Rohacell<sup>®</sup> avec et sans Nanostrength et l'effet de la forme de l'impacteur a été étudiée en comparant la réponse de la plaque sandwich. Trois formes d'impacteur différent ont été utilisées : cylindrique (diamètre 50 mm), et en coin (angle de 120 et de 60). La position de l'impact sur la plaque sandwich a aussi été modifiée selon les essais avant d'évaluer la présence d'effets de bord.

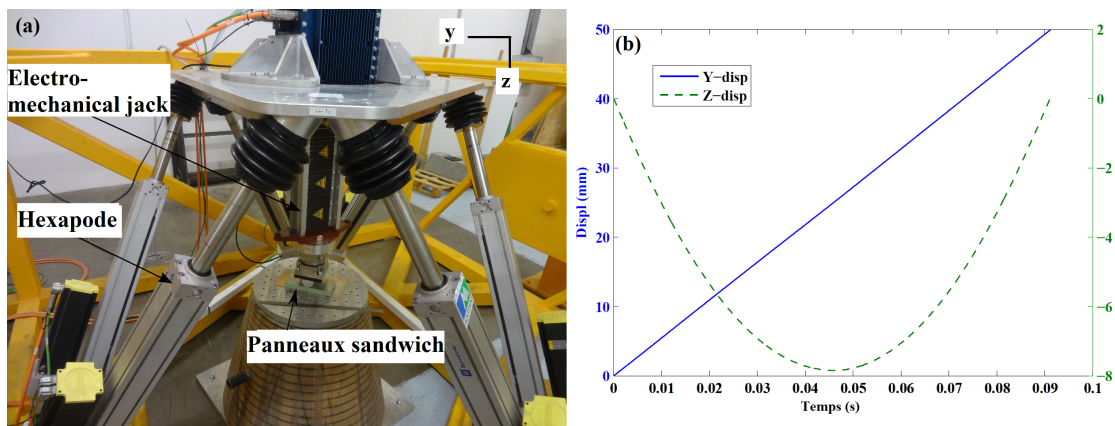


**Figure 0.4.** (a) la configuration hexapode pour les essais d'impact parabolique et (b) trajectoire de déplacement dans les directions y et z

Le modèle LS-Dyna développé précédemment pour la simulation d'impact faible vitesse sur plaque sandwich Kevlar / Rohacell<sup>®</sup> a été utilisé pour modéliser les essais à trajectoire parabolique. Ces simulations permettront de vérifier si le modèle développé peut être utilisé pour d'autres conditions de chargement que celui pour lequel il a été identifié. Lors des essais expérimentaux, un mouchetis a été appliqué sur la tranche de la plaque sandwich et la corrélation d'images numériques a été utilisée pour mesurer les champs de déformation de cisaillement. Ces champs expérimentaux ont ensuite été comparés aux résultats des simulations. Les résultats du modèle EF (figure 5) montrent une bonne corrélation avec les mesures macroscopiques (efforts verticaux et transversaux) expérimentales, mais les modes de rupture complexes, tels que la décohésion et le cisaillement de la mousse n'ont pas été clairement identifiés par les simulations. Des modifications du modèle sont donc

à prévoir pour se rapprocher du comportement d'une structure sandwich soumise à un chargement complexe fortement non proportionnel.

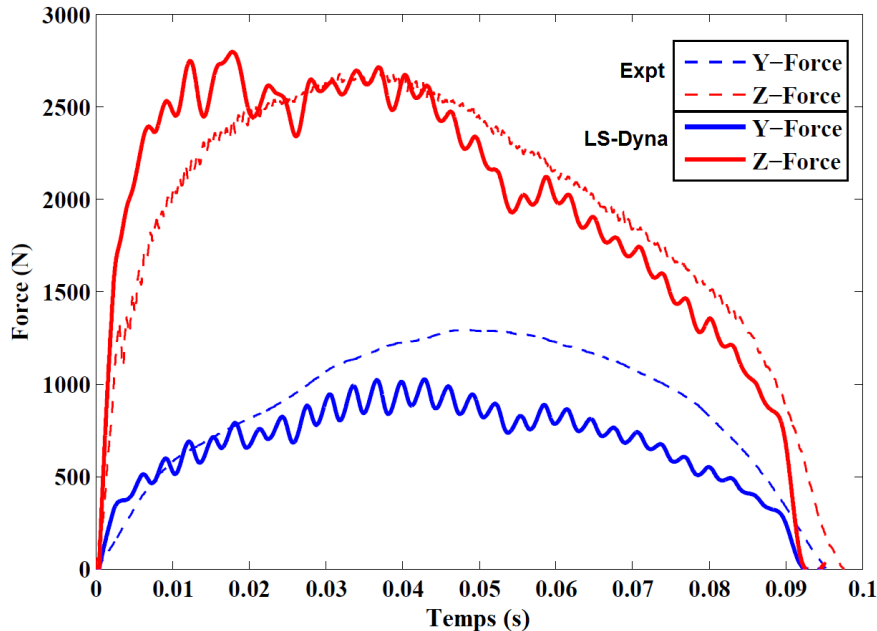


**Figure 0.5.** Comparaison des efforts transversaux (y) et verticaux (z) obtenus expérimentalement et numériquement dans le cas d'un impact parabolique sur plaque sandwich

## Conclusions

Les résultats de ces travaux de thèse trouvent des applications directes dans l'industrie des composites car les conditions de chargement de type impact interviennent fréquemment lors du cycle de vie des structures sandwich. Lors d'un impact, la structure subira des dégradations et donc une diminution de ses propriétés mécaniques. Les panneaux sandwich constitués de résine modifiée à l'échelle nanométrique et de fibres de Kevlar possèdent des propriétés accrues de résistance aux impacts et permettent de minimiser l'endommagement de la structure en cas d'impact faible vitesse. On peut souligner que le développement de panneaux sandwich à matrice renforcée de copolymère tribloc est un domaine prometteur de l'étude, même si le taux de renfort dans la matrice et le type de renfort reste à étudier en fonction du type de fibres.

La principale contribution de cette thèse est l'étude de l'effet des nanoparticules de copolymère tribloc ajoutées à la matrice Epoxy sur les résistances aux chocs de panneaux sandwich. Bien que la ténacité de la matrice d'un composite soit un domaine de recherche

prolifère, l'avènement des nanotechnologies a ouvert la voie à de nouveaux composites hautes performances. Les copolymères à blocs ont un avantage certain sur les autres types de nanoparticules car ils s'auto-assemblent à l'échelle nanométrique et ne s'agglomèrent pas. Par conséquent le processus de fabrication des composites stratifiés et des panneaux sandwich possédant ces nanorenforts n'est pas modifié par rapport aux procédés existants.

Le modèle EF développé dans cette thèse montre que le modèle macroscopique avec une loi de comportement phénoménologique est capable de simuler la réponse macroscopique de composites stratifiés et plaques sandwich soumis à des impacts de faible vitesse. Ces résultats peuvent être utiles pour optimiser, par exemple, la résistance à l'impact d'une structure en minimisant le nombre d'essais expérimentaux à réaliser. La mise en œuvre d'essais d'impact à trajectoire tridimensionnelle est une autre contribution originale et importante de la thèse. Les méthodes d'essais actuelles se limitent à des tests d'impact normal et ce nouveau dispositif permettra de recréer expérimentalement des sollicitations proches de chargements réels appliqués aux structures.

## Bibliographie

- [1] L.A. Carlsson and G.A. Kardomateas. Structural and failure mechanics of sandwich composites, volume 121. Springer Science, 2011.
- [2] A.F. Avila, M.G.R. Carvalho, E.C. Dias, and D.T.L. da Cruz. Nano-structured sandwich composites response to low-velocity impact. *Composite Structures*, 92(3):745 -751, 2010.
- [3] M.O.W. Richardson and M.J. Wisheart. Review of low-velocity impact properties of composite materials. *Composites Part A: Applied Science and Manufacturing*, 27(12):1123 - 1131, 1996.
- [4] L. Sun, R.F. Gibson, F. Gordaninejad, and J. Suhr. Energy absorption capability of nanocomposites: A review. *Composites Science and Technology*, 69(14):2392 - 2409, 2009.
- [5] R. Barsotti. Nanostrength block copolymers for epoxy toughening. Technical report, Arkema Inc., September 2008.
- [6] S. Denneulin. étude du comportement dynamique de matériaux composites sous sollicitations de chocs- Application à un casque aéronautique. PhD thesis, école Nationale Supérieure d'Arts et Métiers, France, 2011.
- [7] S. Denneulin, P. Viot, F. Léonardi, and J.L. Lataillade. The influence of acrylate tri-block copolymer embedded in matrix on composite structures' responses to low- velocity impacts. *Composite Structures*, 94(4):1471 - 1481, 2012.
- [8] S. Guérard, J-L. Barou, L. Mahéo, and P. Viot. Development of a new experimental device for tridimensional impacts - results on foam-core sandwich panels. In 4th International conference on impact loading of lightweight structures, 2014.



# List of publications

## Journal article

1. **KR Ramakrishnan**, S Guérard, P Viot and K Shankar, “Effect of block copolymer nano-reinforcements on the low velocity impact response of sandwich structures”, *Composite Structures*, 2014, 110, p. 174-182

## Conference articles

1. **KR Ramakrishnan**, S Guérard, K Shankar and P Viot, “Drop tower experiments on Glass FRP sandwich plates with nano-elastomeric particles”, *ICILLS Cape Town*, 2014
2. **KR Ramakrishnan**, S Guérard, K Shankar and P Viot, “Development of a Finite Element Model for the study of the impact behaviour of sandwich panels”, *21ème Congrès Français de Mécanique Bordeaux*, 2013
3. **KR Ramakrishnan**, S Guérard, P Viot, F Leonardi and K Shankar, “Effect of block copolymer nano-reinforcements on the low velocity impact response of sandwich structures”, *ICCS - Porto*, 2013
4. **KR Ramakrishnan**, K Shankar, P Viot and S Guérard, “An experimental and numerical study of the impact properties of sandwich plates with different cores”, *7th Australasian Congress on Applied Mechanics-Adelaide*, 2012
5. **KR Ramakrishnan**, K Shankar, P Viot and S Guérard, “A Comparative Study of the Impact Properties of Sandwich Materials with Different Cores”, *Dymat Freiburg*, 2012

## Articles under preparation

1. **KR Ramakrishnan**, S Guérard, K Shankar and P Viot, “Finite element modelling of low velocity impact of composite structures with nano-reinforcements”, submitted to *Composites Part B*
2. **KR Ramakrishnan**, S Guérard, K Shankar and P Viot, “Parabolic impact of sandwich panels with and without nano-reinforcement”, to be submitted to *International Journal of Impact Engineering*
3. **KR Ramakrishnan**, S Guérard, K Shankar and P Viot, “Numerical simulation of impact response of sandwich panels with nano block copolymer embedded in the resin”, to be submitted to *Composite Structures*
4. **KR Ramakrishnan**, K Shankar, S Guérard and P Viot, “An experimental and numerical study on the effect of different cores on the impact behaviour of sandwich composites”, to be submitted to *Composite Structures*



# Contents

Abstract	i
Résumé substantiel	iii
List of publications	xv
Abbreviations	xxxii
Chapter 1 Introduction	1
1.1 Background . . . . .	1
1.2 Aim . . . . .	4
1.3 Scope of thesis . . . . .	4
1.4 Methodology . . . . .	5
1.5 Outline of thesis . . . . .	5
Chapter 2 Literature Review	7
2.1 Introduction . . . . .	7
2.2 Sandwich structures - Materials and construction . . . . .	8
2.2.1 Fibre . . . . .	9
2.2.2 Matrix . . . . .	12
2.2.3 Core . . . . .	13
2.3 Impact behaviour of sandwich structures . . . . .	15
2.3.1 Experimental methods . . . . .	16
2.3.2 Failure mechanisms in sandwich structures . . . . .	21
2.4 Improving impact resistance of sandwich composites . . . . .	29
2.4.1 Modification of sandwich architecture . . . . .	29
2.4.2 Improvement of constituent materials . . . . .	30
2.5 Toughening of Epoxy . . . . .	32
2.5.1 Microparticle reinforcement of epoxy . . . . .	33
2.5.2 Nanoparticle reinforcement of epoxy . . . . .	35
2.6 Block copolymer nano-reinforcements . . . . .	37
2.7 Summary . . . . .	40

---

Chapter 3	Low velocity impact tests of sandwich panels with and without nano-reinforcement: Normal impact	43
3.1	Introduction . . . . .	43
3.2	Manufacturing of sandwich plates with block copolymer nanoparticles	44
3.2.1	Material . . . . .	44
3.2.2	Fabrication of sandwich panels . . . . .	47
3.3	Experimental setup for normal impact tests . . . . .	48
3.4	Results of low velocity normal impact tests of Kevlar - Rohacell sandwich plates . . . . .	53
3.4.1	Energy dissipated . . . . .	59
3.4.2	Post-mortem damage analysis of Kevlar Rohacell sandwich . . . . .	64
3.4.3	Microscopic observation of damage . . . . .	67
3.5	Results of low velocity normal impact tests of Glass - Rohacell sandwich plates . . . . .	70
3.6	Comparison of Kevlar- Rohacell and Glass- Rohacell sandwich . . . . .	75
3.7	Summary . . . . .	81
Chapter 4	Finite Element modelling of low velocity impact response of composite laminates and sandwich panels	83
4.1	Introduction . . . . .	83
4.2	Review of finite element method for simulation of impact of sandwich composites . . . . .	84
4.2.1	Constitutive laws for composite facesheets . . . . .	86
4.2.2	Constitutive modelling of foam core . . . . .	96
4.2.3	Simulation of delaminations and debonding . . . . .	101
4.3	FE model of normal impact of Kevlar composite laminates with and without nano-reinforcement . . . . .	106
4.3.1	Identification of material model parameters . . . . .	108
4.3.2	Results of the low velocity normal impact of Kevlar composite plate . . . . .	110
4.4	Development of FE model of normal impact of Kevlar-Rohacell sandwich panels with and without nano-reinforcements . . . . .	115
4.4.1	Identification of foam properties . . . . .	117
4.4.2	Identification of Interlaminar properties . . . . .	122

---

4.5	Results of LS-Dyna simulation of Kevlar-Rohacell sandwich composites	128
4.5.1	Comparison of results from LS-Dyna model with drop tower tests of Kevlar-Rohacell sandwich panels . . . . .	129
4.6	Summary . . . . .	138
Chapter 5	Parabolic impact of sandwich panels with and without nano-reinforcement	141
5.1	Introduction . . . . .	141
5.2	Experimental setup for parabolic impact testing of sandwich panels . . . . .	142
5.3	Parabolic impact testing of Kevlar Rohacell sandwich . . . . .	145
5.4	Development of FE model of parabolic impact of sandwich panels . . . . .	154
5.4.1	Validation of LS-Dyna model for Aluminium- Divinycell sandwich . . . . .	154
5.5	Results of LS-Dyna simulation for parabolic impact of Kevlar Rohacell sandwich . . . . .	157
5.6	Summary . . . . .	167
Chapter 6	Conclusion and Recommendations	169
6.1	Conclusions . . . . .	169
6.2	Significant contributions . . . . .	171
6.3	Recommendations . . . . .	172
References		185



# List of Tables

2.1	Typical properties for a range of commonly used fibre reinforcements for impact applications [18]	10
2.2	Summary of properties of some foam materials [27]	13
2.3	List of papers on indentation and low velocity impact of sandwich composites	22
3.1	Materials used in fabrication of sandwich composites	46
3.2	Peak force and Maximum displacement of Kevlar sandwich samples	60
4.1	Commonly used material models for composites simulation in LS-Dyna	88
4.2	Material properties for the Kevlar composite with and without nanoparticles	113



# List of Figures

0.1	Schéma du panneau sandwich . . . . .	iii
0.2	Courbe force-déplacement (à gauche) et vue de dessus de l'échantillon après impact (à droite) pour un impact normal de KR et KNR sandwich à l'énergie de 16 J . . . . .	ix
0.3	Comparaison entre un essai tour de chute et la simulation LS-Dyna correspondante pour une plaque sandwich KR et un impact de 16 J . . . . .	x
0.4	(a) la configuration hexapode pour les essais d'impact parabolique et (b) trajectoire de déplacement dans les directions y et z . . . . .	xi
0.5	Comparaison des efforts transversaux (y) et verticaux (z) obtenus expérimentalement et numériquement dans le cas d'un impact parabolique sur plaque sandwich . . . . .	xii
1.1	Schematic diagram of sandwich construction . . . . .	2
2.1	Specific properties of different fibres [19] . . . . .	11
2.2	Chemical structure of DGEBA resin [23] . . . . .	12
2.3	(a) Microstructure of Rohacell foam and (b) Typical Compression properties of Rohacell 51WF foam in three perpendicular axes [25] . . . . .	14
2.4	Schematic diagram of drop tower used for the low velocity impact tests [41] . . . . .	18
2.5	Typical load deflection curves for low velocity impact: a) rebounding impact, b) penetration and c) complete perforation [43] . . . . .	19
2.6	(a) Impact surface, (b) cross-sectional view and (c) Optical micrograph of sandwich plates [45] . . . . .	19
2.7	Different failure modes in sandwich beams subjected to flexure [6] . . . . .	23
2.8	Progression of failure in sandwich plates with honeycomb core [37] . . . . .	24
2.9	Failure modes in Sandwich plates with low velocity impact [42] . . . . .	25
2.10	(a) Typical matrix crack and delamination for 0/90/0 composite and (b) Stress component contributing to matrix crack [9] . . . . .	26
2.11	Failure by skin core debonding (a) Good adhesion and (b) Poor adhesion [33] . . . . .	28
2.12	Core crushing in sandwich with different Polyurethane foam cores [51] . . . . .	29

---

2.13	Effect of CTBN particles in DGEBA epoxy on (a) Fracture energy and (b) Tensile modulus [61] . . . . .	34
2.14	Chemical structure of Triblock copolymer, schematic illustration of the nano-phase structures and TEM image showing 10% triblock copolymers in DGEBA resin [73] . . . . .	38
2.15	Macroscopic behaviour of Kevlar FRP with and without Nanostrength [41] . . . . .	39
2.16	Scanning Electron Microscope observation of Glass FRP with and without NanoStrength [76] . . . . .	40
3.1	(a) Schematic structure and TEM image of MAM block copolymer in DGEBA resin [4]; (b) Schematic mixture of neat and nano matrix system; (c) Mixing of Nanostrength and Degassing . . . . .	45
3.2	(a) Steps involved in the fabrication of sandwich samples, (b) Wet layup process for sandwich manufacture and (c) Curing the sandwich plate in hot press . . . . .	48
3.3	(a) Drop tower setup for low velocity impact testing and (b) Close-up of impactor and target plate . . . . .	49
3.4	Example of displacement measurement using high speed camera . . . . .	51
3.5	Typical results of force and displacement from drop tower test . . . . .	52
3.6	Repeatability of drop tower tests: Force- displacement of three KR sandwich plates . . . . .	54
3.7	Force- displacement curve of KR and KNR sandwich for impact energy of 8J . . . . .	54
3.8	Force- displacement curve of KR and KNR sandwich for impact energy of 12J . . . . .	55
3.9	Force- displacement curve of KR and KNR sandwich for impact energy of 16J . . . . .	55
3.10	High speed camera images of the top facesheet for impact of 16 J . . . . .	57
3.11	Top surface of the Kevlar sandwich samples after impact . . . . .	58
3.12	Force- displacement curve for drop height of 1.25 m and visual inspection of top and bottom surface . . . . .	59
3.13	(a) Peak Force and (b) Max. displacement for Kevlar sandwich samples . . . . .	60
3.14	Energy for Damage Initiation (Zone I) and Total energy dissipated during Impact (Zone I + Zone II) . . . . .	61

---

3.15	Energy up to peak force for KR and KNR sandwich plates . . . . .	62
3.16	Total energy dissipated in the impact of KR and KNR sandwich plates	63
3.17	Cross section of the Kevlar sandwich samples after impact test: (Left) KR sandwich and (Right) KNR sandwich . . . . .	65
3.18	Definition of damage parameters . . . . .	66
3.19	Damage parameters measured from section of the sandwich sample (a)Depth of facesheet $d_1$ , (b) Depth of core $d_2$ and (c) Extent of damage $l_1$ . . . . .	66
3.20	Core cavities in impacted Kevlar sandwich panels . . . . .	67
3.21	Microscopic observations of section of KR sandwich (12 J impact) . .	68
3.22	Microscopic observations of section of KNR sandwich (16 J impact) .	69
3.23	(a)Uncrushed and (b)crushed cells of PMI foam (impact of 12 J) . . .	69
3.24	Force - displacement curve of GR and GNR sandwich for impact energy of 4J . . . . .	70
3.25	Force - displacement curve of GR and GNR sandwich for impact energy of 8J . . . . .	71
3.26	Force - displacement curve of GR and GNR sandwich for impact energy of 16J . . . . .	71
3.27	Top surface of the GR and GNR sandwich samples after impact . . .	73
3.28	(a) Peak force and (b) Maximum displacement of GR and GNR sand- wich samples after impact . . . . .	74
3.29	(a) Energy upto peak force and (b) Total energy dissipated by GR and GNR sandwich samples with and without nanoparticles . . . . .	74
3.30	Comparison of Force- displacement curve for Kevlar and Glass sand- wich for impact of 16 J . . . . .	76
3.31	Force history and bottom surface of the impact on Kevlar plates with and without Nanostrength [41] . . . . .	77
3.32	Force history and bottom surface of the impact on GFRP plates with and without Nanostrength [76] . . . . .	79
3.33	Comparison of the force history of GFRP plates and Glass-Rohacell sandwich panels with and without Nanostrength for impact of 16 J .	80
4.1	Scales considered for composite plates [89] . . . . .	85
4.2	Validation of FE model by comparison of Force, Displacement and Energy history [87] . . . . .	87

4.3	Comparison of different material models for the modelling of composite laminates [102] . . . . .	91
4.4	Stress- strain responses for different values of $E_i$ and $SLIM_i$ [94] . . .	93
4.5	Solution Algorithm for MLT model [99] . . . . .	95
4.6	Results of single element test for validation of MLT model [104] . . .	95
4.7	Fringe plot (a,b) Fibre and matrix tensile damage; (c,d) Fibre and matrix compressive damage; (e,f) Crush damage and delamination [81]	97
4.8	Different plateau regions in cellular material (a) Strain hardening, (b) Strain softening and (c) Perfectly plastic [33] . . . . .	98
4.9	Yield stress vs. volumetric strain input for MAT63 Crushable foam [100]	101
4.10	(a) Composite beam with delamination (b) cohesive springs model and (c) Interlaminar cohesive model behaviour for mode I - bilinear model with loading in A-B and unloading in B-C [111] . . . . .	102
4.11	Comparison of internal energy and contact force for different modelling approaches [110] . . . . .	105
4.12	LS-Dyna model of the composite plate, fixture and hemispherical impactor . . . . .	106
4.13	(a) Coarse mesh, (b) Fine mesh and (c) Mesh sensitivity analysis of Kevlar composite . . . . .	107
4.14	Comparison of stress vs. strain curves for 45 degree samples [5] . . .	109
4.15	3-point bending test setup and strain field $\gamma_{13}$ obtained from image correlation [5] . . . . .	110
4.16	Comparison of Force- displacement response of the Kevlar plate with neat resin: (a)v=3.13 m/s and (b) v=4.43 m/s . . . . .	111
4.17	Comparison of Force- displacement response of the Kevlar plate with Nano resin: (a)v=3.13 m/s and (b) v=4.43 m/s . . . . .	112
4.18	Comparison of bottom surface of the Kevlar composite plate with neat resin: (top) experiment, (bottom) LS-Dyna . . . . .	114
4.19	Displacement vector of the Kevlar composite plate with Nano resin: (left)grid pattern in plate and (centre) vector for experiment, (right) LS-Dyna . . . . .	114
4.20	Comparison of z- displacement of Kevlar plate with Nano resin . . . .	115
4.21	LS-Dyna model for the simulation of impact on sandwich plate . . . .	116
4.22	Quasistatic Compression of Rohacell foam . . . . .	117

4.23	Compression device of Flywheel for dynamic compression of foam [116]	118
4.24	Results of uniaxial compression of Rohacell foam at (a) Quasistatic and (b) Flywheel, for 6 samples of same dimensions and density . . .	120
4.25	SHPB test setup for High strain rate Compression and Stress- strain curve of Rohacell foam . . . . .	121
4.26	Comparison of Compression Stress -strain curve of Rohacell foam . .	122
4.27	Uniaxial compression model of Rohacell foam . . . . .	122
4.28	Experimental setup for Double Cantilever Beam test (a) Aluminium substrate and (b) Kevlar composite with end blocks . . . . .	124
4.29	Force-displacement curve for DCB test of Kevlar composite with neat resin and nano resin . . . . .	124
4.30	DCB samples of Kevlar composite with neat resin and Nanostrength	125
4.31	Force- displacement curve for DCB test of Kevlar composite on Aluminium substrate . . . . .	126
4.32	DCB samples of Kevlar composite with neat resin and Nanostrength on Aluminium substrate . . . . .	126
4.33	Fracture energy calculated for DCB test as a function of crack length (a) Kevlar composite beam and (b) Kevlar - Aluminium beam . . . .	128
4.34	Typical evolution of impact from $t=0$ ms (no contact) to $t= 10$ ms (after rebound) . . . . .	129
4.35	Force, displacement and energy time histories for Kevlar sandwich plate	130
4.36	Comparison of Force -displacement curves for 8 J impact for KR sandwich . . . . .	131
4.37	Comparison of Force -displacement curves for 12 J impact for KR sandwich . . . . .	132
4.38	Comparison of Force -displacement curves for 16 J impact for KR sandwich . . . . .	132
4.39	Comparison of experiment and LS-Dyna simulation for Kevlar Rohacell sandwich: (a) Peak Force and (b) Max displacement . . . . .	133
4.40	Contour plot of damage in longitudinal direction of top facesheet . . .	135
4.41	Core damage in the Rohacell foam sandwich plate impacted at 16 J .	136
4.42	Comparison of Force- displacement curves for 8 J impact for KNR sandwich . . . . .	136

4.43	Comparison of Force- displacement curves for 12 J impact for KNR sandwich . . . . .	137
4.44	Comparison of Force- displacement curves for 16 J impact for KNR sandwich . . . . .	137
4.45	Comparison of energy absorbed by Kevlar/Nano Rohacell sandwich . . . . .	138
5.1	Hexapod setup for tri-dimensional impact of sandwich panels . . . . .	143
5.2	(a) Parabolic trajectory for Aluminium Divinycell sandwich plate and Displacement input for the Hexapod . . . . .	144
5.3	Typical Force- time results obtained for parabolic impact of Aluminium Divinycell sandwich plate . . . . .	145
5.4	(a) Hexapod setup with cylindrical impactor and Kevlar-Rohacell sandwich and (b) Clamping mechanism . . . . .	145
5.5	Parabolic trajectory: Displacement input for the hexapod . . . . .	146
5.6	Parabolic trajectory with different impactor geometries - Cylindrical, 120° and 60° wedge . . . . .	147
5.7	(a) KR sandwich samples after impact by cylindrical impactor, (b) Force -time curve for impact by cylindrical impactor and (c) KNR sandwich samples after impact by cylindrical impactor . . . . .	148
5.8	(a) KR sandwich samples after impact by 120° wedge shape impactor, (b) Force -time curve for impact and (c) KNR sandwich samples after impact by 120° wedge impactor . . . . .	149
5.9	(a) KR sandwich samples after impact by 60° wedge shape impactor, (b) Force- time curve for impact and (c) KNR sandwich samples after impact by 60° wedge impactor . . . . .	150
5.10	Progression of impact for KR sandwich with 60° wedge impactor (a)t= 0ms, (b)t=14ms, (c)t=45ms and (d)t=88ms . . . . .	151
5.11	Comparison of Z- Force history for Kevlar-Rohacell sandwich with different impactor geometries - Cylindrical, 120° and 60° wedge . . . . .	152
5.12	Parabolic trajectory of the cylindrical impactor: (Top) Traj2 and (Bottom) Traj3 . . . . .	152
5.13	Effect of location of impact for KR sandwich plate and cylindrical impactor . . . . .	153
5.14	LS-Dyna model of Aluminium - Divinycell sandwich and cylindrical impactor . . . . .	155

---

5.15	Comparison of Force- time curves for 0.5 mm Aluminium - Divinycell sandwich model with experiment . . . . .	156
5.16	Comparison of Force- time curves for 1 mm Aluminium - Divinycell sandwich model with experiment . . . . .	157
5.17	LS-Dyna model of Kevlar Rohacell sandwich plate with different impactor geometries . . . . .	158
5.18	Comparison of Y-force and Z-force from experiment and LS-Dyna for Traj3 . . . . .	159
5.19	Progression of core strain for KR sandwich plate with cylindrical impactor and Traj3 . . . . .	160
5.20	Comparison of Minimum principal strain history from Digital Image Correlation and LS-Dyna for Traj3 . . . . .	161
5.21	Comparison of y-force and z-force for KR sandwich from experiment and LS-Dyna for cylindrical impactor . . . . .	162
5.22	Comparison of Y-force and Z-force for KR sandwich from experiment and LS-Dyna for 120° wedge impactor . . . . .	163
5.23	Comparison of Y-force and Z-force for KR sandwich from experiment and LS-Dyna for 60° wedge impactor . . . . .	163
5.24	Comparison of minimum principal strain for KR sandwich from DIC and LS-Dyna for cylindrical impactor . . . . .	164
5.25	Comparison of Y-force and Z-force for KNR sandwich from experiment and LS-Dyna for cylindrical impactor . . . . .	165
5.26	Comparison of LS-Dyna force history of KR and KNR sandwich panels for cylindrical impactor . . . . .	165
5.27	Tresca strain for KR sandwich plate and cylindrical impactor with Traj1 . . . . .	167



## Abbreviations/Acronyms

BCW	Buckled cell walls
CB	Carbon Black
CDM	Continuum Damage Mechanics
CNT	Carbon Nanotubes
CTBN	Carboxyl terminated butadiene acrylonitrile
CFRP	Carbon Fibre Reinforced Plastic
DAQ	Data Acquisition
DCB	Double Cantilever Beam
DGEBA	Diglycidyl ether of bisphenol A epoxy
DIC	Digital Image Correlation
EPP	Expanded Polypropylene
EPS	Expanded Polystyrene
ERODS	Erosion strain
FE	Finite Element
FEA	Finite Element Analysis
FEM	Finite Element Method
FRP	Fibre reinforced Plastics
$G_{Ic}$	Mode I interlaminar fracture toughness
$G_{IIc}$	Mode II interlaminar fracture toughness
GFRP	Glass Fibre Reinforced Plastic
GNR	Glass-Nanostrength Rohacell sandwich
GR	Glass Rohacell sandwich
KFRP	Kevlar Fibre Reinforced Plastic
KNR	Kevlar-Nanostrength Rohacell sandwich
KR	Kevlar Rohacell sandwich
LSTC	Livermore Software Technology Corporation
LVDT	Linear Voltage Displacement Transducer
MAM	polymethylmethacrylate- b- polybutylacrylate- b- polymethylmethacrylate tri-block copolymer

---

MLT	Matzenmiller, Lubliner and Taylor Model
MWCNT	Multi-walled Carbon nanotubes
NFLS	Normal strength of contact interface
PEEK	Polyether Ether Ketone
PES	PolyEther Sulphone
PMI	PolyMethacryllimide
PMMA	Polymethyl methacrylate
PUR	Polyurethane
PVC	Poly Vinyl Chloride
REV	Representative Element Volume
ROI	Region of Interest
SBM	styrene- b- butadiene- b- polymethylmethacrylate tri-block copolymer
SEM	Scanning Electron Microscope
SFLS	Shear strength of contact interface
SHPB	Split Hopkinson Pressure Bar
SLIM	Stress Limit
TEM	Transmission Electron Microscope
$T_g$	Glass transition temperature
UHMWPE	Ultra High Molecular Weight PolyEthylene
XPS	Extruded Polystyrene

# Chapter 1

## Introduction

### 1.1 Background

The focus of this study is the low velocity impact behaviour of composite sandwich panels. Sandwich structures are lightweight structures that are based on a simple construction of two thin high strength facesheets of relatively dense material bonded to either side of a thick low density core such as foam and honeycomb. The facesheets or skins are designed to resist bending loads and are usually made of aluminium or fibre reinforced polymers. The core separates and stabilises the outer sheets against buckling under edgewise compression, torsion or bending and is usually made of wood, polymer foams, or expanded metal or polymer honeycombs. An adhesive bonding between the facesheets and the core ensures the load transfer between them. The sandwich concept can be observed in natural materials and structures such as human and animal bones, skulls and wings of birds [1]. A high specific bending stiffness is achieved because of the separation of the stiff facesheets by the core as the sandwich structures behave like I-beams. The outer facesheets correspond to the flanges, and carry most of the direct compressive/tensile bending load, while the lightweight core corresponds to the web of the I-beam. A schematic representation of the sandwich structure is shown in Figure 1.1. Schematic diagram of sandwich construction figure.1.1

Sandwich structures have a high ratio of flexural stiffness to weight, resulting in higher buckling resistance, lower lateral deformations, and high energy absorption. Additionally, they also provide good thermal and acoustic insulation, higher natural frequencies and buoyancy. The sandwich construction allows the optimisation of structures that are weight-critical such as parts of airplanes, space structures, blades for wind power generation, naval structures and sporting goods [1]. Sandwich composites with Fibre reinforced plastic (FRP) facesheets and polymeric foam cores have emerged as a major class of lightweight structural materials in a wide range of engineering fields including aerospace, automotive and marine structures. However, some FRP sandwich structures have very low energy absorption capability when

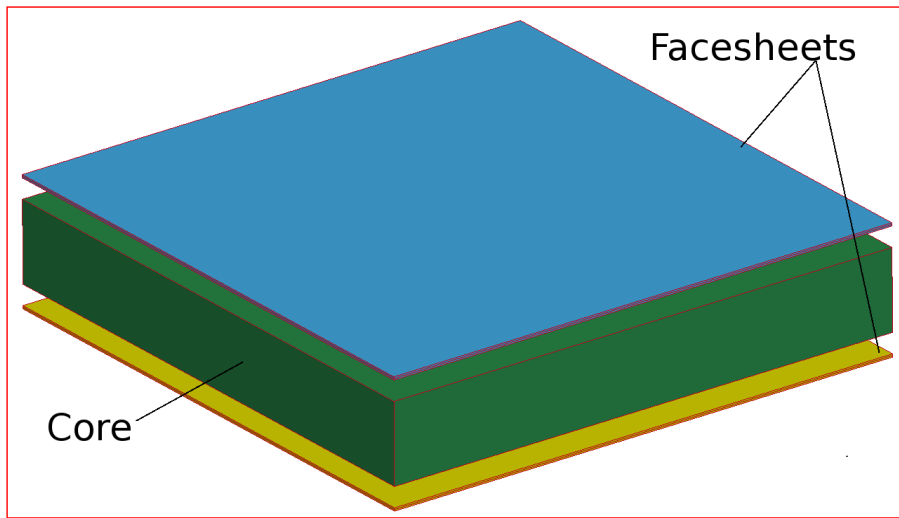


**Figure 1.1.** Schematic diagram of sandwich construction

subjected to impact loads normal to the sandwich plane. This is of concern due to the susceptibility of sandwich structures to damage caused by impact [2]. Impact damage in sandwich structures can be caused by tool drops, runway debris, bird strikes, hailstorms or ballistic loading. Low velocity impact damage is of particular concern in aerospace applications because the impact load may cause no obvious indication of damage except for a small indentation at the impacted location. However, significant damage, such as local core crushing and disbonding of the facesheet from the core has occurred, which severely compromise the structural integrity of the sandwich panel.

The resin systems used as matrix material in the laminated composite facesheets which are typically thermoset resins like epoxy, are relatively brittle materials. Due to the brittle nature of the matrix, even a small amount of internal delamination propagates predominantly at right angles to the applied compressive stress with disastrous results to the sandwich composite. Rubber toughening has proved to be effective and is widely used but the drawback of this approach is that it sacrifices desirable properties e.g., the stiffness and the glass transition temperature of epoxy. One of the proposed solutions is the modification of the thermoset resins with nano-sized organic and inorganic particles. Carbon nanotubes (CNT) or nanoclay and silicate nanocomposites have been investigated by various researchers [3] but a new method to synthesise block copolymers, which self-assemble in the nanoscale would appreciably reduce the problems associated with dispersion of the nanoparticles.

It has been reported that block copolymer-modified epoxies enhanced the fracture toughness and impact performance with minimal sacrifice of thermal properties [4]. Denneulin et al. [5] reported that while carbon nanotubes did not have a significant effect, the damage behaviour of Kevlar FRP with nano-block copolymer modified epoxy was improved substantially. A systematic study on the effect of these nano reinforcements on the mechanical performance of sandwich panels made with these nano-modified resins, especially to impact loading, is lacking. The objective of the PhD thesis is to therefore study the effect of toughening the matrix with nano-elastomeric particles on the low velocity impact performance of sandwich composites.

The effect of the addition of nanoparticles on the impact performance of sandwich panels with FRP facesheets are studied using experimental testing and numerical simulation. The low velocity impact behaviour of sandwich plates is typically studied by applying an initial velocity to a rigid impactor, which comes in contact with the facesheet. The macroscopic response of the sandwich composite to the impact and the microscopic mechanisms by which enhancement of the fracture toughness of the resin translates to improved impact resistance of the sandwich panel will be studied. The thesis will focus on two different types of impact loading; low velocity impact at normal angle of incidence and parabolic impacts. In real engineering situations, the structures are more frequently loaded at some oblique angle. It is easy to carry out normal impact tests using devices like the drop tower, but oblique tests are difficult to characterise experimentally. A tri-dimensional impact device called Hexapod has been developed to experimentally study the impact loading of sandwich plates with a parabolic trajectory.

The PhD thesis was part of a Cotutelle agreement signed between École Doctorale of Arts et Métiers ParisTech, centre de Bordeaux-Talence and the Graduate Research School of the University of New South Wales, Australia. Consequently, the project was conducted partly at the School of Engineering and Information Technology (SEIT) of the Australian Defence Force Academy (ADFA) campus of University of New South Wales, Canberra and the Durabilité Matériaux des Assemblages et des Structures department (DuMAS) of Institut de Mécanique et d'Ingénierie de Bordeaux (I2M). The thesis was done under the supervision of Dr. Krishna Shankar at SEIT and Prof. Philippe Viot and Dr. Sandra Guérard at I2M laboratory. The sandwich samples required for the experimental testing were manufactured in the

materials laboratory at Université de Pau et des pays de l'Adour with support of Dr. Frédéric Léonardi.

## 1.2 Aim

To investigate the enhancement in impact resistance of sandwich panels with FRP facesheets due to the addition of block copolymer nanoparticles in the epoxy matrix. The effect of the nanoparticles on the impact performance of sandwich panels with Kevlar and Glass FRP facesheets and Rohacell<sup>®</sup> foam core with neat resin and 10%Nanostrength<sup>®</sup> embedded in the resin will be studied using experimental testing and numerical simulation.

## 1.3 Scope of thesis

The effect of the addition of nano-elastomeric particles on the impact performance of sandwich panels will be studied using experimental methods as well as through numerical simulation using Finite Element Analysis (FEA) software. The first phase of the experimental studies will consist of instrumented low velocity impact testing using drop tower setup. The second phase of experimentation will involve parabolic impact tests using Hexapod. This presents an exciting new opportunity as the literature is limited to study of normal and oblique impacts. The Hexapod or Stewart platform will enable defining a trajectory of the impact along the surface of the sandwich panel. The third phase of the experimental work will consist of damage analysis using an optical microscope. Numerical simulation of the impact response of sandwich panels with and without nano-reinforcement will be performed to study the effect of the nano-additives on the impact resistance of the panels under different incident velocity conditions. Mechanical characterisation of the component materials of the sandwich structure, such as the strain rate dependent properties of the polymeric foam core and interlaminar properties are required as input parameters for the Finite Element (FE) models. The impact test results will be used to validate the numerical simulation models of the drop tower tests. The validated numerical model will then be employed for the simulation of the parabolic impact with the Hexapod. The key contributions of the thesis will be; (1) investigating how enhancing matrix toughness with block copolymer nanoparticles improve the impact resistance of FRP sandwich panels, (2) developing a phenomenological FE

model for the sandwich panels and (3) studying parallel impacts through parabolic trajectories using the Hexapod.

## 1.4 Methodology

The methodology adopted for the thesis is as follows:

- *Experiments*
  - Drop tower impact tests of KevlarRohacell sandwich plates
  - Drop tower impact tests of GlassRohacell sandwich plates
  - Damage analysis by cutting section of sample
  - Microscopy of sandwich section
  - Compression testing of Rohacell foam core samples at different strain rates
  - Double Cantilever Beam (DCB) test of Kevlar composite with neat and nano resin
  - Parabolic impact tests on KevlarRohacell sandwich plates on Hexapod (Stewart platform)
- *Simulations*
  - Identification of material model of composite and foam core
  - Mesh sensitivity
  - Compression model of Rohacell foam
  - Development and validation of FE model for low velocity impact of Kevlar FRP composite with neat and nano resin
  - Development and validation of FE model for low velocity impact of KevlarRohacell sandwich (with neat and nano resin)
  - Simulation of parabolic impact of Kevlar Rohacell sandwich (with neat and nano resin)

## 1.5 Outline of thesis

**Chapter 2** includes a detailed review of literature on the materials used for sandwich construction and the low velocity impact behaviour of sandwich structures. An overview of the methods used to toughen the matrix, including the use of block copolymers is provided.

**Chapter 3** presents the fabrication method of sandwich plates with and without the nanoparticles in the resin and the drop tower experimental setup used for the

low velocity impact testing. A comparison of the macroscopic behaviour of sandwich composites with Rohacell foam core and Kevlar and Glass fibre reinforced epoxy facesheets with neat resin and resin with 10% M52N Nanostrength is also presented.

**Chapter 4** deals with the development of the Finite element model using *LS-Dyna* for the simulation of low velocity impact loading of sandwich plates. A review of the different material laws used for the composite facesheet and the core material are given. The FE model is validated by comparing the experimental measurements provided in previous chapter with the simulated force versus time responses along with the predicted failure modes and peak loads.

**Chapter 5** is a preliminary study on triaxial impact loading of Kevlar- Rohacell sandwich composites using a modified Stewart platform (Hexapod). The study of impact behaviour of sandwich panels have been limited to normal impacts with some limited literature on oblique impacts. The parabolic impact loading presented in this chapter is innovative in that the impact isolates the effect of shear (or parallel) contact in oblique impacts. The parabolic impact of the sandwich panel is studied for different impactor geometries both experimentally as well as with an FE model developed in LS-Dyna.

Conclusions and recommendations are provided in **Chapter 6**

# Chapter 2

## Literature Review

### 2.1 Introduction

Sandwich panels are a special form of laminated composites comprising of two thin high strength facesheets bonded to either side of a thick low density core such as foams and honeycombs. This provides a lightweight structure with high bending stiffness. The skins are designed to resist tensile and compressive stresses and are usually made of aluminium, polymers or fibre reinforced polymers. The core is designed to resist compression and shear stresses and a range of materials including endgrain Balsa wood, rigid polymer foams, aluminium or Nomex honeycombs are used as cores. Sandwich composites with fibre reinforced plastic (FRP) facesheets have emerged as a major class of lightweight structural materials in a wide range of engineering fields including aerospace, automotive, wind energy and marine structures. In addition, sandwich construction is used in protective headgear such as motorcycle helmets, aeronautical helmets used by fighter pilots and helmets used for recreational activities in hockey or football. Sandwich composites offer immense potential in applications where reduction of weight is an important factor for efficiency or comfort because of their high stiffness to weight ratio. Sandwich construction, in addition, offers the possibility of optimising various aspects of performance by tailoring the core and skin materials and their thicknesses.

The impact performance of sandwich structures has been identified as being of considerable importance [6] and it has been noted that sandwich structures must dissipate the impact energy to protect either the rest of the structure or humans during impact loads. However some sandwich composites have been shown to be vulnerable to impulsive loads normal to the sandwich plane. This is of concern due to the susceptibility of sandwich structures to damage caused by impact [2]. Impact damage in sandwich structures can be caused by tool drops, runway debris, bird strikes, hailstorms or ballistic loading. Marine hull structures are also subjected to “slamming” loads caused by repeated water impacts. Ballistic impacts cause localised damage,

which is clearly visible on inspection while low-velocity impacts involve long contact time between impactor and target which result in global structural deformation with internal damage at points far from the contact region [7]. Bernard and Lagace used X-ray photos to determine the extent of delamination damage and noted that extensive delamination and core damage were found in specimens with no visible surface damage [8]. The failure modes commonly associated with low velocity impact loading in sandwich structures are fibre failure, matrix cracking, delamination and core crushing. Richardson et al. [9] noted that matrix damage is the first type of failure induced by transverse low-velocity impact, and usually takes the form of matrix cracking but also debonding between fibre and matrix. Delamination has also been observed to occur in the presence of matrix cracks.

One of the limiting factors on the impact performance of the FRP sandwich is the brittle nature of the epoxy matrix. In order to improve the impact resistance of the composites, several solutions including thermoplastic resins, toughened epoxies, carbon, steel, or titanium pins driven through the z-direction, stitched fabrics and 3D composites have been proposed [10]. Shih et al. [11] reported that the impact failure mechanism of sandwich panels containing less tough facesheets was found to change from facesheet-dominated to foam-core-dominated behaviour. The toughness of a material is a measure of how much energy it is able to absorb prior to failure. Brittle materials, like a glassy epoxy resin, have high strength but negligible toughness. Conversely, ductile materials have high toughness due to plastic deformation. Strong correlations have been reported in the literature between the toughness of the matrix,  $G_m$ , and the composite mode I interlaminar fracture toughness,  $G_{Ic}$  [12]. According to Liu and Wagner, improving the toughness of brittle matrix represents a worthy challenge, especially in view of potential industrial applications [13].

This chapter provides an extensive literature review of materials used in sandwich structures, the impact behaviour of sandwich structures and the means of improving the impact behaviour of sandwich plates by the toughening of the epoxy matrix by block copolymer particles.

## 2.2 Sandwich structures - Materials and construction

The increasing effort to develop lightweight structures characterised by better mechanical performance has led to the development and the employment of sandwich

structures. A sandwich structure may be defined as a composite component featuring a lightweight core placed between two relatively thin high-strength facesheets. A sandwich structure may be considered as an I-beam with the core represented by the web and the facesheets represented by the flanges of the I-beam. The facesheets are bonded to the core to permit the load transfer between the components. The flanges form an efficient stress couple counteracting the bending moment. The web is designed to allow the flanges to resist shear and buckling and to maintain a constant distance between the two flanges. The core places the facesheets away from the bending neutral axis enhancing the bending resistance of the facesheets. Composite facesheets typically consist of laminates formed by stacking uni-directional plies or woven fabrics embedded in a polymer matrix [1]. Structural sandwich structures with fibre-reinforced composite face sheets are nowadays widely used in aerospace, marine, automobile, locomotive, windmills, building, and consumer industries for their excellent properties like superior bending stiffness, low weight, excellent thermal insulation and acoustic damping, ease of machining, and ease of forming, among others [14]. The use of woven fabrics as facesheets in composite panels is increasing due to interlacing of fibre bundles possessing high ratios of strain to failure in tension, compression or under impact loads [15]. The materials used as core are typically low density materials such as honeycombs, polymeric foams, balsa wood and cork [16].

### 2.2.1 Fibre

A fibre-reinforced composite is composed of three constituents: the fibres, the matrix and a fine interphase region responsible for assuring the bond between the matrix and fibre. The manner in which the material deforms and fractures depends upon both the chemical and mechanical properties of these three constituents [17]. The role of the fibres in a composite structure is extremely important since they are responsible for bearing a significant percentage of the applied load. At present, many types of fibre are available for aeronautical applications these include carbon, glass, and Kevlar fibres [17].

The typical properties of some commonly used fibres are given in Table 2.1 Typical properties for a range of commonly used fibre reinforcements for impact applications [18]table.2.1. Twaron and Kevlar fibres belong to the family of Aramid fibres, while Dyneema and Spectra are made of Ultra High Molecular Weight - PolyEthylene (UHMW-PE). Carbon and glass fibres suffer from a lack of plasticity which

**Table 2.1.** Typical properties for a range of commonly used fibre reinforcements for impact applications [18]

<b>Fibre</b>	<b>Density (g/ cm<sup>3</sup>)</b>	<b>Tensile modulus(GPa)</b>	<b>Tensile strength(MPa)</b>	<b>Failure strain(%)</b>
E Glass	2.58	72	3.5	4.8
S-2 Glass	2.46	87	4.9	5.7
Carbon T400	1.80	250	4.4	1.8
Twaron HM1055	1.45	125	2.8	2.5
Twaron HS2000	1.44	90	3.8	3.5
Kevlar 49	1.45	135	2.9	2.8
Kevlar 129	1.45	99	3.4	3.3
Dyneema SK60	0.97	89	2.7	3.5
Dyneema SK71	0.97	120	4	4.1
Spectra S900	0.97	79	2.1	3.6
Spectra S2000	0.97	116	3	2.9
All-PP tapes	0.78	15	0.45	7.5

means that non-penetrative impact loads can lead to (often invisible, subsurface) fibre damage, which can drastically reduce the residual mechanical properties of the composites. The earliest aramids, which became DuPont's family of Kevlar aramid fibres were initially targeted at reinforcement of rubber goods such as tires, hoses, and belts and as reinforcement of plastics, a field previously dominated by glass, carbon, and boron fibres. The aramid fibres held the distinction of having the highest tensile strength-to-weight ratio of any commercially available reinforcement fibres and this led to the development of numerous high-performance composite applications [19]. Composites with thermoplastic fibres like Dyneema and Spectra typically possess sufficient elastic limits to make them less sensitive to damage from lower energy impacts and are therefore used in specific impact applications, for instance, personal protection for military/police personnel from direct projectile impact, or as spall liners behind ceramic/metallic armour in armoured vehicles to limit proliferation of shrapnel inside a vehicle following impact [18].

It can be seen from the Figure 2.1 Specific properties of different fibres [19] figure.2.1 that the Kevlar fibres have excellent specific properties compared to other fibres [19]. Reis et al. [20] reported that the Aramid fibres are a very important reinforcement for military and civilian systems due to their high degree of toughness and damage tolerance associated with the failure mechanism of aramids which promotes good

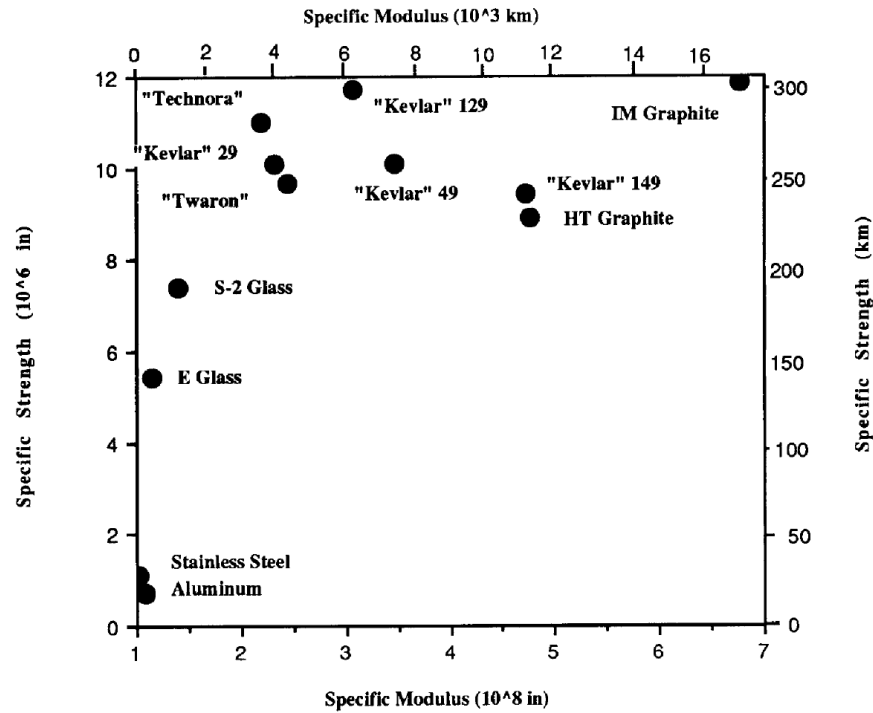


Figure 2.1. Specific properties of different fibres [19]

impact/ballistic performance. Kevlar composites have been extensively utilised as lightweight armor structures in applications ranging from military helmets to large scale vehicle systems such as aircraft, spacecraft, land vehicles, and naval vessels [21]. The extended chain structure of the polymer molecule of the Aramid fibres results in unusually high tensile properties, but is vulnerable to kinking and collapse in compression. Therefore the stress- strain behaviour of the Aramid fibre, and of composites made with it, is highly asymmetric; the material yields at relatively low strain in compression giving rise to elastic-plastic behaviour. Aramid-reinforced composites fail in a controlled, non-catastrophic manner in bending and compression, absorbing a great deal of energy in the process. This makes it possible to design fail-safe structures which retain their integrity and can still withstand significant tensile stress even after failure [19]. Hybrid composites with high modulus/high-cost fibre such as carbon or boron combined with low modulus/low-cost fibre such as glass or Kevlar have been found to provide advantages such as balance of strength and stiffness, reduced weight and/or cost, improved fatigue resistance, improved fracture toughness, and impact resistance [22]. The high modulus fibre provides the stiffness and

load bearing capability, whereas the low modulus fibre makes the composite more damage tolerant and reduces the cost.

### 2.2.2 Matrix

The polymer matrix materials are thermosetting polymers like epoxy, polyester, phenolic, polyimide resins or thermoplastics such as polypropylene, Nylon 6.6, PMMA, PEEK [10]. Thermoset resins such as epoxy and thermoplastic resins like PEEK are the most commonly used matrix materials. Thermosetting resins are usually low molecular weight monomers or oligomers having functional groups for cross-linking reaction. The polymerization or curing reaction of these resins yields a highly cross-linked three-dimensional network structure [23]. The polymeric matrix in a fibre-reinforced composite serves to protect, align and stabilise the fibres as well as assure stress transfer from one fibre to another [17]. Epoxy resins are relatively low molecular weight prepolymers capable of being processed under a variety of conditions. The cured resins have high chemical and corrosion resistance, good mechanical and thermal properties, outstanding adhesion to a variety of substrates, and good electrical properties [23]. The chemical structure of a common epoxy resin called diglycidyl ether of bisphenol A (DGEBA), shown in Figure 2.2, is characterised by the presence of a three-membered ring containing two carbons and an oxygen (epoxy group or epoxide ring).

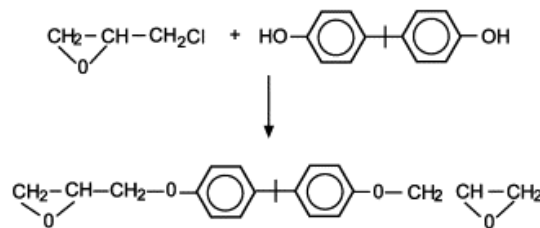


**Figure 2.2.** Chemical structure of DGEBA resin [23]

Typically both the stiffness and strength of the matrix are lower than those of the reinforcing fibres and therefore the fibres are responsible for carrying most of the applied load in a composite component. The role of the matrix is nevertheless critical and damage to the matrix can reduce the load bearing capacity significantly. The methods used to improve the toughness of the matrix and thus the mechanical properties of the composite, are presented in a later section.

### 2.2.3 Core

The core materials are usually divided into four groups; balsa wood, corrugated sheets, honeycombs and cellular foams [24]. Aluminium honeycombs have been used in the aerospace industry but suffer from corrosion damage to the core from water ingress. According to Shipsha [24], though honeycomb sandwich structures offer the highest stiffness to weight ratio, many industrial applications prefer cellular foam cores such as PVC foam (Divinycell<sup>®</sup>) because of their relative low cost of these closed-cell foams, water resistance and a possibility to use traditional manufacturing methods such as hand layup. Foam materials have a cellular structure with a three-dimensional array of cells and this microscopic cellular structure determines their superior performance as an energy absorbing material [25]. One of the other advantages of foam cores is the increased support surface for bonding with the face sheets and provides structural damping [7]. Other foams that are used as core material for sandwich structures include Polyurethane foams, phenolic foams, expanded and extruded polystyrene (EPS and XPS) foams and PolyMethacrylImide (PMI) foams [26]. A summary of properties of some of the foam materials is given by Hazizan and Cantwell [27] in Table 2.2. It can be seen that PMI foam commercially available as Rohacell<sup>®</sup> foam, with a density of 52 ( $kg/m^3$ ) has good specific tensile and shear properties with Tensile modulus of 75 MPa and Shear modulus of 19 MPa.

**Table 2.2.** Summary of properties of some foam materials [27]

Foam	Nominal density( $kg/m^3$ )	Tensile modulus(MPa)	Shear modulus(MPa)
Linear PVC	50	37	11
Linear PVC	80	56	21
PEI	60	37	14
PEI	80	52	22
PVC/PUR	40	28	13
PVC/PUR	55	45	22
PVC/PUR	75	63	30
PVC/PUR	90	81	38
Rohacell (PMI) [25]	52	75	19

Rohacell polymethacrylimide series of closed cell rigid foams have application potential in aerospace and aircraft structures. The manufacturing process of the

Rohacell foams are a two step process with the solid plastic sheet formed by polymerisation reaction in the first step and the thermal expansion of polymer compounds with a blowing agent that produces gases at elevated temperatures in the second step. The blowing agent starts to react and produces small gas bubbles through the plastic giving the characteristic foam structure [24]. The foams are produced in a variety of densities and thicknesses. Arezoo et al. [28] observed that the analysis of the microstructure of Rohacell foam of different density revealed that the material comprises cells of tetrakaidecahedral shape, with different cell diameter and cell-wall thickness for each foam density. The microstructure of the Rohacell foam and a typical uniaxial compressive behaviour of the foam material is given in Figure 2.3(a) Microstructure of Rohacell foam and (b) Typical Compression properties of Rohacell 51WF foam in three perpendicular axes [25]figure.2.3. The stress- strain curves NC1, NC2 and NC3 correspond to loading in three perpendicular directions. The stress- strain curve can be divided into three distinct regions. The first stage corresponds to the elastic region and after the yield point  $\sigma_y$  is followed by a yield plateau, where the stress remains almost constant while the strain is increased. This behaviour is due to the collapse of the cells inside the foam. At the third stage, which corresponds to high compressive strains, the material reaches a region of densification, causing the stress to increase very quickly [29]. Mahfuz et al. [30] noted that in order to improve the performance under impact of sandwich structures with foam cores, a thorough understanding of foam behaviour to high strain rate loading is essential. The impact behaviour of Rohacell foams and sandwich panels containing Rohacell foam cores have been studied by various researchers [8, 24, 25, 31–33].

## 2.3 Impact behaviour of sandwich structures

Impact involves the contact of two bodies namely the impactor and the target plate. The impact response of sandwich plate depends on a large number of variables such as mass of the impactor, impact velocity, contact area and stiffness of the sandwich panel. The mechanical behaviour of sandwich structures depends on the mechanical properties of facesheets and core and has been found to be highly dependent on the rate of loading; while the sandwich plates can exhibit ductile behaviour under static loading, they can have brittle behaviour under impact and fail catastrophically [34]. Flores et al. [33] conducted quasistatic indentation tests on carbon fibre sandwich plates with different density Rohacell foams and various nose shapes. Goldsmith and

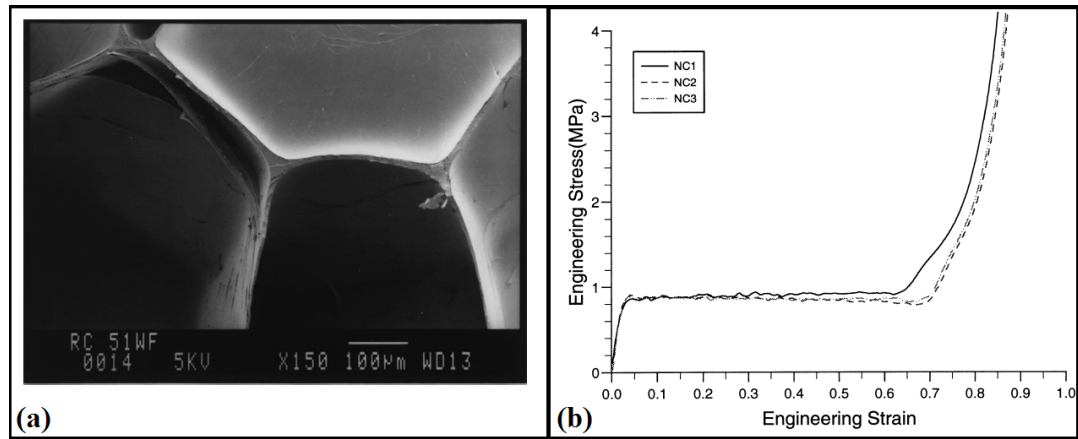


**Figure 2.3.** (a) Microstructure of Rohacell foam and (b) Typical Compression properties of Rohacell 51WF foam in three perpendicular axes [25]

Sackman [35] undertook an experimental investigation of aluminum and Nomex<sup>®</sup> honeycombs and aluminum honeycomb sandwiches with aluminum as well as non-metallic face plates under static as well as dynamic loading in order to determine the energy dissipation and force level transmission characteristics of these structures. Cantwell et al. [16] studied sandwich panels with balsa wood cores as well as with PVC for marine applications and found that both the balsa wood and PVC foam core sandwich panels were able to withstand higher forces under impact loading than in quasi-static conditions. It was also observed that PVC foams where there is no crosslinking in the polymer foam absorbed the most energy under impact. Richardson et al. [9] observed that while impact damage is generally not considered to be a threat in metal structures owing to the ductile nature of the material, most composites are brittle and so can only absorb energy in elastic deformation and through damage mechanisms, and not via plastic deformation. Metals absorb a large amount of energy because at yield stress the material may flow for very large strains (up to 20%) at constant yield before work hardening. In contrast, composites can fail in a wide variety of modes and contain barely visible impact damage (BVID) which nevertheless severely reduces the structural integrity of the component. The transverse impact resistance of composite plates is poor due to the lack of through-thickness reinforcement. A sandwich structure should undergo stable progressive crushing in order to absorb energy efficiently.

There is some discussion about the exact definition of low velocity impact with Cantwell and Morton [17] classifying velocities up to 10 *m/s* as low velocity and

Abrate [34] in his review of impact on laminated composites stated that impact speeds of less than 100  $m/s$  are considered as low-velocity impacts. It is generally accepted that low-velocity impact are events which can be treated as quasi-static, the upper limit of which can vary from one to tens of  $m/s$ . The contact duration is long enough for the entire structure to respond to the impact in low-velocity impact while high-velocity impact response is dominated by stress wave propagation through the material.

### 2.3.1 Experimental methods

Many researchers have studied the dynamic behaviour of sandwich structures [17,27, 35–37]. According to Ramesh [36], impact experiments fall into one of four different categories; High-strain-rate experiments, Wave-propagation experiments, Dynamic failure experiments and Direct impact experiments. Quasi static experiments are typically accomplished through a variety of servohydraulic machines, while Kolsky bar or Split-Hopkinson pressure bar (SHPB) is the experimental technique used in the high-strain-rate domain. Taylor impact and Charpy tests are dynamic experiments to capture impact failure behaviour. According to Cantwell and Morton [17], the impact test fixture should be designed to simulate the loading conditions to which a composite component is subject in operational service and then reproduce the failure modes and mechanisms likely to occur. The impact problem can be divided into two separate conditions: high velocity impact by a small mass (runway debris, small arms fire, etc.), which is tested with a gas gun or some other ballistic launcher and low velocity impact by a large mass (dropped tool), which is tested using a falling weight or a swinging pendulum.

High velocity impact testing at ballistic rates of strain can be achieved using a high pressure gas gun where a gas such as nitrogen is fed to a chamber located at one end of the barrel [17]. When the gas has reached a pre-determined pressure value, a diaphragm is burst (by electrical heating or a mechanical puncturing device), accelerating a projectile down the barrel to strike a specimen or component supported vertically. The velocity of the impactor can be determined just prior to impact using optical sensors or by using a simple break-wire technique. The high velocity impact typically results in large-scale damage and/or perforation of the target. Roach et al. [38] carried out impact tests at 30, 60 and 120  $m/s$  on Glass fibre reinforced polyester laminates with and without a PVC foam core using a nitrogen pressurised

gas gun and found that sandwich panels do not undergo any significant global deformations and as a result, require less energy to penetration than the skins alone. Hampson and Moatamedi [39] provides an extensive review of published literature on the topic of high velocity and hyper velocity impact tests.

The test devices used to study the low velocity impact response of composite materials include the Charpy and Izod pendulums, the falling weight fixtures such as the Gardner and drop dart tests as well as hydraulic machines designed to perform testing at velocities up to 10  $m/s$ . In the typical Charpy tests, the specimen was a thick beam with a notch at its mid point and impacted by the swinging pendulum directly opposite the notch. The energy dissipated during impact can be found but the Charpy tests induced failure modes that are not necessarily observed under low velocity impact loading on operational structures and are therefore not a preferred test method [17].

Most previous studies on low velocity impact damage used drop weight experimental methods of a relatively large mass, which represented the accidental damage caused by dropped tools [39]. For instance, an Instron Dynatup drop tower, Model 9250HV was used for impact testing at different energies by Gustin et al. [15] and by Park et al. [40]. In a drop tower test with normal incidence, a weight is allowed to fall from a pre-determined height to strike the test specimen or plate supported in the horizontal plane. It is possible to use a similar system for oblique impacts by tilting the plane of the target fixture to the required angle. In general, the impact event does not cause complete destruction of the test specimen but rebounds, enabling a residual energy to be determined. In the schematic diagram of the drop tower shown in Figure 2.4 Schematic diagram of drop tower used for the low velocity impact tests [41] figure.2.4, two columns guide the falling carriage on which impactor is fixed. The carriage is raised to the desired impact height by a winch and released by an electromagnet, freely falls under gravity, and strikes the target plate which is mounted on a fixture. The whole setup is attached to a rigid solid base structure [41]. The incident velocity of the impactor can be determined from the equations of motion or by using optical sensors located just above the target. The impactor is instrumented, enabling the measurement of force/time and displacement characteristics to be determined. The energy dissipation during the impact event can be determined from the sensor data. One of the advantages of this test with respect to the Charpy and Izod tests is that it allows a wider range of test geometries

to be tested and it is possible to use different impactor shapes like hemispherical, conical, blunt cylinders or sharp points [17].

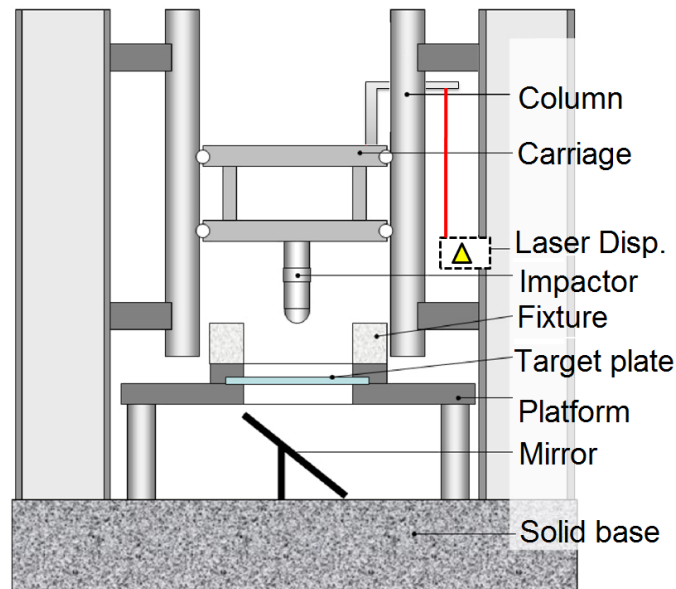


**Figure 2.4.** Schematic diagram of drop tower used for the low velocity impact tests [41]

The damage processes during impact event are associated with the energy absorbing capacity of the structures and can be characterised by the force and energy histories obtained during the impact tests [40]. The deflection and the contact force between the impactor and the target plate are measured during the impact. It is widely accepted that the displacement of impactor is the sum of the indentation of top facesheet and the global bending deflection of the sandwich plate [42]. According to Atas and Sevim [43], the load- deflection curve gives significant information about the damage process. Some typical load deflection responses are shown in Figure 2.5 Typical load deflection curves for low velocity impact: a) rebounding impact, b) penetration and c) complete perforation [43]figure.2.5. There are two basic types; closed curves (a and b), which consists of an ascending loading section and a descending section combining loading and unloading depending on whether the sample has perforation or not and open curves (c), where the contact force does not return to zero because of the friction between the impactor and the penetrated target plate.

Caprino and Teti [44] found that the perforation of the facesheet directly struck by the tup resulted in a sudden, large drop of contact force. Hampson and Moatamedi

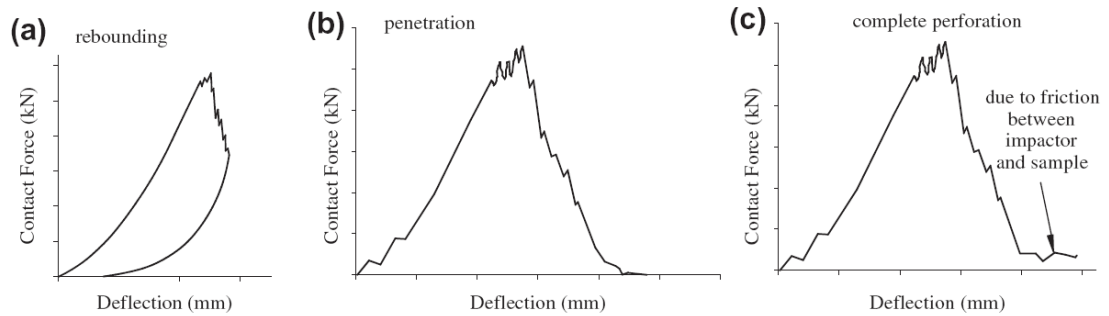


**Figure 2.5.** Typical load deflection curves for low velocity impact: a) rebounding impact, b) penetration and c) complete perforation [43]

[39] observed that as low speed impact usually results in barely visible impact damage visual observation is not sufficient and more accurate assessments using thermography and ultrasonic C-scan methods are necessary to assess the damage. Hosur et al. [45] studied the impact region under an optical microscope to investigate the failure modes of the sample shown in Figure 2.6(a) Impact surface, (b) cross-sectional view and (c) Optical micrograph of sandwich plates [45]figure.2.6 and compared the damage mechanisms in the core, either in terms of width and depth of the region of crushed core or the base width for samples with shear cracking.

Gustin et al. [15] compared the absorbed energy and maximum impact force of sandwich plates with foam-filled and hollow honeycomb cores subjected to low velocity impact. Cantwell et al. [16] compared the impact response of sandwich structures with balsa wood and PVC foam cores for use in marine applications. Bernard and Lagace studied the impact resistance of composite sandwich plates with graphite/epoxy facesheets and three different cores; aluminum honeycomb, Nomex honeycomb and Rohacell foam core using low energy impact tests [8]. Mines et al. studied the perforation due to impact of square sandwich plates with Coremat<sup>®</sup> and aluminium honeycomb cores [37]. The study of the behaviour of sandwich structures to impact loading is usually accomplished by experimental testing [15, 16, 40]. While other forms of impact testing such as charpy tests are available, a drop tower apparatus is the most common method of low velocity impact testing. The macroscopic failure modes, micro failure mechanisms and energy absorbing characteristics of these composite sandwich panels are studied using instrumented impact test and microscopy [11].

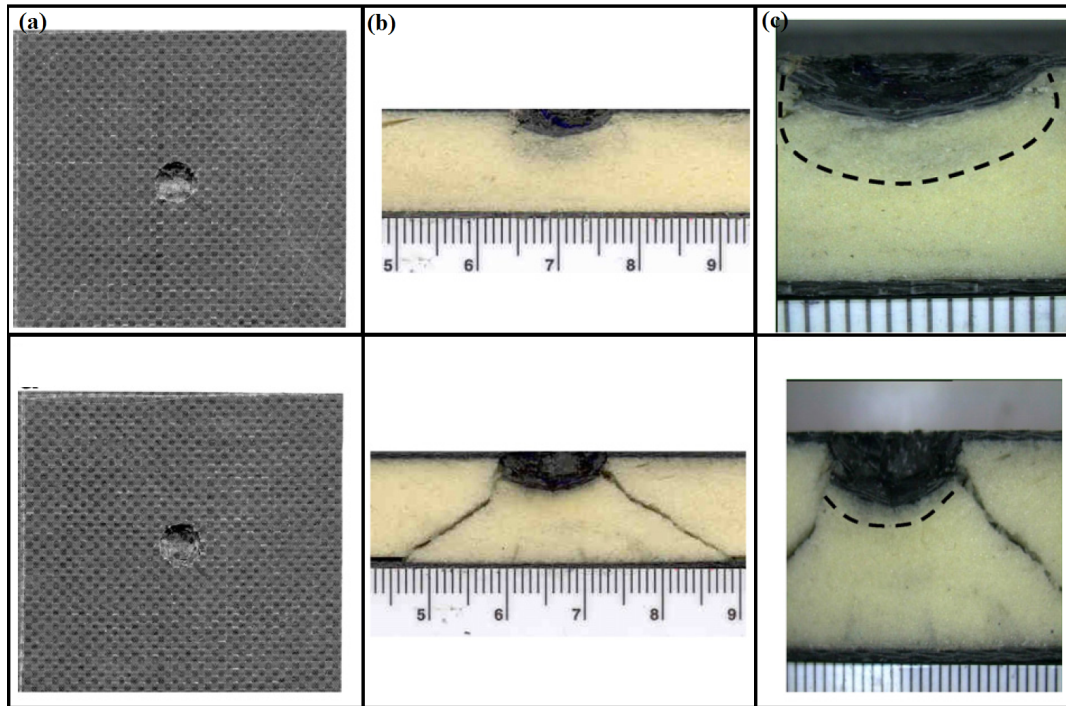


**Figure 2.6.** (a) Impact surface, (b) cross-sectional view and (c) Optical micrograph of sandwich plates [45]

Anderson and Madenci [32] conducted impact tests on a variety of sandwich configurations with graphite/epoxy facesheets and Rohacell foam or honeycomb cores. Contact Force- time history, depth of indentation and cross-sectional views of the impacted sandwich were used to characterise the type and extent of the damage. Dvorak and Suvorov [46] examined the improvement of damage resistance of sandwich plates by inserting a thin, ductile polyurethane interlayer of relatively high stiffness between the exterior facesheet and the foam core and observed that the interlayer protects the foam core from local crushing under the indenter. Bernard and Lagace [8] compared the impact behaviour of sandwich plates with honeycomb cores and Rohacell foam cores and examined the cross-sections of the impact specimens under a microscope to quantify facesheet damage, adhesive layer damage, and core damage through the thickness of the specimen. Damage to the facesheets was primarily delaminations between plies.

Borsellino et al. [47] studied sandwich panels used in windsurf boards construction with a core of expanded polystyrene foam and high density PVC foam, focusing

on the effects induced by different kind of skin arrangements (Kevlar, glass and carbon fibres). Caprino and Teti [44] concluded that the damage development and residual strength after impact were substantially independent of core density and recommended that high strength, compliant core materials offer the best performance under impact conditions.

An impact can produce extensive subsurface delamination and transverse cracking which may not be visible on the laminate surface (i.e., barely visible impact damage (BVID)), and the presence of this damage is known to cause substantial loss in the mechanical properties [48]. Park et al. [40] employed some damage parameters to evaluate the impact response and to observe the contribution of facesheet material and core thickness on the impact response; namely, (1) load at incipient damage  $P_{inc}$ , (2) energy absorbed at incipient damage  $E_{inc}$ , (3) maximum load  $P_{max}$ , (4) total energy absorbed during impact  $E_{ab}$ , (5) plastic energy absorbed by damage  $E_{pl}$  and (6) impact damage area. The load bearing capacity of the target is reduced in the presence of some damage which result in a drop in the force. Thus  $P_{inc}$  and  $P_{max}$  are related to the impact resistance of structures. The energy absorbed ( $E_{ab}$ ) calculated through the impact force history is a measure of the energy dissipated by damage mechanisms through the structure, but it must be noted that this energy consists of elastic and plastic absorbing energy.

A list of some of the papers on the indentation and low velocity impact experiments of sandwich composites with various cores and facesheets is given in Table 2.3. List of papers on indentation and low velocity impact of sandwich composites table.2.3. While this is not a complete list of all the published literature on this topic, they represent a good cross section of studies carried out with different materials. There are more references suggested in review papers written by Hampson et al. [39] and Cantwell and Morton [17].

### 2.3.2 Failure mechanisms in sandwich structures

The different ways by which sandwich structures can fail was shown by Triantafillou and Gibson [49]; (i) the faces and core can yield plastically or fracture, (ii) the compressive face can buckle locally or “wrinkle”, and the bond between the facesheet and core can fracture, causing delamination and (iii) the core may yield in shear, tension or compression or be subject to indentation at the loading points. Richardson et al. [9] noted that due to the heterogeneous and anisotropic nature of fibre

**Table 2.3.** List of papers on indentation and low velocity impact of sandwich composites

<b>Author</b>	<b>Fibre</b>	<b>Core</b>	<b>Test</b>	<b>Ref</b>
Avila et al.	Glass epoxy	Polystyrene foam	Indentation and low velocity impact	[2]
Bhuiyan et al.	Carbon fibre epoxy	Polyurethane foam	Drop tower impact	[7]
Bernard and Lagace	Graphite epoxy	Aluminium and Nomex honeycomb, Rohacell	Gas gun	[8]
Shih and Jang	Graphite, Aramid, PE and Polyester fibres	PVC foam	Drop tower impact	[11]
Xia and Wu	Glass, Carbon and Kevlar fibre	RPU foam	Drop tower impact	[14]
Gustin et al.	Carbon fibre epoxy	Foam filled and hollow honeycombs	Drop tower impact	[15]
Cantwell et al.	Glass epoxy	PVC foam and Balsa	Flexure, buckling and indentation	[16]
Gustin et al.	Kevlar and carbon fibre hybrid	PUR foam filled honeycomb	Drop tower impact	[21]
Hazizan et al.	Glass fibre phenolic resin	PVC/PUR foam	Drop tower impact	[27]
Mahfuz et al.	S2 glass fibre vinylester	PVC foams	Quasi-static and high strain rate	[30]
Rizov et al.	Glass fibre vinylester	Rohacell foam	Indentation	[31]
Anderson and Madenci	Graphite epoxy	Rohacell and Honeycomb	Drop tower impact	[32]
Flores and Li	Carbon fibre epoxy	Rohacell foam	Quasi-static indentation	[33]
Mines et al.	Glass fibre vinylester	Coremat and honeycomb	Indentation and low velocity impact	[37]
Roach et al.	E-glass polyester	PVC foam	Gas gun	[38]
Park et al.	Carbon epoxy and Glass epoxy	Nomex honeycomb	Drop tower impact	[40]
Atas and Sevim	E-glass epoxy	PVC foam and Balsa	Drop tower impact	[43]
Zhu and Chai	Carbon fibre epoxy	Nomex honeycomb	Quasi-static and drop tower	[42]
Caprino and Teti	Glass epoxy	PVC foam	Drop tower impact	[44]
Dvorak & Suvorov	Graphite epoxy	PVC foam and PUR interlayer	Indentation	[46]
Borsellino et al.	Glass, Carbon and Kevlar fibre	Polystyrene and PVC foams	Flatwise and edge-wise compression	[47]

reinforced plastic (FRP) laminates, four major modes of failure can be observed in the composites:

1. matrix mode,
2. Fibre mode,
3. delamination mode, and
4. Penetration.

Mines et al. [6] identified the different modes of failure in sandwich beams under static and dynamic bending. Figure 2.7 Different failure modes in sandwich beams subjected to flexure [6]figure.2.7 shows the various modes of failure in sandwich beams subjected to bending loads. In the figure, the different modes represented are: I - upper skin compression failure;  $I_a$  - stable core crushing then lower skin tensile failure;  $I_b$  - core shear failure; II - upper skin crushing failure; III - core shear failure; IV - lower skin tensile failure. The critical failure mode, which occurs at the lowest load, depends in part on the properties of the facesheet and core materials and, in part, on the design of the sandwich. The beam shear failure is attributed to an initial shear failure at the interface between the upper skin and the core as the shear stresses are greatest in the core and core-skin bondline. Subsequently the core fails in shear and the lower skin debonds [6].

The failure process during perforation for a sandwich plate with Aerolam core is shown in Figure 2.8 Progression of failure in sandwich plates with honeycomb core [37]figure.2.8. Initially, the core crushes and a diamond deformation area is formed and sub-critical cracks emanate from the apex of the diamond. After upper skin failure, the load is transferred to the lower skin and the lower skin/core bonding occurs. The lower skin then tears in mutually perpendicular directions along the fibre 0/90 directions, and full perforation occurs. The elastic bending energy in the panel is converted to damage energy [37].

Triantafyllou and Gibson developed equations describing the failure load for different modes of failure and produced a failure mode map which showed which failure mode is dominant for a particular design and loading condition [49]. Bhuiyan et al. [7] noted that the damage initiation thresholds and damage size depend on the properties of impactor including end-shape, size, mass and the elastic properties of the projectile, property of the target sandwich specimen including elastic properties of core materials, facesheets, their interface, relative thicknesses, as well as size and shape of the structure and the boundary conditions used for the test. Mines

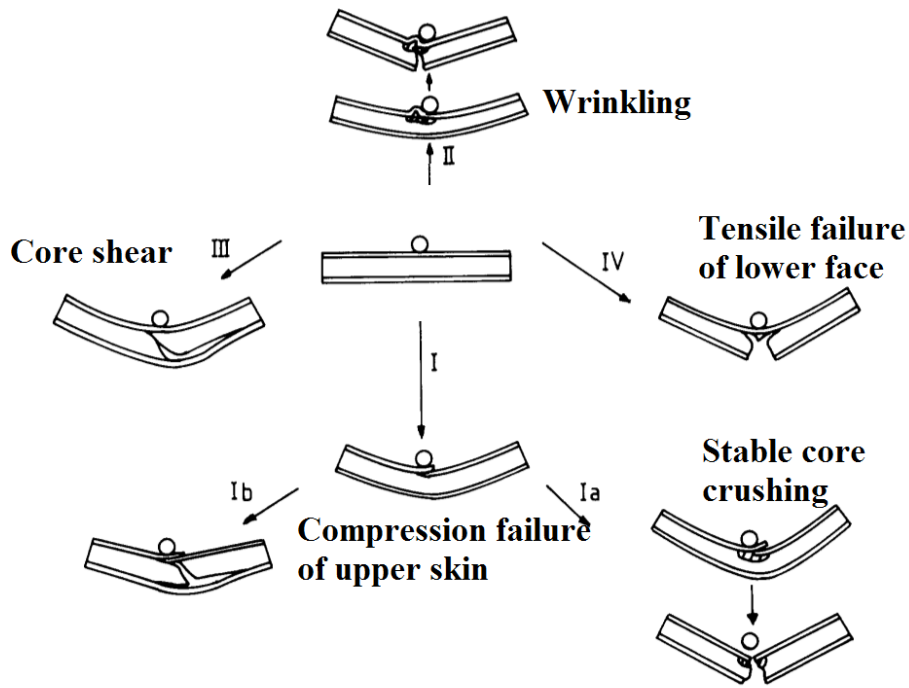


Figure 2.7. Different failure modes in sandwich beams subjected to flexure [6]

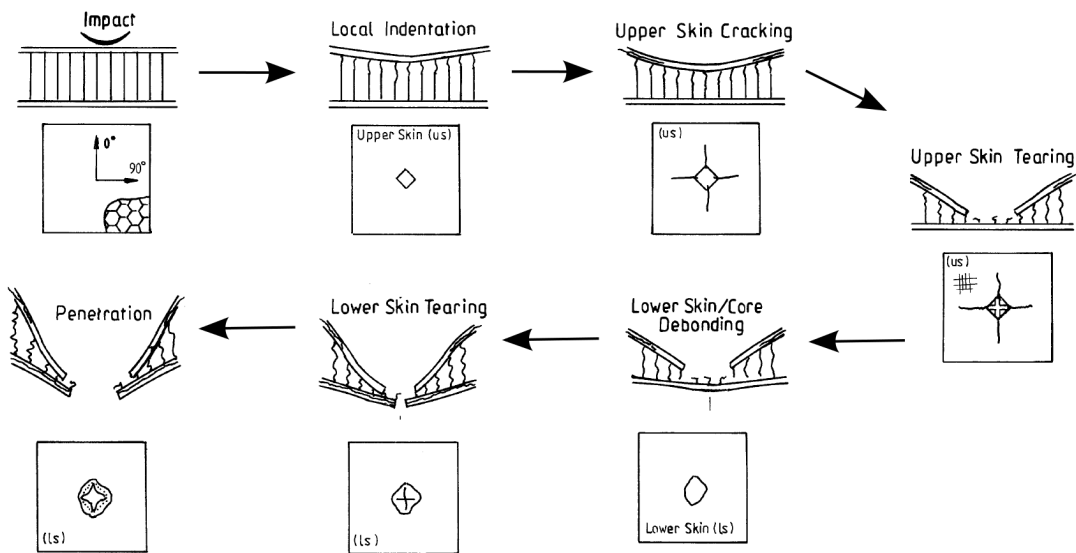
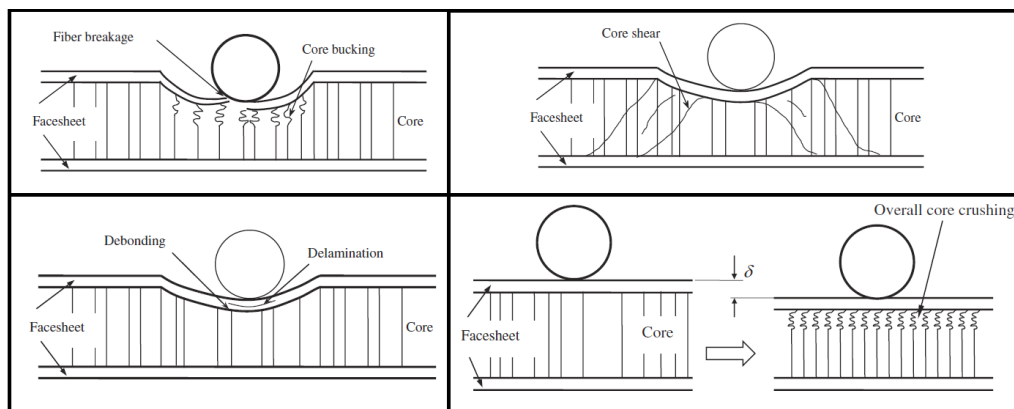


Figure 2.8. Progression of failure in sandwich plates with honeycomb core [37]

et al. [37] showed that much of the incident energy of the projectile is absorbed in crushing the core material within a localised region immediate to the point of

impact. Bernard and Lagace showed that different cores displayed different damage modes; cell wall buckling in the honeycomb structures while in the Rohacell cores, cracks were formed in the foam parallel to the facesheets [8]. Park et al. [40] observed that the damage processes during impact event can be characterised by the force and energy histories obtained during the impact tests. Several damage parameters like load and energy absorbed at incipient damage, maximum load, total energy absorbed during impact and impact damage area have been adopted to evaluate the role of facesheet material and core thickness on impact response [40].

Hazizan et al. [27] observed that the prominent mode of failure in a sandwich panel depends on the core properties and listed three modes of failure; shear cracking in the brittle foam core for low density foams, fibre buckling close to the point of impact for samples with intermediate modulus foams and delaminations in the top facesheet for samples with high stiffness cores. The damage and failure modes of composite sandwich panels, shown in Figure 2.9 Failure modes in Sandwich plates with low velocity impact [42]figure.2.9, were analysed by Zhu and Chai [42]. The figure shows fibre breakage and core buckling, core shear, overall core crushing and delamination in the facesheet and debonding between the facesheet and core. For sandwich panels consisting of very stiff facesheets combined with a very soft core, the impactor and the top skin may move down rigidly while the core crushes uniformly. This is referred as overall core crushing but this phenomenon is not common [42]. Core buckling is widely reported as the first damage mode that occurs in experiments involving low impact energy levels [42] while failure mode of core shear is prominent for sandwich panel with thick skin and weak cores.



**Figure 2.9.** Failure modes in Sandwich plates with low velocity impact [42]

The modes of impact damage on the composite facesheet range from matrix cracking and delamination through to fibre failure and penetration. Matrix cracking occurs parallel to the fibres due to tension, compression or shear and occur due to property mismatch between the fibre and matrix [9]. Matrix damage may decrease the localised stiffness of the panels but is usually not catastrophic until the matrix of the facesheet cracks and finally the fibres in the facesheet breaks [42]. The type of matrix cracking which occurs is dependent on the global structure of the impacted specimens. The shear cracks shown in Figure 2.10(a) Typical matrix crack and delamination for 0/90/0 composite and (b) Stress component contributing to matrix crack [9]figure.2.10 are formed by the very high transverse shear stress through the material, and are inclined at approximately 45°. The bending crack in the 90° layer is caused by a combination of  $\sigma_{11}$  and  $\sigma_{13}$  with a weak contribution of  $\sigma_{33}$  [9]. The inclined shear matrix crack in the upper layer is halted by the change in orientation of the fibres when it reaches the interface and so propagates between the layers as a delamination. Cantwell and Morton [17] emphasised that excessive transverse deflection in long thin specimens cause bending cracks in the lower layers whereas short thick specimens are stiffer and so higher peak contact forces induce transverse shear cracks under the impactor in the upper plies.

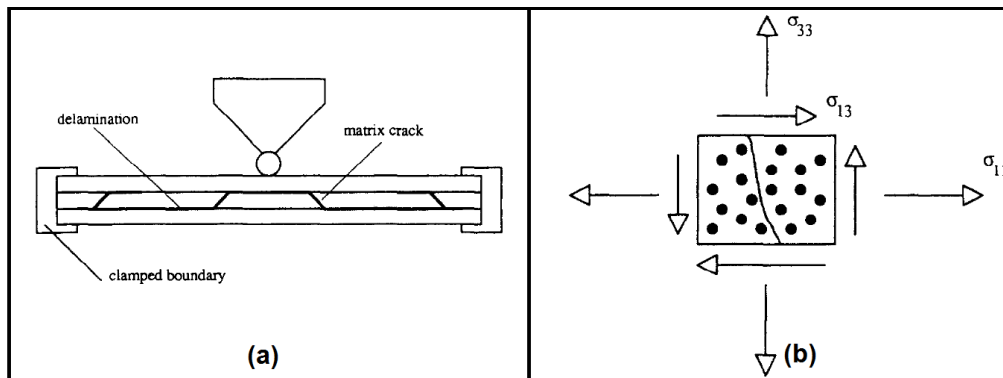


**Figure 2.10.** (a) Typical matrix crack and delamination for 0/90/0 composite and (b) Stress component contributing to matrix crack [9]

A delamination is a crack which runs in the resin-rich area between plies of different fibre orientation as a result of the bending stiffness mismatch between adjacent layers [9]. Delamination is one of the most common damage initiation modes in laminated composites and in sandwich structures. Bernard and Lagace [8] found that the damage in the impacted facesheets was primarily delaminations with the largest

delamination occurring between the bottom two plies in the top facesheet (plies closest to the facesheet-core interface). No damage was observed in the back facesheets for these tests conducted up to 10 J of projectile kinetic energy. The delamination in the facesheets were observed to be peanut-shaped with major axis along weaker fibre orientation [40]. Delamination between plies in laminates and debonding between facesheets and core will occur when the inter-laminar shear strength or bond strength is exceeded. Although not a catastrophic failure mode, debonding is also found to decrease the stiffness and strength significantly [42]. It is also widely agreed that debonding of sandwich panels is not only dependent on geometry but also highly dependent on the Mode II inter-laminar fracture energy,  $G_{IIc}$ . The case of debonding in sandwich panels may be more complicated than delamination in composite laminates since the core is much softer than the facesheet. Cantwell et al. [17] suggested that to suppress impact induced delamination, laminates with sudden large changes in fibre direction should be avoided and also proposed the use of woven fabrics instead of unidirectional plies. Another technique used to reduce delamination was suggested by Gustin et al. [21] by the use of hybridization; by incorporating plies of lower modulus Kevlar fibres to carbon fibre composites.

Richardson et al. [9] observed that the interphase region can affect the failure mode which occurs at a given load; i.e., poor adhesion results in failure at low transverse stress, leaving clean fibres. The bond strength can be manipulated to improve the toughness by absorbing energy in fibre-matrix debond; however, this reduces the mechanical properties. Cantwell et al. [17] also studied the fibre/matrix interphase region and found that if the residual properties of the composite are not important, then a weak interphase encourages failure through gross splitting and delamination but for applications that require damage containment, some level of fibre surface treatment is necessary to strengthen the interphase.

Fibre breakage in the facesheet or facesheet cracking is another common failure mode for sandwich panels subjected to low velocity large mass impact test. The effect of facesheet thickness was found to be vital contribution to the failure mode and its corresponding ultimate load while core density affected the failure mode but not its corresponding ultimate load. For sandwich plates with thin facesheets and stiff cores, tensile cracking is caused by the high in-plane tensile forces due to the large global deflection of the sandwich. Damage initiation was found to occur as a direct result of localised deformation and was independent of the boundary

condition and stacking sequence of the laminated facesheets [42]. Penetration is a macroscopic mode of failure and occurs when the fibre failure reaches a critical extent, enabling the impactor to completely penetrate the material [9]. Wrinkling involves local buckling of the face into the core, causing compression of the core [49] but this mode was not common in low velocity impact tests.

The debonding along the facesheets and the core interface of sandwich panels is found to be predominated by a sliding mode. The effect of elastic modulus of the core on debonding has been found to be significant, and low relative density of the core will result in more critical debonding [50]. Cantwell et al. [16] used a modified peel test to study the skin - core adhesion for glass fibre sandwich with Balsa wood core and PVC foam cores and found that the interface failure in foam based sandwich left a residual foam layer on the composite while there was no evidence of similar behaviour in Balsa sandwich. Bernard and Lagace [8] found that for specimens with lightweight cores such as Rohacell foam, the debonding between the facesheet and the core was not so significant and remarked that debonding appears to increase with increasing core stiffness. The debonding shown in Figure 2.11 Failure by skin core debonding (a) Good adhesion and (b) Poor adhesion [33] figure.2.11 shows the difference between good adhesion between facesheet and core for 51WF Rohacell foam core (a) and skin core debonding for a different type of Rohacell foam with poor resin absorption (b) [33]. It can be seen that the skin/core debonding in the sample with good adhesive interface also causes core failure while the core has very little damage in the case with poor adhesion.

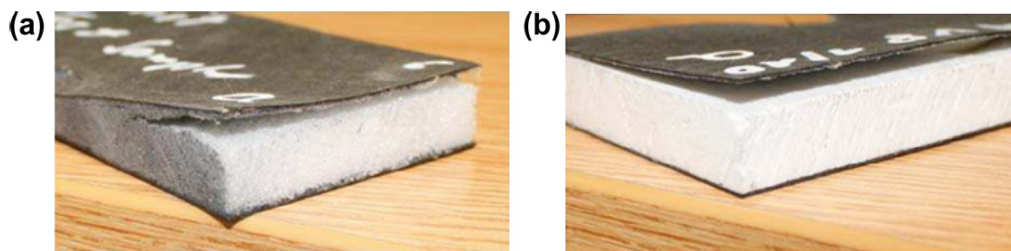


**Figure 2.11.** Failure by skin core debonding (a) Good adhesion and (b) Poor adhesion [33]

Damage in the honeycomb cores was characterised by a buckling of the honeycomb cell walls and the damage was measured by counting the number of the buckled cell walls (BCW) along the +45 cross-section [8]. Bernard and Lagace [8] studied the cross-section photograph of a Rohacell sandwich specimen and found that the

Rohacell core damage was characterised by core crushing, which left an easily detectable depression near the top facesheet in the region directly under the impact. At lower energy levels, they observed a crack running parallel to the facesheets, the length of which was measured by slightly flexing the sandwich cross-section.

Figure 2.12 Core crushing in sandwich with different Polyurethane foam cores [51] figure.2.12 shows the cross section of the damaged sandwich panels with different polyurethane foam cores. Residual indentation and damaged facesheet can be seen for the first case, with the crushed foam creating a cavity between the facesheets and the core in the second case and core crushing extending to a larger depth in the final image [51].

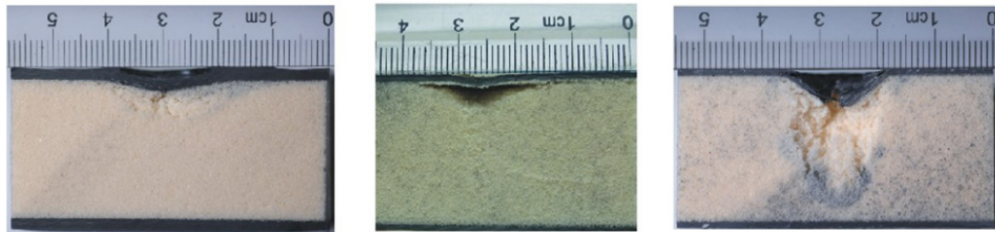


**Figure 2.12.** Core crushing in sandwich with different Polyurethane foam cores [51]

## 2.4 Improving impact resistance of sandwich composites

Several approaches have been employed to improve the impact damage resistance of sandwich composites including matrix modifications, selection of laminate stacking sequence, introduction of through-thickness reinforcements, insertion of interlaminar layers, fibre hybridisation and utilisation of high-strain fibres [52]. Dransfield et al. [53] noted that the limitation of resin-based advanced fibre composites is not strength but sensitivity to mechanical damage from localised impact loads of relatively low velocity. Delamination was identified as a substantial cause of the problem because the composite facesheets possess strength in the fibre direction but lack strength in the through-thickness direction. This essentially limits the strength of a traditional 2D composite to the properties of the brittle matrix alone. The reinforcing techniques to combat the problem of delamination and improve impact resistance can be classified either as modification of the sandwich architecture or improvement of the materials.

### 2.4.1 Modification of sandwich architecture

There are two basic categories of architecture for through-thickness reinforcing: fully integrated (3D) systems, such as weaves or braids produced by textile processing and systems manufactured from planar (2D) lamina with selective through-thickness reinforcing using stitching or interleaving. Through-thickness reinforcing can provide improved interlaminar strength and delamination resistance while producing a more integrated composite structure. Zhong and Jang [52] presented a review of the effect of three-dimensional weave geometries achieved through the interlocking of fabrics with z-direction yarns and showed that the damage zone of the 3-D composites and stitched composites was smaller compared to conventional composites. However, the complexity, limited shapeability and processability minimises the use of 3-D composites to special applications, where highly triaxial stress states are predominant [53].

Dvorak and Suvorov [46] examined the improvement of damage resistance of sandwich plates by inserting a thin, ductile interlayer between the facesheet and the foam core. According to the authors, impact-induced cracks propagate through the interface between the facesheet and the core and polyurethane interlayers of relatively high stiffness and ductility are expected to offer additional support to the facesheet, easily adjust to its deformation, and rebound upon unloading. The global deflection is also reduced by the increase in bending stiffness of the plate. An additional advantage of the interlayer is its ability to hinder moisture penetration into the interior of the sandwich plate in the presence of matrix cracking in the facesheet. Cartié and Fleck [54] explored the strategy of maximising the through-thickness stiffness and strength of the core by adding reinforcement pins to Rohacell foam core, with the ends of the pins embedded in woven carbon fibre facesheets. The pin-reinforced foam cores known by the commercial name of X-Cor have successfully improved the stiffness, strength and energy absorption in a synergistic manner. Nanayakkara et al. [55] investigated the stiffening and strengthening of the core material with through-thickness z-pins made of pultruded rods of T300 carbon/bismaleimide. The through-thickness reinforcement was inserted into the core material at an orthogonal or inclined angle to increase the in-plane and through-thickness properties of the sandwich material and it was reported that the size of damage sustained by the sandwich material was reduced by z-pinning. Mostafa et al. [56] investigated the effect of inserting semi-circular shear keys at the skin-core

interface on the shear performance of the sandwich panel. It was found that by enhancing the skin-core interaction and allowing the skin to share a part of the applied shear load, the shear keys were effective in improving the shear performance of the sandwich panel. However, the method is complex and involves modifying the core and altering the traditional manufacturing process for a small improvement in resistance of sandwich panels.

#### 2.4.2 Improvement of constituent materials

The impact performance of sandwich composites can be improved by choosing appropriate materials for the core and the fibre and matrix of the facesheet. Hosur et al. [45] remarked that there is a growing emphasis on improving the properties of polymers and foam materials through the inclusion of small amounts of nanoparticles like carbon nanotubes and nanofibres,  $TiO_2$ , nanoclay, etc., to improve the materials properties. Sandwich panels with nanoclay reinforced polyurethane foam were studied and it was observed from damage analyses after impact that nanoclay infused foams had smaller damage area than their neat counterparts. Njuguna et al. [57] studied the low velocity impact resistance of nanophased sandwich structures based on polyurethane foam and montmorillonite nanoclay and reported that the nanophased sandwich panels were capable of taking higher peak loads when subjected to low velocity impact than those made of neat PU cores.

Richardson and Wisheart [9] remarked that since the ability to store energy elastically in the fibres is one of the fundamental parameters in determining the impact resistance of the composite laminate, both the fibre modulus and the failure strain are important. Glass fibres despite their lower strength and stiffness can absorb approximately three times the elastic energy of carbon because of their high strain to failure. Composite laminates containing fibres like PolyEthylene (PE) fibres exhibit both high strength and high ductility and therefore have superior impact resistance compared to other laminates. Composites with strong fibres such as graphite have the limitation that they are brittle and ductile fibres like nylon do not have high value of strength [52]. Cantwell and Morton [17] showed that high performance fibres improve both the short- and long-term mechanical properties of composites by increasing the strain to failure of the reinforcing fibres. Hybrid composites are formed by adding glass or Kevlar to carbon composites to improve impact resistance. Gustin et al. [21] improved the impact properties of Carbon fibre sandwich composites by using hybrid facesheets with combination of Kevlar

and Carbon fibres. However, the mismatch in moduli between the different fibres increases the complexity of the design of hybrids [9].

Zhong and Jang [52] remarked that the ability of the resin to undergo plastic deformation during an impact event is essential to improving the damage resistance of sandwich composites. It was shown that better resistance to delamination and matrix cracking achieved with tougher resins led to improved impact resistance. Cantwell and Morton [17] reported that since the first generation of matrix systems for advanced composites lacked toughness, a number of techniques have been developed to improve the toughness including the use of thermoplastic matrices like PEEK and the inclusion of thin, tough layers at ply interfaces. However, it has been reported that the high velocity impact response of carbon fibre/PEEK is relatively poor and that the advantage of using thermoplastic matrices have a velocity threshold. Another method of improving the matrix is by the reduction in the cross-linking density of thermosets such as epoxy resins [52]. The cross-linking density is reduced by incorporating predominantly di-functional constituents. This however affects the glass transition temperature  $T_g$ , which can be mitigated by the addition of stiffened polymer backbone components. Other methods used for toughening of the matrix are the use of plasticizing modifiers, the addition of rubber particles such as carboxylterminated butadiene-acrylonitrile (CTBN) and the addition of thermoplastic particles such as polyethersulphone (PES) and polyetherimide [17].

## 2.5 Toughening of Epoxy

Epoxy resins are used in a variety of applications including as the matrix material for glass-, carbon- and other fibre reinforced composites because of their properties, such as a high modulus and failure strength, low creep, good performance at elevated temperatures, and low density. The cured epoxies are amorphous and highly-crosslinked (i.e., thermosetting) polymers. This microstructure results in many useful properties for structural engineering applications including in the aviation and marine industries as adhesives and matrix materials for many different types of composites [58]. In addition to transferring the load to the fibres, the polymeric matrix in an FRP provides several key functions: it protects the fibres from damaging themselves and aligns and stabilises the fibres. One of the main drawbacks of epoxy resin that makes it unsuitable for wider applications is its brittle nature and subsequent poor resistance to crack initiation and crack growth. Soutis [10]

noted that the first generation of composites used in aircraft construction employed brittle epoxy resin systems leading to laminated structures with a poor tolerance to low-energy impact caused by runway debris thrown up by aircraft wheels or the impacts occurring during manufacture and subsequent servicing operation. Fracture toughness of the matrix can be defined as the resistance to brittle fracture in the presence of a crack. Once a crack is initiated, it will grow until all the stored energy is dissipated and ductility provides the ability to yield and undergo plastic deformation to dissipate energy without crack growth. Garg and Mai [59] noted that of the three most important damage initiation modes in a laminated composite, namely, matrix cracking, delamination and fibre fracture, the first two modes depend to a large extent on the properties of the matrix. The ductility or fracture toughness of the matrix is one of the dominant material parameters affecting the interlaminar fracture toughness of FRP composites even though other factors such as fibre-matrix interfacial adhesion, laminate configuration, presence of pores and residual stress state also play a significant role [60].

### 2.5.1 Microparticle reinforcement of epoxy

The toughening of epoxy by the addition of a rigid or soft second phase of either rubber or inorganic fillers such as alumina and silica particles was identified as a promising solution [59]. In this process, a small proportion, typically between 5 and 20% of rubber or inorganic filler is incorporated as a dispersed phase in a rigid epoxy matrix. When inorganic second phase particles are employed, the modified epoxy polymer is named particulate-filled epoxy while the rubber-modified resin is called “rubber toughened epoxy” [58]. A majority of the studies [12, 58, 59, 61–63] have involved the chemical modification of epoxy with a wide variety of materials, with the most common system being the carboxyl terminated acrylonitrile butadiene (CTBN) elastomer. He et al. [62] studied the dispersion of preformed rubber (acrylic) particles in liquid epoxy monomer in order to vary the concentration without altering other morphological features. Imielinska and Wojtyra [64] studied the effect of toughening epoxy matrix with phenolic microspheres and showed that it improved low velocity impact behaviour because the microspheres absorbed significant amount of energy during fracture through crack front bowing and crack splitting mechanisms. The rubber or thermoplastic particles are typically about 1 - 5  $\mu\text{m}$  in diameter with a volume fraction of about 5 - 20% [65].

Bagheri et al. [58] has given an exhaustive review of the many researchers who investigated various methods to toughen the matrix with additives. One of the extensively used methods to toughen epoxy is by the addition of a suitable rubber to uncured resin and then controlling the polymerization reactions to induce phase separation [12]. Zeng et al. [63] reported that during the polymerization, the rubber phase-separates because it becomes less miscible with the matrix, forming tiny particles of rubber that are dispersed in the epoxy matrix. The second phase of the rubber particles enables ductile deformation to occur via deformation and cavitation in an otherwise linear elastic, brittle polymer [59]. He et al. [62] found that increasing concentration of elastomeric particles up to a certain value, raises the fracture energy as much as 15 to 20 times that of the unmodified epoxy but further additions resulted in significant reductions in fracture energy and other mechanical and thermal properties. Bascom et al. [61] also noted that for CTBN concentrations of more than 15% an elastomer-epoxy blend was formed, instead of a particulate phase as shown in Figure 2.13. Effect of CTBN particles in DGEBA epoxy on (a) Fracture energy and (b) Tensile modulus [61] figure.2.13. This observation suggests an optimum concentration of toughening.

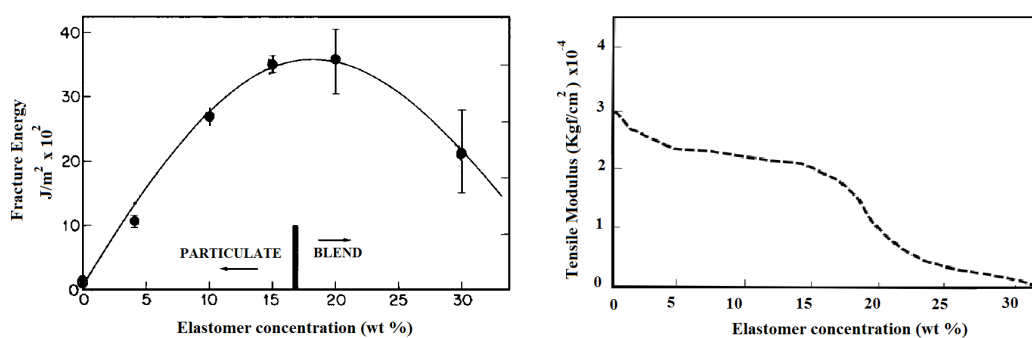


**Figure 2.13.** Effect of CTBN particles in DGEBA epoxy on (a) Fracture energy and (b) Tensile modulus [61]

Garg and Mai [59] provided an overview of the research on failure mechanisms in epoxy resins toughened by various materials. Bascom et al. [61] showed that the principal effect of the elastomer particles was the increase of the plastic zone due to the flexibilised boundary between the matrix and the particles. Kinloch et al. [12] conducted fracture studies of rubber modified epoxies and proposed that the greater crack resistance in the rubber-modified epoxy arises from a greater extent of energy-dissipating deformations occurring in the material in the vicinity of the crack tip.

The deformation processes are (i) localised cavitation in the rubber, or at the particle/matrix interface, and (ii) plastic shear yielding in the epoxy matrix. According to the authors, the main source of energy dissipation and increased toughness is shear yielding. They identified interactions between the stress field ahead of the crack and the rubbery particles as the main reason that shear yielding occurred to a far greater degree in the matrix of the rubber-modified epoxy, compared to the unmodified epoxy [12]. Kim et al. [48] studied the residual mechanical properties and damage tolerance of carbon fibre-reinforced composites containing unmodified and rubber-modified epoxy resins subjected to drop-weight impact. It was shown that while the residual flexural strength and modulus were slightly higher for the unmodified matrix system, the residual Mode I interlaminar fracture toughness was significantly higher when the epoxy matrix was modified with CTBN particles. Imielinska and Wojtyra [64] found that FRP with modified epoxy resin absorbed higher impact energy and identified the ductility of the matrix as one of the parameters controlling impact energy absorption.

Rubber toughening has proved to be effective and is widely used. However, the drawback of this approach is that it sacrifices the stiffness of epoxy significantly and decreases the glass transition temperature. It can be observed in Figure 2.13 Effect of CTBN particles in DGEBA epoxy on (a) Fracture energy and (b) Tensile modulus [61] figure.2.13 that with the increasing concentration of elastomers, the tensile modulus of the epoxy was significantly reduced [61]. Johnsen et al. [65] noted that the rubbery phase typically increases the viscosity of the epoxy monomer mixture and reduces the modulus of the cured epoxy polymer. Soutis [10] noted that the toughened epoxy systems provided some improvement in damage tolerance but were still not as effective as some thermoplastic materials.

### 2.5.2 Nanoparticle reinforcement of epoxy

The addition of rubber particles in the epoxy caused a decrease in the modulus and the thermal properties, and therefore a new approach of forming a nanophase structure in the polymer matrix was proposed for improving the toughness of thermoplastic and thermoset systems. The nanophase has at least one dimension in the nanometer length scale and consists small, rigid particles, whiskers, or tubes (e.g., layered silicates, silica particles or carbon nanotubes). According to Njuguna et al. [66] nano-particles as filler materials in epoxy resins present a high-potential for the improvement of mechanical and physical polymer properties. It was postulated

that due to the molecular size of their reinforcement, polymer nanocomposites offer the possibility to develop new materials with unusual properties.

Carbon nanotubes (CNT), carbon nanofibres and nanoclays were identified as potential nano-scale materials for the reinforcement of epoxy [66]. Gojny et al. [67] identified that the combination of conventional fibres like glass and additional nanophase reinforcement of the matrix such as carbon nanotubes presented a high potential for structural applications. They investigated nanoparticle-reinforced FRPs containing low contents of carbon black (CB) and carbon nanotubes (CNTs) in the epoxy resin and reported significant improvement in interlaminar shear strength, without any adverse effect in tensile properties. Karapappas et al. [68] investigated the fracture energy of unidirectional carbon fibre reinforced polymers modified by the addition of multi-walled carbon nanotubes (MWCNT) into the matrix material. A significant increase in the fracture energy of the laminates was reported for even low contents of 1% wt. of MWCNTs. According to Liu and Wagner [13], the ability to homogeneously disperse nanotubes throughout a matrix and the formation of strong interfacial bonding represent the two key aspects to be dealt with if carbon nanotubes are to be considered as effective reinforcement in future composites.

Iqbal et al. [69] investigated the influence of nanoclay on the impact damage resistance of carbon fibre epoxy composites and observed a transition of failure mechanisms from the brittle buckling mode to more ductile, multi-layer delamination mode due to the presence of nanoclay particles. Siddiqui et al. [60] studied organoclay modified epoxy nanocomposites, as well as the CFRP composites with nanoclay in the matrix and reported significant improvements in both crack growth resistance and fracture toughness of mode I interlaminar fracture of CFRP composites with increasing clay content. Aymerich et al. [70] studied the low velocity impact response of nano-modified Glass/epoxy laminates where the nano-modification of the matrix was achieved by a commercial montmorillonite nanoclay called the Cloisite30B and observed a greater damage extension and noted that the presence of clays seems to promote high energy dissipative mechanisms.

Johnsen et al. [65] and Zeng et al. [63] studied the toughening mechanisms of silica nanoparticle-modified epoxy polymers, where the mean particle size of the nano-silica particles were 20 nm. Manjunatha et al. [71] also studied glass fibre reinforced plastic (GFRP) composite laminates fabricated with silica nanoparticle-modified epoxy resins. They observed suppressed matrix cracking and reduced crack

propagation rate in the nanoparticle-modified matrix and noted that it enhanced the fatigue life of GFRP laminates by about three to four times. Sun et al. [3] compared the different energy absorption mechanisms of nanocomposites and conventional composites and identified some key parameters such as shape and size of nano-fillers, mechanical properties of nano-fillers and matrix materials, interfacial adhesion, interphase characteristics, as well as the volume fraction and dispersion of fillers in the matrix. Kinloch et al. [12] studied fracture and impact of glass-fibre reinforced composites where the epoxy matrix was modified with carboxyl terminated butadiene acrylonitrile (CTBN) rubber particles and nanosilica and observed a synergistic effect between the nanosilica and rubber, resulting in 50% increase in fracture energy when compared to the rubber modified epoxy. However, in a similar study on glass-fibre-reinforced composites with nanoparticle modified epoxy matrix, Wichmann et al. [72] noted that there was no significant effect on interlaminar toughness values ( $G_{IC}$  and  $G_{IIC}$ ) despite a pronounced increase in matrix toughness. The authors speculated that this was due to the poor interface between matrix and fibre. Richardson et al. [9] noted that increased interlaminar fracture toughness invariably reduces mechanical properties and improvements made to the pure matrix are never transferred fully to the composite due to the presence of the brittle fibres, which prevent growth of plastic zones in the matrix.

The energy absorption capability of fully exfoliated nanoparticles will increase with increasing volume fraction of nanoparticles due to the increasing number of initial cracks and increased contact area between nano-particles and matrix which influence the debonding energy between particles and matrix. However, Sun et al. [3] noted that in practice the increasing filler volume fraction led to agglomeration, which brings about local stress concentration. Agglomerates act as defects and initiate catastrophic failure [63]. Iqbal et al. [69] noted that laminates with 5% wt. nanoclay absorbed less energy than the laminates with 3% nanoclay and attributed this phenomenon to nanoclay agglomeration.

## 2.6 Block copolymer nano-reinforcements

While most of the research has been focussed on Carbon Nanotubes (CNT) or nanoclay and silicate nanocomposites, block copolymers have attracted attention as modifiers for toughening of epoxy resins [73]. There is considerable interest on the ability of block copolymers used as thermoplastic nano-elastomers to improve

the mechanical properties of epoxy resin [4, 73–75]. A new method to synthesise block copolymers which self-assemble in the nanoscale by controlled radical polymerization and anionic polymerization was developed by Barsotti under the trade name of Nanostrength<sup>®</sup> [4]. This would appreciably reduce the problems associated with dispersion of the nanoparticles. Kishi et al. [73] reported that the block copolymers themselves have nano-phase structures and when the self-assembly ability of the block copolymers is activated in the epoxy blends, the phase separation of the polymer alloys is controlled in the order of nanometers. Figure 2.14 shows the chemical structure of the triblock copolymer and a schematic illustration of the nano-phase structures in the epoxy resin. Nanostructuring is induced by the strong repulsions between the side and middle block. According to Barsotti [4], the thermodynamic miscibility of the block copolymer leads to a homogenous and reproducible dispersion on a nanometer scale. A TEM image showing 10% triblock copolymers in DGEBA resin is also shown in the Figure 2.14 and it can be seen that there are no signs of agglomeration.

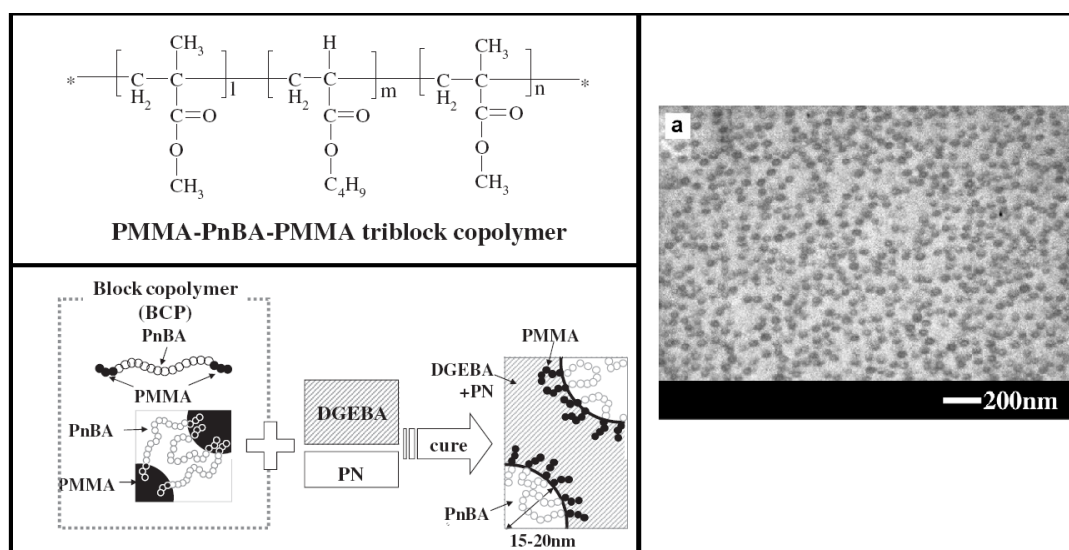


**Figure 2.14.** Chemical structure of Triblock copolymer, schematic illustration of the nano-phase structures and TEM image showing 10% triblock copolymers in DGEBA resin [73]

Barsotti [4] claimed that using block copolymer- modified epoxies enhanced the fracture toughness and impact performance with minimal sacrifice of thermal properties. The block copolymers that were developed were triblock polymers consisting of polymethylmethacrylate- b- polybutylacrylate- b- polymethylmethacrylate (MAM) and styrene- b- butadiene- b- polymethylmethacrylate (SBM) families. The non-reactive backbone of the block copolymers increases the toughness of the resin without sacrificing  $T_g$  or modulus. Thus block copolymers have the potential to provide superior toughening when compared to reactive rubber flexibilisers or core shell toughening agents [4].

A systematic study on the effect of these nano reinforcements on the mechanical performance of FRPs made with these nano-modified resins, especially to impact loading, is lacking. Denneulin et al. [41] identified this deficiency and studied the influence of nano-elastomers of block copolymer embedded in the matrix, on the low velocity impact response of Kevlar fibre reinforced composite structures for helmet shells. It was shown that the addition of copolymers significantly changes the composite behaviour, especially the phenomena involved in dissipating the impact energy. Figure 2.15 Macroscopic behaviour of Kevlar FRP with and without Nanostrength [41] figure.2.15 shows the force- displacement curve for the laminate without the nano-reinforcements (Epoxy-3K) and ones with Nanostrength (Epoxy-NS-3K) and corresponding images of the composite laminate. It can be seen that the addition of the nanoparticles to the resin improved the impact resistance of the Kevlar FRP and prevented catastrophic failure due to fibre breakage and perforation seen in the sample without the nanoparticles. Denneulin et al. [5] reported that while the carbon nanotubes did not have significant effect, the damage behaviour was substantially better for the Kevlar FRP with nano-block copolymer modified epoxy.

Boumbimba et al. [76] prepared Glass fibre/epoxy-modified Nanostrength laminate composites and reported enhancement of impact resistance with the addition of acrylic tri-blocks copolymers consists of 25% improvement in  $F_{init}$ , 33% improvement in  $F_{max}$  and 19% increase in the displacement corresponding to the maximum load. Figure 2.16 Scanning Electron Microscope observation of Glass FRP with and without NanoStrength [76] figure.2.16 shows SEM observations of impact region which reveal a smooth matrix fracture surface, typical of brittle fracture surface for the laminates without nanoparticles (EPO FV 10). However, rougher and more ductile fracture zones were observed for samples with Nanostrength (EPONS FV 10

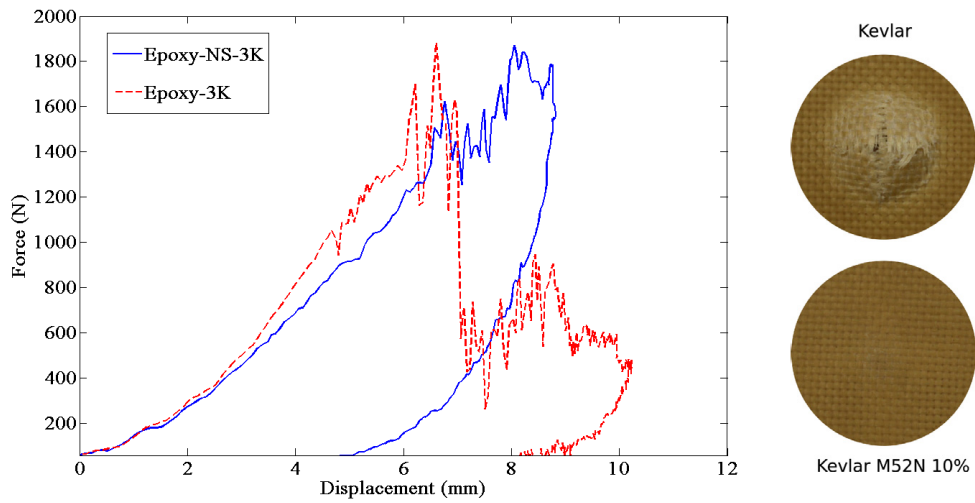


**Figure 2.15.** Macroscopic behaviour of Kevlar FRP with and without Nanostrength [41] composite).

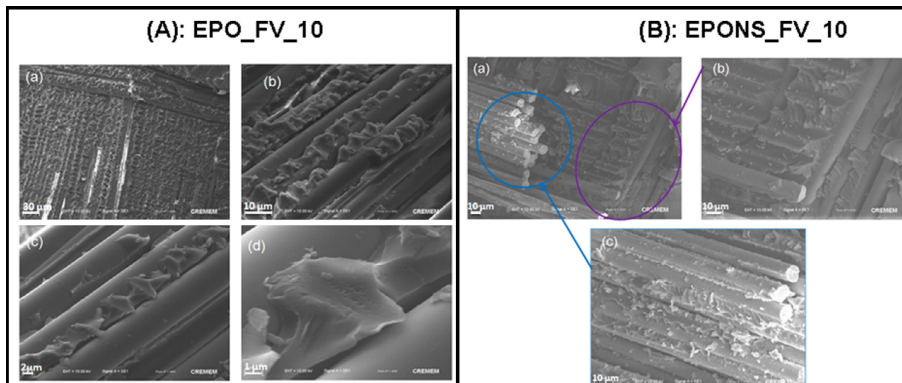


**Figure 2.16.** Scanning Electron Microscope observation of Glass FRP with and without NanoStrength [76]

## 2.7 Summary

An extensive review of the state of the art research on the topic of the impact behaviour of sandwich structures was provided in the chapter. The different experimental methods for impact testing and the different failure modes associated with impact loading were summarised. Garg and Mai [59] noted that of the three most important damage initiation modes in composite facesheets, namely, matrix cracking, delamination and fibre fracture, the first two modes depend to a large

extent on the properties of the matrix. Matrix damage decreases the localised stiffness of the panels but is not catastrophic until fibre failure. Similarly, debonding, although not a catastrophic failure mode, is found to decrease the stiffness and strength significantly [42]. The toughening of matrix (epoxy) has long been identified as a viable means of improving impact resistance of composites and research has been conducted on this for many decades, initially with micro and then with various nano- reinforcements. The limitation with the microparticles like CTBN was that it reduced desirable properties such as stiffness and thermal stability. It is our contention that of the different nano-reinforcements currently being investigated such as nanoclay, carbon nanotubes and block copolymer, the block copolymer is the most promising material to enhance the mechanical properties of sandwich composites. The main advantage of block copolymers is that they disperse well and do not suffer from problems of agglomeration of other nanoparticle reinforcements. Previous studies have confirmed that block copolymer nanoparticles produce tenfold increase in fracture energy of the epoxy resin modified with merely 2.5% weight of nano-elastomers [4]. Nanostrength, a triblock copolymer has also been shown to improve the damage resistance of FRP composite laminates [41, 76]. In the subsequent chapters, existing research on the toughening of epoxy with block copolymer will be extended to evaluate the effect of the nano elastomeric particles in the case of sandwich structures made of Kevlar and Glass FRP skins. The mechanisms of failure and the cause of the improvement in impact resistance will be compared with the composites with neat resin.



## Chapter 3

# Low velocity impact tests of sandwich panels with and without nano-reinforcement: Normal impact

### 3.1 Introduction

The literature review presented in the previous chapter has shown that the toughening of the matrix has the potential to improve the impact resistance of sandwich composites with fibre reinforced polymer facesheets. It was noted that the use of nano- block copolymers for toughening the epoxy matrix is particularly promising as it does not have the disadvantage of micro-toughening mechanisms (that other mechanical properties get unfavourably affected) or that of other nano-reinforcements (no agglomeration). The aim of this chapter is to compare the normal impact response of sandwich structures with and without Nanostrength<sup>®</sup> in the epoxy matrix under low velocity. The sandwich structures chosen for the study have facesheets made of Glass fibre or Kevlar fibre reinforced epoxy laminates and a core made of closed cell PMI foam. The method of mixing the Nanostrength particles to the resin and the fabrication procedure for the sandwich composites are presented. A series of low velocity impact tests are performed using an instrumented drop tower. The experimental setup and the results from the drop tower tests are presented. The macroscopic response of the sandwich panels based on Force- displacement curves, the energy absorbed during impact and post-mortem observations are employed to compare the impact resistance of the sandwich structures with neat resin and Nano resin. The microscopic observation of damage modes are also presented in the chapter.

## 3.2 Manufacturing of sandwich plates with block copolymer nanoparticles

### 3.2.1 Material

The sandwich panels with FRP facesheets require the selection of appropriate fibre material for the facesheet (with the matrix of neat and nano-modified epoxy) and foam core. Two types of facesheets were employed in this experimental study: Kevlar/epoxy and Glass/epoxy. Kevlar fabric is an obvious choice as Denneulin et al. [5] have already shown that the block copolymer nanoparticles have a significant effect on the impact resistance of Kevlar reinforced epoxy composite laminates. As explained in the previous chapter, Kevlar composites are extensively utilized as lightweight armor structures in applications ranging from military helmets to large scale vehicle systems such as aircraft, spacecraft, land vehicles, and naval vessels [21]. One of the objectives of the thesis is to verify if the improvement observed in the composite laminates are transferred to sandwich structures with Kevlar facesheets. Kevlar129 (Saatarlar Style 802; Taffeta 190  $g/m^2$ ; thickness: 260  $\mu m$ ) was chosen for this study because of its very high tensile toughness ( $\sigma_r = 3.4$  GPa,  $\epsilon_r = 3.5\%$ ). Sandwich composites with Kevlar fabric facesheets were shown to possess the best impact resistance and the least extent of damage compared to glass, carbon and carbon/Kevlar hybrid facesheets [14]. Three layers of plain woven fabric with the ply orientation [0/90] were used. Sandwich panels with plain weave laminated facesheets are becoming prevalent, because plain weave fabrics have balanced ply properties and improved interlaminar properties compared to unidirectional laminates, and high stiffness and strength to weight ratios compared to metal sheets [51]. Quasi-isotropic ply orientation of [0/90] was chosen to avoid the additional parameter of the effect of ply angle in the stacking sequence in the study of the effect of the block copolymer nanoparticles. Sandwich panels with Glass fibre facesheets were chosen to study the effect of the fibre material on the block copolymer nano-reinforcements. This study will follow the project of Boumbimba et al. [76] who investigated if the improvements in impact performance observed in Kevlar composites are replicated for other fibre materials. For the sandwich with Glass fibre facesheets, five layers of bidirectional plain woven Glass fabric (200 $gsm$ ; thickness: 150  $\mu m$ ) supplied by Composites Distribution were used. Five plies with the ply orientation [0-90] were chosen to keep the thickness of the cured composite facesheet similar to the three layer Kevlar (approximately 0.8 mm).

Closed cell PolyMethacrylImide (PMI) foam commercially available as Rohacell<sup>®</sup> was chosen as the core material for the sandwich panels. Closed cell foams like Rohacell foam are typically preferred for aerospace structures due to their low density and excellent mechanical properties. The high performance closed-cell foams can also significantly improve the performance of sandwich structures with their superior environmental properties such as water resistance, and sound insulation [51]. The characteristic cell-wall size and cell-wall thickness are 0.3 mm and 12  $\mu\text{m}$ , respectively. One of the reasons for choosing the Rohacell foam instead of other foams such as Divinycell which is a closed cell PVC foam, is the high temperature resistance of Rohacell foam which allows the sandwich to be cured in the hot press at elevated temperatures. Rohacell foam is available in different densities and thickness and a foam with density of 51  $\text{g}/\text{cm}^3$  and thickness of 20 mm was chosen for our study. The sandwich panels with the Kevlar or Glass fibre reinforced epoxy skins were manufactured using a wet layup process.

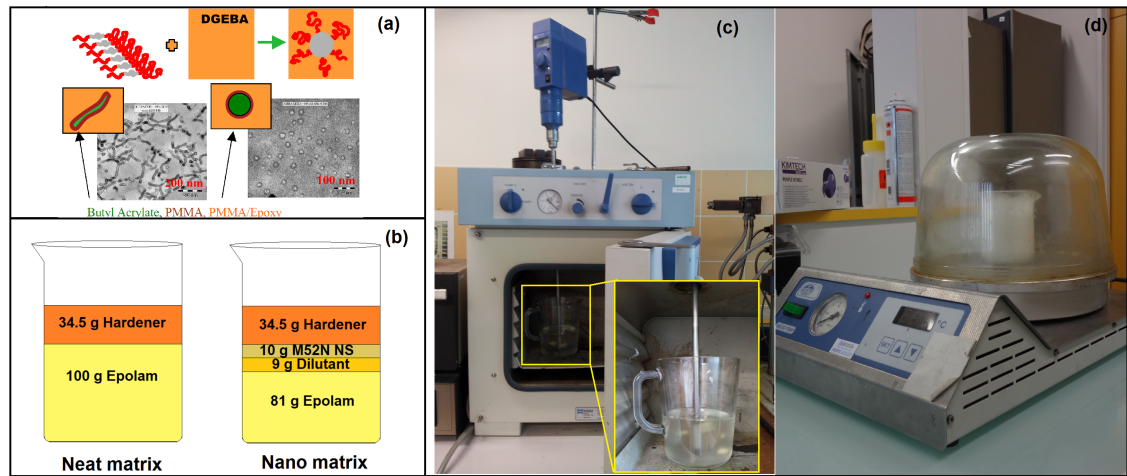


**Figure 3.1.** (a) Schematic structure and TEM image of MAM block copolymer in DGEBA resin [4]; (b) Schematic mixture of neat and nano matrix system; (c) Mixing of Nanostrength and Degassing

The diglycidyl ether of bisphenol A (DGEBA) thermoset epoxy resin Epolam 2020 and hardener supplied by Axson Technologies was chosen as matrix material. The resin system was chosen owing to its low viscosity and long gel time (60 mins) at room temperature. The hardener was used in the ratio 0.345 (w/w) (34.5 g of hardener for 100 g of resin) as recommended by supplier. The resin was used in two configurations: as supplied (Neat) or toughened with nanoparticles (Nano). For the

resin with nano-reinforcements, Nanostrength<sup>®</sup>, supplied to us by Arkema (GRL, France), was used. 10 g of triblocks copolymer M52N Nanostrength, which belong to a family of symmetric MAM copolymers with two poly(methyl methacrylate) blocks surrounding a center block of poly(butyl acrylate) were added to Epolam resin such that 100 g of the Nano-modified resin contains 10 g of Nanostrength. Denneulin et al. [41] have shown from tests on Kevlar composites with three different formulations of block copolymer (M22, M42, and M52N), that M52N Nanostrength in the epoxy resin system provided improvements in impact resistance. 10 % M52N Nanostrength was chosen out of the different percentages of reinforcements, as it has been shown to be the optimum percentage to improve the impact resistance without adversely affecting the stiffness or other desirable properties [41]. The viscosity of the nano-modified resin was also a crucial factor in choosing 10% of Nanostrength.

The materials used are summarized in the Table 3.1. Materials used in fabrication of sandwich composites table.3.1

**Table 3.1.** Materials used in fabrication of sandwich composites

Material	Specifications	Supplier
Epoxy resin	DGEBA (Epolam 2020)	Axson technologies
Dilutant	RD107	Epotec
Matrix reinforcement	M52N Nanostrength	Arkema polymers
Kevlar fabric	Kevlar129 (190 gsm)	Saatilar, Saati Italy
Glass fabric	Plain weave (200 gsm)	Composites distribution
PMI foam	Rohacell $\rho = 51g/cm^3$	Evonik industries, France

Nanostrength, which is in powder form, is added to the resin by mixing, using a mechanical stirrer (shown in Figure 3.1(a) Schematic structure and TEM image of MAM block copolymer in DGEBA resin [4]; (b) Schematic mixture of neat and nano matrix system; (c) Mixing of Nanostrength and Degassing figure.3.1) at 290 rpm at 110° C for a duration of two hours. The powder is added to the resin in small quantities to prevent clumping. A dilutant containing epoxy monomers was also added to the resin to reduce the viscosity of the resin and to help the addition of 10% by weight of the nanoparticles. Barsotti has reported that the MAM triblock copolymers like the M52N chosen for this study can easily be dissolved in a typical DGEBA resin with the application of heat and a low amount of shear. It has been shown that when dissolved in DGEBA resin, the MAM block copolymer self-assemble into nanostructures, wherein the PMMA block will associate

with the epoxy resin, forming an effective shell surrounding an immiscible PBuA core [4]. Schematic structure of the MAM blocks before mixing with the DGEBA resin and the self assembling structure after nanostructuration is also shown in Figure 3.1(a) Schematic structure and TEM image of MAM block copolymer in DGEBA resin [4]; (b) Schematic mixture of neat and nano matrix system; (c) Mixing of Nanostrength and Degassingfigure.3.1 along with TEM images of MAM block copolymer in DGEBA resin. Transmission Electronic Microscopy (TEM) was used by Denneulin et al. [41] to check the self-assembling process of the block copolymer nanoparticles. The solution (Epolam+RD107+Nanostrength) is allowed to cool to room temperature and it is observed that the addition of nanoparticles turns a transparent resin into a translucent one. The stirring action agitates the mixture and produces a foaming solution. The solution becomes clear of any particle agglomeration and bubbles after the degassing step. The Epolam resin with Nanostrength is prepared in a large quantity and required amount of this precursor is mixed with the hardener. The Epolam resin-Nanostrength mixture is heated at 40° C for 5 minutes for degassing before adding the hardener. The pre-heating also helps to reduce the viscosity of the resin making it easier to apply on the fabric. The layers of fabric were impregnated with this mixture.

### 3.2.2 Fabrication of sandwich panels

The sandwich samples were manufactured using a wet lay-up process. The different steps involved in the fabrication of a Kevlar sandwich plate are shown in Figure 3.2(a) Steps involved in the fabrication of sandwich samples, (b) Wet layup process for sandwich manufacture and (c) Curing the sandwich plate in hot pressfigure.3.2. The manufacturing process was similar to the method explained in [41] for the fabrication of Kevlar composite plates. In the first step, each layer of the fabric was cut to desired dimensions and was impregnated with the resin-hardener mix manually with a brush. Care was taken to not distort the alignment of the fibres as this will result in variability of behaviour. The three impregnated layers of fabrics were placed between two sheets of baking paper and compressed in the press for 5 minutes at room temperature and a pressure of 1.5 bars. This step ensures that excess resin is ejected from the facesheet. The process was repeated for both the top and bottom facesheet of the sandwich. It is possible to manufacture the facesheets separately and bond them to the core or the sandwich could be co-cured. Co-curing the sandwich was chosen as it was recommended that co-curing the facesheets ensure

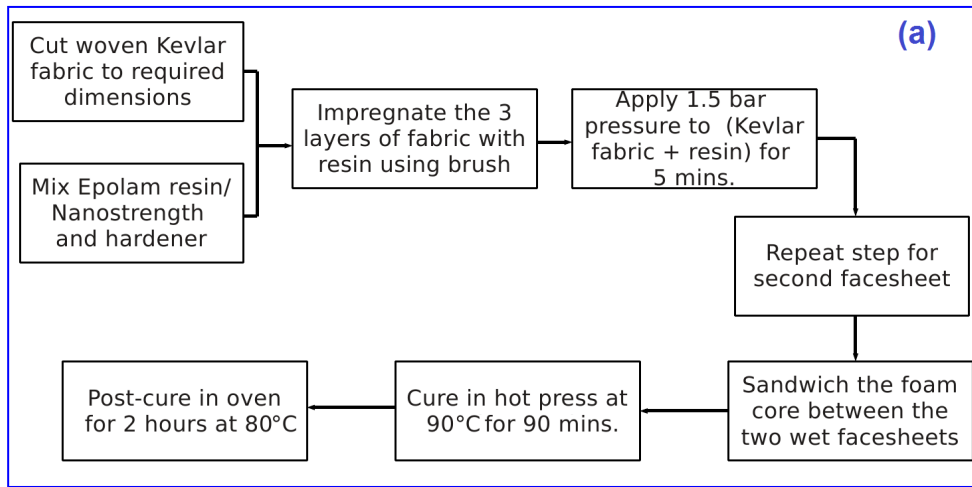


**Figure 3.2.** (a) Steps involved in the fabrication of sandwich samples, (b) Wet layup process for sandwich manufacture and (c) Curing the sandwich plate in hot press

good adhesion with the core [45]. The two facesheet layers of  $[0/90]_3$  Kevlar fibre were then bonded on each side of the core material and the sandwich panel was co-cured in a hot press at  $90^\circ\text{C}$  for 90 minutes at pressure of 1.5 bars. No additional adhesive was introduced between the face sheets and the core. Finally, the sandwich composites were post-cured in an oven at  $80^\circ\text{C}$  for two hours. Square plates of side 200 mm were fabricated using this method. The nominal thickness of the cured sandwich plates were 20 mm. This is because there is some compression in the foam core while the sandwich is cured in the hot press. The same method was used for the fabrication of the sandwich plates with Glass fibre reinforced composite facesheets with the only modification being that 5 layers of Glass woven fabric were

used instead of the Kevlar fabric.

### 3.3 Experimental setup for normal impact tests

Low velocity normal impact testing was accomplished using an instrumented drop tower. Drop towers are widely used for impact testing as they have several advantages over other dynamic testing machines and provide a quick and inexpensive mean of conducting low velocity impact tests. The typical setup of the drop tower setup consists of an instrumented impactor that is secured to a carriage that falls along guideposts and collides with the plate. An electromagnet holds the carriage lifted to a pre-determined height and the impact event is initiated by switching off the electromagnet and letting the carriage fall freely under the action of gravity. The potential energy achieved by raising the level of the carriage is transferred to kinetic energy on release of the electromagnet and the impactor head transfers the impact energy to the test specimen. The energy of the impact can be varied by either changing the mass of the carriage or by changing the drop height. The maximum impact energy that can be obtained is therefore limited by the weight of the impactor carriage and the maximum height of the tower.

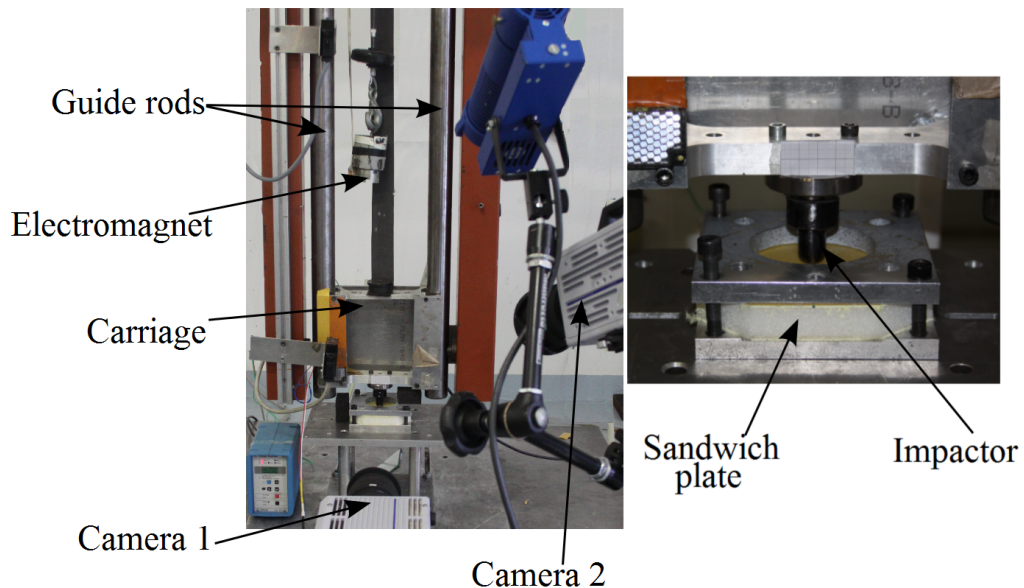


**Figure 3.3.** (a) Drop tower setup for low velocity impact testing and (b) Close-up of impactor and target plate

The drop tower setup used for the low velocity impact testing is shown in Figure 3.3(a) Drop tower setup for low velocity impact testing and (b) Close-up of impactor and target plate figure.3.3. The experimental device present in the dynamic platform of I2M laboratory in Talence consists of two rectified columns attached to a metallic gantry and these two columns guide the falling carriage, on which different impactor geometries can be fixed. A winch with an electromagnet was used to lift the projectile to the desired impact height. During the test, the impactor carriage is released by the electromagnet, freefalls, and strikes the structure. A rebound-catcher has been implemented to avoid a second impact, which could further damage the structure and prevent an accurate post-mortem analysis of the damage and residual strain. The drop height is varied to give a range of impact energies while the mass of the impactor is kept constant. A 16 mm diameter hemispherical headed steel impactor strikes the centre of the square target plate which is clamped with square aluminium plates with a circular hole of diameter 70 mm. The circular boundary condition is widely used so that the central point of impact is at the same distance from the edge and the diameter of 70 mm is chosen to allow global deformation in the plate. A small diameter hemispherical impactor is the standard impactor geometry used for low velocity impact testing of composites by researchers, for instance Park et al. [40] used a hemispherical impactor with a diameter of 12.7 mm and opening of the round-clamped fixture of 76.2 mm. The bolts were tightened to a torque of 5 Nm using a torque wrench, in order to provide consistent clamping from experiment to experiment. The force response of the sandwich structure during impact was measured using a piezoelectric force sensor (Kistler force transducer, force range of 5 kN). The ring type force sensor is attached between the hemispherical impactor and the carriage using supplier specified studs. The displacement of the carriage is measured using a Laser Displacement sensor (Keyence France SAS, maximum range 100 mm). The signals of both sensors were recorded by a National Instruments DAQ card at a frequency of 30 kHz. A typical impact duration is of the order of 10 ms and this frequency of data acquisition enables measurement of force and displacement including initiation of damage. In addition to these sensors, two high-speed video cameras (Photron FASTCAM- APX RS and Photron SA3) were used to measure displacement of the impactor and to observe the top facesheet, respectively. A frame rate of 10000 frames per second and image resolution of 512 pixels x 512 pixels was chosen for the image acquisition of impactor displacement. The second high-speed

camera had a frame rate of 6000 fps and image resolution of 512 x 512 pixels.

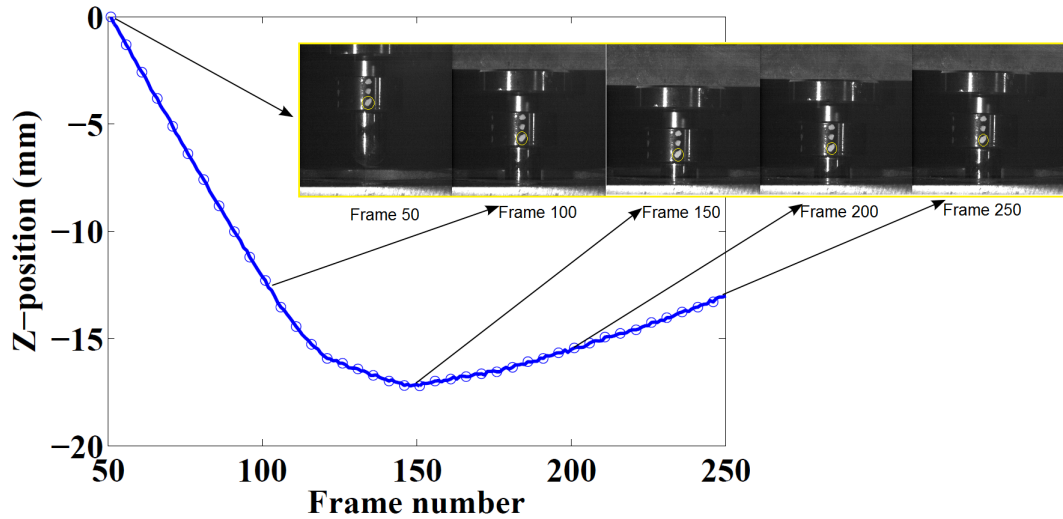


**Figure 3.4.** Example of displacement measurement using high speed camera

Figure 3.4 Example of displacement measurement using high speed camera figure.3.4 shows the displacement measured using an image correlation subroutine written in ImageJ software for a typical case. The subroutine follows a white dot made of correction fluid on the impactor through the images from the high speed camera. An initial Region of Interest (RoI) is chosen from a reference image with known location of the dot. The ImageJ command for checking circularity of the dot and the diameter/ area of the circle are used in the identification of the dot in subsequent images. In the case shown, Frame 50 is chosen as the reference image against which all the subsequent images are compared and the image correlation is initiated to obtain the position of the target point for 200 frames. A calibration image is used to convert the pixels to *mm* measurements. The displacement in both *x* and *y* directions are measured to correct for any off-axis displacement. Ideally, the guide posts do not interfere with the free flight of the weight in the vertical direction and serves strictly as a safety device, acting to constrain lateral movements and rotations of the carriage. However, the theoretical value of the velocity  $v_{th} = \sqrt{2gh}$  was not used for the initial velocity as it was expected that there will be some frictional losses in the columns. The measured velocity  $v_o$  was obtained by a linear regression of the displacement before contact. The initial energy of the impact was calculated from

the mass of the impactor (1.8 kg) and initial impact velocity found from the slope of the displacement before contact.

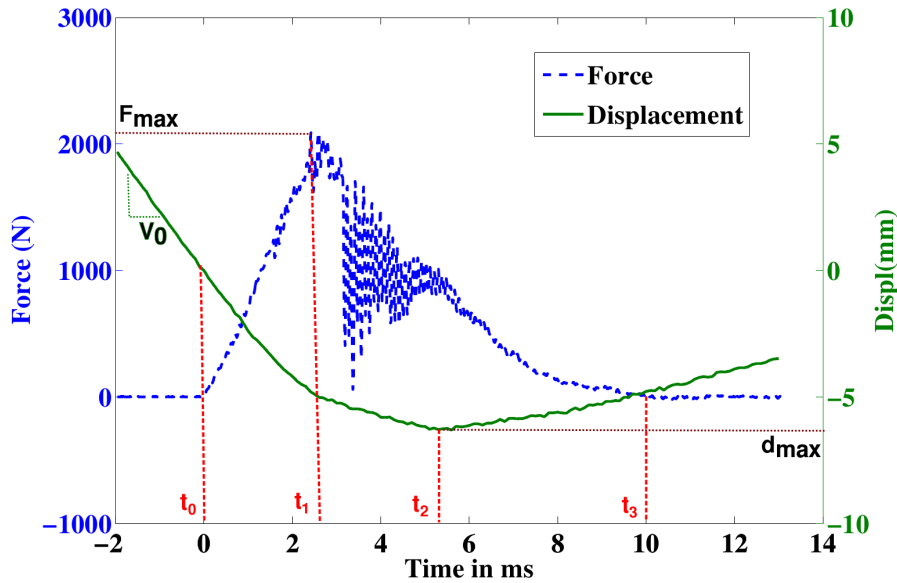


**Figure 3.5.** Typical results of force and displacement from drop tower test

A typical force and displacement- time history of low velocity impact is shown in Figure 3.5. Typical results of force and displacement from drop tower test figure.3.5. The curves shown correspond to 8 J impact on Kevlar sandwich plate with neat resin, i.e., without any nano-reinforcements. Time  $t_0$  and  $t_3$  corresponds to the beginning and end of impact, respectively. The beginning of the test was defined when the force reached 50 N and the force and displacement curves were adjusted to consider this instant  $t_0$  as the starting point of the impact. Four distinct phases are identified from the force- time history; the first phase corresponds to elastic bending of the sandwich panel, the second corresponds to a first change of the stiffness because of damage initiation upto the peak force, the third phase is from the significant and sharp drop of load after the peak force which is due to damage propagation in the composite facesheet and the last phase corresponds to the unloading of the sandwich panel due to its residual strength and in the case of penetration, the dry friction between the impactor and the perforated sample. It can be seen that the total duration of the impact in this case is about 10 milliseconds. The contact force of the sandwich composite exhibits a linear increase with respect to time as the indenter comes in to contact with the specimen and is followed by a sudden drop

in the load after it reached the first peak value at  $t_1$ . The maximum displacement of the impactor occurs at  $t_2$  and marks the beginning of the unloading phase. The unloading is finally followed by the rebound, which is represented by the contact force value reaching zero i.e., the impactor is no longer in contact with the sandwich plate. In the case of an elastic impact, the force-time history has a parabolic curve which is symmetric about the peak force, i.e., loading and unloading portion are identical. It can be seen that for this case there is some damage which is marked by the sharp drop in the force corresponding to the initiation of fibre failure and therefore there is no symmetry between the loading and unloading phases. The final displacement value is not zero and denote the permanent deformation in the sandwich sample.

### 3.4 Results of low velocity normal impact tests of Kevlar - Rohacell sandwich plates

The sandwich plates with the neat resin are designated KR sandwich plate (to denote Kevlar-Rohacell sandwich) while the plates with Nanostrength embedded in the epoxy matrix are designated KNR sandwich plate (Kevlar-Nanostrength-Rohacell sandwich). The sandwich panels were tested for three drop heights of 0.5 m, 0.75 m and 1 m corresponding to impact energies 8 J, 12 J and 16 J. These energies were chosen to correlate with different levels of damage in the sandwich panel. Three samples were tested for each configuration in order to verify the repeatability of the test. The measurements of time-history of contact force and displacement of the impactor made it possible to plot the force vs. displacement curve for each type of sandwich plate tested.

Figure 3.6 Repeatability of drop tower tests: Force- displacement of three KR sandwich plates figure.3.6 shows the force- displacement curves for KR sandwich plate impacted with an initial energy of 8 J. It can be observed that these curves follow each other closely and that only a weak dispersion of material behaviour exists between the different samples. The initial linear portion of the curve is robust with force values of 1495, 1515 and 1530 N for a displacement of 5mm. The large oscillations that marked the beginning of fibre fracture and other damage processes are not reproducible. Fibre fracture causes a large loss of stiffness which is observed from the sharp drop in the force. However, it is safe to assume that the tests are

repeatable and only a representative sample from each energy is used for comparison with other samples henceforth.

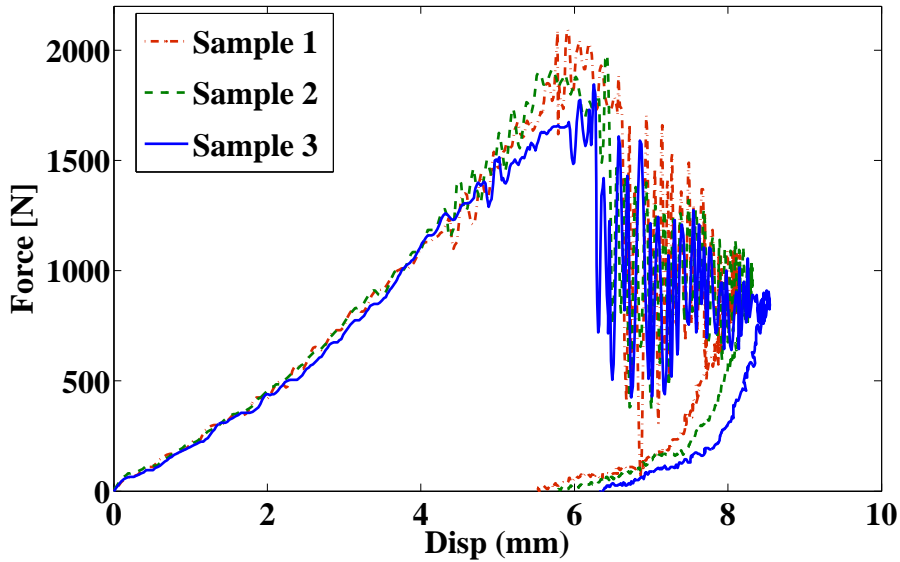


**Figure 3.6.** Repeatability of drop tower tests: Force- displacement of three KR sandwich plates

The force- displacement curve of Kevlar - Rohacell sandwich panels with neat resin and with 10% M52N Nanostrength (KR sandwich and KNR sandwich) are compared for the impact energies of 8 J, 12 J and 16 J (drop height of 0.5 m, 0.75 m and 1 m) in Figures 3.7 Force- displacement curve of KR and KNR sandwich for impact energy of 8J figure.3.7, 3.8 Force- displacement curve of KR and KNR sandwich for impact energy of 12J figure.3.8 and 3.9 Force- displacement curve of KR and KNR sandwich for impact energy of 16J figure.3.9.

It is observed that the force- displacement curve of the sandwich panels show a quasi-linear behaviour for low values of indentation, followed by a non-linear regime. It can also be observed that the stiffness of the sandwich panel during the elastic bending phase, i.e., slope of the linear portion of the curve, the elastic stiffness is slightly reduced by the addition of copolymers, which is likely due to the more compliant elastomeric phase. This is particularly notable as the toughening of the resin with rubber particles resulted in a considerable loss of stiffness and the addition of block copolymer has not significantly reduced the stiffness.

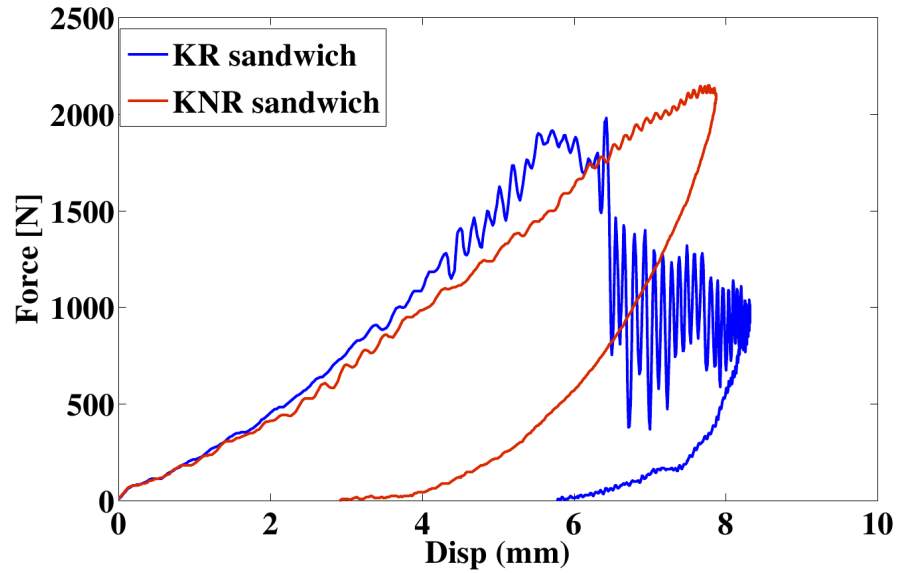


Figure 3.7. Force- displacement curve of KR and KNR sandwich for impact energy of 8J

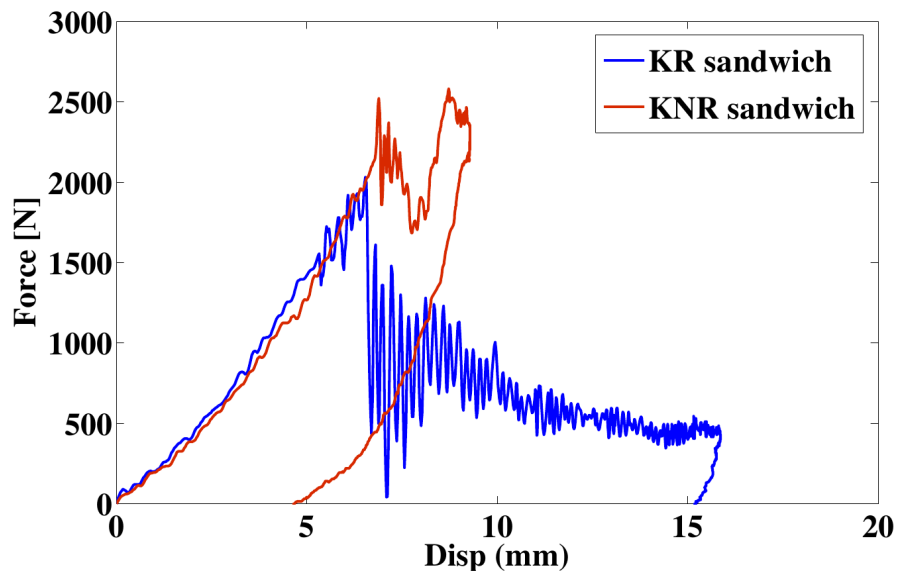
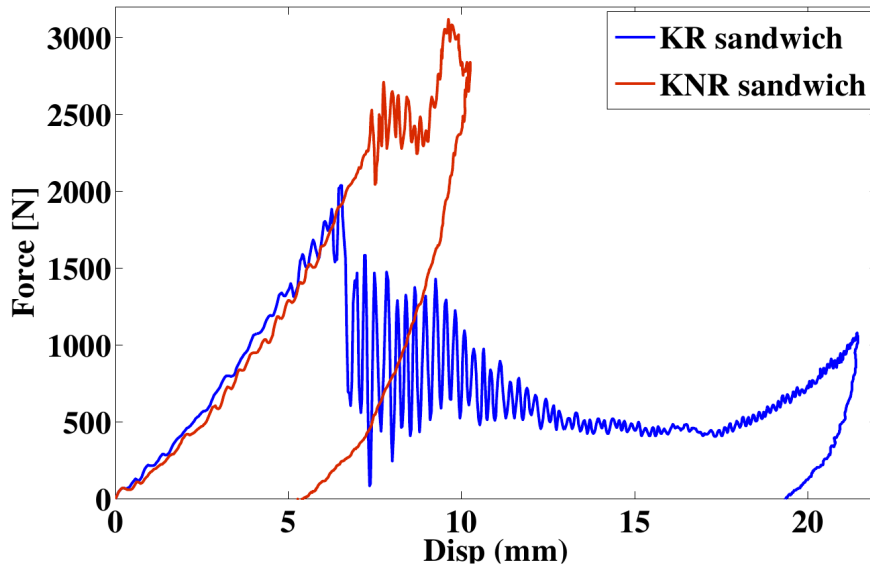


Figure 3.8. Force- displacement curve of KR and KNR sandwich for impact energy of 12J



**Figure 3.9.** Force- displacement curve of KR and KNR sandwich for impact energy of 16J

The force- displacement curves for the lowest impact of 8 J (Figure 3.7 Force-displacement curve of KR and KNR sandwich for impact energy of 8J figure.3.7) show that there is a sharp drop in the force at a displacement of 6.7 mm for the KR sandwich plate, followed by large oscillations in the signal. The unloading phase is characterised by the return of the force values to zero and it can be seen that there is a large permanent deformation as the displacement values do not return to zero which indicates considerable permanent damage. The behaviour of the KNR sandwich is distinctly different from the KR sandwich. The load displacement curve remains smooth, even in the unloading phase, without any oscillations, which indicates that there is no significant damage, although there is some permanent deformation after the impact. At this low impact energy (8J), the peak load with the nano-block co-polymers is only about 10% higher than that of the panel without nano-reinforcement and the maximum displacement is about the same. However, with increasing levels of impact energy, not only the load deflection behavior changes, but also the peak load and maximum displacement differ significantly with the addition of nano particles. For instance, in Figure 3.8 Force- displacement curve of KR and KNR sandwich for impact energy of 12J figure.3.8, the peak force values for KR

sandwich and KNR sandwich for an impact of 12 J were 2025 N and 2580 N respectively (27% increase). For the sandwich with neat resin (KR), a sharp drop in force is observed which corresponds to the failure of facesheets through fibre breakage and perforation. Fibre fracture is confined to a small region close to the point of contact but the loss of flexural stiffness due to it is enough to soften the area around the impactor. The behaviour after this peak exhibits a core-dominant behaviour and follows regions of plastic plateau in which the cellular structure collapse initiate by buckling of the cell walls and edges and densification of the core.

The force- displacement curve for the sandwich samples impacted from drop height of 1 m, shown in Figure 3.9 Force- displacement curve of KR and KNR sandwich for impact energy of 16J figure.3.9 has a similar curve to the previous case with fibre perforation for the KR sandwich plate and large displacement corresponding to crushing of the foam. The second peak seen for sandwich plates impacted at the higher energy shows that the lower facesheet has begun to play a role in the deformation. The KNR sandwich has a higher peak force and lower maximum displacement.

The second high speed camera was used to observe the top facesheet as there is no damage in the bottom surface of the sandwich that can be observed for the energies tested. Figure 3.10 High speed camera images of the top facesheet for impact of 16 J figure.3.10 shows the images at different times during the impact event, corresponding to an impact test at 16 J on the KR (neat resin) sandwich panel (Top) and the KNR (nano resin) sandwich panel (Bottom). The images begin 6 milliseconds before the beginning of contact and shows the impactor come into contact with the top facesheet. It can be seen that in the case of the KR sandwich, the impactor has penetrated the top facesheet completely by  $t=3$  ms whereas, in the case of the nano-reinforced sandwich panel even after 8 ms, there is no perforation and the impactor rebounds, as seen in the last image at 14 ms.

Typical images of the top facesheet post-impact are shown in Figure 3.11 Top surface of the Kevlar sandwich samples after impact figure.3.11. It can be seen that even for the lowest energy, there is beginning of fibre failure and perforation in the sandwich plates with neat resin. This is consistent with our observation of the force- displacement curve, where a sudden drop and large oscillations were seen in KR sandwich sample impacted at 8 J. There is complete penetration of the top facesheet in the neat resin sandwich impacted at higher energy. The sandwich plates

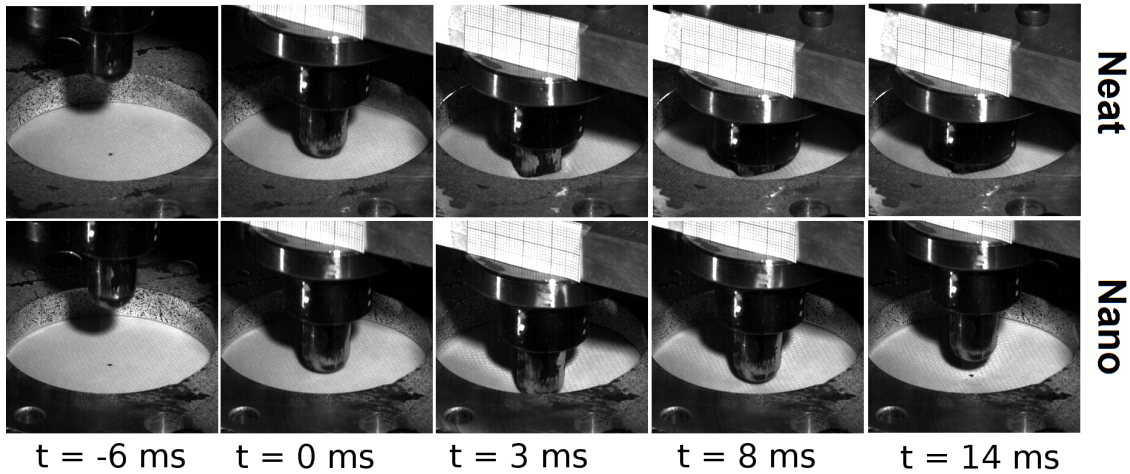


**Figure 3.10.** High speed camera images of the top facesheet for impact of 16 J

with nano-modified resin do not show any perforation even at the highest energy but some discolouration in the fibre directions [0-90], are clearly visible. Some bands in the +/- 45 directions are also observed, which are indicative of permanent stretching of the fibres and possibly, matrix failure. It can also be observed from visual examination of the top facesheet that the load is spread over a larger area for the samples with nano-modified resin while the sandwich plate with neat resin shows more local damage. It can be concluded that the KNR sandwich plate exhibits a higher strength and greater durability or damage resistance (absence of the fibre breakage and perforation).

An additional test was carried out at an initial energy of 20 J (drop height 1.25 m) to observe if the KNR sandwich had perforation at this higher energy. Figure 3.12 Force- displacement curve for drop height of 1.25 m and visual inspection of top and bottom surface figure.3.12 shows the Force- displacement curve of the 20 J impact on KR and KNR sandwich plate. It can be observed that the 20 J impact caused penetration failure in the top facesheet of the KNR sandwich plate (bottom left picture), but no damage in the bottom facesheet (Bottom right), while there is penetration in the top and damage in the bottom facesheets of the KR panel (top left and right images). The second peak observed for KR sandwich is the result of the bottom facesheet taking the load. This second peak is almost as high as the first peak where most of the load is resisted by the top facesheet. Visual examination of both the top and bottom facesheets confirm that there is considerable failure in the

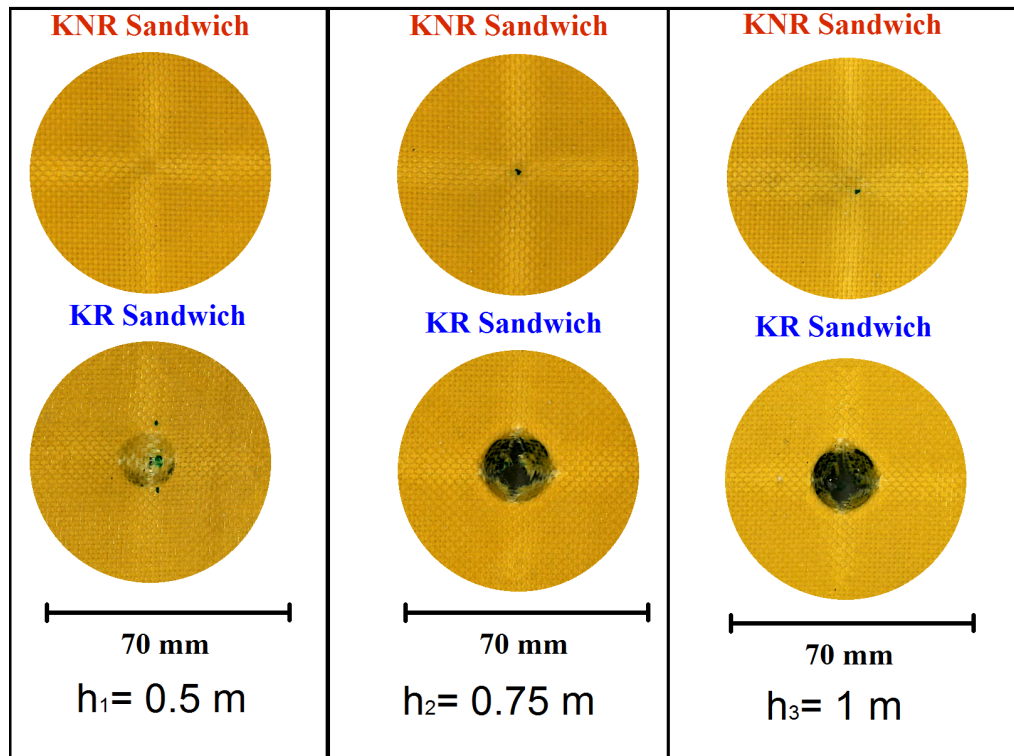


**Figure 3.11.** Top surface of the Kevlar sandwich samples after impact

bottom facesheet of the KR sandwich plate, whereas the bottom skin of the KNR sandwich shows little damage.

Figures 3.13(a) Peak Force and (b) Max. displacement for Kevlar sandwich samples figure.3.13(a) and (b) respectively shows the peak force and maximum displacement of the KR and KNR sandwich plates for the different initial impact energies. It can be seen that the peak force for the KNR sandwich plates show a steady increasing trend up to the 16 J impact but falls for the 20 J impact. This can be explained by the fact that there was no fibre perforation of the top facesheet until the 20 J impact case. The peak forces for the KR sandwich plate are lower than the corresponding peak values for KNR sandwich for all the four impact energies. It also does not increase significantly for higher energy levels, suggesting that the maximum force is achieved before the facesheet ruptures, and this occurs even at the lowest energy level of 8J. The trend of maximum displacement, on the other hand, shows KR sandwich having consistently higher values than the KNR counterparts and increasing at a much higher rate with increasing impact energy. These large displacements are associated with the crushing of the foam, which also reduces the

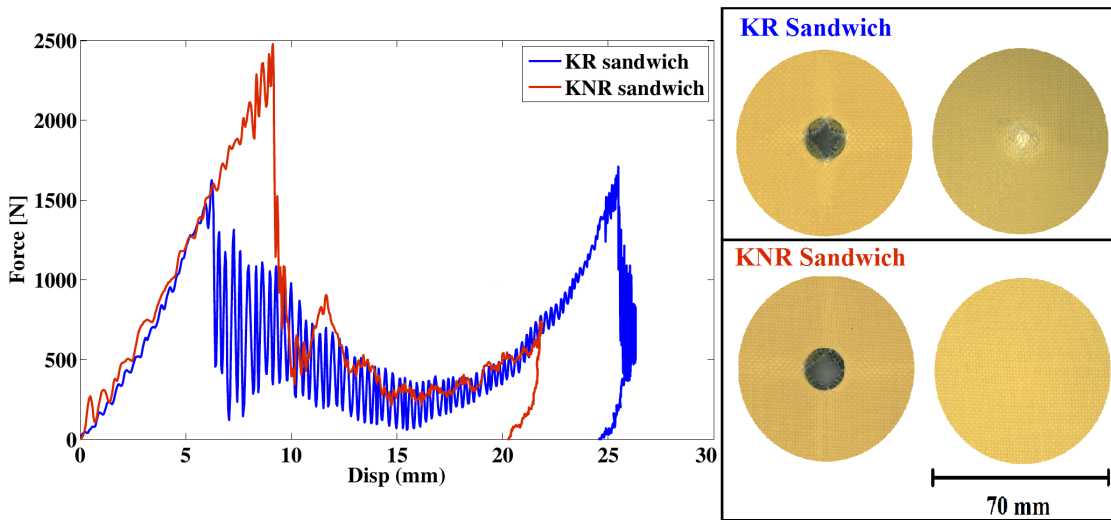


**Figure 3.12.** Force- displacement curve for drop height of 1.25 m and visual inspection of top and bottom surface

bending stiffness allowing for more overall bending of the panels. In the case of the KNR sandwich where the top facesheet did not fail, the crushing of the core is appreciably less. This observation is supported by the 20 J impact case where the top facesheet of the KNR sandwich perforated and the maximum displacement shows a sharp increase. It should also be noted that the maximum displacement exceeds the thickness of the sandwich sample (20 mm) which suggests that there is some bending of the plate component to the deformation. The values of the peak force and maximum displacement of Kevlar sandwich samples with and without nanoparticles are summarized in the Table 3.2 Peak force and Maximum displacement of Kevlar sandwich sample table.3.2.

### 3.4.1 Energy dissipated

One of the criteria that is widely used to compare the impact resistance of different composites is the energy criteria. The energy dissipated during the impact can be computed from the numerical integration of the Force- displacement curve. The energy computed as the integral of the Force- displacement curve up to the displacement corresponding to the peak force as shown as the yellow shaded region (I) in Figure 3.14 Energy for Damage Initiation (Zone I) and Total energy dissipated during Impact (Zone I + Zone II) figure.3.14 is the energy available for damage initiation. It is the energy available in the target for major damage to occur, being the elastic strain energy stored in the target minus energy lost through matrix damage,

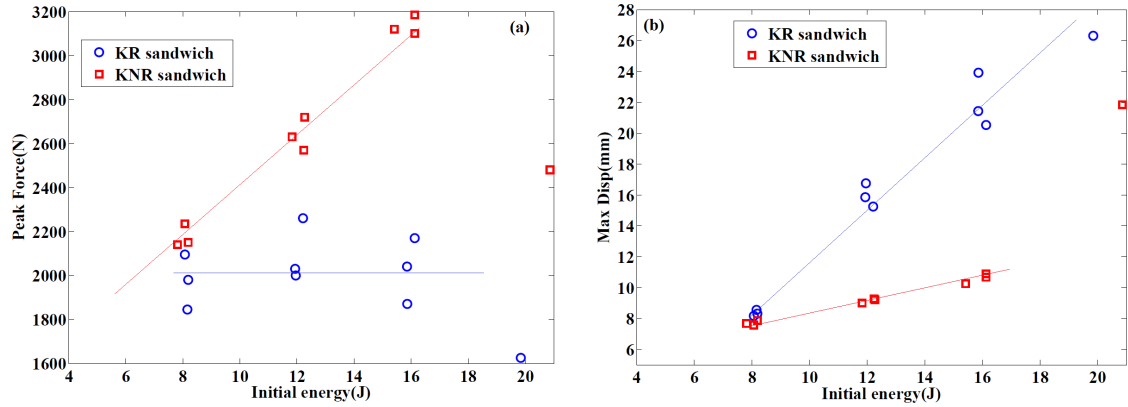


**Figure 3.13.** (a) Peak Force and (b) Max. displacement for Kevlar sandwich samples

**Table 3.2.** Peak force and Maximum displacement of Kevlar sandwich samples

KR sandwich			KNR sandwich		
Impact energy (J)	Peak force (N)	Max. Displ. (mm)	Impact energy (J)	Peak force (N)	Max. Displ. (mm)
8.07	2095	8.16	8.07	2235	7.57
8.19	1980	8.32	8.19	2150	7.87
8.16	1845	8.55	7.82	2140	7.67
12.21	2260	15.25	11.83	2630	9
11.96	2000	16.75	12.27	2720	9.2
11.94	2030	15.86	12.24	2570	9.27
15.87	1870	23.92	16.13	3185	10.66
16.13	2170	20.53	16.13	3100	10.89
15.86	2040	21.43	15.42	3120	10.25
19.85	1625	26.31	20.87	2480	21.85

friction, wave propagation (although this is negligible at low velocities) and non-elastic deformation of the target. For cases where there is no fibre failure indicated by a sudden drop in the force, this is the only energy available for damage initiation (and is usually equal to the input (impact) energy, since it cannot be more). However, in cases where there is substantial damage, then this is the energy required for damage initiation. The energy of damage initiation is an important parameter for comparing impact performance, as obviously we would prefer to have a material or structure which would require a higher level of energy before damage initiates. The energy up to the peak force clearly represents the energy required to generate sufficient damage to reduce the stiffness of the plate and affect its structural integrity

severely. A second criterion can also be defined as the total energy dissipated during the impact. This, includes the area dissipated through damage (area II in Figure 3.14 Energy for Damage Initiation (Zone I) and Total energy dissipated during Impact (Zone I + Zone II) figure.3.14) and is therefore corresponds to the total area under the force - displacement curve from the beginning of impact until the end of unloading phase when the force reaches zero again.

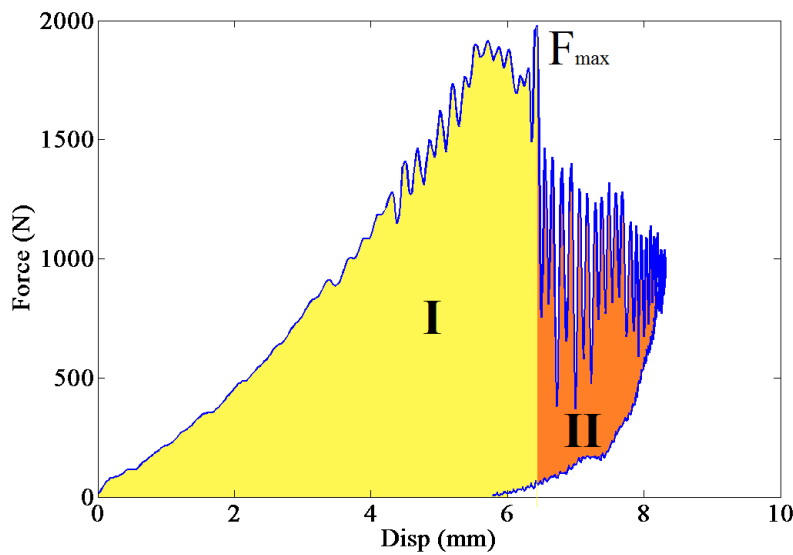


**Figure 3.14.** Energy for Damage Initiation (Zone I) and Total energy dissipated during Impact (Zone I + Zone II)

The energy required to initiate failure for the KR and KNR sandwich plates is compared in Figure 3.15 Energy up to peak force for KR and KNR sandwich plates figure.3.15. It is observed that the elastic energy has similar trend to the results presented by Reis et al. [20] for the addition of nanoclay particles in Kevlar composites. The difference in energy for damage initiation due to the addition of nano-block copolymers increases with increasing impact energy. It may be noted that, for the KNR samples, at impact energy of 8J, the energy up to peak force is about the same as the input energies (8J), and is only marginally lower for input energies of 12 J and 16 J, indicating that some damage has initiated; however, it is significantly lower (only 10J) for the impact energy level of 20J. Whereas, for the KR sandwich panels, the peak energy is well below the input energy at all levels of impact (input) energy, indicating that the peak force is limited by damage initiation in the non-reinforced Kevlar panels at all impact energy levels. A ranking regarding

perforation resistance can be performed with this criterion [5]. A polynomial fit was not attempted given the limited number of impact energies tested, but the trends are shown as dotted lines and it is evident that the addition of Nanostrength increases the penetration threshold for the Kevlar sandwich plates.

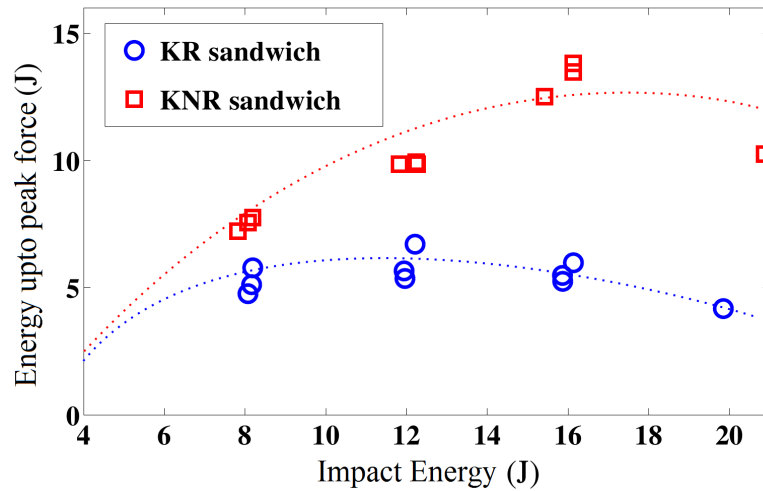


**Figure 3.15.** Energy up to peak force for KR and KNR sandwich plates

Figure 3.16 Total energy dissipated in the impact of KR and KNR sandwich plates figure.3.16 shows the plots for the total energy dissipated against the initial kinetic energy of the impactor for the KR and KNR samples. The 45° line is the total available energy, i.e., for initial impact energy of 8 J, the maximum energy that can be dissipated during the impact is 8 J and so on. It can be seen that penetration occurs when the dissipated energy curve approaches the 45° line, i.e. samples that undergo penetration absorbs a large portion of the kinetic energy of the impactor in damage of the different components of the sandwich plate.

For the impact energy of 8J, the total energy dissipated or absorbed by the KR sandwich panels is below the 45 degree line, indicating that the damage is not significant and part of elastic energy is returned to the impactor. At 12J and 16 J of impact energy, the total dissipated energies of the KR panels lie on the 45 degree line, indicating that all the available energy is absorbed by the damage caused to the sandwich panels. On the other hand, the total energies absorbed by the KNR sandwich panels at all impact energy levels lie below the 45 degree line indicating that a significant portion of the input energy is returned by the nano-reinforced

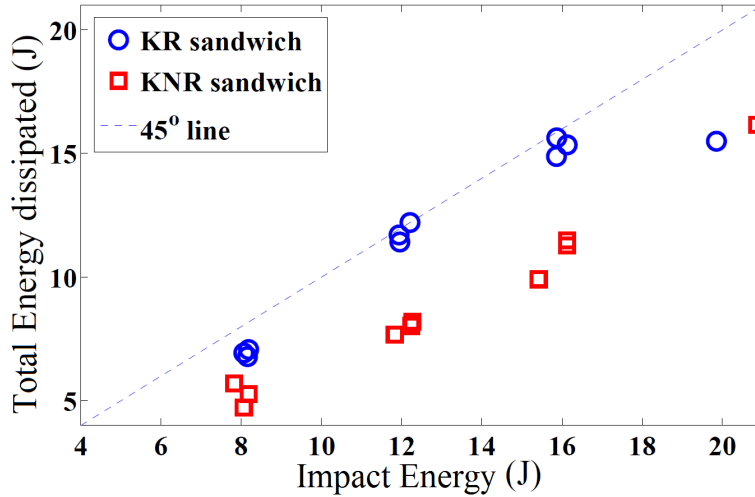


**Figure 3.16.** Total energy dissipated in the impact of KR and KNR sandwich plates

and relatively undamaged sandwich panel to the impactor (in the cases of impact energies up to 16J) or penetration occurs (in the case of 20J impact). Compared to the nano-reinforced (KNR) panels, the non-reinforced Kevlar sandwich panels (KR) absorb a higher amount of total energy because they develop significantly larger amounts of damage in the form of perforation of the facesheet and extensive core crushing. The maximum displacement reached for the 16 J impact is almost 22 mm. This core dominated region is involved in dissipating a large portion of energy. Even though the KNR sandwich plates have a higher peak force value than the KR sandwich counterparts, there is sufficient recovery of the samples in the unloading phase, that it has a lower total energy dissipated. The remaining energy is returned to the impactor as rebound energy.

It is understood that higher values of dissipated energy relates to lower elastic recovery and consequently major damage while the lower values of the sandwich plate with nanoparticles implies that the KNR sandwich plate can withstand higher impact energies. The residual strength of the sandwich plate after the impact will be higher for the KNR sandwich because it has less damage than the KR sandwich. It can be seen that for the present loading conditions, the limit of the impact energy of KNR sandwich is over 16 J before the plate begins to fail by perforation whereas that limit is lower for the KR sandwich plate. It is also interesting to note that for the impact at 20 J, the KR sandwich plate has reached a saturation limit of energy absorption. Higher impact energies do not cause an increase of absorption after

complete penetration and the remaining energy in the impactor exists as residual kinetic energy. The KNR sandwich continues to have an increasing trend in the energies tested and has not reached the saturation limit, that is, the KNR sandwich plates can be used in cases where the impact energy is higher than 20 J without reaching the maximum possible energy absorption.

### 3.4.2 Post-mortem damage analysis of Kevlar Rohacell sandwich

The results presented in previous sections indicate that the addition of the nanoparticles in the epoxy resin improves the damage resistance of Kevlar sandwich panels based on the Force- displacement curves and visual inspection of the top and bottom facesheet after impact. It is not possible to observe the true extent of damage, especially in the core material by inspection of the outer layer of facesheets. A detailed analysis of the damage in the samples has been carried out by sectioning the samples. The impacted sandwich sample is cut in the middle in order to observe the section view. The sandwich sample is embedded in a coloured resin before cutting to preserve the shape of the damage of the facesheets as well as the core. For the sandwich plates in which there is no perforation of the top facesheet, a small hole is drilled on the top facesheet, through which the coloured resin is injected. A room temperature curing epoxy resin was used along with a red dye for this purpose. The sandwich plate was cut using a diamond-toothed saw and the section of interest is embedded in a clear Mecaprex resin under vacuum. Mecaprex resin was chosen for its transparency as well as fast cure time. The mounted samples are then polished under progressively finer abrasive papers. The section view of the KR and KNR sandwich plates for impact energies of 8, 12, 16 and 20 J are shown in Figure 3.17. Cross section of the Kevlar sandwich samples after impact test: (Left) KR sandwich and (Right) KNR sandwich figure.3.17. Images (a,b,c,d) correspond to KR sandwich plate and (i,ii,iii,iv) are for the KNR sandwich plates.

It can be seen that for both the un-reinforced and the reinforced samples, the extent of damage increases with increasing impact energy level, progressively moving down from the top face, into the core and finally into the bottom face sheet. It is also immediately apparent that the damage is more extensive, for each impact energy level, in the KR samples than in the KNR samples. The indentation and deformation of the upper facesheet in images (a), (b) and (c) is much more severe than those in (i), (ii) and (iii). It can also be seen that the core damage and debonding between the upper facesheet and the core is more extensive in the KR samples than in the

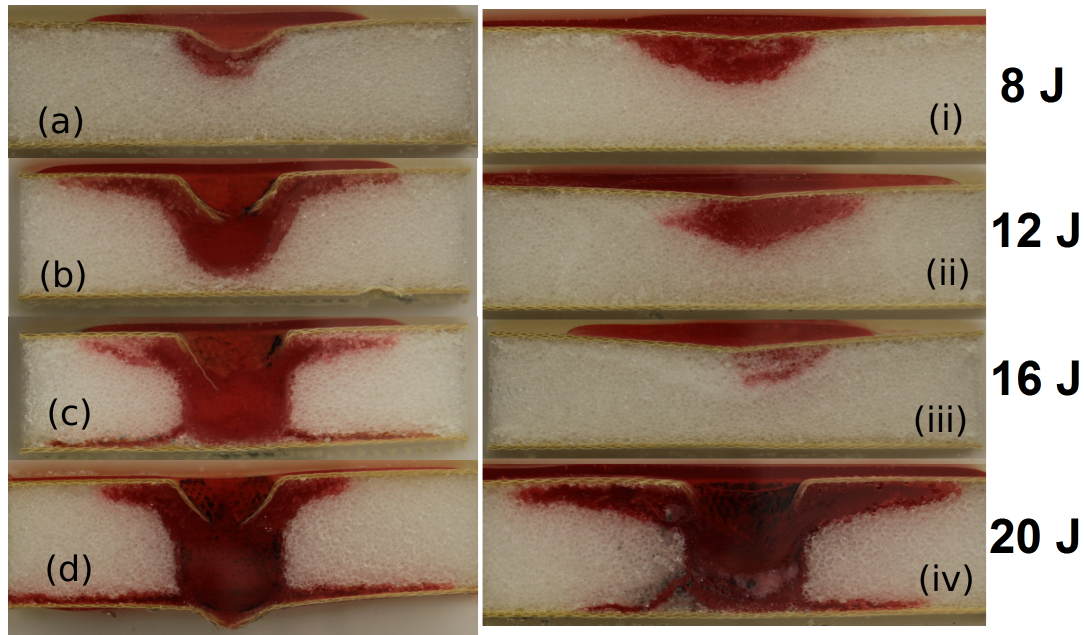


**Figure 3.17.** Cross section of the Kevlar sandwich samples after impact test: (Left) KR sandwich and (Right) KNR sandwich

KNR samples for the same energy levels. After impact at 16J, there is extensive disbonding between the core and the lower facesheet in the Kevlar sample with neat resin, but none in the nano-reinforced Kevlar sample. It can also be seen that at 20J, the bottom facesheet of the KR sample is severely damaged, while that of the KNR sample is still intact which would allow for more energy to be dissipated before complete failure of the sandwich plate.

Three damage parameters, indicative of the extent of damage, have been identified for measurement from the sections of the impacted specimen as shown in Figure 3.18. Definition of damage parameters figure.3.18. They are:

1. Depth of indentation of the top facesheet ( $d_1$ )
2. Depth of indentation of the core ( $d_2$ )
3. Width of debonding between facesheet and core ( $l_1$ )

Figures 3.19 Damage parameters measured from section of the sandwich sample (a) Depth of facesheet  $d_1$ , (b) Depth of core  $d_2$  and (c) Extent of damage  $l_1$  figure.3.19 shows the comparison of these damage parameters for the KR and KNR sandwich plates. It can be seen for KR sandwich plates that both the depth of indentation in facesheet and core ( $d_1$  and  $d_2$ ) exhibit an increasing trend with initial energy

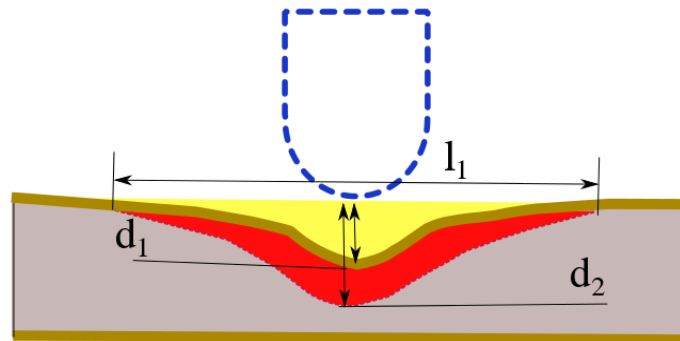


**Figure 3.18.** Definition of damage parameters

while the KNR sandwich shows an almost constant value for impacts up to 16J. At 20J of energy, there is significant jump in both  $d_1$  and  $d_2$  for the KNR samples. It is also clear that depths of indentation of the facesheet and the core are much larger in the KR samples than the KNR samples, at least for energies up to 16J. The higher values observed for the KR sandwich plates are due to the more local damage observed in them. The extent of damage  $l_1$  which corresponds to the amount of debonding between the top facesheet and the core have higher values for KNR sandwich plates which confirm that the load is spread over a larger area in the sandwich plate with nano-reinforcements. It should be noted that there are some challenges in quantifying these parameters precisely and a qualitative comparison of the damage parameters is more appropriate.

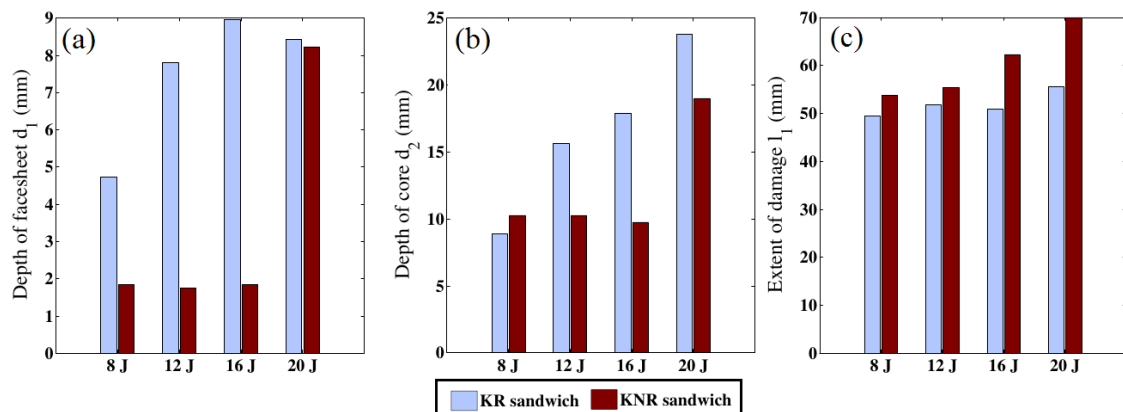


**Figure 3.19.** Damage parameters measured from section of the sandwich sample (a) Depth of facesheet  $d_1$ , (b) Depth of core  $d_2$  and (c) Extent of damage  $l_1$

In addition to the above damage parameters, the core cavity represented by area of the red region in the core in the schematic diagram has also been plotted in Figure 3.20. Core cavities in impacted Kevlar sandwich panels figure.3.20. Both the KR and KNR sandwich samples show a clear trend of increasing core cavity damage with higher energies. It is however difficult to make any comparisons between the two types of sandwich plates. This is because the core damage is more spread out in width, in general, in the KNR samples than in the KR samples; while the damage in the latter goes much deeper. Obviously the depth of core damage seems to be more critical in determining the load capacity of the sandwich panel, since (a) even when the upper facesheet is damaged it can carry significant load, preventing the impactor from penetrating deeper and (b) the depth of damage in the core determines when the damage reaches the bottom facesheet and it starts getting damaged. It would therefore appear that the area of core cavity is not a good indicator of the severity of damage, unlike the depths of indentation of the facesheet and the core.

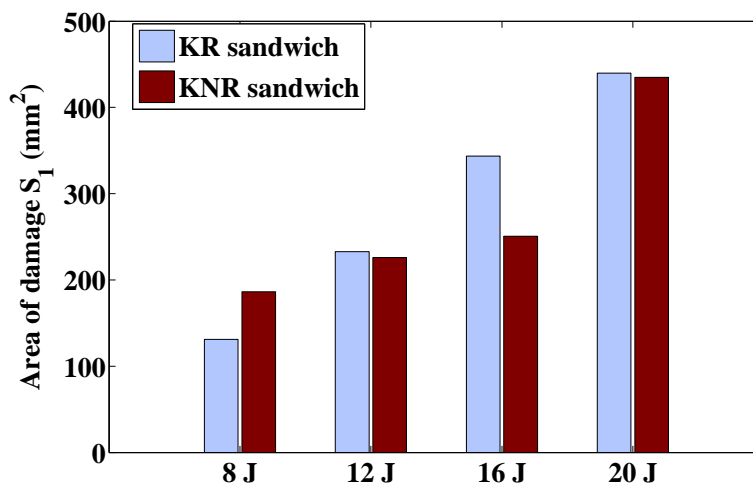
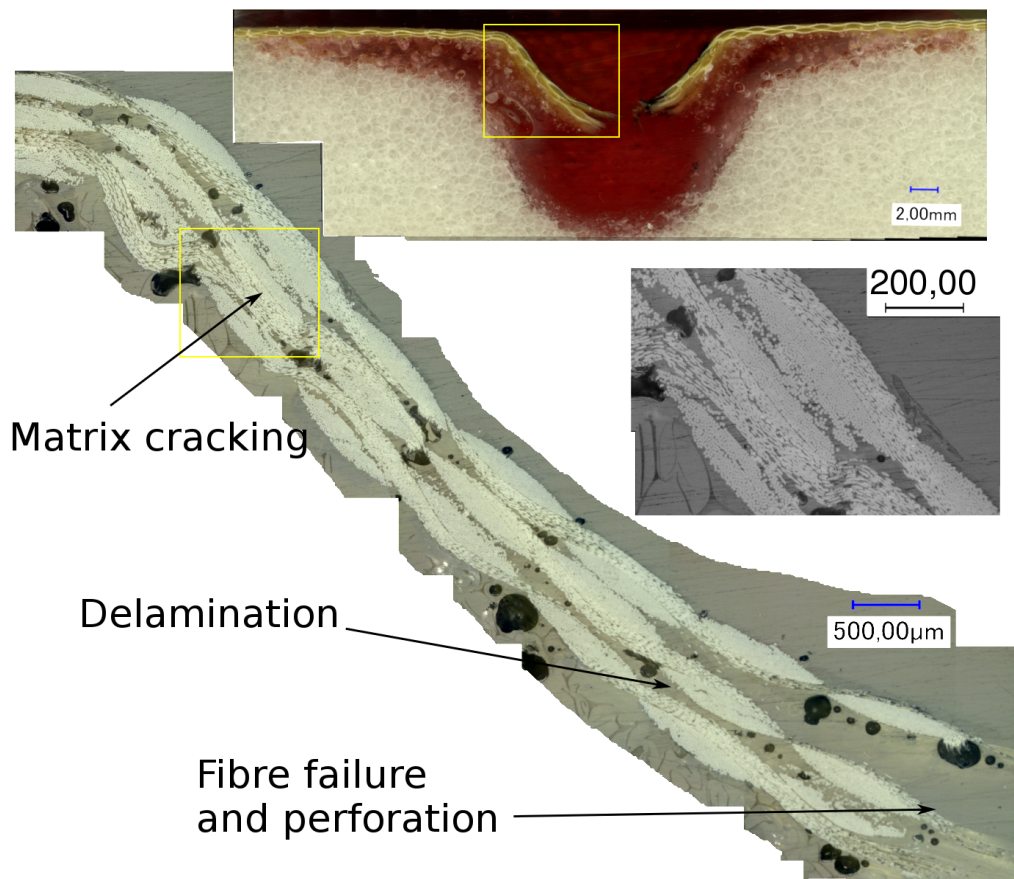


Figure 3.20. Core cavities in impacted Kevlar sandwich panels

### 3.4.3 Microscopic observation of damage

The section of the sandwich plate is also observed under an digital optical microscope. Microscopy reveals the three prominent modes of failure in the top facesheet; matrix cracking, delamination, fibre breakage and perforation. Sections of the KR sandwich plate viewed under an optical microscope after an impact of 12 J is shown in Figure 3.21. Microscopic observations of section of KR sandwich (12 J

impact)figure.3.21. The image shows the three plies of the Kevlar facesheet and it is possible to discern the wavy weft of the plain woven fabric ( $0^\circ$ ) and the warp ( $90^\circ$ ) is visible as fibre bundles. It can be seen that the damage in the KR sandwich plate was concentrated in the indentation zone corresponding to the dimensions of the impactor. Fibre breakages are clearly visible close to the point of impact. In the second zone, a gap can be detected between the three layers of the Kevlar fabric, corresponding to the delamination failure. Finally, matrix cracking is observed in the  $90^\circ$  fibre yarns.



**Figure 3.21.** Microscopic observations of section of KR sandwich (12 J impact)

Microscope images of KNR sandwich plate after an impact of 16 J is shown in Figure 3.22. Microscopic observations of section of KNR sandwich (16 J impact)figure.3.22. A high density of matrix cracks between  $90^\circ$  fibre yarns is observed in the sandwich

plates with nanoparticles. These matrix cracks are mainly responsible for the dissipated energy. It is hypothesised that these matrix cracks and the resulting delamination are responsible for the increase in dissipation of the impact energy before initiation of fibre failure. It is also interesting to note that the matrix cracks are not limited to the impact zone but are present farther from the point of impact as well.

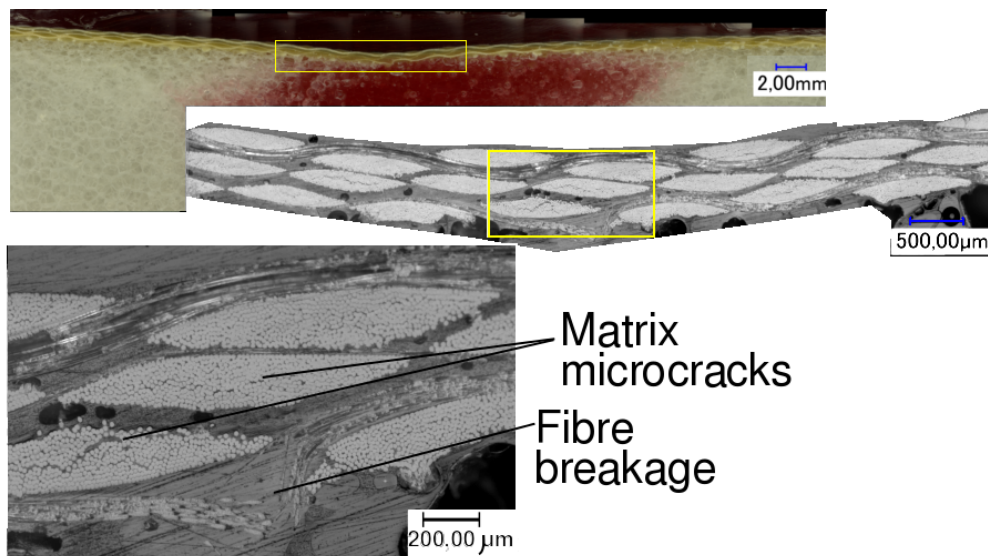


**Figure 3.22.** Microscopic observations of section of KNR sandwich (16 J impact)

Figure 3.23(a) Uncrushed and (b) crushed cells of PMI foam (impact of 12 J) figure.3.23 shows the uncrushed and crushed cells of the Rohacell foam core for 12 J impact. Buckling of the cell walls can be clearly observed in the crushed core. The foam core plays an important role in the energy absorbed by the sandwich structure as a large amount of energy is dissipated in the core crushing.

### 3.5 Results of low velocity normal impact tests of Glass - Rohacell sandwich plates

Drop tower impact tests were conducted on sandwich panels with Rohacell foam core and Glass FRP facesheets with and without nanoparticles in the resin. Results of the low velocity impact tests with the 16 mm diameter hemispherical impactor on square sandwich plates with facesheets containing five layers of Glass fibre reinforced epoxy and a Rohacell foam core are presented in this section. The experimental conditions are identical to the impact test on Kevlar- Rohacell sandwich plates.

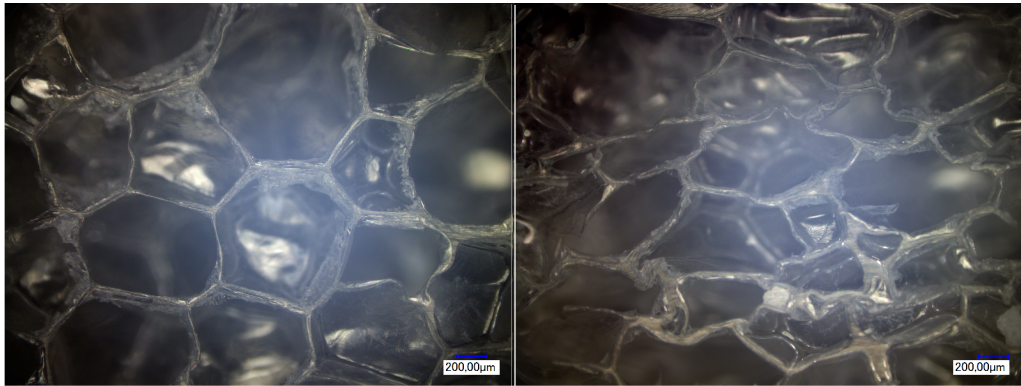


**Figure 3.23.** (a)Uncrushed and (b)crushed cells of PMI foam (impact of 12 J)

Figures 3.24 Force - displacement curve of GR and GNR sandwich for impact energy of 4J figure.3.24, 3.25 Force - displacement curve of GR and GNR sandwich for impact energy of 8J figure.3.25 and 3.26 Force - displacement curve of GR and GNR sandwich for impact energy of 16J figure.3.26 show the Force- displacement curves for Glass fibre sandwich plate impacted from a height of 0.25 m, 0.5 m and 1 m corresponding to impact energies of 4 J, 8 J and 16 J. The sandwich plates with the neat resin and Glass fibres are designated GR sandwich plate (to denote Glass-Rohacell sandwich) while the plates with Nanostrength embedded in the epoxy matrix are designated GNR sandwich plate (Glass-Nanostrength-Rohacell sandwich).

The lower drop height of 0.25 m was chosen in addition to the 0.5 and 1 m tested in the Kevlar sandwich plate because the Glass fibres are considerably weaker than the Kevlar fibres. It can be observed from the force- displacement curves that the elastic stiffness has not changed dramatically for the sandwich plate due to the addition of copolymers. This is similar to the results observed in the Kevlar sandwich composites and is significant because according to the literature the toughening of the resin with rubber particles resulted in a considerable loss of stiffness. It can be seen that at the lowest impact energy of 4 J, the sandwich plate with Nanostrength has a slightly higher peak force when compared to the Glass sandwich without the nanoparticles; 1557 N compared to 1473 N for the sandwich with neat resin, only a 5% difference.

The sharp drop in force after the peak marks the beginning of fibre breakage. For the higher energy of impact shown in Figures 3.25 Force - displacement curve of GR and GNR sandwich for impact energy of 8J figure.3.25 and 3.26 Force - displacement

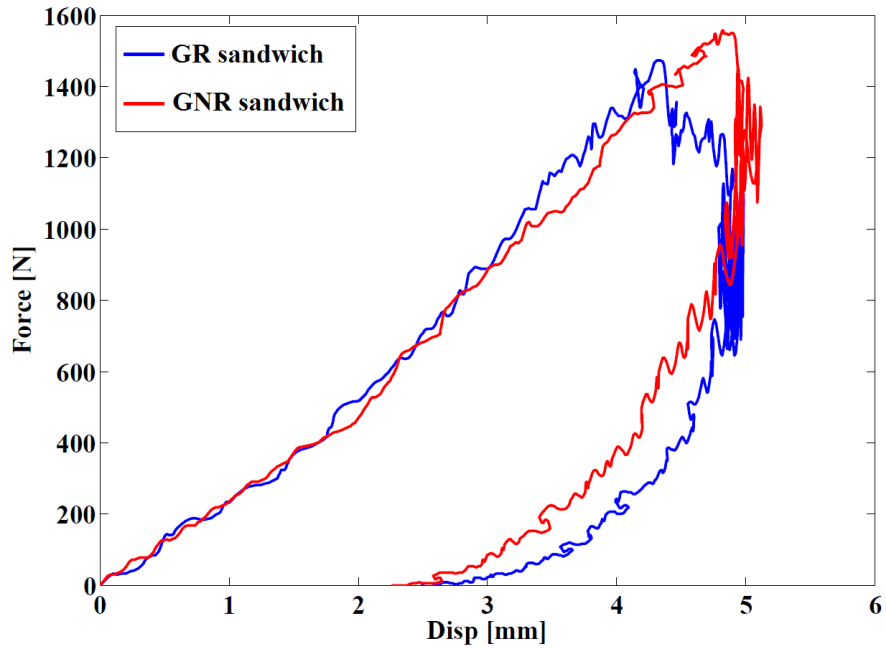


Figure 3.24. Force - displacement curve of GR and GNR sandwich for impact energy of 4J

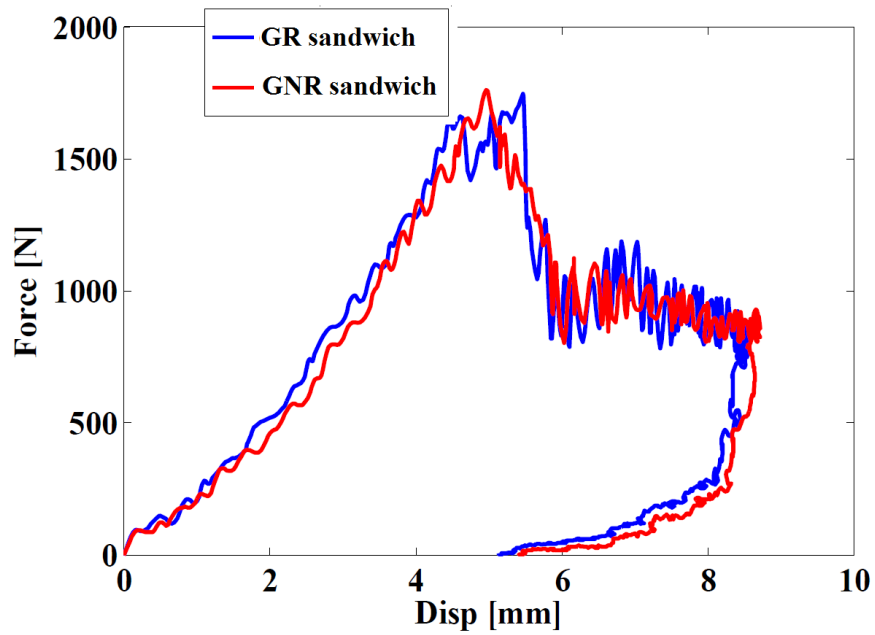
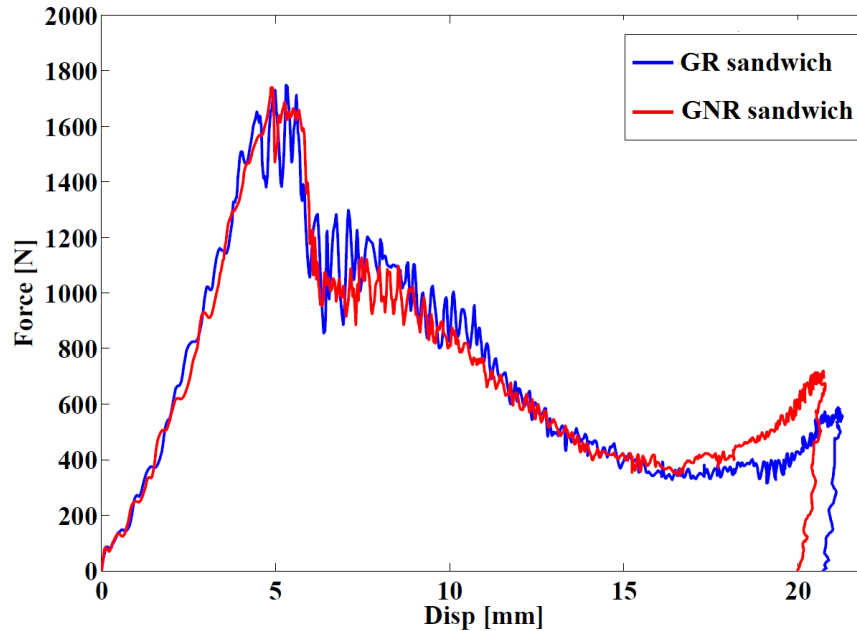


Figure 3.25. Force - displacement curve of GR and GNR sandwich for impact energy of 8J



**Figure 3.26.** Force - displacement curve of GR and GNR sandwich for impact energy of 16J

curve of GR and GNR sandwich for impact energy of 16Jfigure.3.26, there is no significant difference between the two sandwich plates in terms of peak force; 1746 N and 1761 N for the neat matrix and Nano matrix respectively. There is marginally more elastic recovery in the sandwich plates with Nanostrength but the improved behaviour observed in the KNR sandwich plates are not obtained. It can be seen that the top facesheet of the Glass/Nano - Rohacell sandwich is not able to prevent perforation and undergoes rupture at the same peak force as the sandwich with neat resin.

Photographs of the top facesheet of the GFRP sandwich panels after impact are shown in Figure 3.27Top surface of the GR and GNR sandwich samples after impactfigure.3.27. It can be observed that there is no perforation of the top facesheet at the lower impact energy of 4 J (drop height of 0.25 m) but as the energy of impact increased, there was perforation of the top skin. It is interesting to note that there is no visible difference between the failure in the samples with neat resin and the samples with Nanostrength embedded in the resin. This supports our observation from the force- displacement curves that there is no significant effect of the block copolymers on the impact behaviour of the sandwich panels with GFRP facesheets.

There was no damage visible on the bottom facesheets for the impact energies tested and they are not considered for comparison.

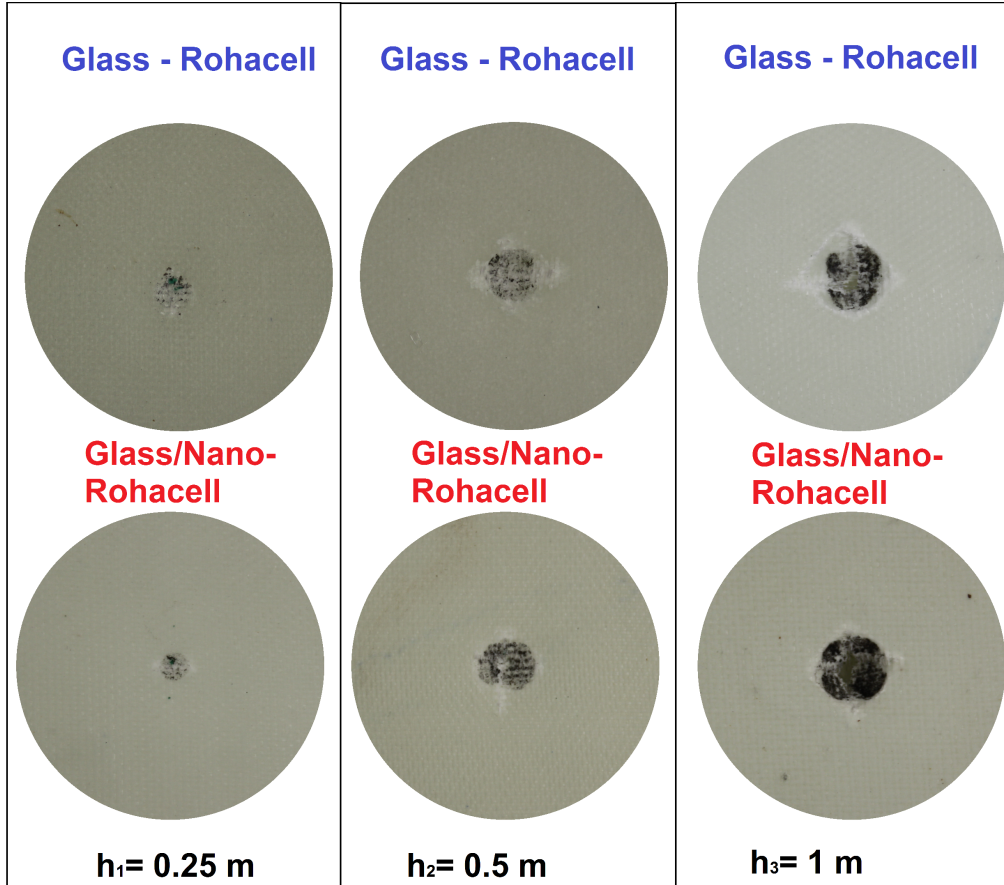


**Figure 3.27.** Top surface of the GR and GNR sandwich samples after impact

Figures 3.28(a) Peak force and (b) Maximum displacement of GR and GNR sandwich samples after impact figure.3.28(a) and (b) respectively, show the peak force and maximum displacement of the GR and GNR sandwich plates for the initial impact energies of 4 J, 8 J and 16 J. It can be seen that the peak force for both the GR and GNR sandwich plates increase with increasing impact energy but have a reached their maximum limit for 8 J impact and there is no increase of the peak force for higher energy of impact. This can be explained by the fact that there was fibre perforation of the top facesheet for these impact cases. The trend of maximum displacement, on the other hand, shows consistently higher values with increasing impact energy. These large displacements are mainly related to the crushing of the Rohacell foam core, but will also contain a component of increased

global bending of the panels due to the reduction of bending stiffness. There was no appreciable difference between the sandwich plates with neat resin and the panels with Nanostrength.

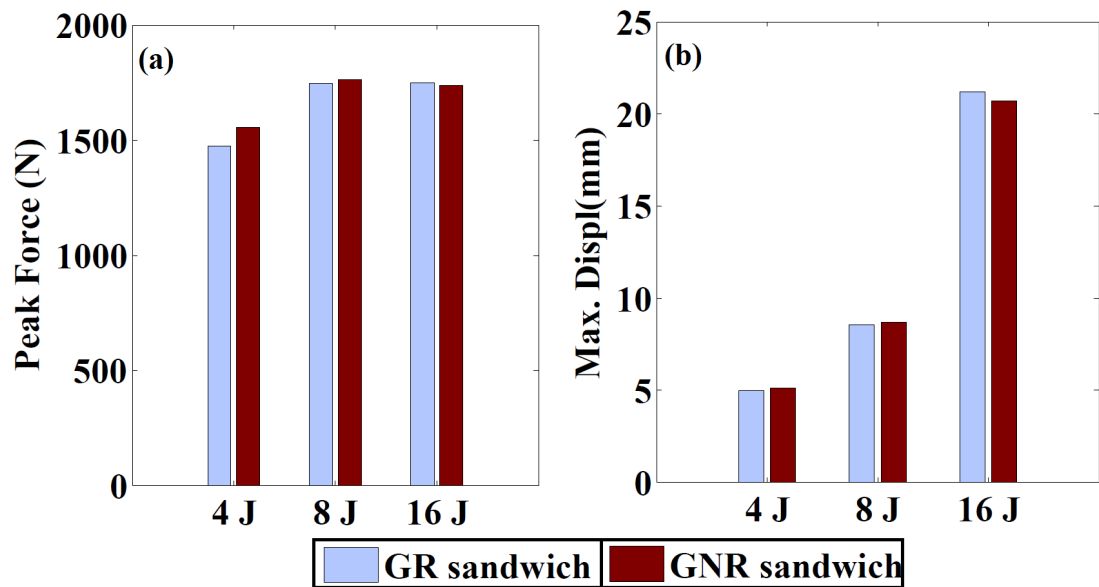


**Figure 3.28.** (a) Peak force and (b) Maximum displacement of GR and GNR sandwich samples after impact

The energy required to initiate failure, computed as the integral of the force-displacement curve up to the displacement corresponding to the peak force and the total energy dissipated during the impact of the sandwich panels with GFRP facesheets, corresponding to the area under the force - displacement curve from the beginning of impact until the end of unloading phase are shown in Figure 3.29(a) Energy upto peak force and (b) Total energy dissipated by GR and GNR sandwich samples with and without nanoparticlesfigure.3.29.

It is observed that the elastic energy has similar trend to the results presented for the addition of Nanostrength in Kevlar sandwich panels. The effect of the addition of nano-block copolymers on energy for damage initiation is however not increasing for higher impact energies. Similarly, the total energy dissipated follows the results observed for Kevlar sandwich plates but the effect is less pronounced (about 2%). This is because the mode of failure has not changed for the sandwich panels with Nanostrength in the matrix. Both the sandwich plates with neat resin and Nano resin have fibre perforation in the top facesheet followed by core crushing.

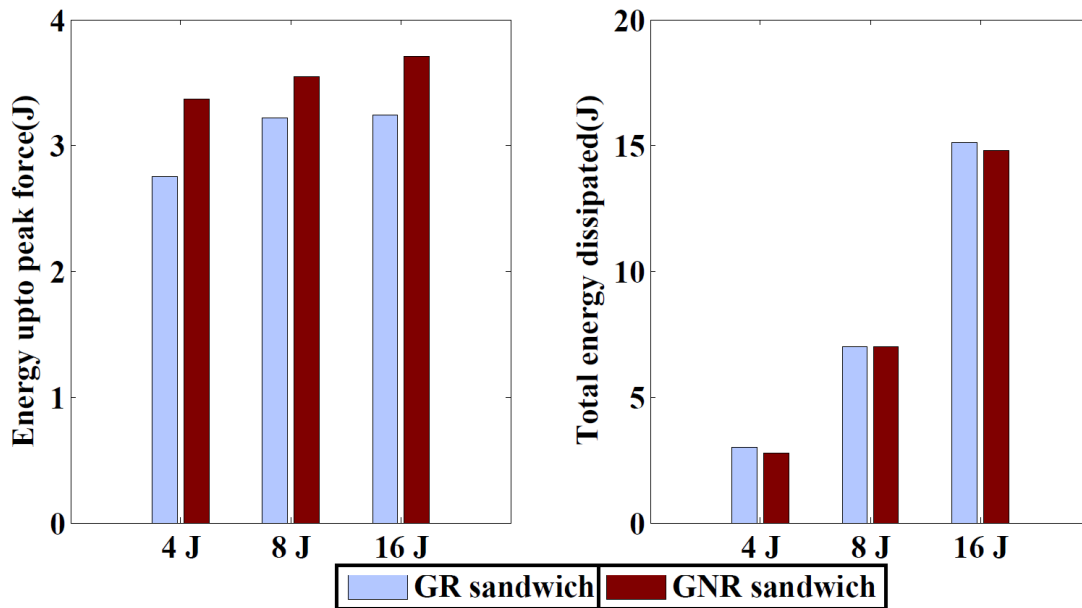


**Figure 3.29.** (a) Energy upto peak force and (b) Total energy dissipated by GR and GNR sandwich samples with and without nanoparticles

### 3.6 Comparison of Kevlar- Rohacell and Glass- Rohacell sandwich

The effect of the block copolymer nanoparticles on the impact resistance of sandwich panels made with Kevlar facesheets are compared with Glass FRP sandwich plates. A comparison of the Force- displacement response of the Kevlar-Rohacell sandwich and Glass-Rohacell sandwich, both with neat resin and with Nanostrength, for an impact of 16 J (i.e. drop height of 1 m) is shown in Figure 3.30. Comparison of Force-displacement curve for Kevlar and Glass sandwich for impact of 16 J figure.3.30. The stiffness represented by the initial linear part of the Force- displacement response of GR and GNR sandwich is higher than the KR and KNR sandwich plates. The peak force of the KR and GR sandwich samples (with neat resin) have values of 2040 N and 1743 N respectively but they follow a similar pattern of peak and post-peak response associated with fibre failure and perforation in the top facesheet and extensive core crushing. The maximum displacement values are almost identical at 21.4 mm. However, the response of the sandwich plates with the Nanostrength modified resin is very different. While the KNR sandwich has a higher peak force of 3120 N and some elastic recovery to have final displacement of 5.5 mm, the GNR

sandwich plate follows the same trajectory as the GR plate with a peak force of 1740 N and post-peak response characterised by sudden drop due to the perforation and large displacement of the impactor due to core crushing similar to the sample with neat resin.

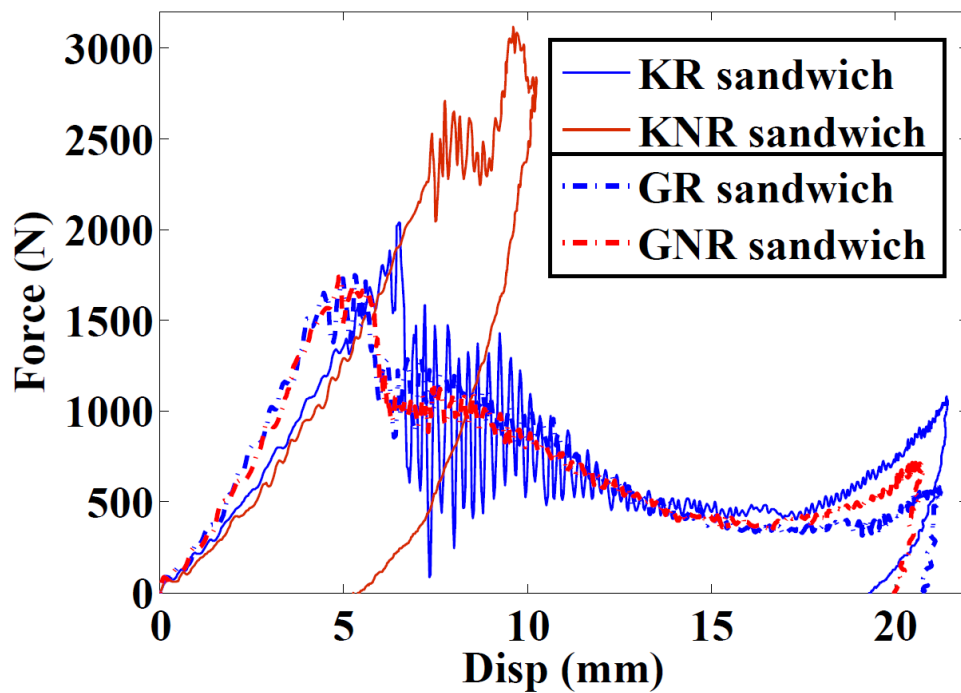


**Figure 3.30.** Comparison of Force- displacement curve for Kevlar and Glass sandwich for impact of 16 J

The results presented for the sandwich panels with the Kevlar and Glass FRP facesheets are compared with the drop tower test results published by Sébastien Denneulin et al. [5] and Rodrigue Boumbimba et al. [76] who studied the low velocity impact behaviour of composite plates made of Kevlar and Glass fibres, respectively. The setup and sensors used by them are the identical to experimental conditions explained in the previous section with the only difference being that the second high-speed camera was used to observe the bottom surface of the composite. It should be noted that while their project was focussed on the behaviour of composite plates, the focus of my PhD thesis is on the behaviour of sandwich plates where such composites were used as facesheets.

Figure 3.31 Force history and bottom surface of the impact on Kevlar plates with and without Nanostrength [41] figure.3.31 shows the Force vs. time response obtained from the drop tower impact tests on Kevlar  $[0 - 90]_3$  composite plates with and without nanoparticles for a drop height of 0.5 m and images from the second high-speed camera (Photron SA3) which was used to observe the bottom surface of the composite plate with a mirror placed at  $45^\circ$  angle below the clamping fixture. The images correspond to different points during the impact (Images (i, ii, iii and iv) are for the Kevlar plate with neat resin and images (a, b and c) are for the Kevlar plate with 10% M52N Nanostrength). The image (ii) shows the beginning of the damage propagation in the composite with neat resin which is clearly visible in image (iii). The image (b) corresponds to the peak force and the beginning of the unloading phase for the Kevlar composite plate with nano resin. It can be observed that the Kevlar plate with Nanostrength do not show any sign of perforation, while the impactor is clearly visible after perforation in the Kevlar plate with neat resin. The Kevlar with neat resin has a peak force of 1.6 kN while the peak force of the Kevlar with Nano resin is 1.88 kN, an increase of 17.5%.

A similar investigation was done for composite plates with Glass  $[0 - 90]_5$  FRP with neat resin and nano-modified resin [76]. It can be observed from the Figure 3.32 Force history and bottom surface of the impact on GFRP plates with and without Nanostrength [76] figure.3.32 that while the addition of the nanoparticles did not prevent the perforation of the composite in this case, there were still differences in the force- time history between the composites with neat resin and nano resin. Fibre breakage, which can be observed in image (ii) for the neat resin sample and image (b) for the nano resin sample is marked by strong decrease in force due to a loss of rigidity and resistance in the composite structure. The fibre breakage is a brief phenomenon of duration less than 1 ms. Boumbimba et al. [76] have reported an improvement of 25% in the force required to initiate damage and a 33% increase in  $F_{max}$ . In fact, both  $F_{init}$  and  $F_{max}$  increase from 1195 N and 1250 N to 1530 N and 1665 N, respectively, with the addition of 10% wt. of Nanostrength. It was also reported that the dissipative energy, corresponding to the area of the force displacement curve also increases with the addition of Nanostrength. Boumbimba et al. [76] concluded that the improvements in the energy absorbed and impact resistance while not as high as for Kevlar were not insignificant for Glass fibre composite laminates.

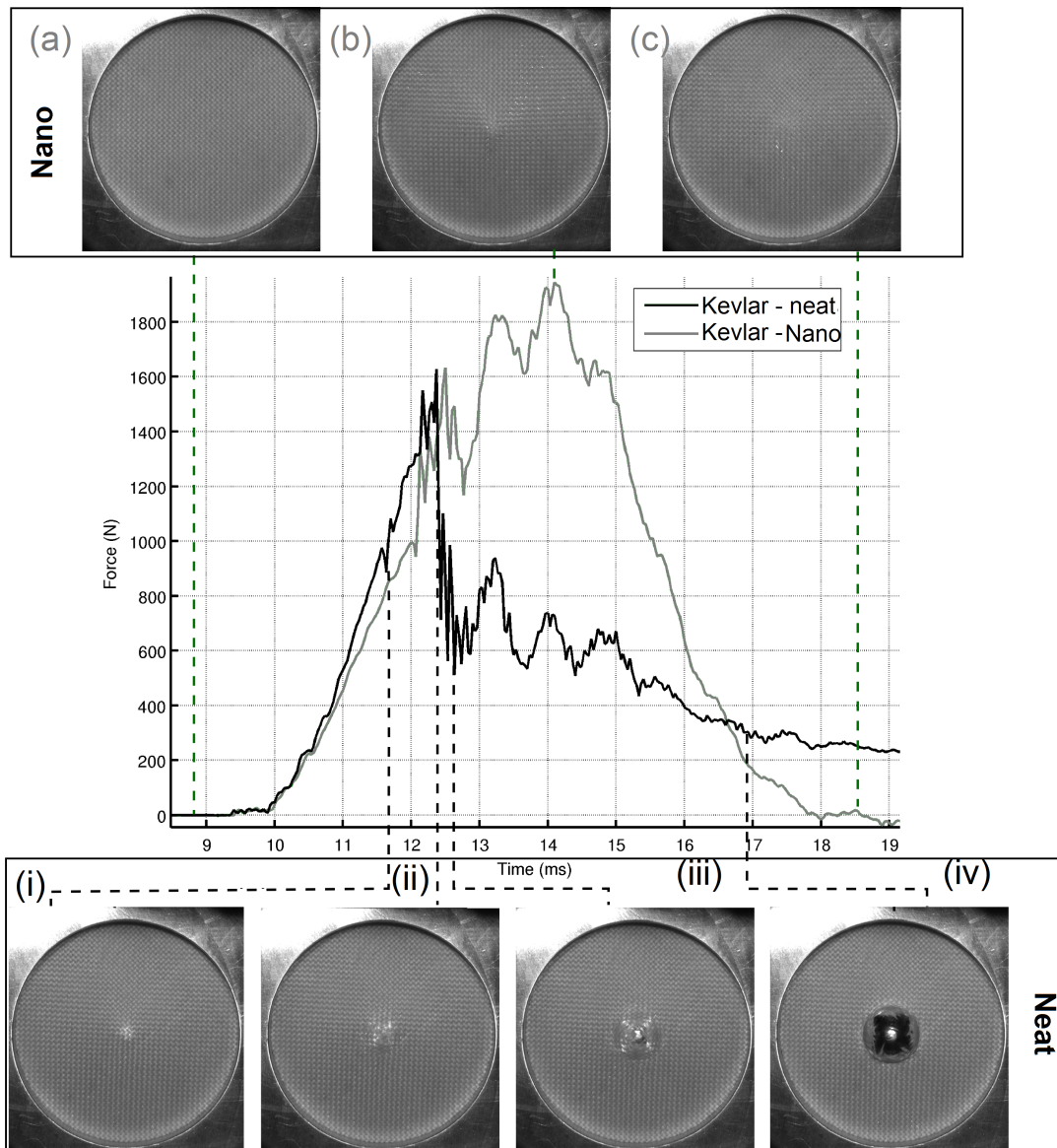


**Figure 3.31.** Force history and bottom surface of the impact on Kevlar plates with and without Nanostrength [41]

These prior investigations on the effect of nano block copolymers on impact resistance of Kevlar and GFRP composite laminates indicate that Nanostrength has significant beneficial effect for both materials, with prospective applications in manufacturing helmets, boat hulls and aerospace structures. However, the results of drop tower tests on sandwich panels with Glass FRP facesheets with and without

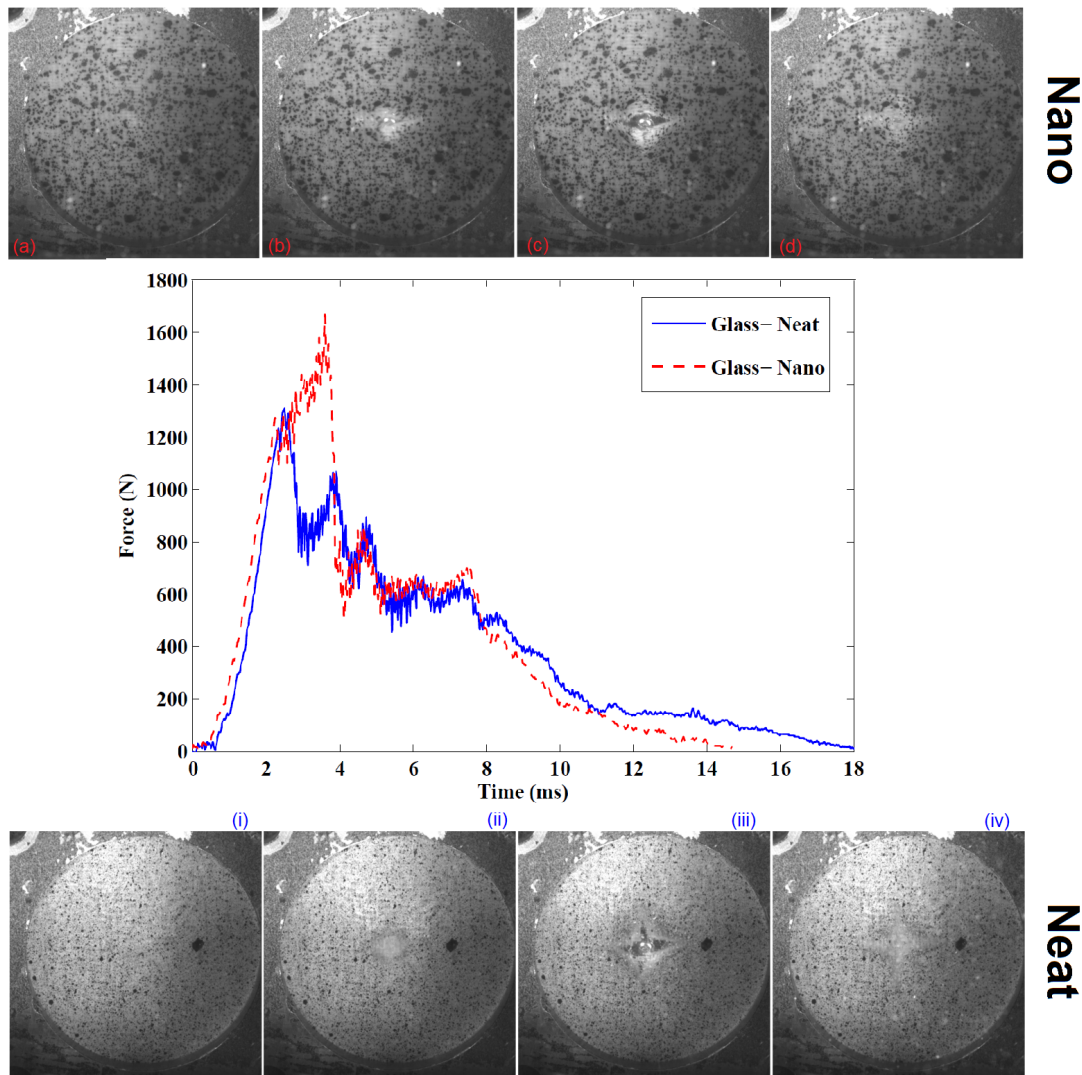


**Figure 3.32.** Force history and bottom surface of the impact on GFRP plates with and without Nanostrength [76]

Nanostrength seem to suggest that the block copolymer reinforcements do not improve the impact resistance of these sandwich panels. It was our expectation that the toughening of the resin matrix with the nanoparticles would have similar effect independent of the fibre reinforcements.

A comparison of the force history of the impact on GFRP plates and Glass-Rohacell sandwich panels with and without Nanostrength for an impact of 16 J is given in Figure 3.33. Comparison of the force history of GFRP plates and Glass-Rohacell sandwich panels with and without Nanostrength for impact of 16

Figure 3.33. The peak forces for the sandwich panels are higher than those for the GFRP laminate; 1749 and 1740 N the Glass fibre sandwich panels with neat resin and Nano resin, respectively compared to 1310 and 1670 N and for the GFRP laminates tested by Boumbimba et al. [76]. Both the composite laminates and the sandwich panels exhibit similar modes of fibre failure as observed from the sharp drop in the force after the peak values. The sandwich panels exhibit a second rise in the contact force, which is typical of the densification of the core below the point of impact.

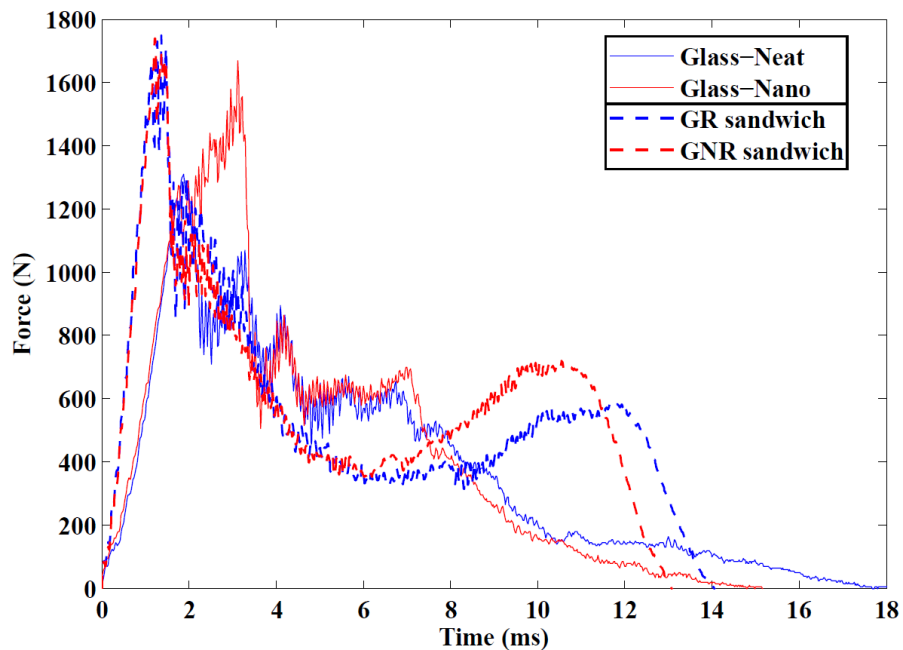


**Figure 3.33.** Comparison of the force history of GFRP plates and Glass-Rohacell sandwich panels with and without Nanostrength for impact of 16 J

The addition of the nano block copolymers did not alter the macroscopic failure modes observed in the Glass fibre laminates or in the sandwich panels where such laminates were used as facesheets. The laminates, however show a clear improvement in terms of peak force and energy absorbed which are not apparent for the sandwich panels. The cause of this phenomenon is not clear but several reasons have been hypothesised. It is possible that the glass fibres fail before a threshold stress for delamination initiation and this results in the Glass fibre reinforced composite facesheet having no time for the improvement of the resin by the addition of the nanoparticles. On the other hand, the aramid fibres in Kevlar have a greater

strain to failure, which could provide an opportunity for the improvement in the ductility of the matrix to have an effect. The fibre- matrix adhesion of Kevlar is notoriously weak when compared to Glass- epoxy and it is possible that the addition of the Nanostrength improved this adhesion and thus provided enhanced impact resistance. A strong composite interphase, which is the region between the fibre and the matrix, promotes the involvement of the fibre and thus increases the composite strength. It has been shown that at high level of fibre -matrix adhesion failure is initiated by matrix cracks. It has also been argued that the improvement in interlaminar shear strength can have inverse relation to impact resistance [77]. A strong interface bond results in a brittle composite as effective crack diverting is inhibited. Several researchers are investigating the fibre-matrix interphase and their effect on mechanical properties [77–79]. Wichmann et al. [72] postulated that the fibre volume fraction is also a significant factor in determining the effectiveness of nano-reinforcements. It should also be noted that Denneulin [5] found that different formulations of the same triblock copolymer (MAM) had different effect on Kevlar composite laminates, with M22N and M42N formulations not improving the impact resistance appreciably compared to M52N Nanostrength.

This is a fertile area of enquiry and more work needs to be done to better understand the effect of the nano block copolymers on different composites. The research group at DuMAS in I2M laboratory and the industrial partners at Arkema and Thales have shown interest in pursuing this line of enquiry. However it is beyond the scope of this project and has been identified for future work. In the rest of the thesis, the focus is on sandwich composites with Kevlar facesheets as they have shown considerable promise for modification by the block copolymers.

### 3.7 Summary

The objective of this chapter was to evaluate the effect of including block copolymer nanoparticles to the matrix on the low velocity impact behaviour of sandwich composites based on Kevlar and Glass fibre reinforced epoxy and Rohacell<sup>®</sup> foam. A 10% M52N Nanostrength<sup>®</sup> triblock copolymer was chosen for the study. The method of manufacturing the sandwich panels with neat and nano-modified resin was presented. A drop tower setup was used to conduct low-velocity impact tests with normal incidence on the two types of sandwich plates at different initial energies. The effect of the nano-reinforcements on the sandwich plates under normal

impact was firstly studied at the macroscopic level based on the Force -displacement curves and visual examination of the samples after impact. While the KR sandwich plate failed by fibre failure and perforation, no perforation was detected in the top facesheet for the sandwich plate with nano-reinforcements for the same impact energy. KR sandwich plates exhibited perforation of top facesheet for impact at 12 J whereas KNR sandwich plates did not have perforation even at 16 J impact. The Glass fibre sandwich showed no significant improvement for the addition of the nanoparticles in the resin. Some possible reasons for this behaviour were posited but were not pursued. It is beyond the scope of this project and has been identified for future work. The focus of the thesis is therefore on sandwich composites with Kevlar facesheets as they have shown considerable promise for modification by the block copolymers. A comparison of the Kevlar sandwich panels in terms of the energy absorbed by the panel was undertaken. The KNR sandwich plates required higher energy to fail and also did not exhibit perforation failure of the facesheets as the sandwich plates without the nano-reinforcements. The damage in the foam core was also not localised in the impact zone but was spread across a significant part of the structure. Different damage parameters were described to compare the two types of sandwich structures. Optical microscopy was undertaken to observe the different failure mechanisms in the Kevlar facesheet and the foam core. It was observed that the damage phenomena in the KNR sandwich plate consist mainly of matrix cracking and it is proposed that this may explain the improvement in impact resistance. It can be concluded that the M52N elastomeric nanoparticles significantly improved the resistance of Kevlar FRP sandwich structures under low velocity impact. In the next chapter, a numerical model is developed to simulate the low velocity impact at normal incidence of Kevlar- Rohacell sandwich plates.



## Chapter 4

# Finite Element modelling of low velocity impact response of composite laminates and sandwich panels

### 4.1 Introduction

Experiments are time consuming, expensive and require ancillaries such as strain gauges and high speed cameras to find stress and deformation state of the structure. Extensive experimental testing is not practical also because these tests provide response data for particular plate and loading conditions and do not provide adequate information about the effect of a wide range of variables. Further, predicting the response of sandwich plates is complicated due to effects such as material and geometric non-linearities, transverse shear effects and multiple and coupled damage modes [80]. These problems and cost of experimentation can be avoided by using numerical methods, which can help in predicting the energy absorption and peak loads for a given combinations of materials and geometry by considering competing mechanisms [81–83]. The combination of improved constitutive modelling of constituents and decreased computational costs make it possible to utilise continuum modelling of sandwich composites to numerically simulate impact response for a much wider range of impactor geometries and velocities [84]. A comprehensive review of analytical models has been given in [34], classifying the previous studies into three categories: (1) energy-balance models that assume a quasi-static behaviour of the structure; (2) spring-mass models that account for the dynamics of the structure in a simplified manner; and (3) complete models in which the dynamic behaviour of the structure is fully modeled. According to Feng and Aymeric [85], the complexity of physical phenomena involved in an impact event restricts the applicability of analytical models to the investigation of simple geometries and loading cases. However, numerical finite element (FE) tools based on appropriate fracture models may provide an efficient alternative to costly experimental tests for prediction of the impact response of sandwich composite structures. Finite element method

(FEM) has become the prevalent technique used for analyzing physical phenomena in the field of structural, solid, and fluid mechanics as well as for the solution of field problems [80]. In this chapter, an overview of the current state-of-the-art on finite element modelling of sandwich panels is presented. An FE model is developed using LS-Dyna software for the simulation of normal impact on Kevlar composite laminates and sandwich panels with Kevlar facesheets and Rohacell foam core. The developed numerical model is validated by comparison to experimental data.

## 4.2 Review of finite element method for simulation of impact of sandwich composites

The finite element method has been an important way to study the impact dynamics of foreign objects on sandwich structures. It is cost-saving and time efficient compared to experiments, and it can be used to model more complex structures and boundary conditions and obtain a more realistic distribution of stress and damage progression compared to an analytical approach. The modelling of damage in facesheets and core material has been a key factor in FE analysis of the impact event [51]. Collombet et al. [86] studied the impact behaviour of laminated composites using a hybrid approach which combined experimental tests and numerical modelling (within the explicit FE code, PLEXUS) to predict matrix cracking and delamination in glass-epoxy laminated plates when subjected to heavy mass/low velocity impact. A finite element (FE) analysis provides the capability to model the impact event, including the complex internal damage mechanisms in a relatively short time [87] and can help in predicting the energy absorption and peak loads for a given combinations of materials and geometry. The contribution of the individual elements of the sandwich panel to the energy absorption can also be obtained. Nemes and Simmonds [84] developed a methodology based on knowledge of the constitutive behaviour of each of the constituents of the sandwich, namely, the core, facesheets, and bond layers to predict the response of foam-core sandwich composites to low velocity impact.

The modelling approaches used for sandwich panels and shells can be divided into four categories: detailed models; three-dimensional continuum models; two-dimensional plate and shell models; and simplified models [88]. The numerical modelling of FRP composites is possible in different scales as shown in Figure 4.1 Scales considered for composite plates [89] figure.4.1: micro, meso and macro scales [89].

At the microscopic scale, a Representative Element Volume (REV) is defined at the level of basic components; the fibre, matrix, the interphase and optionally voids. By modelling the interaction between the fibre and the matrix, obtained by means of patterns, the behaviour of a strand can be simulated. At the mesoscopic scale, the REV is defined at the level of the strand and individual fibres and the matrix is no longer discernible. This scale allows us to understand the behaviour of a part of the fold or part of composite (in the case of thin composites). The simulation of composites at the meso-scale using physically based anisotropic material models for modelling the individual plies and cohesive interface elements for modelling delamination can result at a better understanding of laminate behaviour [89]. Each layer of the composite is modelled in the case of the macroscopic scale model. Modelling at the macroscopic scale considers the layer as homogeneous and therefore the phenomena occurring within the layer must be defined implicitly through the material law. The simplest models consider only the elasticity of the composite and more complicated material laws take into account a large number of phenomena such as damage and viscoplasticity. According to May et al. [89], micro-mechanical simulations require a high resolution and significant computational power. Modelling of impact onto a composite wing at the micro-scale, capturing all these effects is currently not feasible, with multi-scale modelling being one possible solution.

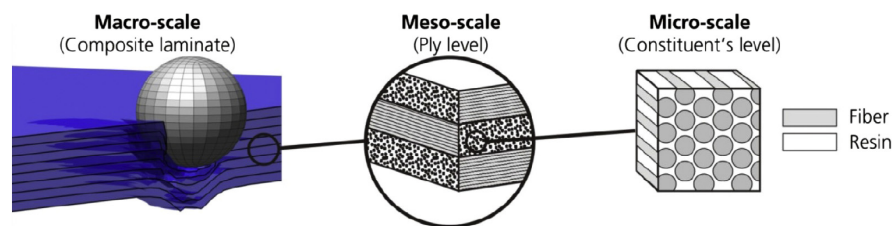


**Figure 4.1.** Scales considered for composite plates [89]

Numerical models for the low velocity impact analysis of sandwich plates have been developed using different finite element software by [29,81–83,90]. The state-of-the-art FE codes used to predict damage of composites and metallic materials subjected to impact loading are LS-DYNA, ABAQUS Explicit, RADIOSS, and PAM-CRASH [91]. The analysis of the quasi-static behaviour or the low-velocity impact performance of foam-cored sandwich structures using numerical models require failure criteria to predict the failure of the composite facesheets, and a crushable foam

model for the core [29]. The challenge is to simulate, with the same model, damage during impact and in particular permanent indentation, and the residual mechanical characteristics after impact, in order to be able to numerically optimise design of composite structures with impact damage tolerance [82]. Early models such as the one developed by Borsellino et al. [47] with 8-node quadrilateral elements (Plane 82) using ANSYS 5.6 finite element software to simulate Flatwise Compression, Edgewise Compression and 3-point Flexural tests of sandwich beams with different facesheets were limited in their applicability. Though the static-mechanical behaviour of the composite structure was well approximated by numerical simulations in elastic zone, the model did not show a good compatibility with the experimental data at high deformation (plastic regime). Rajaneesh et al. [83] developed a numerical simulation of sandwich plates with a core made of aluminium alloy foam with faceplates made of either aluminium or carbon fibre reinforced plastic (CFRP) using 3D finite element models in LS-DYNA . Nguyen et al. [90] used a Sandmesh tool along with LS-Dyna to construct FE models of honeycomb core sandwich materials. The Sandmesh software allowed the authors to explicitly model each core cell of the honeycomb core using shell elements. Heimbs et al. [92] developed an approach for modelling sandwich structures with a Nomex honeycomb core and phenolic composite faces in LS-DYNA. Zhang et al. [93] developed a numerical model for composite laminate plates to predict the damage (matrix crack and delamination) initiation and propagation in low velocity impact tests using the user subroutine in ABAQUS. A damage evolution law which combines stress-based and fracture-mechanics-based failure criteria was used.

The finite element model developed is usually validated by comparison of the impact force-time history, maximum displacement, specimen damage area, core crushing or buckling behaviour and resulting indentation with the impact experiment [90]. In the Figure 4.2 Validation of FE model by comparison of Force, Displacement and Energy history [87]figure.4.2, the Force- time, Force- displacement and Energy- time response of the sandwich plate was compared with the experimental data to validate the numerical model.

#### 4.2.1 Constitutive laws for composite facesheets

The damage inflicted on the composite facesheet is a complex phenomenon due to the different damage mechanisms involved: matrix cracking, tensile and compressive fibre breakage, delamination, etc., which depend on various parameters

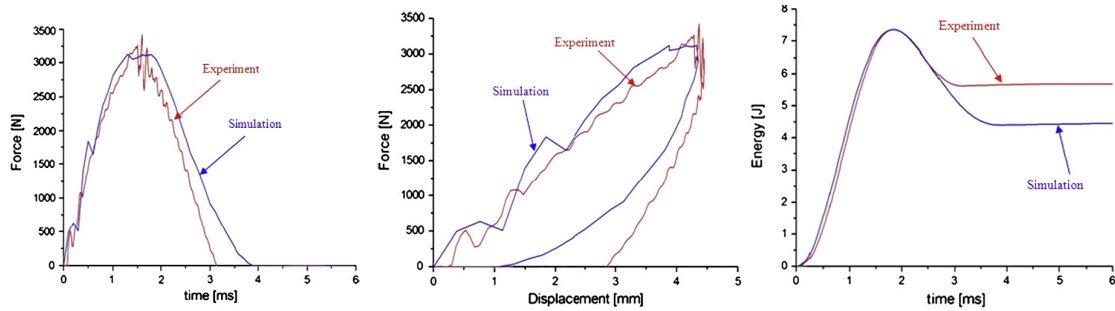


**Figure 4.2.** Validation of FE model by comparison of Force, Displacement and Energy history [87]

including fibre and matrix properties, characteristic of the fibre - matrix interface, manufacturing process, etc. [9]. An accurate FE analysis of a composite structure requires a complex material model capable of capturing the mechanical behaviour of the composite [86]. For example, Shi et al. [87] modelled the damage development in a simple cross ply composite laminate subjected to low velocity impact using a stress-based failure criterion and the damage propagation in the form of intra- and inter-laminar cracking was simulated by energy based criteria. Xiao et al. [94] noted that the existing constitutive models for composite laminates in crash application may be classified into two major categories: micro- mechanics models and phenomenological models. A true micro-mechanics model captures the deformation, damage and fracture of individual fibre yarns, matrix, their interface and interaction in a unit cell based on the constituent properties. The model predicts the overall stress strain response of the unit cell as damage progresses, which is then used in the global model for the element. Phenomenological models, on the other hand, describe the global constitutive behaviour. In fact, most of the material models in FE codes are phenomenological models as it is difficult to model every type of damage and its subsequent softening effects in a complicated 3D microstructure with micro-mechanics models. The plasticity models, for instance, describe the nonlinear deformation through a stress strain relation measured at the macroscopic level. It is also important that the material properties used in the finite element model can be easily obtained from characterisation tests. LS-Dyna has many material models in its library from which to choose the appropriate model.

between the delamination and the matrix cracking damages. Fiber failure was

considered by reducing to zero the longitudinal stiffness when the maximum longitudinal strain is reached. These models were implemented in SAMCEF FE code and very good correlation with the experimental data was found, specially the delamination patterns.

The requirements related to industrial problems have necessitated the choice of a macroscopic approach and the choice of a constitutive law implemented in the computer code LS-Dyna. Table 4.1 Commonly used material models for composites simulation in LS-Dyna shows the most commonly used material models in LS-Dyna for simulation of composite materials. Schweizerhof et al. [95] reviewed the various material models available in LS-Dyna for composite materials. LS-Dyna has a handful of preexisting composite material models such as MAT22 and MAT54/55, which are progressive failure models that use a ply discount method to degrade elastic material properties; and MAT58, MAT158, and MAT162, which use continuum damage mechanics to degrade the elastic properties after failure [91]. The composite damage models available in LS-Dyna generally assume that the behaviour of laminated composite materials can be considered linear elastic until the laminate begins to fail. The models use various criteria for initiating the damage. The continuum damage mechanics-based phenomenological models are characterised by the use of damage variables and damage evolution laws. The damage variables are internal variables that cannot be measured readily by standard material tests. Therefore, various forms of post-peak behaviours were assumed and the damage parameters were selected by best fit to a component test curve by a process of calibration [94].

**Table 4.1.** Commonly used material models for composites simulation in LS-Dyna

Mat. Model no.	Material model	References
22	Composite Damage	[22]
54	Composite Damage with Chang Failure	[95]
58	Laminated Composite Fabric	[94]
59	Composite Failure (Plasticity Based)	[83]
161,162	Composite MSC	[96]

Wang et al. [51] assumed that both the moduli along the weft and warp yarn directions and the in-plane shear modulus will be affected by matrix micro-damage to account for the nonlinear behaviours observed in the plain weave facesheet tests, and all these three moduli will degrade with growing damage. For plain weave plies,

only the Youngs moduli  $E_{11}$ ,  $E_{22}$  and the shear modulus  $G_{12}$  change with growing damage, while the Poisson's ratio  $\nu_{12}$ , is assumed to be independent of structural damage. The mechanical behaviour in the weft and warp yarn directions are identical for a 0/90 plain weave laminate, hence,  $E_{11}$ ,  $E_{22}$  have the same degradation process. Basu et al. [97] used a thermodynamics based theory developed by Schapery (referred to as ST) that uses internal state variables (ISVs) to predict the nonlinear response, including damage initiation and evolution, of fibre reinforced laminates under in-plane loads and integrated this user defined material behaviour with the existing element library of ABAQUS through user defined material subroutine, UMAT.

Rajaneesh et al. [83] modelled unidirectional composite faceplates using three dimensional composite failure material model MAT COMPOSITE FAILURE SOLID MODEL, (MAT59). A maximum principal strain criterion was implemented for the failure of composite faceplate using MAT ADD EROSION. Gama et al. [96] described a progressive composite damage model developed by Materials Sciences Corporation and implemented in LS-Dyna 971 as MAT162. The material model requires a total of 34 material properties and computational modelling parameters to describe the response of orthotropic uni-directional and/or woven composites. There are nine elastic constants (three Youngs moduli, three shear moduli and three Poisson's ratios), ten failure strength properties which can be typically determined from standard test methods and a set of quadratic failure functions which are used to define the initiation of different damage mechanisms related to fibre fracture, fibre crush, fibre shear, in-plane matrix crack and delamination. According to Brooks et al. [98], MAT 162 allows damage growth to be applied to damage for each of the above failure mechanisms. Seven damage threshold variables, r1 to r7, are calculated from the relevant failure criteria expressions for fibre damage in tension (r1- x direction, r2- y direction), fibre damage in compression (r3- x direction, r4- y direction), fibre through-thickness crush (r5), in-plane matrix damage (r6), and delamination damage (r7). Four m values; m1 and m2- fibre damage in the local x- and y- directions, m3- fibre through-thickness crush damage and m4- matrix damage, were used to describe the shape of the seven damage evolution curves.

Sevkat et al. [22] modeled composite materials using MAT COMPOSITE DAMAGE (MAT 022). This model is also called the Chang-Chang composite damage model. According to Heimbs et al. [92], the Chang - Chang model is one of the most commonly used failure models for the composite laminate. It is an orthotropic

material where optional brittle failure for composites can be defined. Dynamic force, strain histories and post impact damage patterns obtained from finite element calculations were in good agreement with the experiments. The lamina is assumed to be linear elastic up to failure but after failure, a ply loses its entire load carrying capacity in the dominant stress direction associated with the failure mode. The failure is considered to be instantaneous and the elastic constants are reduced to zero in a predetermined number of time steps based on the dynamic stability of the model. The model uses a variety of criteria to predict failure due to fibre breakage, matrix cracking and matrix compression failure. The models typically assume that the laminate behaves in a brittle manner in the post-failure regime. Williams et al. observed that this is problematic as it was noted that the stress release and stiffness reduction occurred gradually, not abruptly [99].

MAT54 and MAT55 are progressive failure models designed specifically to handle orthotropic materials such as unidirectional tape composite laminates. Material 54 uses Chang matrix failure criterion (as Material 22), and material 55 uses the Tsai- Wu criterion for matrix failure [100]. The LS-DYNA MAT 54 material model is of interest for large full-scale structural damage simulations because it is a relatively simple material model which requires minimal input parameters. The relative ease of use of the MAT54 material model, however, causes notable shortcomings as a consequence of over-simplification of the complex physical mechanics occurring during the failure of composite material systems [91].

Another material model recommended for modelling the composite facesheet is the LAMINATED COMPOSITE FABRIC material model available in the LS-DYNA material model library (MAT58). This constitutive model is based on the theory of Continuum Damage Mechanics (CDM) approach developed by Matzenmiller, Lubliner and Taylor - called MLT model [101]. The damage inflicted on a composite laminate is a complex phenomenon due to the different damage mechanisms involved: matrix cracking, tensile and compressive fibre breakage, delamination, etc., which depend on various parameters including fibre and matrix properties, characteristic of the fibre- matrix interface, manufacturing process, etc [29].

Figure 4.3 Comparison of different material models for the modelling of composite laminates [102] figure.4.3 shows a comparison of the different composite material models for a single element test in uniaxial tension. MAT2, which is an orthotropic

elastic material is used as a baseline for comparison of the different composite material models. It can be seen that the Chang-Chang model (MAT22) has a brittle failure while MAT54 and MAT59 have an elastic-plastic behaviour. MAT58 which is the LAMINATED COMPOSITE FABRIC material model shows a more realistic softening behaviour after the peak at  $E_{11T}$  with element deletion defined by ERODS command.

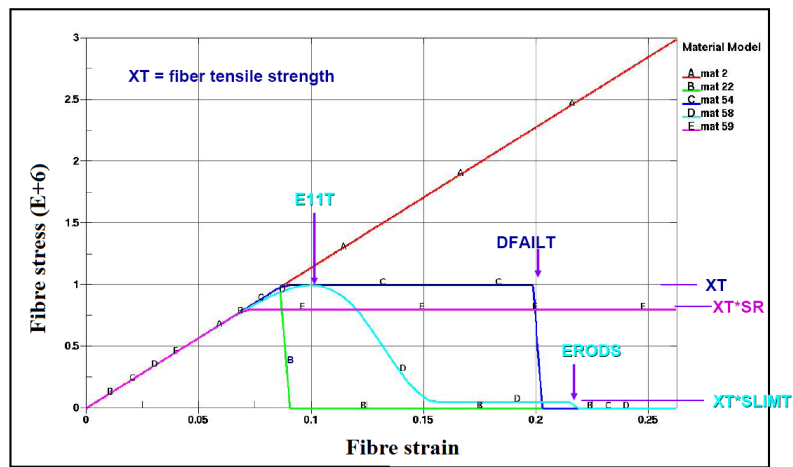


**Figure 4.3.** Comparison of different material models for the modelling of composite laminates [102]

The key concept in CDM is the assumption that a micromechanical process (microcrack growth) can be treated at a macro level by homogenising the damage over a representative volume. It is assumed that the deformation of the material introduces micro-cracks and cavities, which reduce the material stiffness. This is expressed through internal damage parameters, which describe the evolution of the damage state under loading and hence the stiffness degradation [95]. Damage is accumulated within a material based on deformation and loading in various directions:

- Longitudinal (tensile/compressive)
- Transverse (tensile/compressive) , and
- In-plane Shear

Williams and Vaziri [99] explained that the MLT formulation assumes that each unidirectional lamina of a laminated composite can be represented as a homogenized continuum, irrespective of the damage state. This leads directly to the type of damage that is assumed to exist in the lamina. Damage takes the form of disk-like cracks oriented parallel or normal to the fibre direction. In this manner, symmetry

of the lamina is preserved throughout the damage evolution. Two damage variables,  $\omega_1$  and  $\omega_2$ , are introduced to represent the relative size of the two damage areas (i.e. the area of the disk-like cracks). An additional damage parameter,  $\omega_s$  is introduced to account for the effect of damage on the shear response. Note that the definition of the damage parameters as representative of the damage area is by no means a strict assumption. It would be equally correct to consider a dependency on more fundamental variables that describe the attributes of the crack (e.g. crack geometry). A function for the effective stress is derived in terms of the applied stress and the damage parameters. Williams and Vaziri [99] showed that in an uniaxial case, the damage parameter is analogous to the loss of the load bearing cross-sectional area resulting from the damage and for a 2-D case the stress components are multiplied by a transformation matrix to yield the effective stress matrix.

The constitutive matrix, obtained from the compliance matrix of the undamaged lamina and the transformation matrix, is a function of the undamaged elastic constants and the damage state and is given by the equation:

$$\begin{bmatrix} \sigma_1 \\ \sigma_2 \\ \tau_{12} \end{bmatrix} = \frac{1}{D} \begin{bmatrix} (1 - \omega_1)E_1 & (1 - \omega_1)(1 - \omega_2)\nu_{12}E_2 & 0 \\ (1 - \omega_1)(1 - \omega_2)\nu_{21}E_1 & (1 - \omega_2)E_2 & 0 \\ 0 & 0 & (1 - \omega_s)G_{12} \end{bmatrix} \begin{bmatrix} \epsilon_1 \\ \epsilon_2 \\ \gamma_{12} \end{bmatrix} \quad (4.1)$$

where,

$$D = 1 - (1 - \omega_1)(1 - \omega_2)\nu_{12}\nu_{21} > 0 \quad (4.2)$$

The next step is to determine the damage thresholds associated with each damage parameter. The concept of a threshold function, as implemented in the MLT model, is similar to the yield surface in plasticity theory. Within a certain region in stress space (or strain space), the state of damage in the material will not change. This region, the elastic region, is bounded by a series of surfaces associated with the different lamina failure modes. The threshold function,  $r$ , which is analogous to the flow stress in plasticity theory, then becomes a function of  $\sigma$  and  $\omega$  thereby defining the size of the elastic region as damage progresses [99]. A modified version of the MLT model was implemented in LS-Dyna as MAT58b [94]. Two sets of parameters  $E_i$  ( $i=11T, 11C, 22T, 22C, S$ ) and  $SLIM_i$  ( $i=T1, C1, T2, C2, S$ ) were introduced.  $E_i$  is defined as the strain at the maximum stress response and  $SLIM_i$  as the

minimum stress limit of damaged material. A parametric study like the one shown in Figure 4.4 Stress- strain responses for different values of  $E_i$  and  $SLIM_i$  [94] figure.4.4 indicated that varying  $E_i$  changed the slope of the pre- and post-peak response, the same way as  $m_i$  in MAT58a except that  $E_i$  appears to be reciprocal to  $m_i$ , i.e., a greater  $E_i$  value results in a smaller slope of the stress-strain response while the  $SLIM_i$  sets a predefined limiting stress.

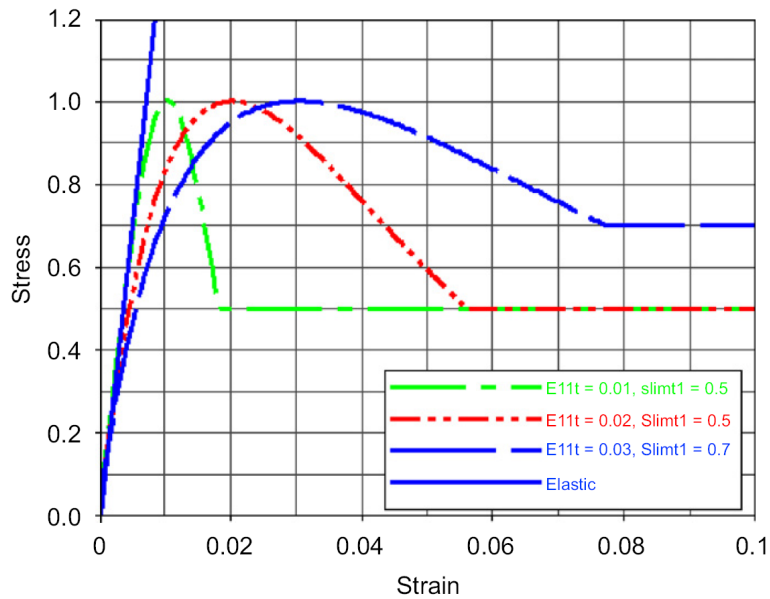


**Figure 4.4.** Stress- strain responses for different values of  $E_i$  and  $SLIM_i$  [94]

Fan et al. [103] adopted various failure criteria to predict macroscopic failures based on the tensile, compressive, and shear strengths of the individual lamina. Hashin's failure criteria are used to predict the onset of facesheet damage in a complex stress state, e.g., fibre breakage and/or matrix cracking. Assuming that fibres are aligned with the first material principal direction (1-direction), thus making the material transversely isotropic about this direction, the tensile and compressive ply strengths in the fibre direction are defined as  $X_T$  and  $X_C$  respectively while the tensile and compressive ply strengths in the direction perpendicular to the fibre direction, i.e., 2- direction are defined as  $Y_T$  and  $Y_C$ . The shear strengths in the 1-2 plane and 2-3 plane are defined as  $S_{12}$  and  $S_{23}$ . The Hashin's criteria read as follows:

$$\left( \frac{\sigma_{11}}{X_t} \right)^2 + \left( \frac{\tau_{12}}{S_{12}} \right)^2 + \left( \frac{\tau_{13}}{S_{13}} \right)^2 \geq 1 \text{ if } \sigma_{11} > 0 \quad (4.3)$$

$$\left(\frac{\sigma_{11}^2}{X_c}\right) \geq 1 \text{ if } \sigma_{11} < 0 \quad (4.4)$$

$$\left(\frac{\sigma_{22} + \sigma_{33}}{Y_t}\right)^2 + \left(\frac{\tau_{12}}{S_{12}}\right)^2 + \left(\frac{\tau_{13}}{S_{13}}\right)^2 + \left(\frac{1}{S_{23}^2}\right) (\tau_{23}^2 - \sigma_{22}\sigma_{33}) \geq 1 \text{ if } \sigma_{22} + \sigma_{33} < 0 \quad (4.5)$$

$$\left(\frac{\sigma_{33}}{Z_t}\right)^2 + \left(\frac{\tau_{23}}{S_{23}}\right)^2 + \left(\frac{\tau_{13}}{S_{13}}\right)^2 = 1 \text{ if } \sigma_{33} > 0 \quad (4.6)$$

$$\left(\frac{\tau_{23}}{\sigma_{23}}\right)^2 + \left(\frac{\tau_{13}}{\sigma_{13}}\right)^2 = 1 \text{ if } \sigma_{33} < 0 \quad (4.7)$$

Matzenmiller et al. [101] have proposed that when one of Hashin's failure criteria is satisfied at a point in a composite structure, damage ensues at that point and it can be characterised by introducing internal variables for fibre breakage in tension and compression, matrix cracking in tension and compression, and crushing. The evolution of these internal variables depends upon values of stresses in Hashins failure criteria which are expressed in terms of stress invariants for a transversely isotropic body and the strength parameters for the composite. Values of damage variables depend upon values of the five internal variables, and determine values of material elastic constants. Alternatively, the damage variables can be used to modify the six stress components used to characterise subsequent deformations of the material point.

A simplified algorithm for the MLT model is shown in Figure 4.5 Solution Algorithm for MLT model [99]figure.4.5, where  $\hat{\sigma}$  is the effective stress matrix,  $r$  denotes the threshold functions associated with the fibre and matrix damage and  $\epsilon$  is the strain matrix.

Deslauriers et al. [104] conducted single element tests to verify the behaviour of the material law based on MLT theory. The predicted stress/strain and damage/strain curves of the element subjected to monotonic tension and compression are shown in Figure 4.6 Results of single element test for validation of MLT model [104]figure.4.6 and it can be seen that damage is accumulated after a strain of 1% and is followed by softening behaviour. Deslauriers et al. [104] concluded that the behaviour of the 1-element model matched the expected response based on the

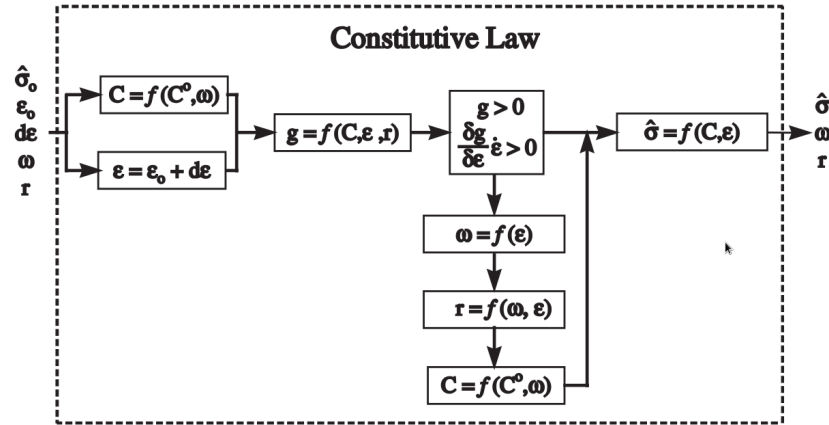


Figure 4.5. Solution Algorithm for MLT model [99]

constitutive equations and the different failure stresses and strain values input to the model.

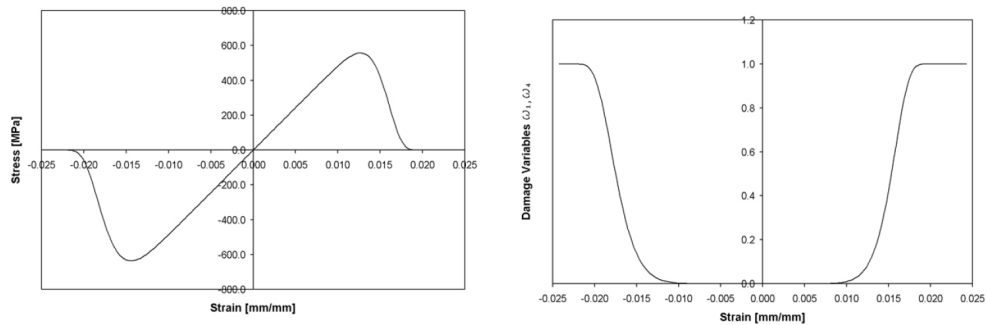


Figure 4.6. Results of single element test for validation of MLT model [104]

According to Schweizerhof et al. [95], the MLT model is considered more appropriate for the modelling of the composite facesheets because unlike the Chang Chang model available in the LS-Dyna library as MAT54, the MLT model provides a smooth increase of damage. There is no sudden change of material behaviour as observed in other models and this represents a realistic simulation of the composite. Failure criteria based on Hashin criteria are used for the woven fabric composite: tensile and compressive failure in warp and weft direction as well as shear failure. The Hashin criteria is capable of distinguishing the fibre and matrix failure modes. A modified version of the MLT model is also capable of including strain rate effects into consideration. A viscous stress tensor is calculated on the basis of a generalised

Maxwell model, where up to six terms in the Prony series expansion can be defined through their shear relaxation modulus and shear decay constant [99].

According to Polanco et al. [105], the ERODS parameter in MAT58 has been utilised to simulate damage of composites in the past but the parameter was typically set high since the Kevlar/Epoxy composite fails at very high strains, and the deletion of elements from the model led to distortion of neighbouring elements responsible for driving down the time step. In addition, the strength values in tension, compression, and shear are important in characterising the Kevlar/Epoxy composite. The behaviour of the material after it fails is determined by the ultimate strength specified in tension, compression, and shear, in addition to the SLIM factors. High strength values could lead to stiffening of the composite, while a low strength value could lead to under-prediction of the crush response.

Batra et al. [81] implemented an MLT model as a user-defined material model in ABAQUS. In the Figure 4.7 Fringe plot (a,b) Fibre and matrix tensile damage; (c,d) Fibre and matrix compressive damage; (e,f) Crush damage and delamination [81]figure.4.7, fringe plots for the three damage modes; fibre and matrix tensile damage (a,b), fibre and matrix compressive damage (c,d), Crush damage and delamination (e,f) are shown. Five damage variables Q1, Q2, ..., Q5 were defined and an element is assumed to have failed when the value of at least one of the damage variables exceeds 0.95 and either the ratio of its final volume to the initial volume is less than 0.1 or more than 4.0. Fibre tensile damage signified by values of Q1, initiates along the top-most layers of the composite plate after impact and the image (b) suggests that the matrix tensile damage (Q4) has increased in the bottom layers of the laminate while the fibre compressive damage (Q2) has spread out in the top layers of the laminate. The compressive matrix damage, decipherable from values of Q5 is shown to be limited to points near the top surface of the composite plate (d). Batra et al. [81] remarked that compressive damage mode is insignificant to warrant a drop in the contact force and predicted that the drop in force is due to the accumulation of the fibre tensile damage along the bottom layers of the composite laminate.

#### 4.2.2 Constitutive modelling of foam core

Feng and Aymerich [85] contrasted monolithic laminates and sandwich plates and found that the simulation of the impact behaviour of sandwich composites is usually more complex than that of monolithic laminates, since the response of the



behaviour of core materials as compared to the facesheets. Foams are a type of cellular solids which can be described as a collection of regular or irregular thin-walled cells. The macroscopic compressive behaviour is determined by the compressive behaviour of individual cells and the collective interactions between neighbouring cells [33].

The modelling of the foam core behaviour requires the use of models to reproduce the crushing behaviour of these cellular materials [29]. Croop and Lobo [106] described that irrespective of the type of the foam, there are generally three zones in the compressive stress-strain relationship of foam, namely, initial elastic region up to  $\sigma_y$ , plateau compaction region and a densification region. Figure 4.8 Different plateau regions in cellular material (a) Strain hardening, (b) Strain softening and (c) Perfectly plastic [33] figure.4.8 shows three different plateau regimens for cellular material under uniaxial compression loading. Depending on the nature of the cells, the foams can be classified as Type-I and Type-II structures, where Type-I structures have a stable load-deflection plateau and frequently show hardening feature in the plateau regime and Type-II structures are unstable, which shows softening feature in the unit cell load-deflection curve or a perfectly plastic regime in the macroscopic compressive deformation [33]. The existence of an elastic regime is a common feature for most cellular solids. The linear elastic relationship between macroscopic stress and strain is mainly due to the collective microscopic elastic bending of the cell wall. The compressed gas inside the closed cells and the viscoelasticity of the cell walls may be responsible for some non-linear responses of the foam material, e.g. non-linear elasticity and viscoelastic recovery of the foam material. In practice, the non-linear elastic deformation of the closed cell foam is idealised by a linear elastic relationship in order to simplify the problem. In elastic regime, the compressive stress increases with cell-wall bending deformations and the macroscopic deformation is uniform within the gauge length of the specimen.

According to Triantafillou et al. [49], both normal and shear stresses can be significant in the core material and therefore a criterion for yield under combined stresses, such as the von Mises yield criterion for fully dense solids, is required to predict failure by yielding. No such criterion exists for foams. Instead, we assume that yielding occurs when the maximum shear stress in the core equals its shear strength or when the maximum principal stress equals the uniaxial yield strength of the core. The foam core can be modelled as an isotropic porous solid, with the

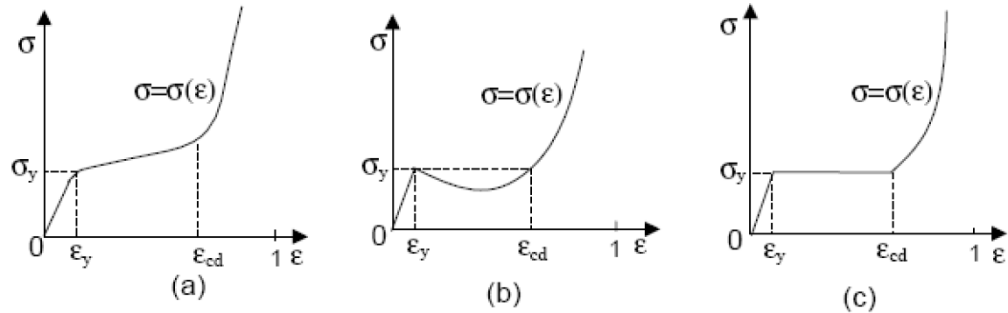


**Figure 4.8.** Different plateau regions in cellular material (a) Strain hardening, (b) Strain softening and (c) Perfectly plastic [33]

constitutive description which utilises a principal stress-yield surface under compression and a quadratic-yield surface elsewhere in the stress space or as a homogeneous isotropic material using the Von-Mises yield criterion [29].

LS-Dyna offers a variety of material models, each with capabilities designed to capture the unique behaviour of different types of foam, for instance, open cell foams and closed cell foams. The selection of the correct material model depends to a large extent, on the observed behaviour of the foam during the test. Croop and Lobo reviewed the various models available for foams and pointed out that selection of material model for foam is not a simple matter because of the complex and highly varied behaviour of foams [106]. Since the available models are limited in one way or another and a full expression of all relevant behaviours is not possible, it was suggested that a pragmatic choice must be made depending on both the material and its behavioural characteristics [106]. MAT LOW DENSITY FOAM, MAT CRUSHABLE FOAM and MAT FU CHANG FOAM corresponding to MAT57, MAT63 and MAT83 in the LS-Dyna library are some of the most commonly used foam models. Typically, the stress- strain curve from uniaxial compression tests are used to model both the elastic and inelastic behaviour of the foam [33]. It is also possible to model the strain rate dependency of the foam using LS-Dyna models. For instance, MAT163 which is a Modified Crushable Foam model accepts uniaxial compression curves at multiple strain rates. Serifi et al. [107] modelled Expanded Polypropylene foam (EPP foam) using MAT FU CHANG FOAM (MAT83), a one dimensional material model with uni-axial compression load curves under different strain rates. LS-Dyna interpolates linearly between the strain rates to calculate the stress- strain values for the applied strain rate. The MAT83 model allows the input of tensile load

curves as negative values of uniaxial compression curves and triaxial curves can be introduced as hydrostatic curves.

Brooks et al. [98] modelled the core material with MAT142 transversely anisotropic crushable foam material model in LS-Dyna. The model requires direct input of stress-strain curves in compression and shear and stiffness over the range of strain rates of interest. Failure was based on a modified TsaiWu yield surface and the yield surface hardens or softens as a function of volumetric strain. The model also assumes a single yield value for tension and compression at each value of volumetric strain, i.e., it is symmetric. In addition to anisotropic elastic properties, the model requires characterization input data in the form of full stress strain curves for compression and shear. Strain rate effects are taken into account by scaling elastic properties and yield strengths based on the input of a single high rate stress strain curve for compression and shear.

Jackson et al. [108] compared different material models for cores including MAT CRUSHABLE FOAM MAT63 which was developed to represent the properties of isotropic crushable foam and includes optional damping and a tensile cutoff stress. MAT63 allows input of a user-defined curve representing the yield stress versus volumetric strain response of the material as shown in Figure 4.9 Yield stress vs. volumetric strain input for MAT63 Crushable foam [100] figure.4.9. An example of unloading from point **a** to the tension cut-off stress at **b** followed by unloading to point **c** and finally reloading to point **d**, where it begins to follow the loading curve again is shown in the figure. The Young's modulus is assumed to be constant and the stress is updated using an elastic behaviour equation.

$$\sigma_{ij}^{trial} = \sigma_{ij}^n + E \dot{\epsilon}_{ij}^{(n+1/2)} \Delta t^{(n+1/2)} \quad (4.8)$$

The magnitude of the principal values of the stress are then checked to see if it exceeds the yield stress and are scaled back to the yield surface using the following equation

$$|\sigma_i^{trial}| > \sigma_y \text{ then } \sigma_i^{n+1} = \sigma_y \frac{\sigma_i^{trial}}{|\sigma_i^{trial}|} \quad (4.9)$$

The stress tensor is transformed back into the global system after scaling the principal values. It is important to note that volumetric strain is defined as  $(1-V_r)$ , where  $V_r$  is the ratio of the current volume to the initial volume. Thus, as crushing

starts, the volumetric strain is low and increases as crushing progresses. Tension is represented using an elastic perfectly-plastic response at the tension cut-off value. Unloading is fully elastic to the tensile cut-off stress and reloading follows the loading curve. It is recommended that it is important to use nonzero values for the tension cutoff to prevent disintegration of the material under small tensile loads [100]. High values of tension cutoff results in the material model having the same behaviour in tension and compression.

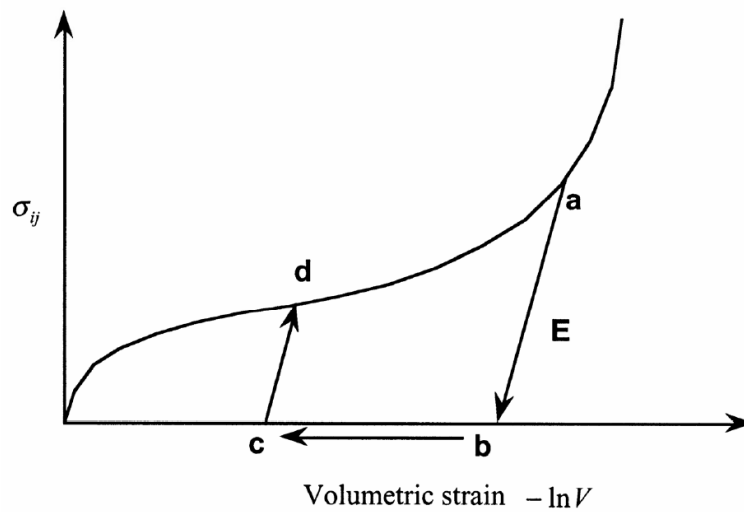


**Figure 4.9.** Yield stress vs. volumetric strain input for MAT63 Crushable foam [100]

Mostafa et al. [109] simulated the response of PVC foam under compression, tension and shear using a Crushable foam- plasticity model in ABAQUS and noted that one of the limitation of the plasticity model is that the response is assumed to be the same in both tension and compression, using the same material property values. However, the tensile and compressive response of many foams including PVC foam are quite different, with the material exhibiting more brittle behaviour in tension, with a higher yield stress, and no plateau or densification. This asymmetry between tension and compression is not captured in foam material models.

Rajaneesh et al. [83] reported that incorporating erosion in homogenized foam models require a selection of suitable erosion criterion such as volumetric plastic strain criterion, and maximum principal stress criterion with accompanying Cockcroft and Lathams energy- based criterion to avoid premature element deletion and

also found that the maximum principal stress criterion was able to predict the correct failure mode as compared to the maximum plastic volumetric strain criteria.

### 4.2.3 Simulation of delaminations and debonding

Dogan et al. [110] defined delamination as the separation of plies in the low resistance thin resin-rich interface between adjacent layers particularly under compressive loading and impacts. Debonding is the failure of the adhesive bond between the facesheets and the core. A necessity for applied sandwich structures in practice is the effective bond between the facesheets and the core material. The bond has to be strong, stiff and tough. The effect of adhesive joints between interfaces on the load transfer and the static and dynamic response of sandwich structures can be studied by the finite element method [80]. There are several methods for modelling the delamination or debonding including using Tiebreak contacts and using Cohesive elements.

Dogan et al. [110] presented a review of the different methods of delamination modelling using both Cohesive elements available in LS-Dyna as MAT COHESIVE MIXED MODE (MAT138), MAT COHESIVE ELASTIC (MAT184), MAT COHESIVE GENERAL (MAT186), etc. and tiebreak contacts available as CONTACT AUTOMATIC SURFACE TO SURFACE TIEBREAK. The Cohesive Zone Model considers fracture as a gradual phenomenon in which separation takes place across an extended crack tip or cohesive zone and the separation is resisted by cohesive tractions. The cohesive elements therefore do not represent any physical material but describe the cohesive forces generated when material elements are pulled apart. The traction separation law can be bilinear, trilinear, parabolic or exponential.

Elder et al. [111] reviewed methods for predicting delamination under impact load in composite materials and reported that the cohesive fracture mechanics model implemented by LS-Dyna uses a bi-linear critical stress for initiation of the delamination, and fracture energy dissipation to determine crack propagation. Crack advancement is determined by a minimum energy iterative approach. The connectivity of each solid-to solid node is achieved by a three degree-of-freedom bilinear spring shown in Figure 4.10(a) Composite beam with delamination (b) cohesive springs model and (c) Interlaminar cohesive model behaviour for mode I - bilinear model with loading in A-B and unloading in B-C [111]figure.4.10. At small loads the springs will remain in the linear section between A and B and as the load increases,

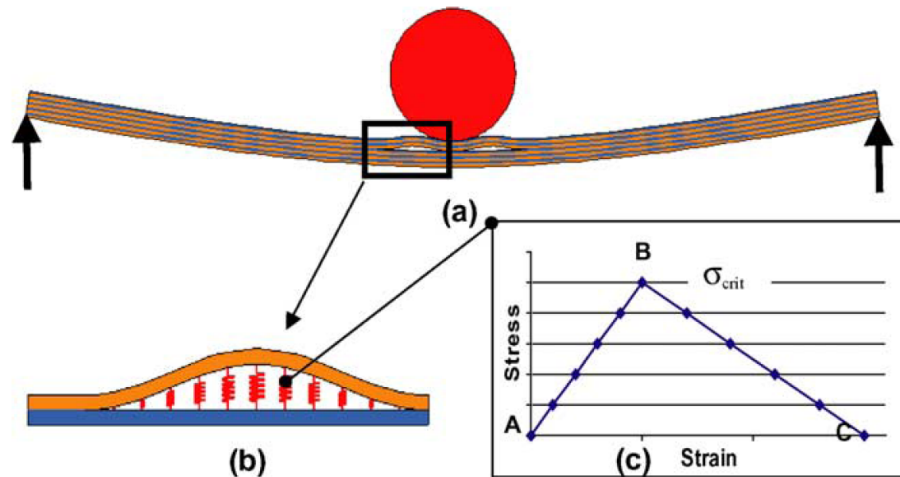


**Figure 4.10.** (a) Composite beam with delamination (b) cohesive springs model and (c) Interlaminar cohesive model behaviour for mode I - bilinear model with loading in A-B and unloading in B-C [111]

some of the springs will start to dissipate energy by unloading in the softening region B-C. This represents the initiation of some damage (micro-cracking), however only after the critical fracture energy is dissipated, where the area under the bilinear graph is equal to the material fracture toughness,  $G_C$ , is a crack deemed to be formed. Meo and Thieulot [112] compared different approaches including methods based on a cohesive zone model, a method based on simulation of the interface with solid elements with element deletion and the last approach based on the definition of a tiebreak contact for simulation of the Double Cantilever Beam (DCB) test and found that the cohesive elements and solid elements were effective techniques for modelling delamination growth.

Feng and Aymerich [85] modelled the delaminations between layers of the composite skins and skin/core debonding by interface cohesive elements, defined by a traction separation constitutive law for Mode II and III as well as Mode I. The traction separation law similar to the one shown in Figure 4.10(a) Composite beam with delamination (b) cohesive springs model and (c) Interlaminar cohesive model behaviour for mode I - bilinear model with loading in A-B and unloading in B-C [111] figure.4.10 consists of an initial linear elastic stage until a damage initiation condition is satisfied (a stress-based quadratic interaction criterion was used in the

calculations), followed by a linear softening phase that simulates the progressive decohesion of the interface with increasing damage. Complete fracture of the interface is assumed to occur when cohesive tractions vanish at the end of the degradation phase. The evolution of damage was monitored by a damage indicator  $d$ , ranging from the value of 0 for the undamaged interface to the value of 1 corresponding to complete decohesion of the interface. One of the disadvantages of the cohesive elements method is the addition of zero-thickness elements at each interface which lead to larger models and longer computation time [113]. Fleming [114] also reported that difficulties in obtaining proper values for the quasi-static pure mode toughness and for the mixed-mode exponent required for the cohesive element model and uncertainty pertaining to strain rate effects inhibits effective use of the cohesive elements for delamination modelling.

LS-Dyna offers a large number of contact types. Suri Bala [115] remarked that accurate modelling of contact interfaces between bodies is crucial to the prediction capability of the finite element simulations. In LS-Dyna, a contact is defined by identifying (via parts, part sets, segment sets, and/or node sets) what locations are to be checked for potential penetration of a slave node through a master segment. At the beginning of the simulation, the nearest master segment for each slave node is located based on an orthogonal projection of the slave node to the master segment. If the slave node is deemed close to the master segment based on established criteria, the slave node is moved to the master surface. In this way, the initial geometry may be slightly altered without invoking any stresses. As the simulation progresses, the isoparametric position of the slave node with respect to its master segment is held fixed using kinematic constraint equations. A search for penetrations, using any of a number of different algorithms, is made every time step. In the case of a penalty-based contact, when a penetration is found a force proportional to the penetration depth is applied to resist, and ultimately eliminate, the penetration. It is extremely important to have the contact segment orientation aligned appropriately as it determines the tensile and compression direction [115]. Tiebreak contacts are penalty based contact types which allow for the definition of failure parameters. Failure can be based on the forces or stress along the normal (tensile) and shear directions.

The criterion for delamination between the composite layers is governed by:

$$\left(\frac{|\sigma_n|}{NFLS}\right)^2 + \left(\frac{|\sigma_s|}{SFLS}\right)^2 \geq 1 \quad (4.10)$$

where,  $\sigma_n$  and  $\sigma_s$  are the normal and shear stresses acting on the layer interface, respectively, while NFLS and SFLS are the normal and shear strengths of the layer interface, respectively. This criterion was incorporated into LS-Dyna through the command: CONTACT AUTOMATIC SURFACE TO SURFACE TIEBREAK. There are different types of tiebreak contacts which are defined by the OPTION parameter. For instance OPTION=-3 defines a tiebreak contact with a general behaviour with failure criterion defined in equation 4.10 but for OPTION=8, the damage of the material is a linear function of the distance between two points which are initially in contact and when the critical opening defined by the user is reached, the contact is broken and the sublaminae are converted into separate surfaces with a regular surface to surface contact to prevent penetrations. According to Dogan et al. [110], this option is the most commonly used contact for delamination modelling.

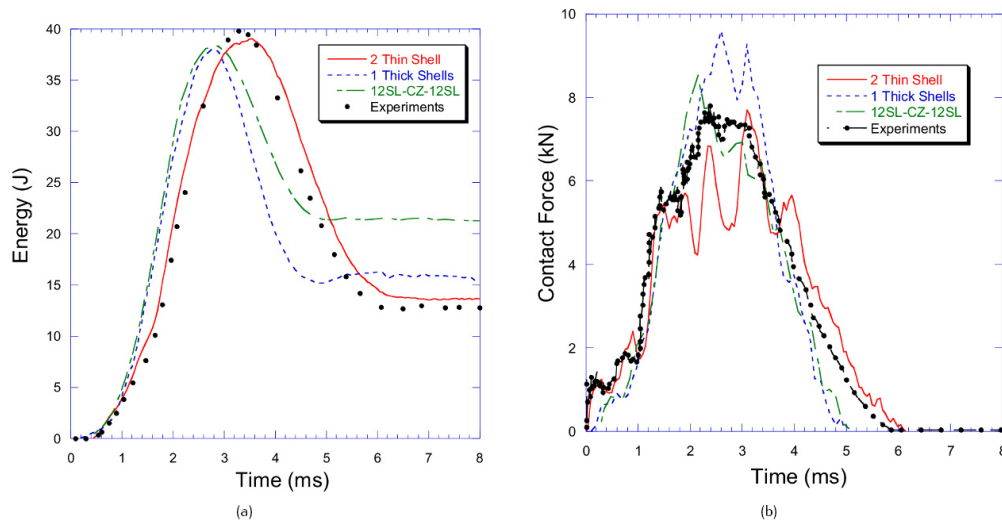


**Figure 4.11.** Comparison of internal energy and contact force for different modelling approaches [110]

A comparison of internal energy and contact force for different approaches for delamination modelling was given by Dogan et al. [110] in Figure 4.11. Comparison of internal energy and contact force for different modelling approaches [110] figure.4.11. The Thick shell (blue dotted lines) and solid elements (green line) approach used

MAT185 Cohesive elements while the thin shell approach shown as red line used a tiebreak contact. It can be seen from the figure that the thin shell approach with tiebreak contact performed well compared with the cohesive elements approach and presents an easy and efficient solution for the modelling of delamination. Dogan et al. [110] also found that the behaviour of the tiebreak contact was dependent on contact option as well as different contact parameters such as SOFT option.

The SOFT=1 option is recommended optional input as a contact parameter for impact analysis where dissimilar materials come into contact [115]. This non-default method calculates the stiffness of the linear contact springs based on the nodal masses that come into contact and the global time step size. The resulting contact stiffness is independent of the material constants and is well suited for treating contact between bodies of dissimilar materials. The stiffness is found by taking the nodal mass divided by the square of the time step size with a scale factor to ensure stability. It is also possible to use SOFT=2 option which uses mass and time step based penalty stiffness as in SOFT=1. This option, however invokes a segment-based contact algorithm which has its origins in Pinball contact developed by Belytschko and his co-workers [100]. With this contact algorithm, contact between segments is treated rather than using the usual node-to-segment treatment. When two 4-noded segments come into contact, forces are applied to eight nodes to resist segment penetration. Bala [115] concluded that this treatment has the effect of distributing forces more realistically and sometimes is quite effective for very stubborn contact problems.

### **4.3 FE model of normal impact of Kevlar composite laminates with and without nano-reinforcement**

The response of the composite plate to impact loading was examined using the Finite element method. Commercially available Finite Element software LS-Dyna was used for the numerical modelling. LS-DYNA is chosen as the desired FE code for the low velocity impact analysis of composite structures as it is a general-purpose finite element code for analysis of large deformation dynamic response of structures based on explicit time integration. The dimensions of the square plates were 100 mm x 100 mm. 3 layers of plain woven fabric with the ply orientation  $[0/90]_3$  were modelled with the keyword *\*PART COMPOSITE*, which enables a simplified method for defining composite layups. The *\*PART COMPOSITE* formulation allows the input

of the thickness of each layer and a material angle, relative to the material direction of the element along with different material data for the layers. The geometry of the composite plate and the impactor are shown in Figure 4.12. LS-Dyna model of the composite plate, fixture and hemispherical impactor figure.4.12.

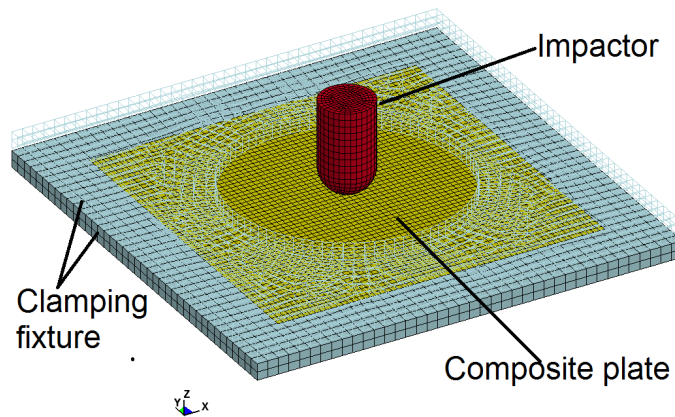


**Figure 4.12.** LS-Dyna model of the composite plate, fixture and hemispherical impactor

The impactor is modelled with 3000 solid elements, while the Kevlar composite is represented by 3600 shell elements. This element size was the best compromise between calculation time and accuracy of the local material fracture representation. The mesh on the composite plate has to be refined adequately enough to have a fine mesh in regions of interest, that is, areas where there are high stress gradients or large deformations. A mesh sensitivity analysis shown in Figure 4.13(a) Coarse mesh, (b) Fine mesh and (c) Mesh sensitivity analysis of Kevlar composite figure.4.13 was done varying the number of elements in the plate from 500 to 10000. It can be seen that the results of the FE model are highly mesh-dependent. An optimal mesh size was determined as the mesh that provided the results most similar to the experiment and the resulting model (3600 elements) was used in all subsequent analyses.

The composite plate has a clamped boundary condition along a 70 mm diameter hole of the support fixture similar to the one used in the experiment of Denneulin et al. [41]. For normal impact, the nodes in the hemispherical impactor have an initial velocity defined to them. The density of the steel impactor is modified to obtain the same kinetic energy as in the experiment. Two initial velocities,  $3.13m/s$  and  $4.48m/s$  were simulated. To reduce the runtime, all simulations commenced

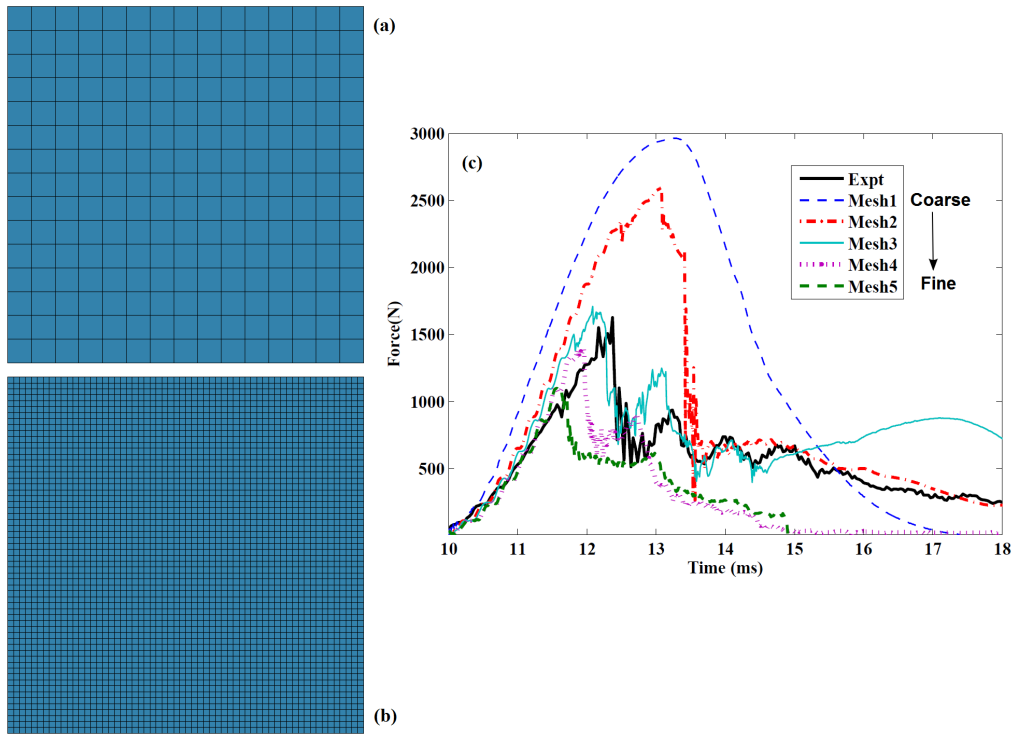


**Figure 4.13.** (a) Coarse mesh, (b) Fine mesh and (c) Mesh sensitivity analysis of Kevlar composite

with the impactor situated just 0.5 mm above the plate. An Automatic Surface to Surface contact is defined between the impactor and the composite plates.

The composite was modelled as Material 58 (LAMINATED COMPOSITE FABRIC material model) available in the LS-Dyna material model library. The model requires input of material properties in shear, tension, and compression to define stress-strain behaviour within the laminate. The constitutive model is based on the theory of continuum damage mechanics (CDM) approach developed by Matzenmiller, Lubliner and Taylor called MLT model [100]. The FRP composite materials are treated as linear elastic orthotropic before failure. The key concept in CDM is the assumption that a micromechanical process (microcrack growth) can be treated at a macro level by homogenizing the damage over a representative volume. As explained earlier, it is assumed that the deformation of the material introduces micro-cracks and cavities, which reduce the material stiffness. This is expressed through internal damage parameters, which describe the evolution of the damage state under loading and hence the stiffness degradation [99]. Damage is accumulated within a material

based on deformation and loading in various directions. Five failure criteria for the woven fabric composite, based on Hashin's criteria are used: tensile and compressive failure in warp and weft direction as well as shear failure. The Hashin criteria is capable of distinguishing the fibre and matrix failure modes. A modified version of the MLT model is also capable of including strain rate effects into consideration. A viscous stress tensor is calculated on the basis of a generalized Maxwell model, where up to six terms in the Prony series expansion can be defined through their shear relaxation modulus and shear decay constant [100].

#### 4.3.1 Identification of material model parameters

The elastic damage law chosen (MAT58) requires the identification of a set of input parameters. Three categories of parameters must be identified: i) the elastic properties of the material, ii) parameters related to damage and breakage, and iii) those related to behaviour after fracture. The material parameters for the Kevlar composite have been identified by tensile tests and 3-point bending tests. In addition to the elastic properties, the properties related to damage and breakage is described by maximum deformations and stresses. Strain rates achieved in the material during the impact are in the order of  $10s^{-1}$ , it is essential to identify the material behaviour at these strain rates. The definition of other parameters, even if they can be connected to a physical phenomenon (e.g., SLIMT parameter to a residual tensile strength), is based on the results of the literature or through optimisation.

Quasistatic tensile tests were done by Denneulin [5] in a Zwick electromechanical testing machine (Zwick GmbH & Co., Ulm, Germany) with dogbone specimen of the woven Kevlar fibre composite specimen with and without the nanoparticles. This was done to obtain the material inputs such as the Young's modulus in the 0 degree and 90 degrees of the manufactured plate (corresponding to the fibre directions). Additional dogbone samples with fibres in the +/- 45 degrees were tested to study the shear behaviour of the composite. Tensile tests were also done using an inertial wheel to measure the response at higher strain rate. The in-plane properties of the composite shows relatively small decreases in Young's modulus (13%), and shear modulus (8%) with the introduction of the Nanostrength. They are explained by the introduction of the more flexible nano-phase. The yield stress increased to a loading in the direction of the fibres (8%), but fell significantly (37%) for testing at 45 degrees as shown in Figure 4.14 Comparison of stress vs. strain curves for 45 degree samples [5]figure.4.14. A significant decrease in yield stress (34%) is observed.

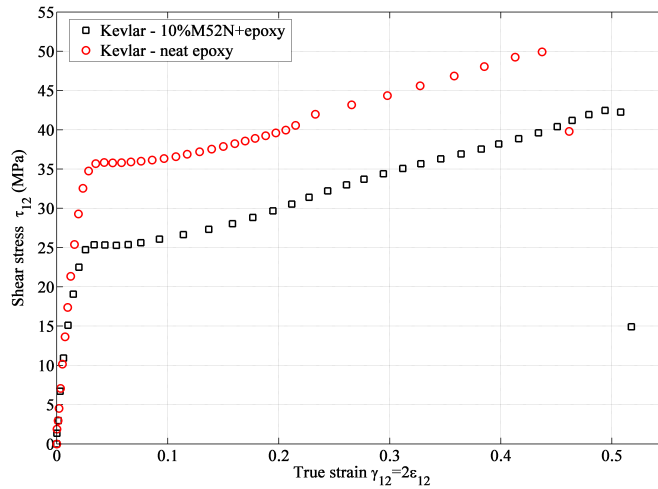


**Figure 4.14.** Comparison of stress vs. strain curves for 45 degree samples [5]

The flexural behaviour of the composite was studied through the 3-point bending test of thick composite on close support and characterization by ultrasonic method. The test setup and image correlation is shown in Figure 4.15 3-point bending test setup and strain field  $\gamma_{13}$  obtained from image correlation [5]figure.4.15. The detailed study of the bending tests showed a slight decrease in modules  $G_{13}$  (5%) with the addition of NS , but a significant decrease (43%) of the yield strength. It can be surmised that the addition of Nanostrength primarily affects the damage thresholds.

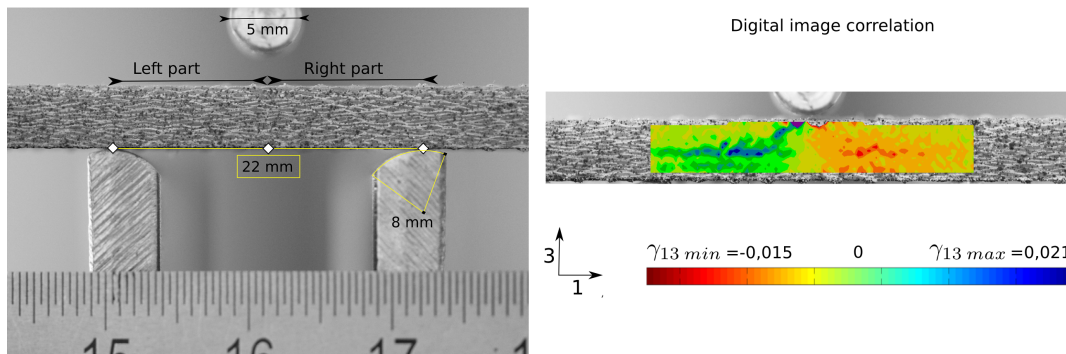


**Figure 4.15.** 3-point bending test setup and strain field  $\gamma_{13}$  obtained from image correlation [5]

The properties used for the Kevlar composite are summarised in the Table 4.2 Material properties for the Kevlar composite with and without nanoparticle stable.4.2. The parameters required for the model such as the moduli in different directions and the method used to obtain the input are indicated. The compressive properties such

strength and strain are obtained from published literature. The strength values in tension, compression, and shear are important in characterizing the Kevlar/Epoxy composite. The behaviour of the material after it fails is determined by the ultimate strength specified in tension, compression, and shear. In addition to these parameters, MAT58 requires the input of SLIM parameters, which are factors to determine the minimum Stress Limits after peak. The SLIM parameters are required for tension and compression in both fibre and matrix direction as well as shear. The ERODS parameter in MAT58 has been utilised to simulate damage of composites. For the results presented here, the ERODS parameter was set high since the Kevlar/Epoxy composite fails at very high strains, and it was recommended by Polanco et al. [105] that the deletion of elements from the model leads to distortion of neighboring elements responsible for driving down the time step.

**Table 4.2.** Material properties for the Kevlar composite with and without nanoparticles

Parameter	Method	Kevlar	Kevlar-Nano
Young's Modulus in 0 and 90° ( $E_1$ and $E_2$ )	Tensile Test	34.5 GPa	30.7 GPa
Shear Modulus ( $G_{12}$ )	45° Tensile test	2.96 GPa	2.94 GPa
Shear Modulus ( $G_{23}, G_{31}$ )	Flexure & Ultrasound	4 GPa	3.8 GPa
Shear stress ( $\tau_1$ )	45° Tensile test	40 MPa	35 MPa
Shear strain ( $\gamma_1$ )	45° Tensile test	0.04	0.04
Longitudinal and Transverse Compressive strength ( $X_C, Y_C$ )	From Literature	266 MPa	266 MPa
Strain at Compressive strength ( $E_{11C}, E_{22C}$ )	From Literature	0.0623	0.0623
Longitudinal and Transverse Tensile strength ( $X_T, Y_T$ )	Tensile Test	480 MPa	522 MPa
Strain at Tensile strength ( $E_{11T}, E_{22T}$ )	Tensile Test	0.022	0.029
Shear strength ( $SC$ )	45° Tensile test	40 MPa	34.5 MPa
Strain at shear strength ( $GMS$ )	45° Tensile test	0.496	0.55

### 4.3.2 Results of the low velocity normal impact of Kevlar composite plate

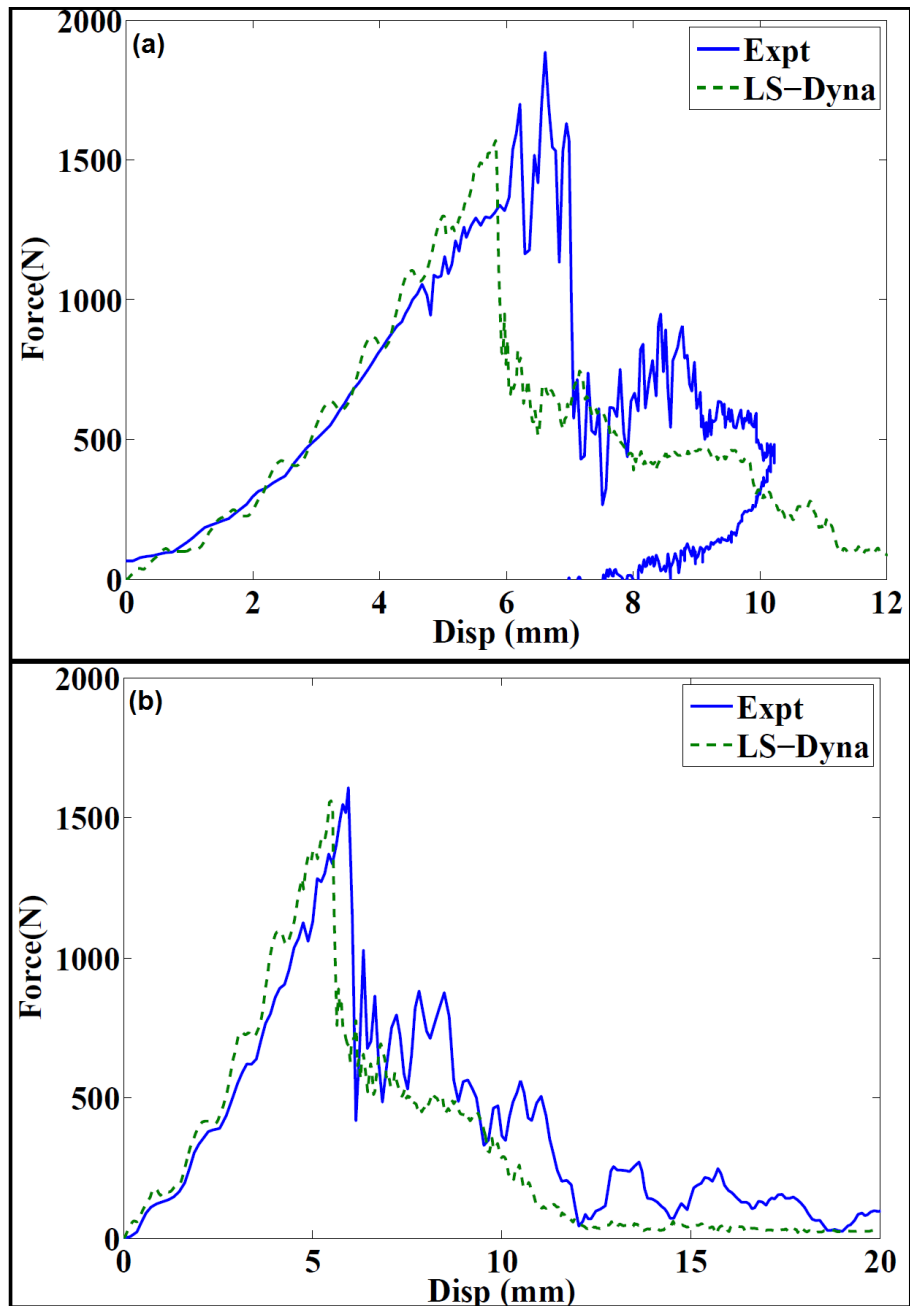
The mechanical response of the panels is typically recorded and analyzed in terms of peak load, absorbed energy, and deflection at peak load. It can be seen from the

Figure 4.16 Comparison of Force- displacement response of the Kevlar plate with neat resin: (a)  $v=3.13$  m/s and (b)  $v=4.43$  m/s figure.4.16 that the finite element results match the experimental data very closely for the composite with neat resin. The peak force values are comparable and the post peak failure of the composite which is indicated by the sudden drop in the force values are also well represented. It should be noted that the force value does not reach zero because there is perforation of the composite plate and there is some residual force from the impactor being in contact with the hole caused by the impact.

A similar analysis was accomplished for the composite plate with the Nanostrength particles embedded in the matrix of the composite (Figure 4.17 Comparison of Force- displacement response of the Kevlar plate with Nano resin: (a)  $v=3.13$  m/s and (b)  $v=4.43$  m/s figure.4.17). The comparison of the force-time response of the composite plate with nanoparticles show a very good correlation with the overall response though the stiffness of the plate in the numerical model is lower than in the experiment. The residual displacement after the 3.13 m/s impact, where there was no penetration of the composite plate, is under-estimated, with the experimental displacement being 5.1 mm and the simulation data showing a lower value of 3.9 mm.

A comparison of the behaviour of the plate accomplished by observing the bottom surface of the Kevlar composite plate with the neat resin can be seen in Figure 4.18 Comparison of bottom surface of the Kevlar composite plate with neat resin: (top) experiment, (bottom) LS-Dyna figure.4.18. The image corresponds to time  $t_1$ , which is the initiation of damage and a small loss in stiffness can be seen (time = 1.8 milliseconds). Time  $t_3$  corresponds to the peak force point and  $t_4$  relates to a time of 5 milliseconds from beginning of impact when there is complete perforation of the facesheet and the impactor is clearly visible from the bottom of the test setup. Kevlar laminates show tensile failure modes, demonstrated by bending at the perimeter of the impactor and tearing at the centre of impact. It can be seen that images from the simulation have very good correlation with the high speed camera data from the experiments.

A similar comparison for the Kevlar plate with Nanostrength is not as illuminating as there is no penetration of the plate and the out of plane displacement is not captured by the high-speed camera. A 2-D image correlation technique is used to plot the planar displacement vector of the lower surface of the plate. The rough



**Figure 4.16.** Comparison of Force- displacement response of the Kevlar plate with neat resin: (a)  $v=3.13$  m/s and (b)  $v=4.43$  m/s

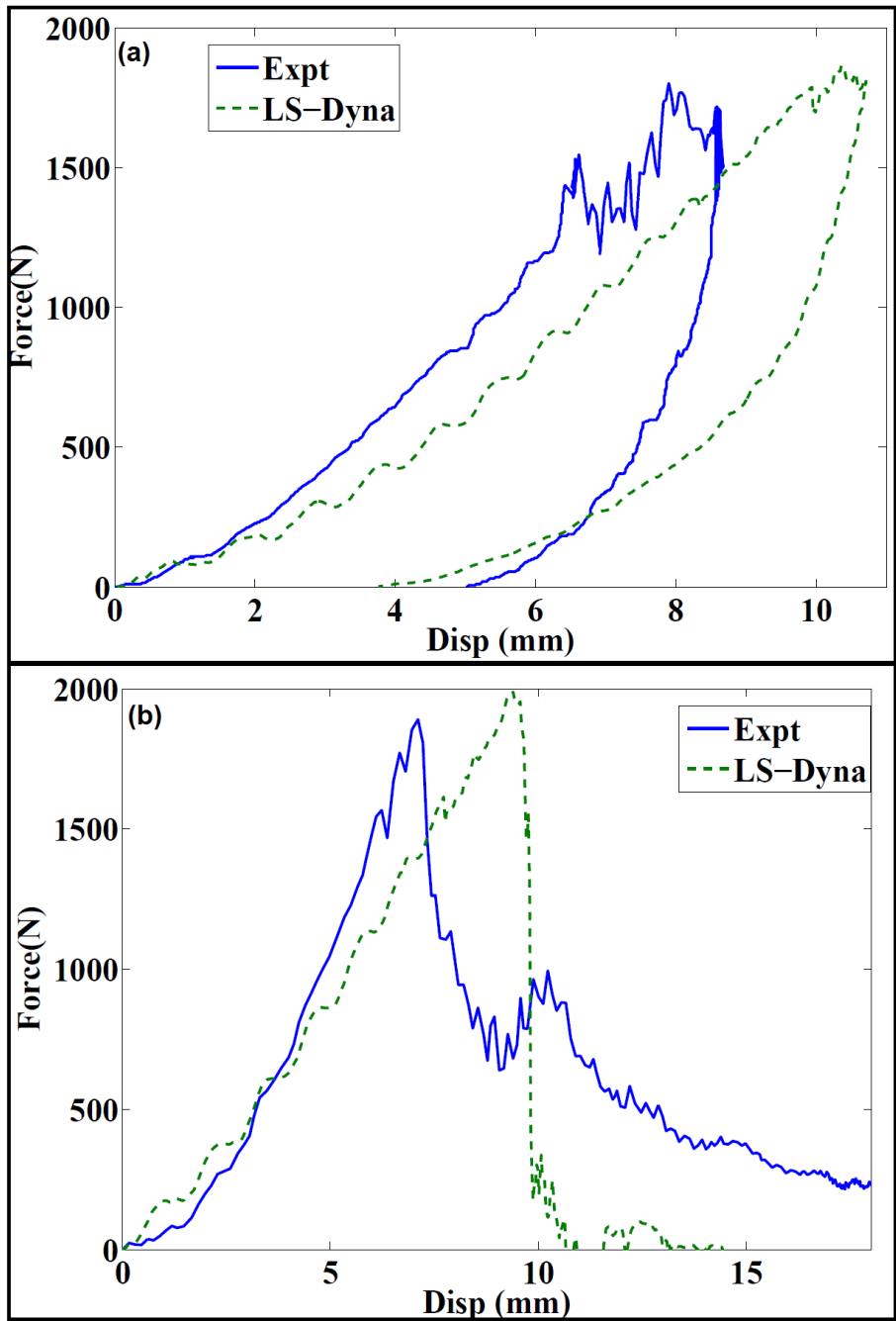


**Figure 4.17.** Comparison of Force- displacement response of the Kevlar plate with Nano resin: (a)  $v=3.13$  m/s and (b)  $v=4.43$  m/s

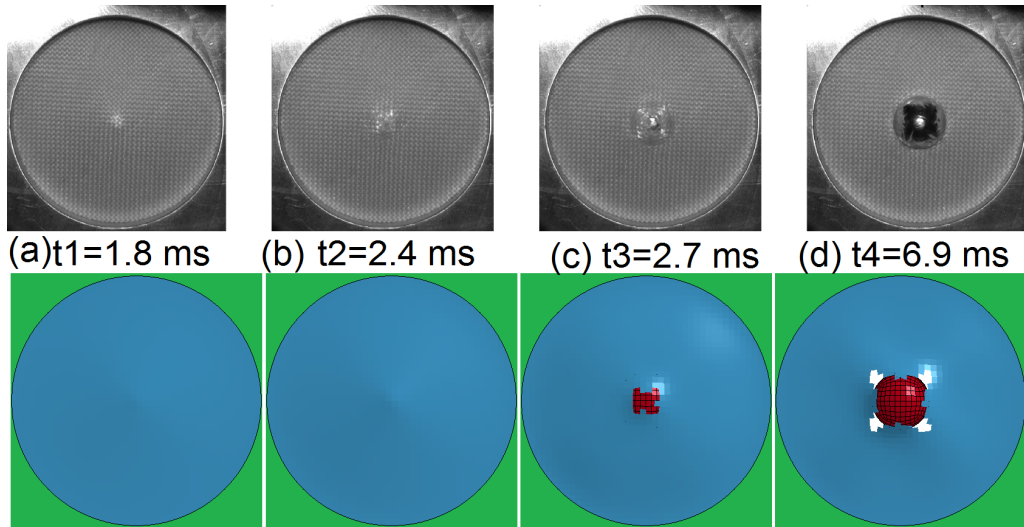


**Figure 4.18.** Comparison of bottom surface of the Kevlar composite plate with neat resin: (top) experiment, (bottom) LS-Dyna

surface of the plate is directly used for this technique instead of adding speckles to the plate. An asymmetry is observed in the planar displacement which is probably due to the point of impact being not exactly at the centre of the plate. A comparison with the simulation results is also shown in Figure 4.19. Displacement vector of the Kevlar composite plate with Nano resin: (left) grid pattern in plate and (centre) vector for experiment, (right) LS-Dyna figure.4.19. It can be seen that the plate is pulled in at the centre in the LS-Dyna simulation.

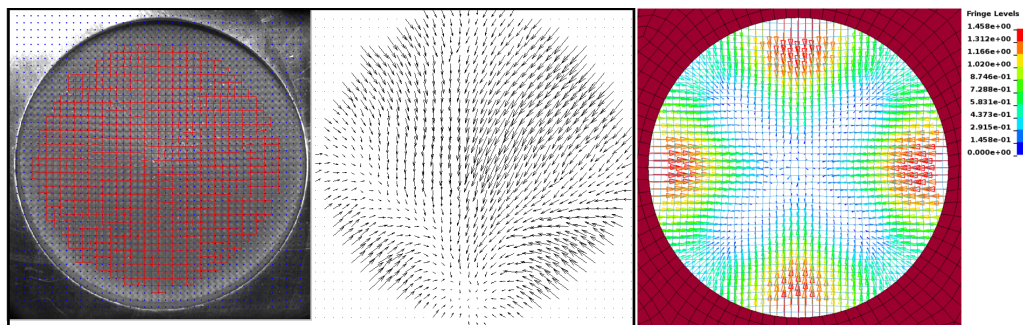


**Figure 4.19.** Displacement vector of the Kevlar composite plate with Nano resin: (left) grid pattern in plate and (centre) vector for experiment, (right) LS-Dyna

Figure 4.20 Comparison of z- displacement of Kevlar plate with Nano resin figure.4.20 shows the comparison of the cross-section at the centre of the Kevlar plate with Nanostrength after the 3.13 m/s impact and z-displacement vector obtained from

the LS-Dyna simulation. It can be seen that the displacement is spread over a larger area in the case of the Kevlar plate with the nanoparticles; i.e. there is less localised damage at the point of impact. This has resulted in the prevention of catastrophic failure and penetration of the composite.

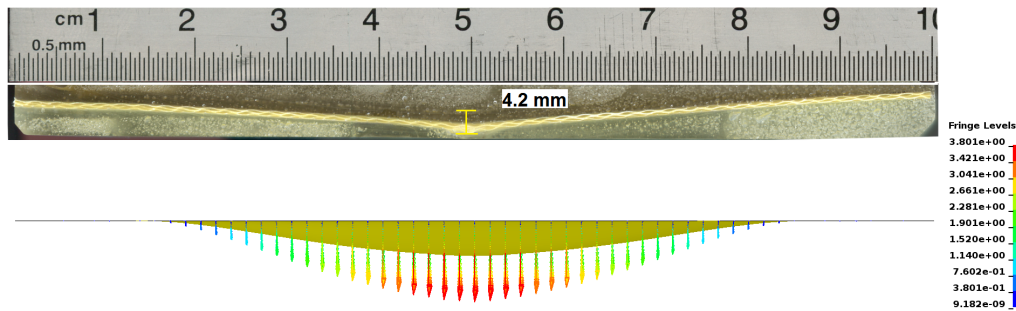


**Figure 4.20.** Comparison of z- displacement of Kevlar plate with Nano resin

#### 4.4 Development of FE model of normal impact of Kevlar-Rohacell sandwich panels with and without nano-reinforcements

An FE model was developed in LS-Dyna to examine the response of Kevlar Rohacell sandwich panels with and without nanoparticles in the resin to normal impact loading. It has been recommended that the appropriate approach to model the sandwich structure is with solid elements for the core and shell elements for the thin facesheets. The sandwich panels with the Kevlar fibre reinforced epoxy skins had a nominal thickness of 21.6 mm, with a 20 mm thick Rohacell foam core and 0.8 mm thick facesheets on either side of the core. The dimension of the square plates was 135 mm. The geometry of the sandwich plate and the impactor are shown in Figure 4.21. LS-Dyna model for the simulation of impact on sandwich plate figure.4.21.

The Kevlar facesheets containing 3 layers of plain woven fabric with the ply orientation  $[0/90]_3$  were modelled with the keyword *\*PART COMPOSITE*, similar to the method explained in the previous section for the composite laminates. The material model validated for the Kevlar composite laminate with and without nanoparticles can be used for the facesheets of the sandwich panels. The core is modelled with under-integrated constant stress hexahedral brick elements while the impactor is

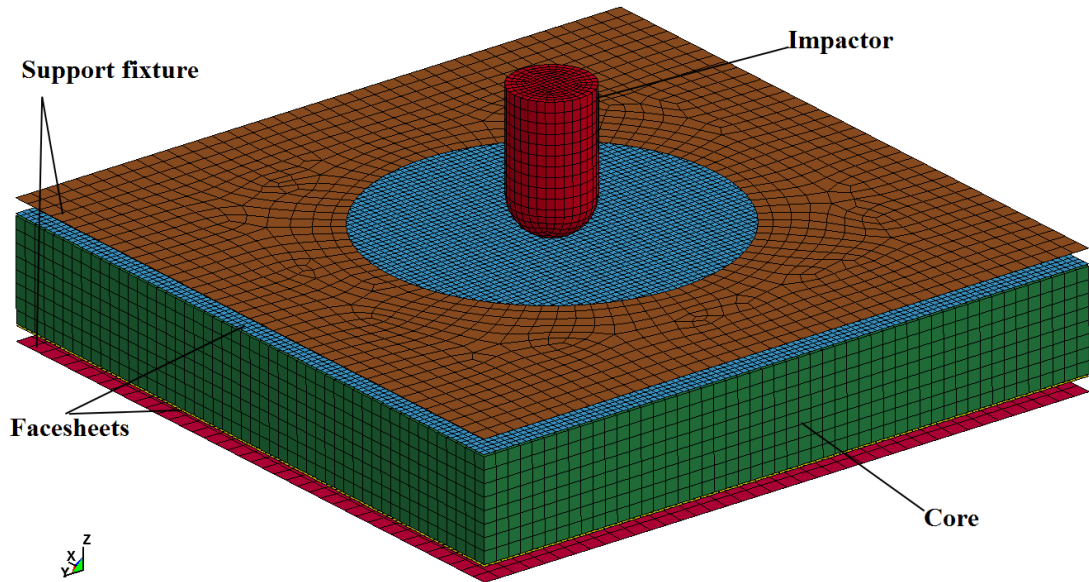


**Figure 4.21.** LS-Dyna model for the simulation of impact on sandwich plate

modelled with 3000 solid elements. A Crushable Foam model represented by LS-Dyna Material Type MAT63 was chosen to model the behaviour of the Rohacell foam core. The stress- strain response for the foam under uniaxial compression was required as input to the material model. A contact is defined between the impactor and the sandwich plates. \*CONTACT AUTOMATIC SURFACE TO SURFACE is the recommended contact type for most impact applications as it employs a two-way contact treatment, i.e. the subroutines in addition to checking the slave nodes for penetration, also check the master nodes for penetration through the slave segments.

In the experiments, an aluminium support fixture was used to obtain the clamped boundary condition. It is possible to simulate this boundary condition by prescribing fixed displacement for nodes outside the circular area with diameter i.e. all nodes outside 70mm in the sandwich plate, to be fixed. The six translational and rotational degrees of freedom can be set to zero but it was observed during the experiments that in reality the nodes on the edge of the circular fixture are not fixed and there is some deformation outside the circumference. Therefore the fixture is modelled as rigid elements with an additional contact defined between the fixture and the sandwich plate. For the simulation of normal impact, the nodes in the hemispherical impactor have an initial velocity defined to them. To reduce the runtime, all simulations

commenced with the impactor situated just 0.5 mm above the plate.

#### 4.4.1 Identification of foam properties

CRUSHABLE FOAM MODEL MAT63 was chosen as the material model for the Rohacell foam core. Since it is expected that the Rohacell foam will exhibit rate dependency, it was considered that a modified form of the MAT63 model which includes strain rate effects, achieved by using the rate dependent stress-strain data, was more appropriate. According to Croop and Lobo [106], MAT63 is useful when there is no recovery and can be considered a more suitable candidate than MAT83, for the Rohacell foam considered for the thesis. Stress vs. volumetric strain data obtained from the compression test is input. The volumetric strain is easily obtained from uniaxial strain as the Poisson's ratio is nearly zero. Uniaxial compressive material tests were conducted in three strain rates to get the strain-rate dependent properties of the Rohacell foam. The quasistatic tests were conducted on a standard Zwick/Roell Z010 electromechanical testing machine (Zwick GmbH & Co., Ulm, Germany) at a quasi-static loading rate of 1 mm/ min, which gives an engineering strain rate of  $4.2 \cdot 10^{-3} s^{-1}$ , according to standards ASTM D3574-91 and ASTM C365-57. Stress was derived from the load cell and engineering strain was derived from crosshead displacement. The Young's modulus defined by the tangent of the secant line from the origin to the yield stress point, the average Young's modulus is 20.4 MPa for quasi-static loading.

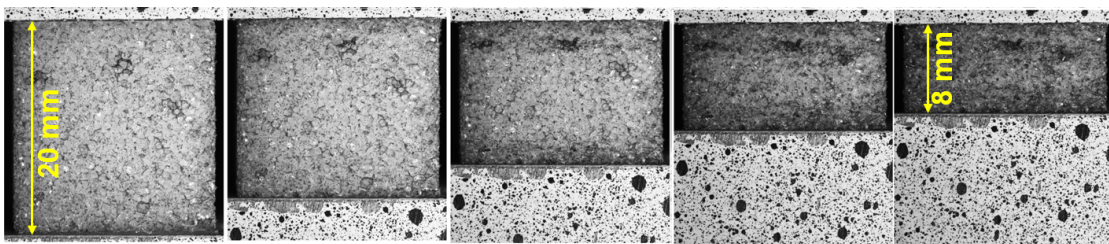


**Figure 4.22.** Quasistatic Compression of Rohacell foam

Figure 4.22 Quasistatic Compression of Rohacell foam figure.4.22 shows the compression of the Rohacell foam sample under quasistatic loading. The crushing of the cells is clearly visible and there is also a stratification of the compression. The uppermost layers of the foam undergo large amount of crushing before the lower layers are compressed. The cell-wall collapse in compression could be one of cell-wall buckling, cell-wall breaking and the formation of plastic hinges in the cell wall, or

their combinations [25]. It is also evident that there is no lateral displacement and that the Poisson's ratio is effectively zero for this kind of foam. Rizov et al. [31] explained that the process of plastic deformation (crushing) of foam under compression at the beginning is localised into the weakest cell layer. When the compressive deformations in this layer attain the densification strain (about 70% for Rohacell foam), the stresses in the layer rapidly increase (i.e., plastic hardening occurs) and this triggers the next layer to start crushing.

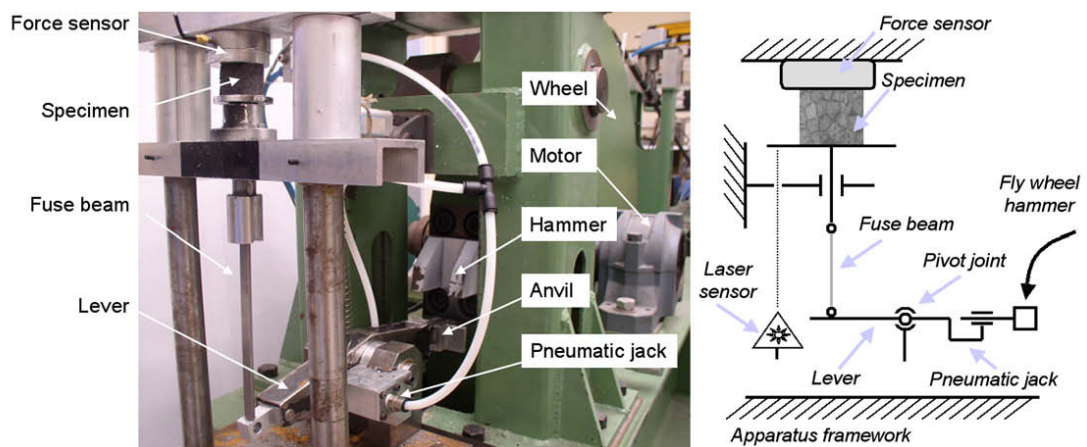


**Figure 4.23.** Compression device of Flywheel for dynamic compression of foam [116]

The medium strain rate tests were conducted on the Flywheel or inertial wheel setup shown in Figure 4.23. The Flywheel is an experimental device that can be used for both tension as well as compression tests. The use of Flywheel for compression testing of foams has been presented by Bouix et al. [116]. The essential element of this machine is a wheel (diameter 1 m, weight 620 kg) and a pendulum system. The wheel, provided with a hammer in the periphery, is rotated by an asynchronous motor. The speed servo is programmable to obtain a velocity of a point located on the diameter from 2 m/s to 40 m/s and the stored energy is then between 530 J and 200 kJ. This device, due to its high moment of inertia, allows the compression of the foam sample under constant velocity. When the desired rotation velocity of the wheel is reached, a pneumatic jack pushes the anvil alongside the wheel which is grabbed by the hammer. The impact lever which is linked to the apparatus framework through a pivot joint causes the compression loading. Once the specimen is totally crushed or the compressive force reaches a threshold value, a fuse beam buckles

and stops further specimen compression. The compressive stress is measured by a piezo-electric force sensor and the compression punch displacement is determined by a dynamic laser sensor (Keyence LC 2100) as well as high-speed camera. A strain rate of  $100 \text{ s}^{-1}$  was reached by the flywheel.

The results of the compression test conducted at quasistatic and intermediate strain rate are shown in Figure 4.24. Results of uniaxial compression of Rohacell foam at (a) Quasistatic and (b) Flywheel, for 6 samples of same dimensions and density figure.4.24. This curve can be divided into three distinct regions; the first corresponding to the elastic region and is determined by the value of the Young's modulus. After the yield point ( $\sigma_y = 0.63 \text{ MPa}$ ), the elastic region is followed by a yield plateau, where the stress remains almost constant while the strain is increased. This behaviour is due to the collapse of the cells inside the foam. At the third stage, which corresponds to high compressive strains, the material exhibits a densification region which results in the sharp increase of stress for small strain increments.

Compression tests were also carried out high strain rates using a Split Hopkinson Pressure Bar (SHPB) shown in Figure 4.25. SHPB test setup for High strain rate Compression and Stress- strain curve of Rohacell foam figure.4.25. The Rohacell foam test specimen was placed between two slender bars (inset figure). According to Bouix et al. [116], bars made of Nylon PA6 provide a better match of the acoustic impedance between the bars and the specimens and ensures the best measurement of signal gage accuracy. The projectile strikes the free face of the input bar and the stress wave generated by the impact allows the loading of the specimen at high velocities. The high strain rate behaviour of the foam is then computed using the strain history generated by the stress waves in the input and output bars. The specimen and bar dimensions have been chosen in order to obtain the stress- strain curves shown in Figure 4.25. SHPB test setup for High strain rate Compression and Stress- strain curve of Rohacell foam figure.4.25.

The compression properties at all the three strain rates are shown in Figure 4.26. Comparison of Compression Stress -strain curve of Rohacell foam figure.4.26. It can be seen that there is not a strong influence of the strain rate on the plateau stress, which is quite similar for the three strain rates at an approximate value of  $0.63 \text{ MPa}$ . There is rate dependence for the beginning of the densification strain. At quasistatic loading, the strain is  $0.49 \text{ mm/mm}$  while at the intermediate strain rate and high strain rate, the densification strain was  $0.59$  and  $0.63 \text{ mm/mm}$  respectively.

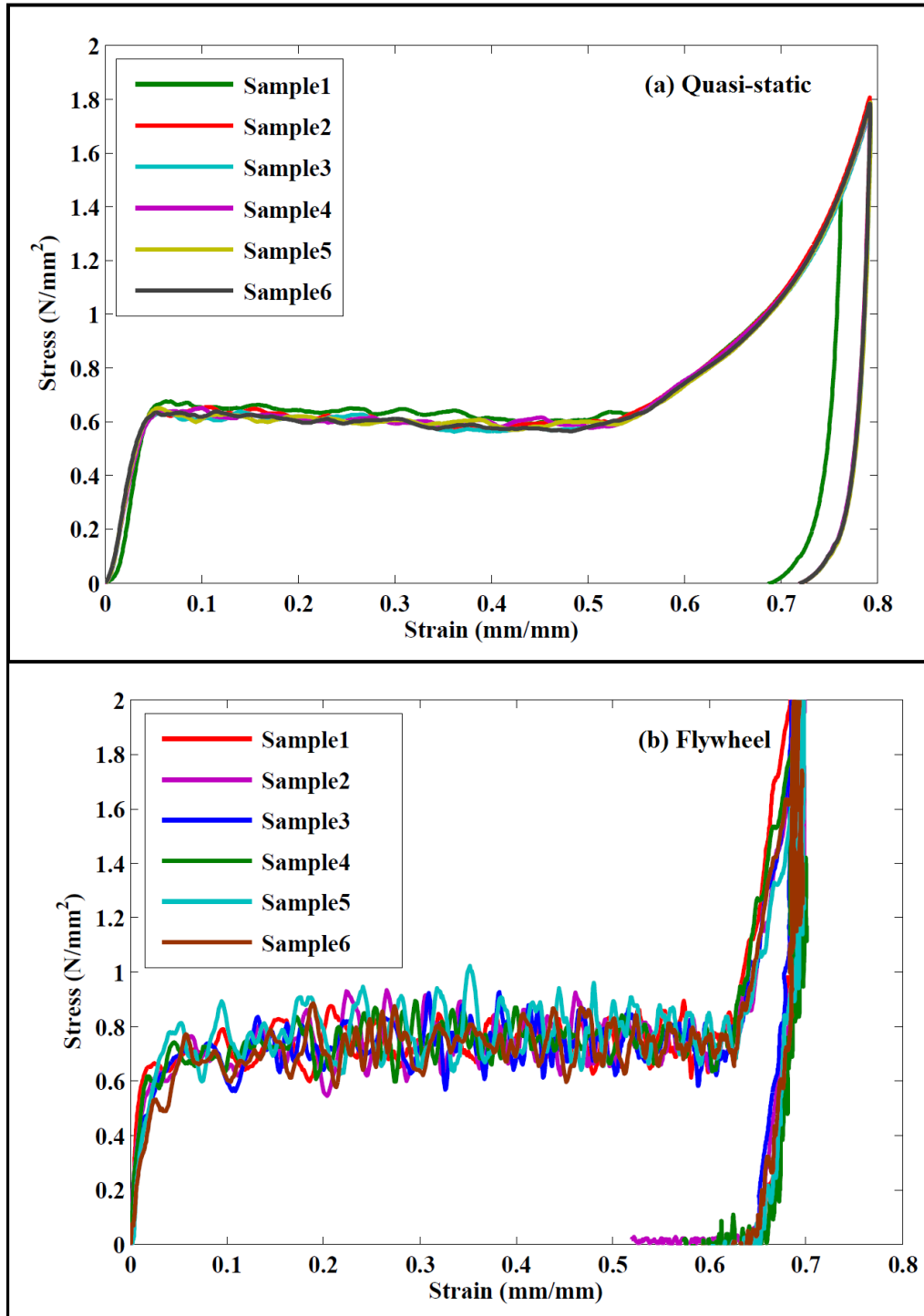


**Figure 4.24.** Results of uniaxial compression of Rohacell foam at (a) Quasistatic and (b) Flywheel, for 6 samples of same dimensions and density

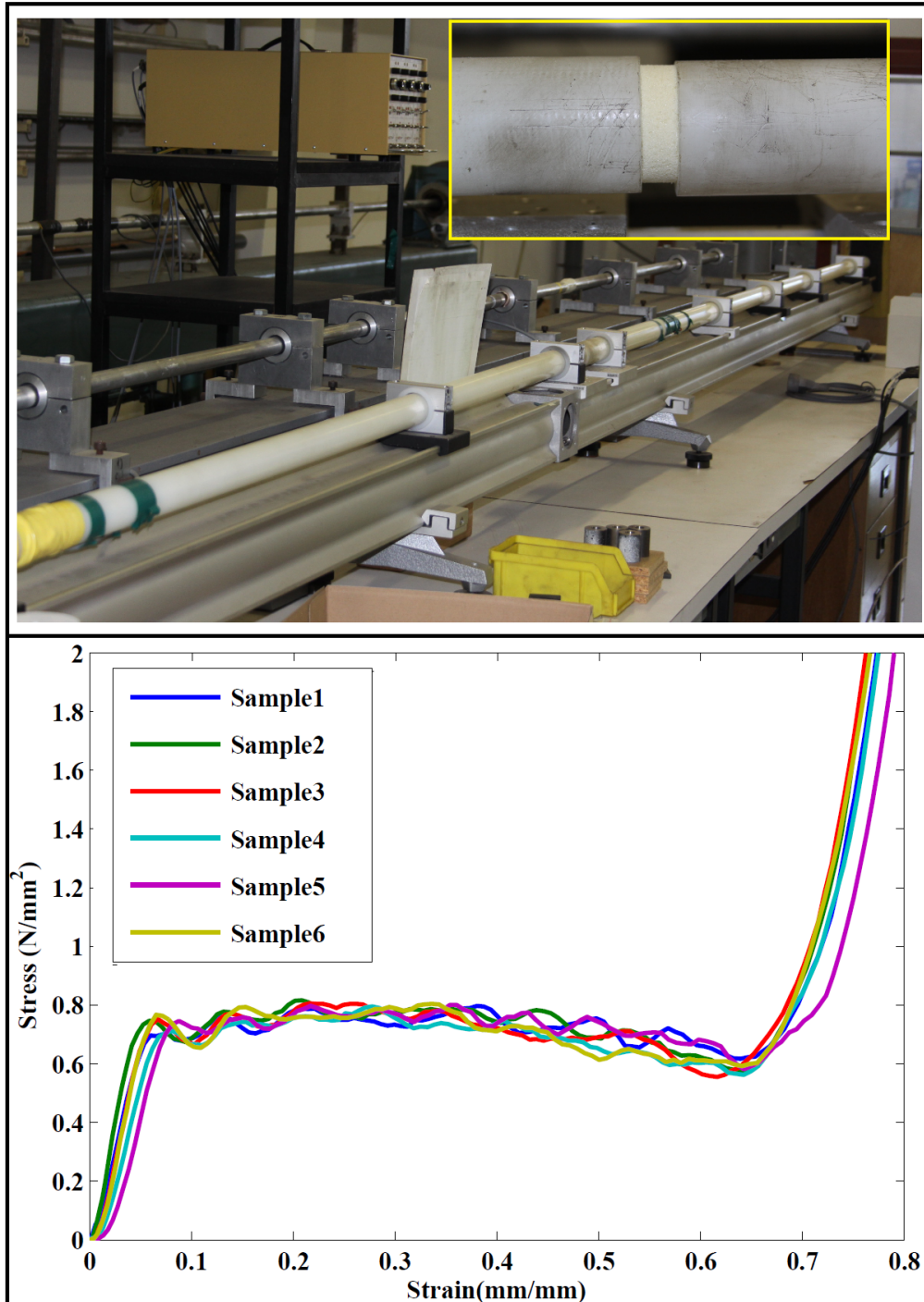


Figure 4.25. SHPB test setup for High strain rate Compression and Stress- strain curve of Rohacell foam

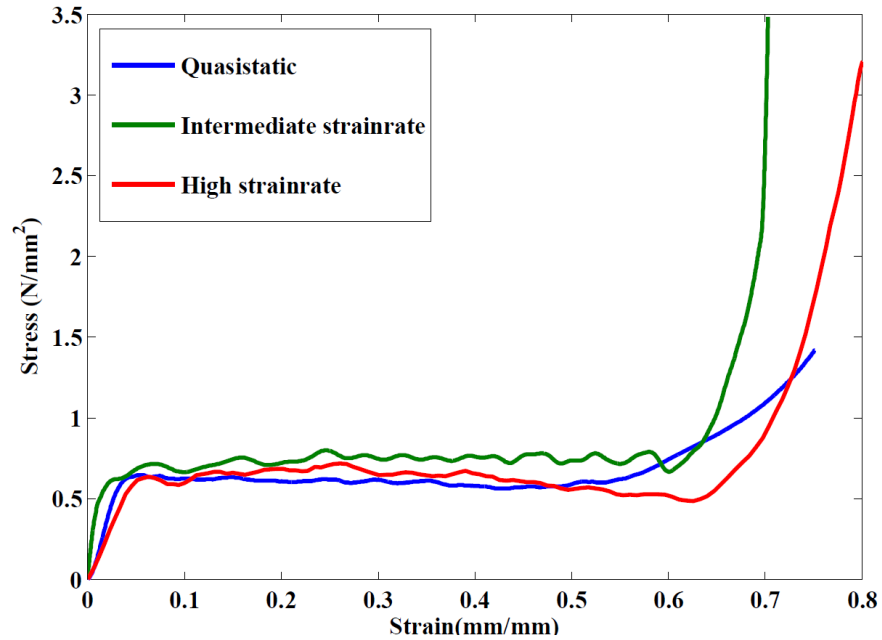


Figure 4.26. Comparison of Compression Stress -strain curve of Rohacell foam

A strain rate dependent model was not used as the effect of strain rate was not significant in the range of strain rates tested. The use of the Crushable foam model is also more computationally efficient than the Modified Crushable Foam model. A simple model of the compression test of the foam shown in Figure 4.27 Uniaxial compression model of Rohacell foam figure.4.27 was used to validate the material model.

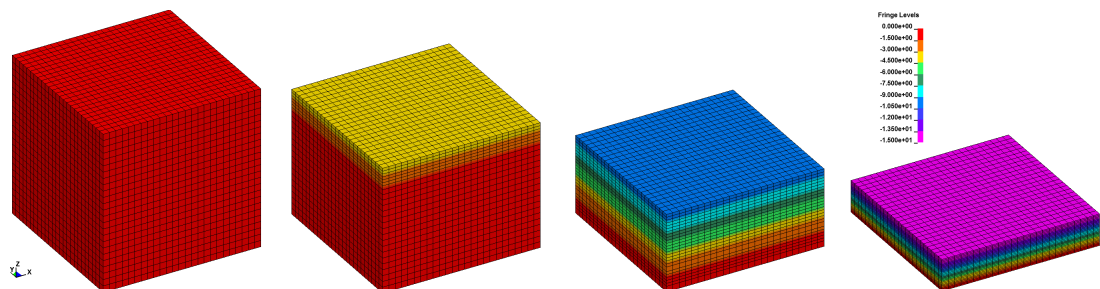


Figure 4.27. Uniaxial compression model of Rohacell foam

#### 4.4.2 Identification of Interlaminar properties

Surface to surface contact with TIEBREAK option was defined between the core and both the top and bottom facesheets to prevent the nodes in the facesheet and

core parts from interpenetrating each other under compression. Traditional contacts transmit only compressive forces and parts in contact that experience tensile forces undergo separation with no resistance. Tiebreak contacts, on the other hand, are penalty based contacts that allow the modelling of connections that transmit both compressive as well as tensile forces with optional failure criteria [115]. It is possible to examine the effect of debonding between the laminate layers using the failure criteria of the tiebreak contact. Failure can be based on the forces or stress along the normal (tensile) and shear directions.

Double Cantilever Beam (DCB) tests were conducted to determine the contact parameters. Figure 4.28 Experimental setup for Double Cantilever Beam test (a) Aluminium substrate and (b) Kevlar composite with end blocks figure.4.28 shows the methodology used for conducting a standard DCB test. The test plan consists of DCB experiments performed on specimens consisting of 12 layers of plain weave Kevlar [0-90] with an initial delamination in the midplane created by using a Teflon film between layers 6 and 7 during the manufacturing of the composite plate. Two types of tests are performed; one where beams of length 180 mm and width of 25 mm are cut from the plate and loaded with end blocks. In the second type, the Kevlar composite beams are glued to a pair of Aluminium substrates using a Hysol EA9395 epoxy paste. The surface of the aluminium substrates are prepared by a process explained by Ben Salem et al. [117], which includes sandblasting the 10 mm thick aluminium alloy, washing in an ultrasonic bath in ethanol, rinsing with acetone and drying the samples before bonding to the Kevlar composite beam. Load is applied in the crack opening mode at constant displacement rate using a universal tensile testing machine (Zwick/Roell Z010, Zwick GmbH & Co., Ulm, Germany). The specimen was attached to the machine with an end block system. The crosshead speed was 0.3 mm/min. The applied force,  $F$ , was measured with a 10 kN load cell (Zwick/Roell, KAF-TC) and the opening displacement,  $D$ , was measured with 50 mm range LVDT sensor and the cross-head.

Typical experimental force versus opening displacement for the Kevlar composite beams without the aluminium substrate is shown in Figure 4.29 Force-displacement curve for DCB test of Kevlar composite with neat resin and nano resin figure.4.29. This result was observed during a DCB test with a 0.3 mm/min controlled transverse displacement speed on samples with neat resin (a) and with nano-modified resin (b). It can be seen that for both samples, during the first stage of the experiment, the



**Figure 4.28.** Experimental setup for Double Cantilever Beam test (a) Aluminium substrate and (b) Kevlar composite with end blocks

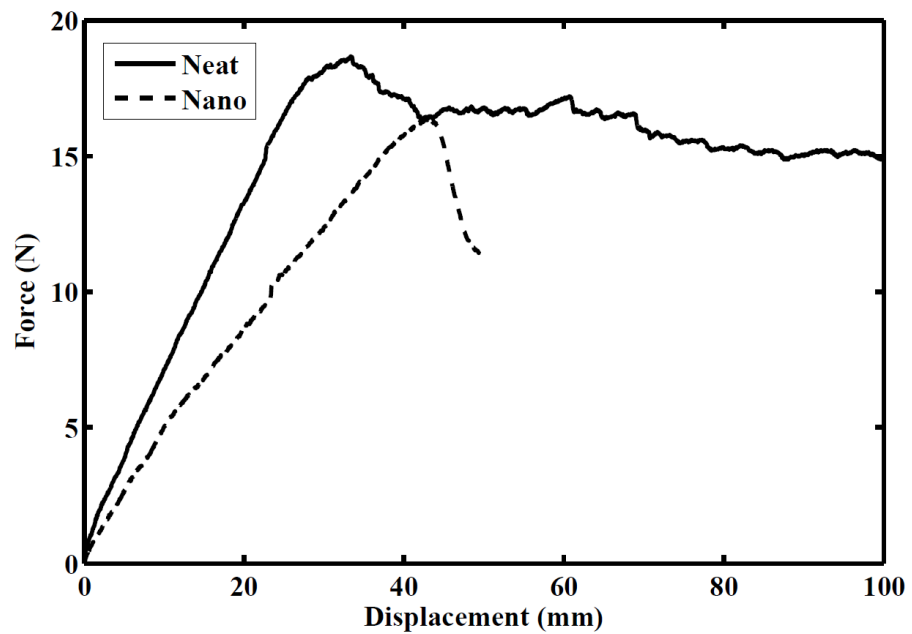
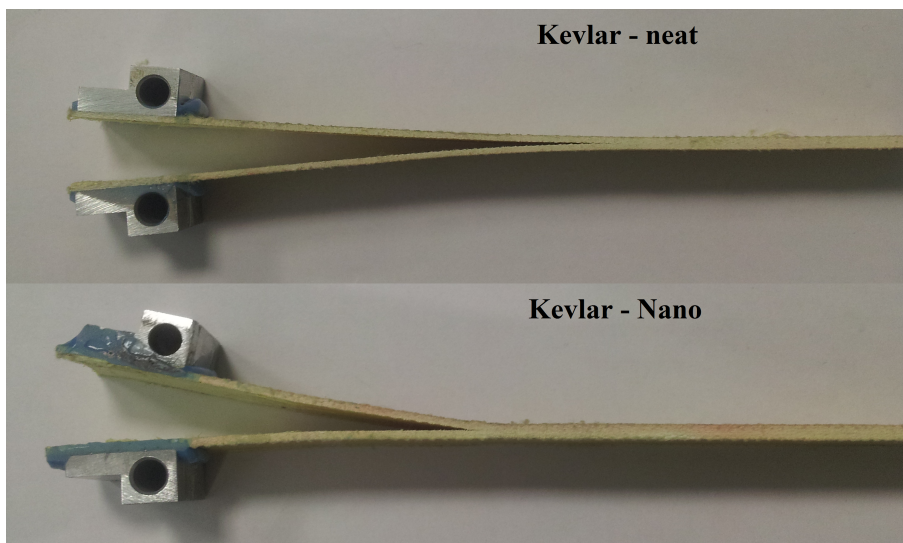


**Figure 4.29.** Force-displacement curve for DCB test of Kevlar composite with neat resin and nano resin

force- displacement evolution is virtually linear until it reaches 18 N ( $D = 30$  mm) maximum applied load, which corresponds to fracture initiation. The applied load

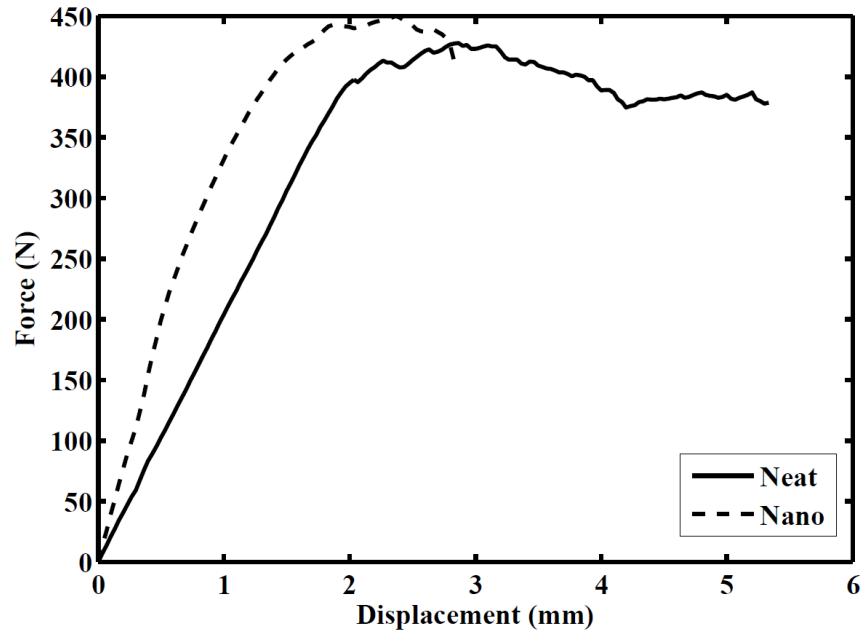
then decreases continuously and stable crack propagation is observed for the sample with the neat resin. However, there is plastic deformation in the sample with the Nano resin which results in the early termination of the test. It should also be noted that the opening displacement is very large for the Kevlar samples without the aluminium substrate.

Figure 4.30 DCB samples of Kevlar composite with neat resin and Nanostrength figure.4.30 shows the Kevlar samples after the DCB test. It is evident that while the delamination crack propagates through the middle for the sample with neat resin, a plastic hinge is formed for the composite with Nanostrength. It is not clear from this test if the addition of the Nanostrength has actually increased the Mode I fracture toughness of the composite laminate. This results in the unusable data for the Kevlar Nano samples.



**Figure 4.30.** DCB samples of Kevlar composite with neat resin and Nanostrength

As an alternative, another DCB test was devised where the composite laminate is glued to a pair of Aluminium beams. This increases the stiffness of the beam and reduces the opening displacement. The Force- displacement results of the Kevlar laminate with Aluminium substrate is shown in Figure 4.31 Force- displacement curve for DCB test of Kevlar composite on Aluminium substrate figure.4.31. It can be seen that the force values are very high when compared to the earlier samples owing to the added stiffness of the aluminium. For the sample with the neat resin, the crack initiation force is about 400 N and a stable crack growth is observed.



**Figure 4.31.** Force- displacement curve for DCB test of Kevlar composite on Aluminium substrate

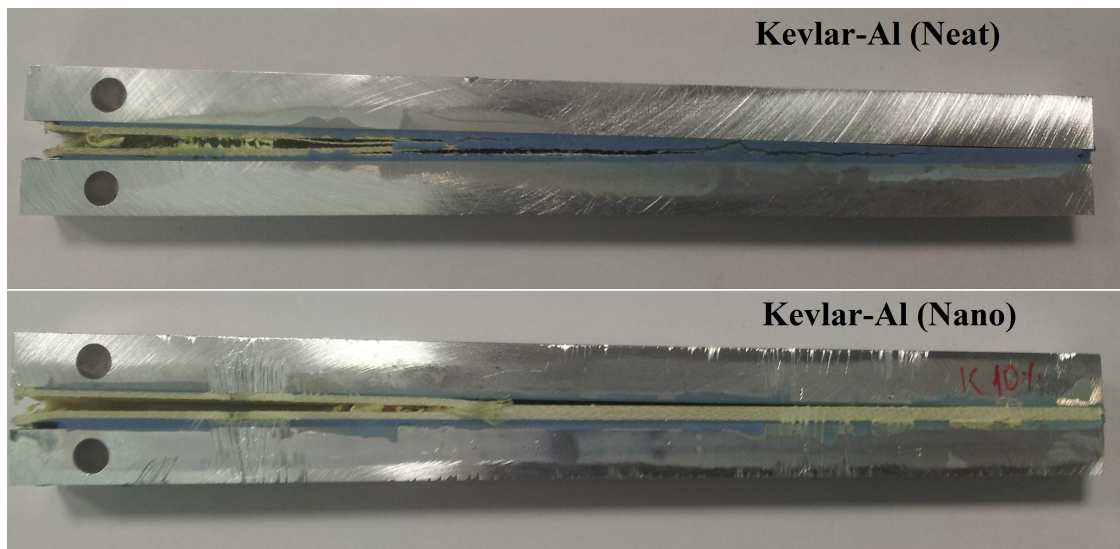


**Figure 4.32.** DCB samples of Kevlar composite with neat resin and Nanostrength on Aluminium substrate

The crack initiation force is higher for the samples with Nanostrength (b) at a value of 450 N. However, the Force- displacement curves do not show a stable crack growth. This is verified by the visual inspection of the samples shown in

Figure 4.32 DCB samples of Kevlar composite with neat resin and Nanostrength on Aluminium substrate figure.4.32 where it can be seen that the crack is propagated through the middle for the samples with neat resin. There is some crack branching to other plies but the delamination growth remains in the composite. But for the sample with nano resin, the crack as soon as it is initiated moves to the interface between the Kevlar composite and the Aluminium beam. This results in premature termination of the DCB test. The moving of the delamination from the composite to the aluminium supports the hypothesis that the addition of the nanoparticles has increased the fracture toughness and the weakest link in the test beam; i.e. the adhesive bond between the aluminium and composite has failed.

The energy release rate  $G_I$  can be derived using Linear Elastic Fracture Mechanics (LEFM) methods and equations described by Ben Salem et al. [117].

$$G_I = \frac{F^2 \delta C}{2b \delta a} \quad (4.11)$$

where  $b$  is the specimen width,  $a$  is the crack length defined as the length between the crack tip and the applied load. The compliance stiffness can be estimated using simple beam theory (SBT). Modelling the adherends with EulerBernoulli beam bending theory, the specimen compliance is given by:

$$C = \frac{\Delta}{F} = \frac{2a^3}{3EI_b} \quad (4.12)$$

where,  $EI_b$  is the flexural rigidity of the beam.

$$G_I = \frac{12(Fa)^2}{Eb^2h^3} \quad (4.13)$$

Ben Salem et al. [117] used the instantaneous crack length evaluated according to SBT and also established that under the LEFM hypothesis, and assuming brittle behaviour of the adhesive, the fracture energy  $G_I$  should not vary significantly during the test, so that when stable crack propagation occurs, load variation should be proportional to  $1/\Delta$ , came up with the equation for the interface fracture energy as

$$G_I = \frac{F^2 a_{SBT}^2}{2b} \left( \frac{1}{EI_b} + \frac{1}{EI_{eff}} \right) \quad (4.14)$$

It was found that the apparent crack length was higher than the real, geometrical crack length since the specimen compliance is higher than that determined with

SBT due to the effect of adhesive layer compliance. Taking the effect of specimen induced asymmetry into account with the effective stiffness, the force versus opening displacement evolution during crack propagation was used to obtain the fracture energy for Mode I delamination shown in Figure 4.33. Fracture energy calculated for DCB test as a function of crack length (a) Kevlar composite beam and (b) Kevlar - Aluminium beam (Figure 4.33). It can be seen that the values for the Kevlar Nano composite are not calculated correctly in both cases because of the lack of steady crack growth. We obtain average  $G_{Ic}$  values from the curve of  $270 J/m^2$  for samples without the aluminium substrate and  $1350 J/m^2$  for the samples bonded on the aluminium beam. These values and the force displacement curves are used as a baseline for the estimation of contact parameters for the delamination simulations.

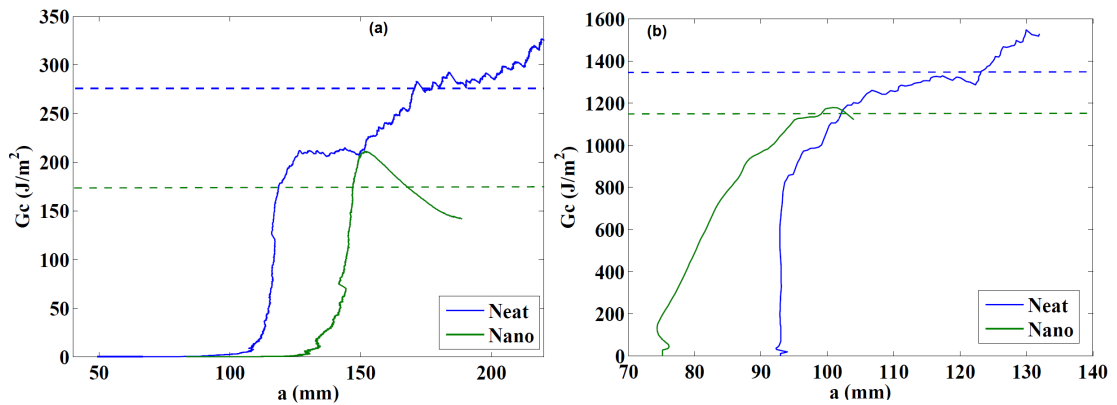


**Figure 4.33.** Fracture energy calculated for DCB test as a function of crack length (a) Kevlar composite beam and (b) Kevlar - Aluminium beam

## 4.5 Results of LS-Dyna simulation of Kevlar-Rohacell sandwich composites

The typical evolution of the impact loading is shown in Figure 4.34. Typical evolution of impact from  $t=0$  ms (no contact) to  $t=10$  ms (after rebound) (Figure 4.34). A section of the sandwich plate cut in the centre is shown to clearly see the loading on the sandwich plate. At time  $t=0$ , shown in Figure 4.34 (a), the impactor is not in contact with the plate. It should be noted that the facesheets which are modelled by shell elements represent the mid-plane of the composite laminate. The impactor has an initial velocity in the  $z$ -direction and comes into contact with the top facesheet.

When time  $t=1.5$  milliseconds (b), there is some loading in the top facesheet which in turn is transferred to the core because of the surface to surface contact defined between the two. As the time progresses to 5 milliseconds the impactor reaches the maximum displacement (c). It begins to rebound and at time  $t=10$  milliseconds, it can be seen that the impactor is no longer in contact with the sandwich plate and there is some damage and permanent indentation observed (d).

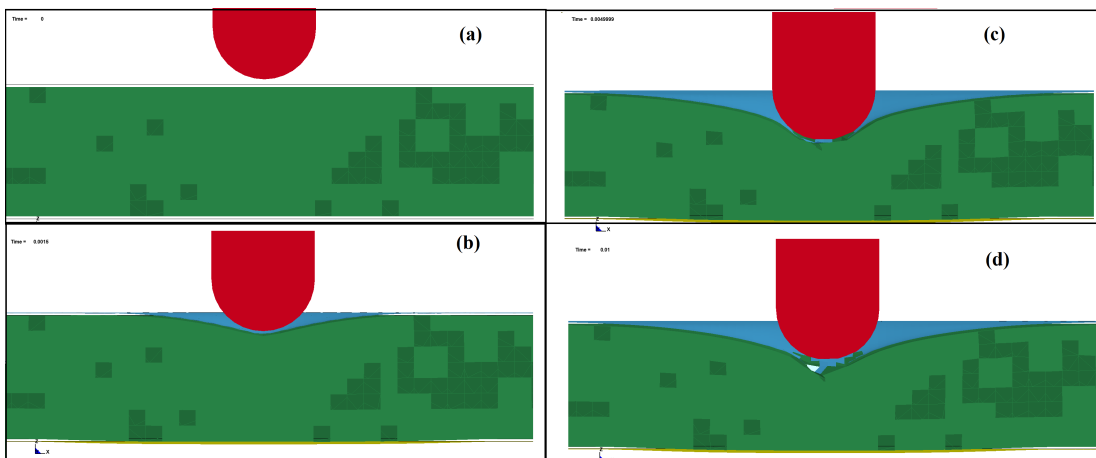


**Figure 4.34.** Typical evolution of impact from  $t=0$  ms (no contact) to  $t=10$  ms (after rebound)

The typical force, displacement and energy time histories for the same case are shown in Figure 4.35. Force, displacement and energy time histories for Kevlar sandwich plate figure.4.35. The contact force history shows the linear loading of the sandwich plate until the peak and then a sharp drop corresponding to failure of the facesheets. It can be seen that the peak force is about 1780 N and the maximum displacement is about 9.5 mm. The kinetic energy of the impact begins at a value of 8.1 J to simulate the actual velocity and kinetic energy of the impactor in the experiment. This initial kinetic energy of the impactor is transferred to the sandwich plate once contact is made. During the impact event, part of this energy is the absorbed energy by the plate in the form of elastic deformation (elastic energy), while a larger amount is dissipated in the various forms of damage and the friction between projectile/facesheet. The kinetic energy of the impactor is completely transferred to the plate when its velocity reaches zero. After this point, the elastic energy stored by the plate is transferred back to the impactor which causes it to rebound. Finally, the energy absorbed by the composite reaches a stable value

resulting from the damage and friction. It can be seen that the rebound energy in this case is very low as most of the kinetic energy has been dissipated in the plate as damage.

#### 4.5.1 Comparison of results from LS-Dyna model with drop tower tests of Kevlar-Rohacell sandwich panels

As explained earlier, the accuracy of the finite element model developed was typically evaluated by comparing experimental results with numerical predictions in terms of contact force history and back surface out of plane deflection. The comparison of the Force -displacement curves for impact of 8 J, 12 J and 16 J for the Kevlar-Rohacell sandwich is shown in Figures 4.36 Comparison of Force -displacement curves for 8 J impact for KR sandwich figure.4.36, 4.37 Comparison of Force -displacement curves for 12 J impact for KR sandwich figure.4.37, and 4.38 Comparison of Force -displacement curves for 16 J impact for KR sandwich figure.4.38. It can be seen that in the initial phase of contact some oscillations can be seen in the time interval of 0 ms to approximate 0.7 ms due to the elastic vibration induced by the initial contact between the impactor and the composite laminate. After that, intense oscillations occur near the peak force value that indicates initiation of damage. The impactor then bounces back and the load is reduced to zero. It is evident from the curves that the numerical model is able to capture the experimental behaviour of the sandwich plate very closely especially in the early part of the curves before the initiation of damage. However, there are some inaccuracies in modelling of the rebound phase of the impact which leads to some differences in the final energy absorbed in the plate.

The peak force and maximum displacement obtained from the simulation is compared to the experimental values in Figure 4.39 Comparison of experiment and LS-Dyna simulation for Kevlar Rohacell sandwich: (a) Peak Force and (b) Max displacement figure.4.39. It can be seen that the peak forces and the maximum displacement compares well with the experiment. The maximum force for the impact of 8 J obtained from the experiment is 1790 N and increases to 2200 and 2490 N for the 12 J and 16 J impact respectively while the average experimental values are 1973, 2097 and 2027 N for the three impact cases. Similarly, the corresponding maximum displacement values obtained from the drop tower tests of 8.4, 16 and 22 mm are comparable to the results from the LS-Dyna simulation of 8.6, 14 and 20 mm.

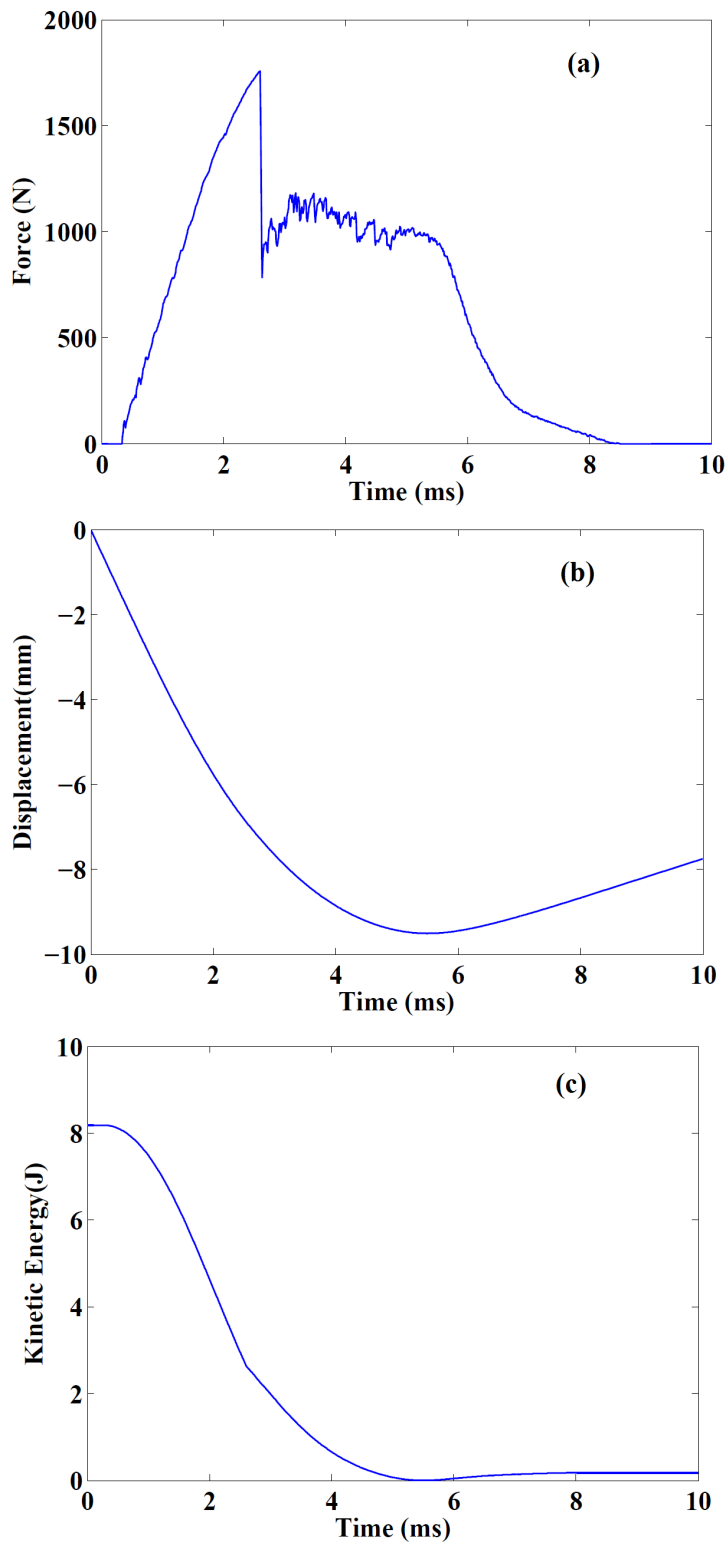


Figure 4.35. Force, displacement and energy time histories for Kevlar sandwich plate

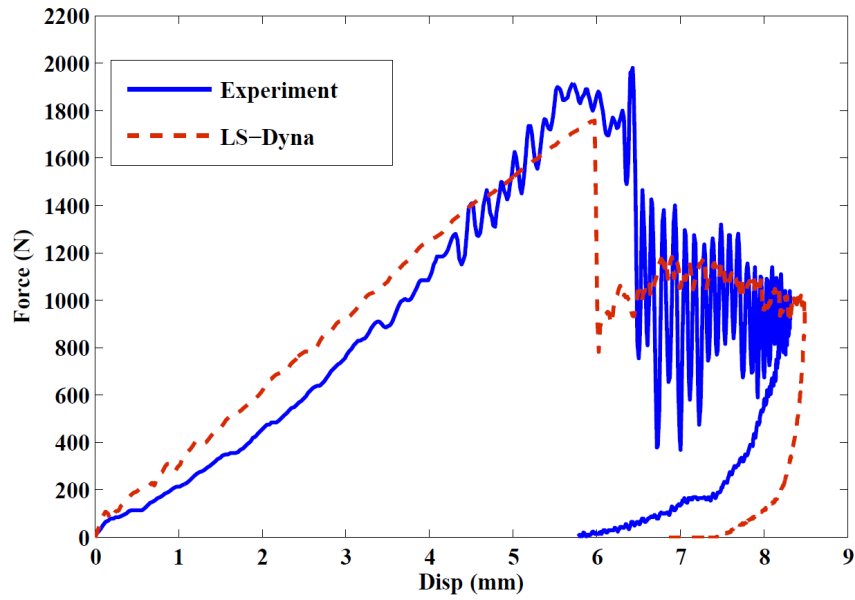


Figure 4.36. Comparison of Force -displacement curves for 8 J impact for KR sandwich

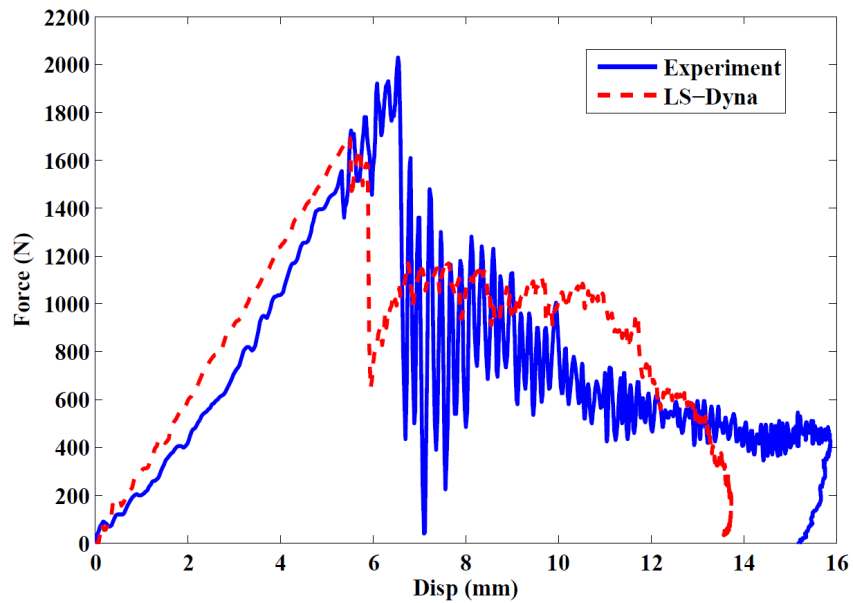
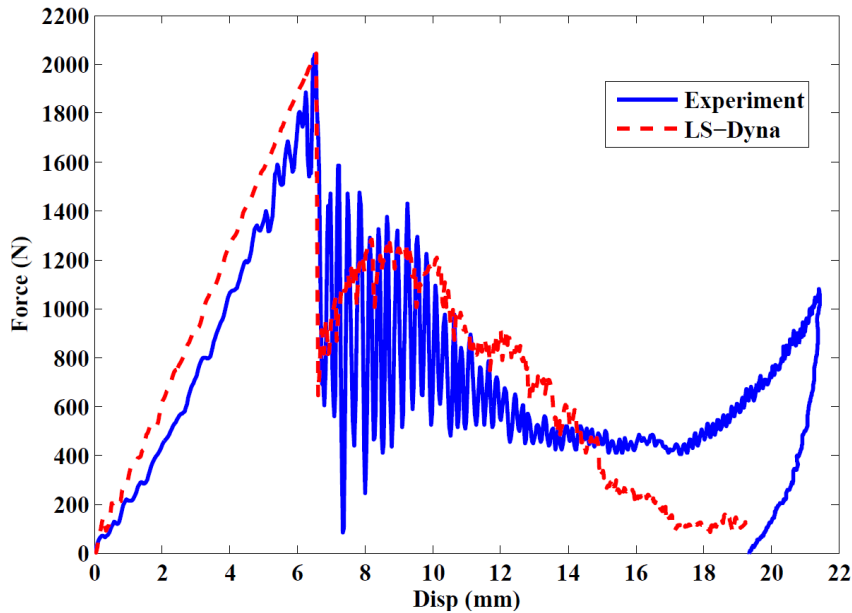


Figure 4.37. Comparison of Force -displacement curves for 12 J impact for KR sandwich



**Figure 4.38.** Comparison of Force -displacement curves for 16 J impact for KR sandwich

Figure 4.40 Contour plot of damage in longitudinal direction of top facesheet figure.4.40 shows the contour plot of History variable 1 which corresponds to damage in longitudinal direction of top facesheet for an impact of 16 J. The first image shows the accumulation of damage in the centre of the impact just before the element deletion is initiated. The damage variable in longitudinal, transverse and shear directions have a maximum value of 1 and on reaching that value, the element is deleted. It can be seen that as the impact progresses, the elements close to the centre of impact are deleted to create a penetration failure, which is approximately the size of the diameter of the impactor. This causes the foam core material underneath these elements to come directly in contact with the impactor. The solid elements of the foam core undergo severe deformation and eventual erosion. The erosion of the foam elements are dependent on maximum principal strain criterion. In order to avoid, negative volume errors that are typically associated with the simulation of large deformation in foam materials, an Hourglass control was defined.

The large displacement in the core for a case of 16 J impact is shown in Figure 4.41 Core damage in the Rohacell foam sandwich plate impacted at 16 J figure.4.41. It can be seen that the elements of the foam directly under the impactor have been eroded once they reach the maximum principal strain criteria for element erosion.

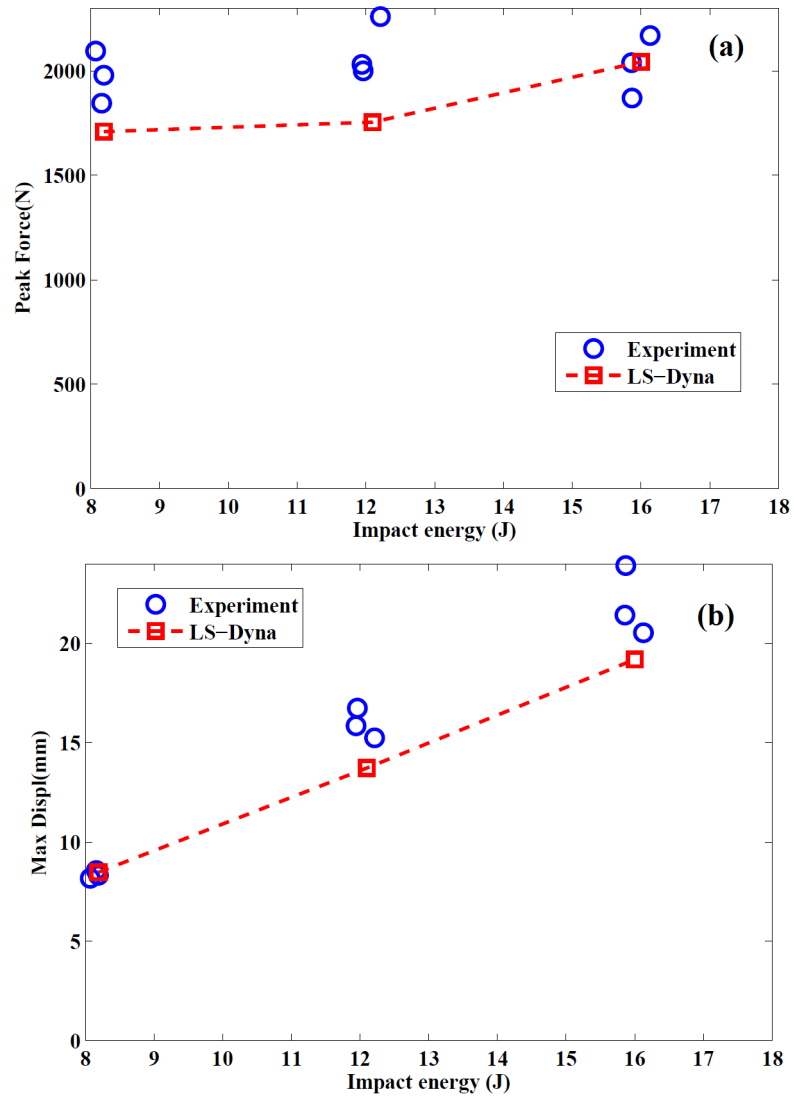


**Figure 4.39.** Comparison of experiment and LS-Dyna simulation for Kevlar Rohacell sandwich: (a) Peak Force and (b) Max displacement

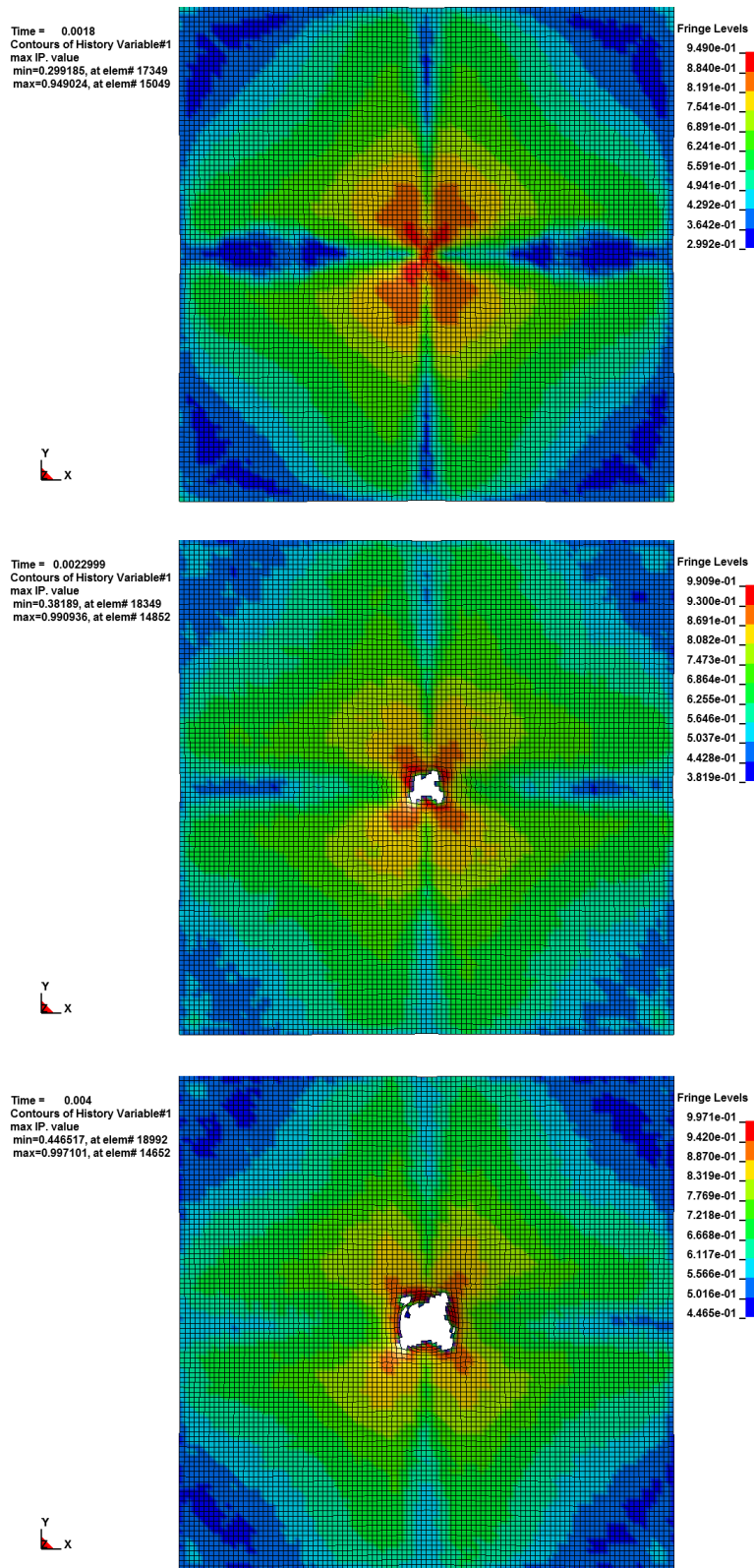
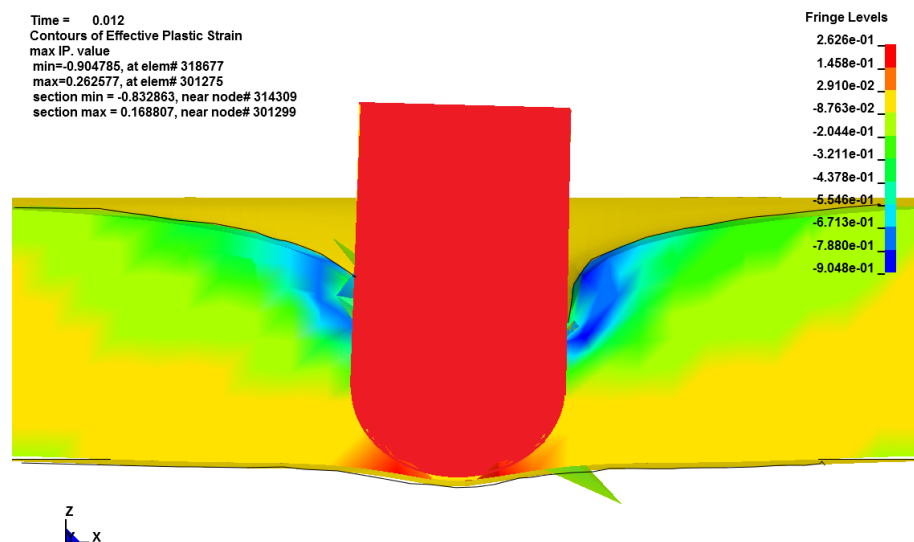


Figure 4.40. Contour plot of damage in longitudinal direction of top facesheet

It should be noted that foam elements encounter Negative Volume issues, which is avoided the definition of internal contact treatment using \*CONTACT INTERIOR specifically designed for soft materials. According to Bala [115], once the part set of the soft materials is determined, LS-Dyna monitors the smallest thickness dimension of each solid element in the part set checks if its value is less than the product of a scale factor and initial smallest thickness dimension. If the current smallest thickness dimension falls below the value, LS-Dyna applies contact forces to separate them much like in classical contact definitions. This additional force help to keep the opposing surfaces of the element away from each other to avoid element inversion problem.



**Figure 4.41.** Core damage in the Rohacell foam sandwich plate impacted at 16 J

The comparison of the Force -displacement curves for impact of 8 J, 12 J and 16 J for the Kevlar/Nano-Rohacell (KNR) sandwich is shown in Figures 4.42 Comparison of Force- displacement curves for 8 J impact for KNR sandwich figure.4.42, 4.43 Comparison of Force- displacement curves for 12 J impact for KNR sandwich figure.4.43, 4.44 Comparison of Force- displacement curves for 16 J impact for KNR sandwich figure.4.44. The difference in peak force in the KR and KNR sandwich panels is due to the different failure modes, because the Kevlar facesheets have different tensile and shear properties. It can be seen that there is good agreement of the initial phase of contact

upto the initiation of damage. The peak forces of the LS-Dyna model of KNR sandwich are 1782, 2198 and 2488 N for the impact of 8 J, 12 J and 16 J, respectively. The corresponding maximum displacements of the impactor are 7.7, 9.5 and 10.7 mm.

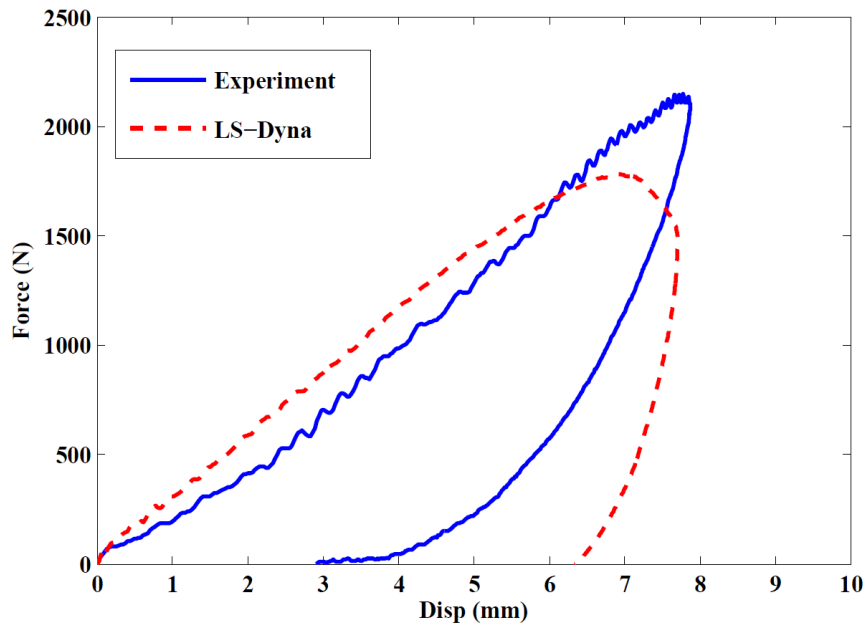


**Figure 4.42.** Comparison of Force- displacement curves for 8 J impact for KNR sandwich

It can be seen that the FE model is not able to reproduce the matrix damage modes which are characterised by the first drop and oscillations in the force values. The peak force and maximum displacement are captured in the simulation. The impactor then bounces back after the peak and the load is reduced to zero but the simulation predicts large residual displacement for the KNR sandwich panels. The inaccuracies in the modelling of the unloading phase of the impact in the case of the sandwich plate with nanoparticles is more pronounced than the case with neat resin. The elastic recovery in the experimental response of KNR sandwich is not replicated. The inability to model the elastic rebound of the sandwich and some of the failure modes associated with matrix damage causes some differences in the final energy absorbed in the plate. Figure 4.45 Comparison of energy absorbed by Kevlar/Nano Rohacell sandwich figure.4.45 shows the comparison of energy absorbed calculated as the area under the force - displacement curve to the experimental result. The final absorbed energy with different impact energies predicted by the numerical model

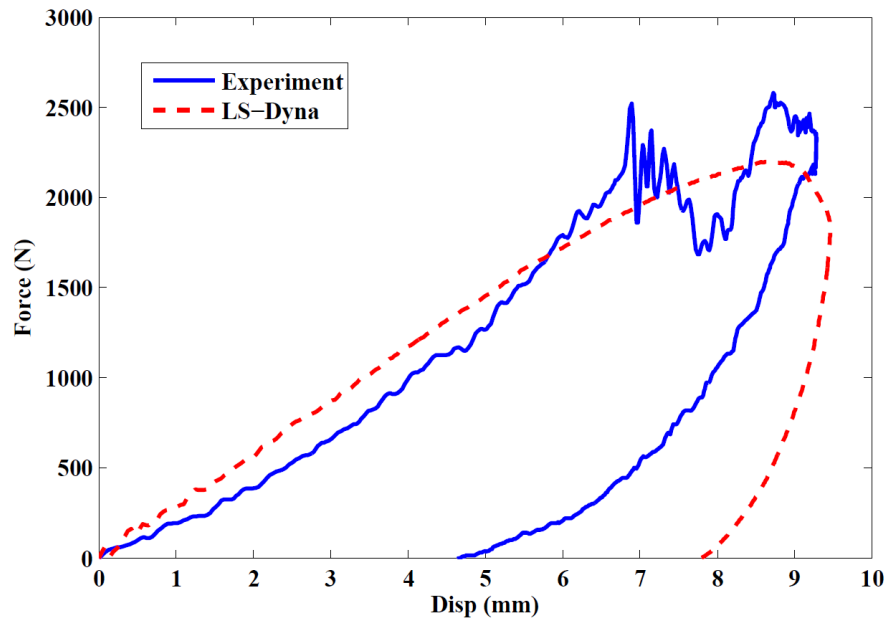


Figure 4.43. Comparison of Force- displacement curves for 12 J impact for KNR sandwich

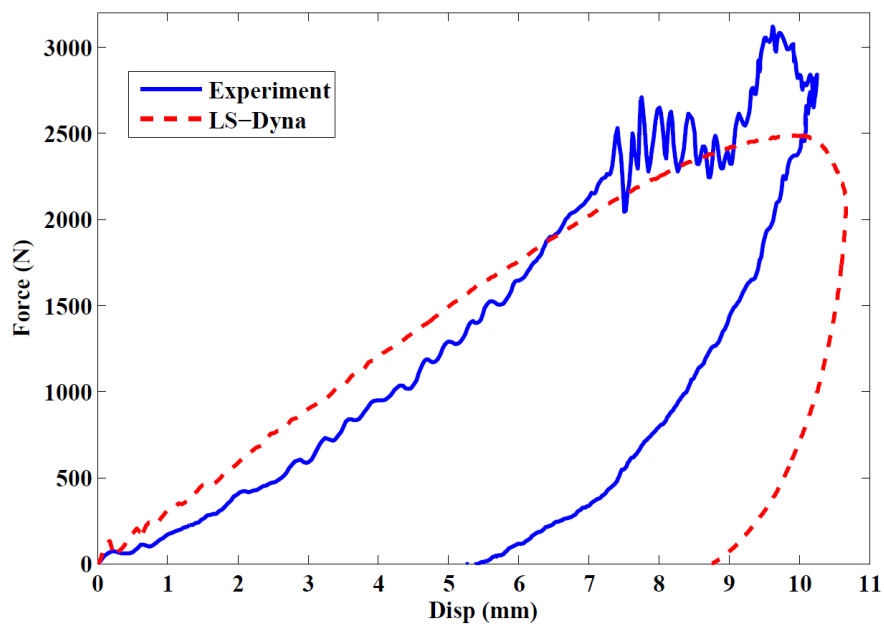
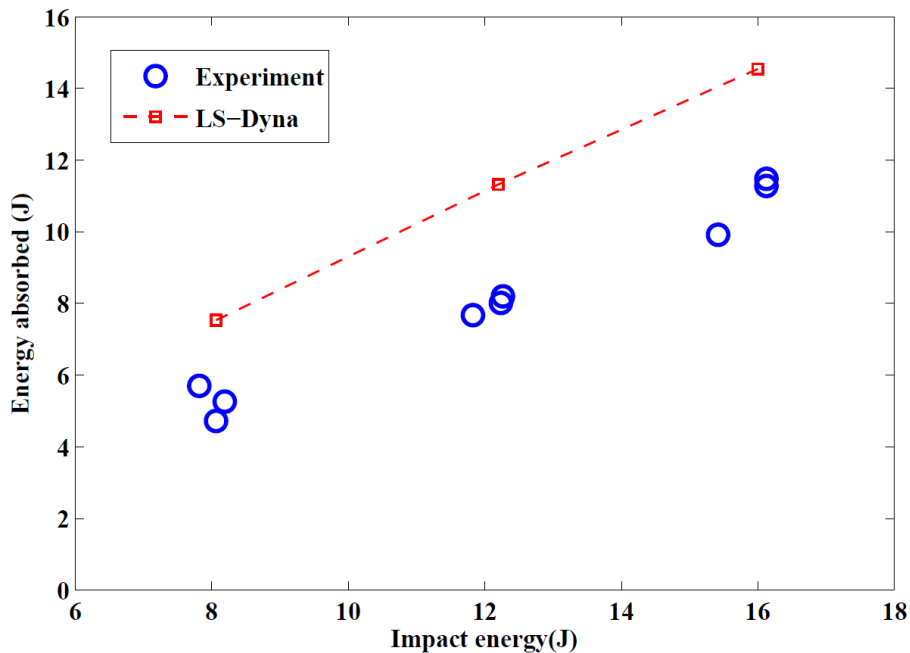


Figure 4.44. Comparison of Force- displacement curves for 16 J impact for KNR sandwich

is higher than the experimental results. The higher energies observed in the LS-Dyna model relate to lower elastic recuperation and consequently major damage. However, the trendlines are maintained, which will provide a good framework for the designer to choose appropriate sandwich materials.



**Figure 4.45.** Comparison of energy absorbed by Kevlar/Nano Rohacell sandwich

## 4.6 Summary

The objective of this chapter was to develop a numerical model based on explicit FE software LS-Dyna to study the low velocity impact behaviour of sandwich panels. An overview of the current state-of-the-art on finite element modelling of sandwich panels was presented. An LS-Dyna model was developed for the simulation of normal impact on Kevlar composite laminates and sandwich panels with Kevlar facesheets and Rohacell foam core. A constitutive law based on Continuum Damage Mechanics available in the material library as Laminated Composite Fabric model (MAT58) was used for the simulation of the composite plate. The input parameters to the material model were obtained by a combination of mechanical tests and parametric studies. A Crushable foam model (MAT63) was used for the foam core. The macroscopic properties of the Kevlar-epoxy facesheets with 10% M52N Nanostrength triblock copolymer was also studied to develop FE models of the sandwich

---

plate with nanoparticles. The simulated contact force and impactor displacement responses along with the predicted failure modes of the sandwich panel are in good agreement with that of the experimental measurements provided in previous chapter. The LS-Dyna model developed had some limitations in the modelling of the failure modes associated with matrix damage and the elastic rebound observed in sandwich plates with nano-reinforcements was not replicated. However, the overall response of the sandwich panels with and without nanoparticles were reproduced with reasonable accuracy and the validated FE model can be used by designers for studying the impact problem for other conditions. The FE model will result in reducing the cost and time required for extensive experimental tests. In the next chapter, the FE model developed here is validated for a case of parabolic impact where the trajectory of the impactor is defined as a parabola with long contact duration. This mode of tests simulate the real world situations that sandwich plates can encounter. Hexapod tests done using a modified Stewart platform and the simulation of parabolic impact are presented in the next chapter.



## Chapter 5

# Parabolic impact of sandwich panels with and without nano-reinforcement

### 5.1 Introduction

Low velocity impact response of sandwich panels is typically tested under impact conditions explained in the previous chapters and the response of the panels are analysed in terms of peak load, absorbed energy and deflection at peak load. The impact loading is applied along one fixed direction that is perpendicular to the plane of the sandwich specimen. The standard test method for impact testing are for normal incidence impact and the test devices are designed for normal impact condition. However, normal impacts described in the previous chapters rarely occur in real engineering situations. Instead, the structures are more frequently loaded at some oblique angle or complex trajectory. While normal incidence impact tests are easy to carry out using devices such as the drop tower, oblique tests are difficult to undertake experimentally, given the need to guide the projectile, coupled with the presence of a horizontal force component that applies a load to the required guide rails. Zhou et al. [118] found that the impact energy for an oblique impact of sandwich composite is dissipated in shearing both the composite and the foam around the perimeter of the projectile, as well as crushing the foam ahead of the impactor. The perforation energy was found to increase with increasing angle of incidence. Goswami et al. [50] found that the debonding along the facesheets and the core interface of sandwich panels is predominated by a sliding mode and observed that low relative density of the core will result in more critical debonding [50]. Zhou et al. [118] also observed that the shear fracture properties of the foams had a significant effect on the perforation resistance of the sandwich structures, suggesting that this mode of failure is important in determining the impact resistance of sandwich structures. Chai and Zhu [119] reviewed the existing literature on the low velocity impact of sandwich structures and found that studies on sandwich panel subjected to low- velocity impact at angles other than perpendicular to the plane of the sandwich

were limited. Guérard et al. [120] noted that normal impacts do not correspond to the complex loading that real structures encounter and developed a tri-dimensional impact device called Hexapod to experimentally study the impact loading of sandwich plates with a parabolic trajectory. Sandwich plates with metallic facesheets were investigated but a proper study of sandwich plates with laminated facesheets subjected to parabolic impact has not been undertaken. This chapter is focussed on the study of parabolic impact testing of Kevlar Rohacell sandwich plates with and without nanoparticles in the epoxy matrix. The experimental setup used for the parabolic impact is described in the next section. A preliminary finite element model is developed to simulate the parabolic impact of Aluminium- Divinycell sandwich and the model is validated by comparison with reported literature. An LS-Dyna model of the Kevlar Rohacell sandwich described in the previous chapter is then used to model the parabolic impact case.

## 5.2 Experimental setup for parabolic impact testing of sandwich panels

Low-velocity impact tests were performed using the Hexapod facility available in the Dynamics platform of DuMAS of I2M laboratory in Arts et Métiers Paris-tech, Bordeaux. Figure 5.1 Hexapod setup for tri-dimensional impact of sandwich panels figure.5.1 shows the Hexapod, which is a modified Gough-Stewart platform, a type of parallel robot constituted of a fixed and a moving platform. Devices placed on the top plate can be moved in the six degrees of freedom, corresponding to three translation axes and three rotation axes, independently. Its horizontal velocity can reach 1.4 m/s and the maximal vertical velocity is 1 m/s. A seventh electromechanical jack (of maximum velocity 3.5 m/s) is implemented on the top plate to increase the vertical speed. The velocity achieved with this configuration of Hexapod is equivalent to the drop tower but with the advantage of imposing a 3D trajectory to the projectile [120]. The tri-axial load cell (Kistler, 9377C, Fx and Fy range: 3000 N, Fz range: 5000N) is placed between the cylindrical impactor and the bottom end of the seventh jack. The Hexapod is setup in such a way that it is possible to change the impactor easily with other geometries such as wedge-shaped impactor.

A high-speed camera (Photron Fastcam APX RS, 5000 frames per second) was used to film the impact. The side of the tested sample was coated with a fine spray of paint to enhance the random texture of the foam and allow for Digital Image

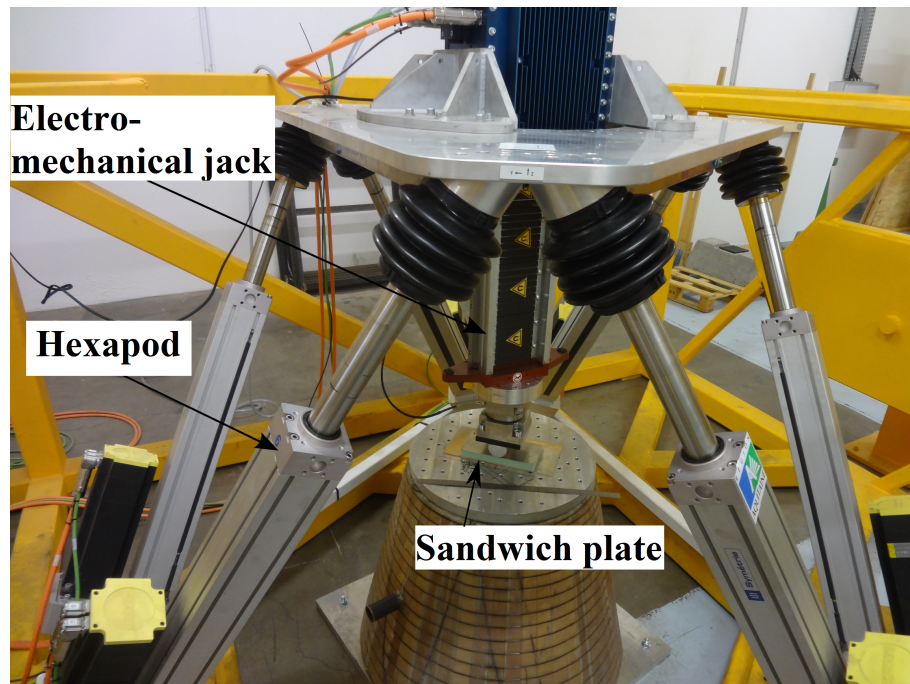
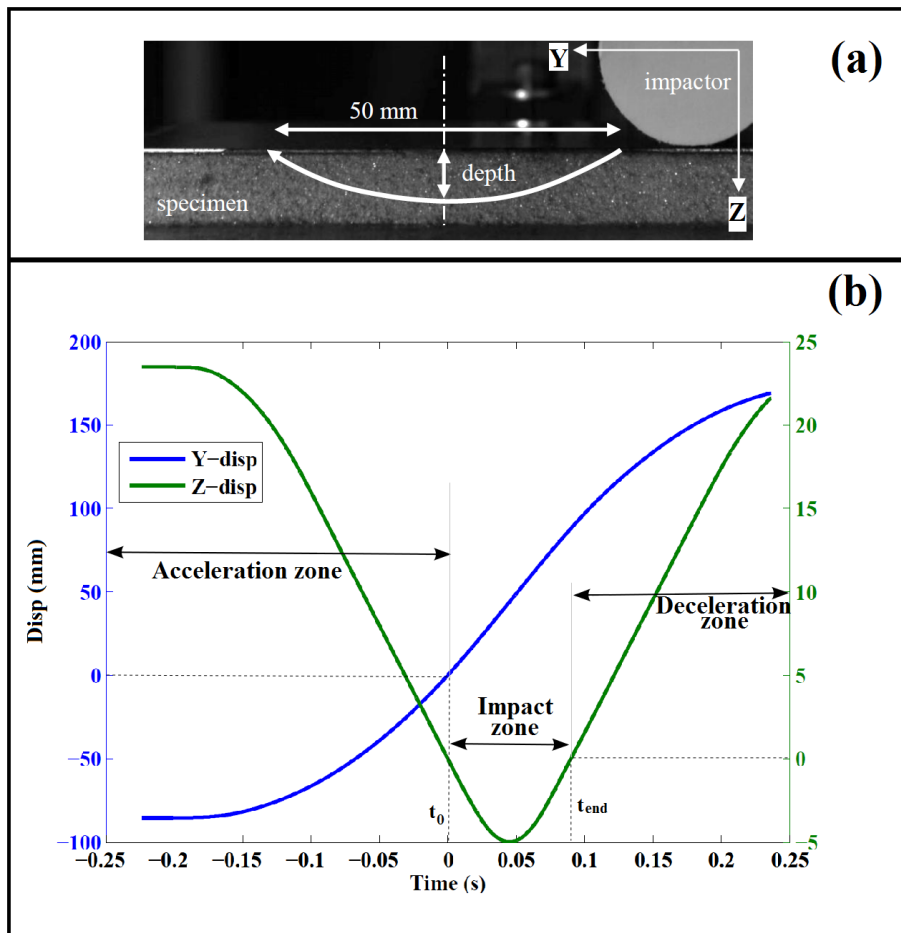


**Figure 5.1.** Hexapod setup for tri-dimensional impact of sandwich panels

Correlation (DIC) calculation (VIC-2D, Correlated Solution). Load history of each impact event was measured by the 3D load cell located between the impactor and the jack extremity. In the case of a normal impact using a drop tower, the impactor is raised to a particular height and released and the potential energy of the impactor is converted to kinetic energy. In the parabolic impact, a trajectory is imposed to the impactor in terms of displacement curves in the Y- and Z- axis, corresponding to the horizontal and vertical directions. The parameters defining the impact are the depth of penetration into the impacted specimen and the width or opening of the parabola.

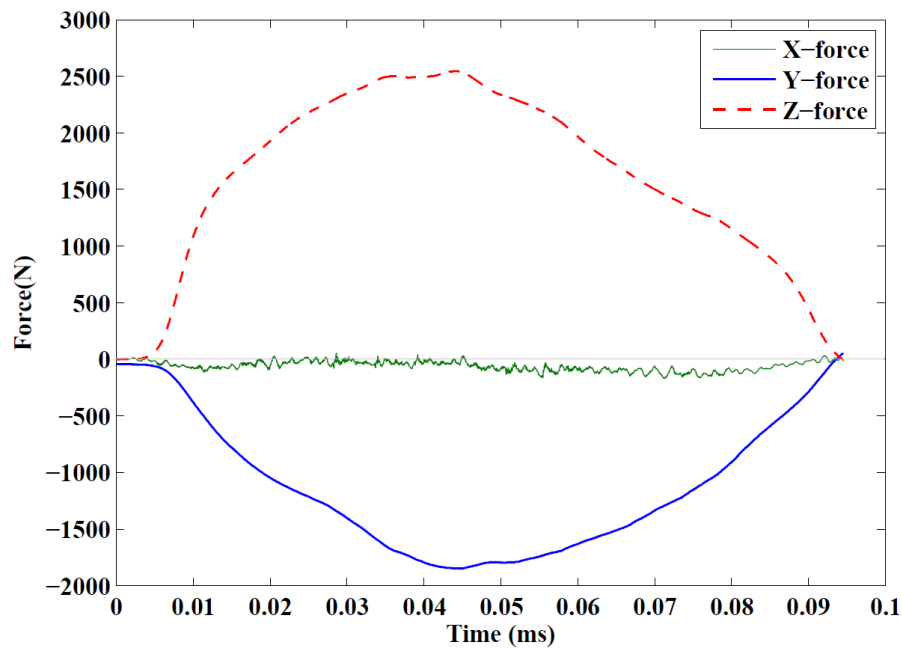
The Hexapod setup was used for three dimensional impact testing of sandwich samples made of Aluminium facesheets and PVC closed-cell foam (Divinycell<sup>®</sup>) core by Guérard et al. [120]. Sandwich samples with two different thicknesses of the 2024 aluminium facesheets: 0.5 mm and 1 mm were considered. The PVC foam core had a 20-mm thickness. The sandwich panels were assembled using a two-component epoxy adhesive (Araldite AW 106R/hardener HV 953U) which was chosen for their high shear and peel strength. The dimensions of the sandwich samples were 200 mm long and 120 mm wide. A parabolic displacement shown

in Figure 5.2(a) Parabolic trajectory for Aluminium Divinycell sandwich plate and Displacement input for the Hexapodfigure.5.2 was imposed to the impactor with a depth of penetration of 5 mm into the impacted specimen and the width of the parabola was 50 mm. Figure 5.2(a) Parabolic trajectory for Aluminium Divinycell sandwich plate and Displacement input for the Hexapodfigure.5.2 also shows the translation displacement in the Y- direction and Z- direction, which is input to the hexapod. This represents the entire trajectory input to the impactor with the beginning of the contact with the sandwich target represented by  $t_0$  and the end of contact denoted by  $t_{end}$ . The horizontal velocity during impact (along Y direction) was constant and equal to 1 m/s and the vertical acceleration was equal to 4 m/s<sup>2</sup>.



**Figure 5.2.** (a) Parabolic trajectory for Aluminium Divinycell sandwich plate and Displacement input for the Hexapod

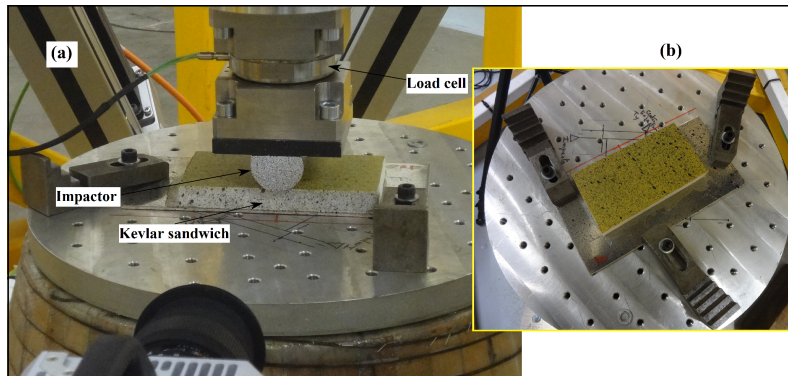
The force- time history obtained from the Kistler load cell is shown in Figure 5.3 Typical Force- time results obtained for parabolic impact of Aluminium Divinycell sandwich platefigure.5.3. This case corresponds to a parabola with maximum depth of penetration of 5 mm and an opening of 50 mm. It can be seen that the vertical force (Z-force) is larger in magnitude than the horizontal component of force (Y-force). The transverse force (X-direction) can be considered negligible compared to vertical and horizontal force components.



**Figure 5.3.** Typical Force- time results obtained for parabolic impact of Aluminium Divinycell sandwich plate

### 5.3 Parabolic impact testing of Kevlar Rohacell sandwich

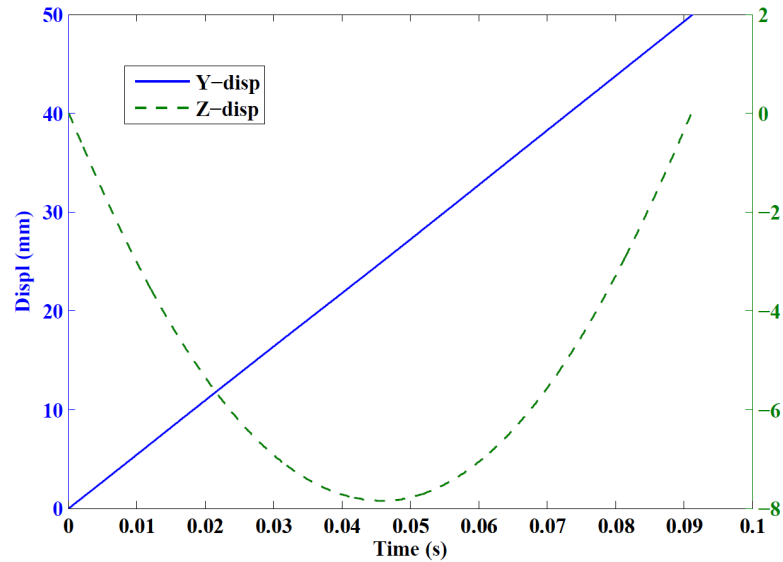
Parabolic impact tests were conducted on sandwich plates with Kevlar facesheets with neat resin and with nano-modified resin and Rohacell foam core, in order to study the effect of the nanoparticles on the behaviour of the sandwich plate. Since the behaviour of the sandwich samples were shown to be repeatable for the normal impact tests, only one sample of each type was tested for each configuration. Figure 5.4(a) Hexapod setup with cylindrical impactor and Kevlar-Rohacell sandwich and (b) Clamping mechanismfigure.5.4 shows the Hexapod setup for the parabolic impact of Kevlar Rohacell sandwich plates. A cylindrical impactor is shown in the



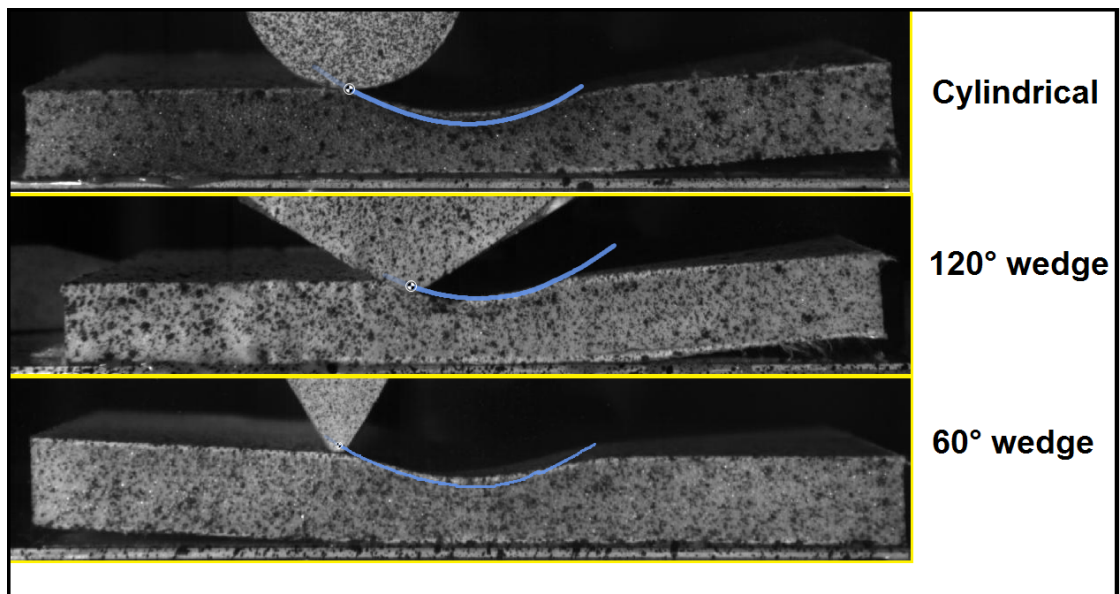
**Figure 5.4.** (a) Hexapod setup with cylindrical impactor and Kevlar-Rohacell sandwich and (b) Clamping mechanism

image but it is possible to change the impactor to study the effect of the impactor geometry on the impact behaviour of the sandwich plate. Figure 5.4(a) Hexapod setup with cylindrical impactor and Kevlar-Rohacell sandwich and (b) Clamping mechanism. Figure 5.4 (b) shows the clamping mechanism for the sandwich plate. The sandwich plate is bonded to an aluminium sheet approximately 300 mm long and 180 mm wide using the Araldite adhesive specified in the previous section. A set of jaws are strategically placed at three points around the plate to clamp the aluminium sheet to a rigid base and to prevent the movement of the Kevlar sandwich plate during the impact.

Figure 5.5 Parabolic trajectory: Displacement input for the hexapod. Figure 5.5 and Figure 5.6 Parabolic trajectory with different impactor geometries - Cylindrical, 120° and 60° wedge. Figure 5.6 show the trajectory of the parabola (Traj1) that was input to the impactor and the different geometry impactors tested. The three impactors correspond to a cylindrical impactor with radius of 25 mm, a wedge shaped impactor with wedge angle of 120° and a sharp wedge impactor with angle of 60° wedge. The parabolic trajectory corresponding to the contact period that is input to the Hexapod is shown in the Figure 5.5 Parabolic trajectory: Displacement input for the hexapod. Figure 5.5 and has Y- displacement of 50 mm, which is centered on the plate, i.e., the maximum displacement in the vertical direction coincides with the geometric centre of the plate in order to minimise edge effects. The displacement in the horizontal direction increases linearly, while the displacement in Z- direction is a parabolic curve with a maximum of 8 mm. The contact duration for the parabolic impacts are fixed and are close to 90 milliseconds representing a prolonged contact



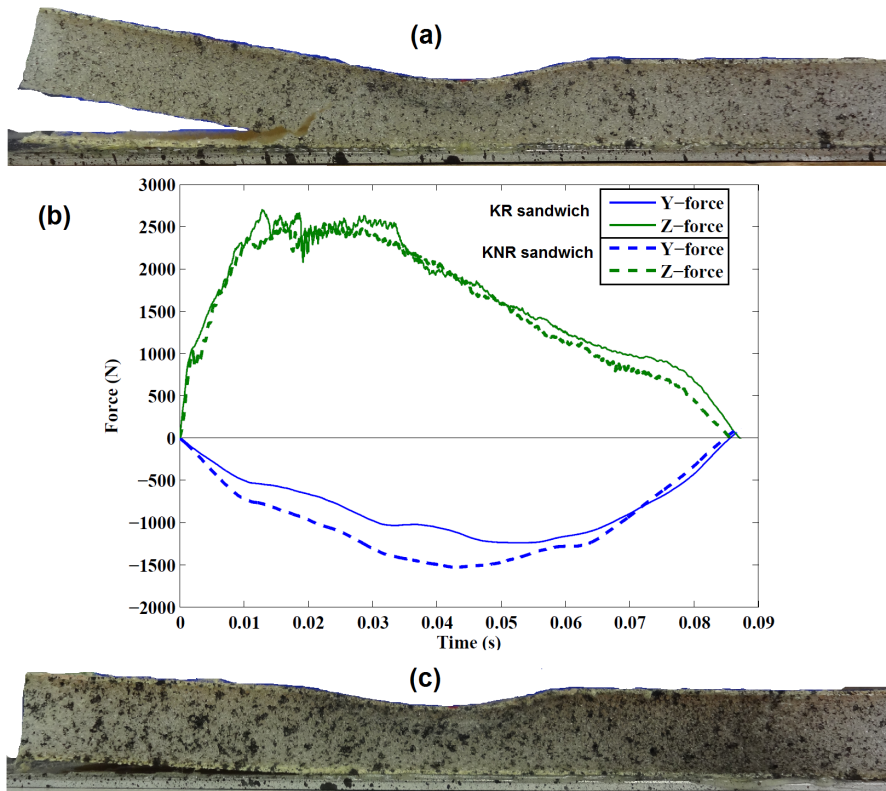
**Figure 5.5.** Parabolic trajectory: Displacement input for the hexapod



**Figure 5.6.** Parabolic trajectory with different impactor geometries - Cylindrical, 120° and 60° wedge

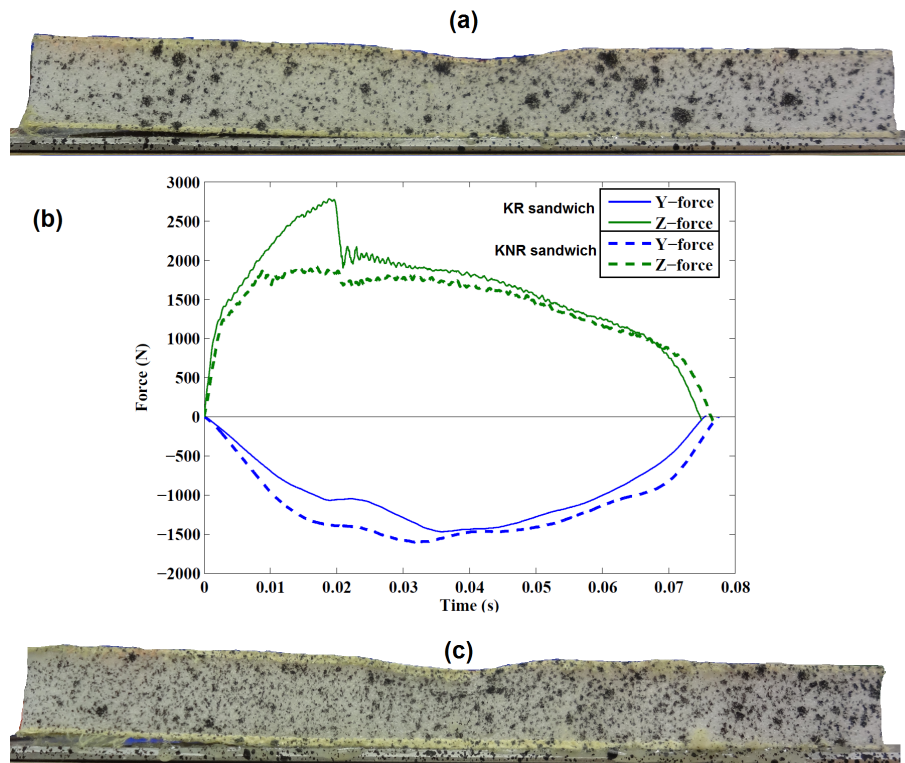
with the sandwich panel, while the contact duration for the normal impact case in the drop tower are a function of the target plate and are typically of the order of 10 milliseconds.

Figure 5.7(a) KR sandwich samples after impact by cylindrical impactor, (b)



**Figure 5.7.** (a) KR sandwich samples after impact by cylindrical impactor, (b) Force - time curve for impact by cylindrical impactor and (c) KNR sandwich samples after impact by cylindrical impactor

Force -time curve for impact by cylindrical impactor and (c) KNR sandwich samples after impact by cylindrical impactor. Figure 5.7 shows the Force- time curve (b) for impact by cylindrical impactor for both KR and KNR sandwich plates. The forces correspond to the vertical component of the force (Z-Force) and the horizontal component of the force (Y-force). It can be seen that the force curves are very similar for the sandwich plates with and without Nanostrength. But the damage observed in the two plates are different. Figure 5.7(a) KR sandwich samples after impact by cylindrical impactor, (b) Force -time curve for impact by cylindrical impactor and (c) KNR sandwich samples after impact by cylindrical impactor. Figure 5.7(a) and (c) show KR and KNR sandwich samples respectively, after impact by the cylindrical impactor. It can be seen that there is shear damage in the foam core of the sample with neat resin which results in the debonding between the bottom facesheet and the core. However, in the samples with Nano resin, the debonding is between the



**Figure 5.8.** (a) KR sandwich samples after impact by  $120^\circ$  wedge shape impactor, (b) Force -time curve for impact and (c) KNR sandwich samples after impact by  $120^\circ$  wedge impactor

bottom facesheet and the aluminium support.

The Force- time curve for impact by  $120^\circ$  wedge shape impactor and Traj1 for both KR and KNR sandwich plates are shown in Figure 5.8(a) KR sandwich samples after impact by  $120^\circ$  wedge shape impactor, (b) Force -time curve for impact and (c) KNR sandwich samples after impact by  $120^\circ$  wedge impactorfigure.5.8. The horizontal component of the force (Y-force) is similar for the sandwich plates with and without Nanostrength, while the KR sandwich plate has higher peak force in vertical axis (Z- force). The contact durations are also slightly different, which can be explained by the small variation in thickness between the two samples. Debonding is observed between the bottom facesheet and the aluminium support for both sandwich plates (Figure 5.8(a) KR sandwich samples after impact by  $120^\circ$  wedge shape impactor, (b) Force -time curve for impact and (c) KNR sandwich samples after impact by  $120^\circ$  wedge impactorfigure.5.8(a) and (c)). The trajectory of the

impactor is from left to right in these figures. It can also be observed that the contact duration for the Wedge120 sample is much lower than the other two, i.e., 74 milliseconds compared to 88 milliseconds for the cylindrical and Wedge60 impactor. Though the parabolic trajectory, in terms of the depth and opening of parabola defined to all the three samples are the same, the trajectory for the Wedge120 sample had a different parameter for velocity and acceleration which resulted in shorter contact duration.

The Force- response for impact by 60° sharp wedge impactor for both KR and KNR sandwich plates and the post-impact samples are shown in Figure 5.9(a) KR sandwich samples after impact by 60° wedge shape impactor, (b) Force- time curve for impact and (c) KNR sandwich samples after impact by 60° wedge impactorfigure.5.9. It can be seen that the Y-force for KNR sandwich plate has higher peak force and in fact reached the maximum of the sensor range as observed in the saturation at 3000 N. This is due to the formation of shear failure in the core very early in the trajectory of the impact, which resulted in a hinge formation. The KR sandwich on the other hand has failure of the adhesive bond between the aluminium support and the sandwich on the opposite side of the impact. This test is not representative of the difference in behaviour of the sandwich plates with and without the nanoparticles and further testing is necessary to draw any conclusions about the effect of Nanostrength on the parabolic impact response of sandwich panels.

The progression of impact for the parabolic impact of KR sandwich with 60° wedge impactor is shown in Figure 5.10Progression of impact for KR sandwich with 60° wedge impactor (a)t= 0ms, (b)t=14ms, (c)t=45ms and (d)t=88msfigure.5.10. It can be seen that the impactor comes into contact with the sandwich plate at t=0 ms and image (b) corresponds to t=16 ms, which is immediately after the peak force is reached. It can be noticed that there is debonding of the sandwich panel from the aluminium support plate, which causes the sudden drop in the Z- force observed in the Figure 5.9(a) KR sandwich samples after impact by 60° wedge shape impactor, (b) Force- time curve for impact and (c) KNR sandwich samples after impact by 60° wedge impactorfigure.5.9. The image (c) relates to the point of maximum z-displacement and the image (d) at t=88 ms is the end of the contact between the impactor and the sandwich target.

A comparison of the Force- displacement response in the vertical direction for parabolic impact of KR sandwich plate with the three different impactor geometries

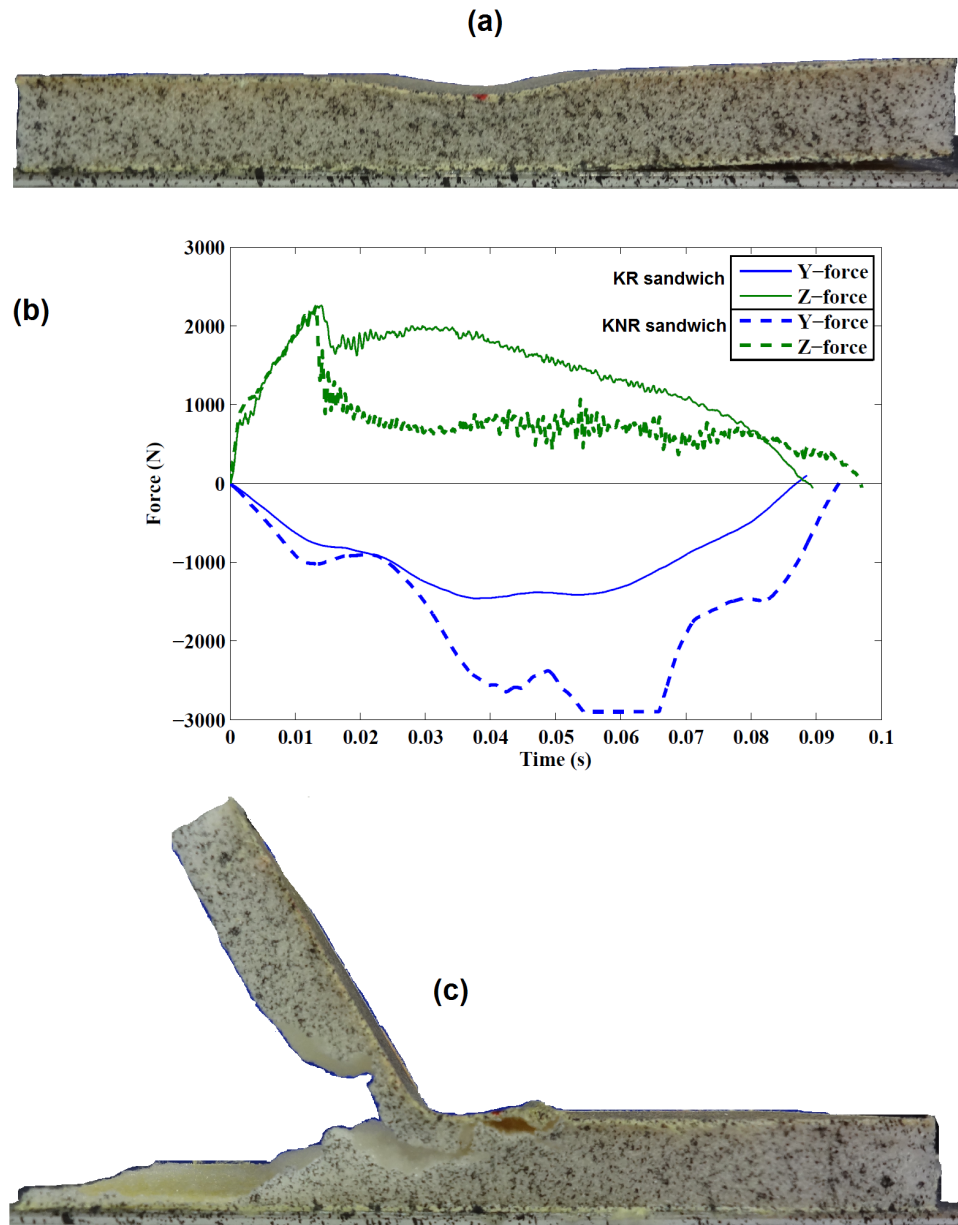


**Figure 5.9.** (a) KR sandwich samples after impact by  $60^\circ$  wedge shape impactor, (b) Force- time curve for impact and (c) KNR sandwich samples after impact by  $60^\circ$  wedge impactor

is given in Figure 5.11 Comparison of Z- Force history for Kevlar-Rohacell sandwich with different impactor geometries - Cylindrical,  $120^\circ$  and  $60^\circ$  wedge figure.5.11. It can be seen that the initial linear region i.e., the stiffness of the plate at the beginning of the contact is nearly identical for the samples irrespective of the impactor

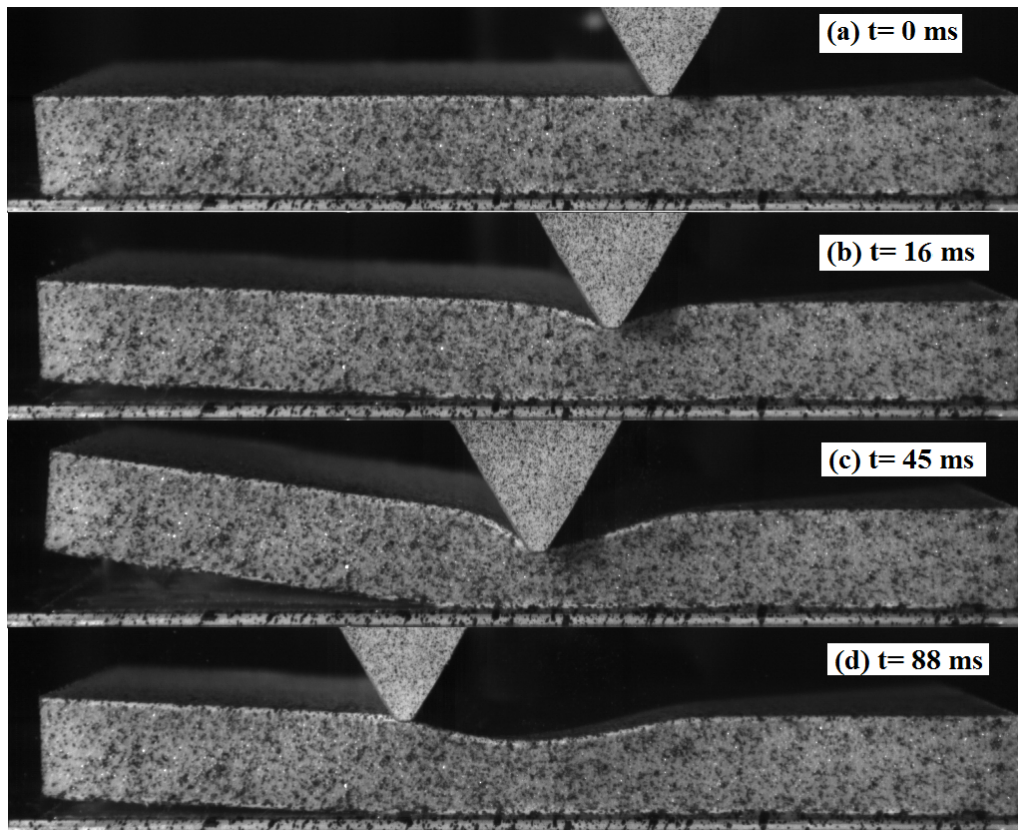


**Figure 5.10.** Progression of impact for KR sandwich with  $60^\circ$  wedge impactor (a) $t=0$ ms, (b) $t=14$ ms, (c) $t=45$ ms and (d) $t=88$ ms

geometry. The stiffness or slope changes for a displacement of 0.5 mm and remains constant until the peak force is reached and a drop in force is observed. It should also be noted that the Force- displacement curves shown in Figure 5.11 Comparison of Z- Force history for Kevlar-Rohacell sandwich with different impactor geometries - Cylindrical,  $120^\circ$  and  $60^\circ$  wedge figure.5.11 are different from the curves for the normal impact case described in the previous chapters.

In addition to the trajectory tested with depth of the parabola of 8 mm and opening of 50 mm, two other tests were conducted with cylindrical impactor to study edge effects. In the second trajectory (Traj2), shown in Figure 5.12 Parabolic trajectory of the cylindrical impactor: (Top) Traj2 and (Bottom) Traj3 figure.5.12, the width and depth of the parabola are maintained as before (50 mm and 8 mm, respectively) but the impact is not centered on the plate but is offset in such a way that the impact begins 50 mm to the right of the centre of the plate and ends in

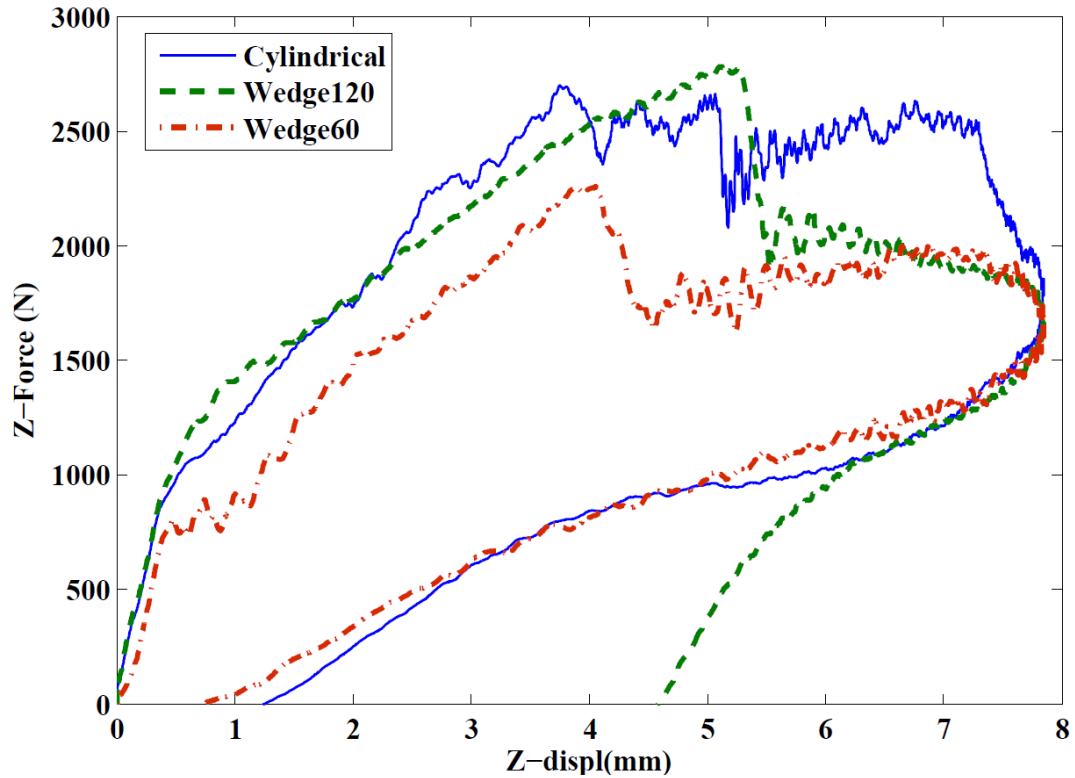


**Figure 5.11.** Comparison of Z- Force history for Kevlar-Rohacell sandwich with different impactor geometries - Cylindrical, 120° and 60° wedge

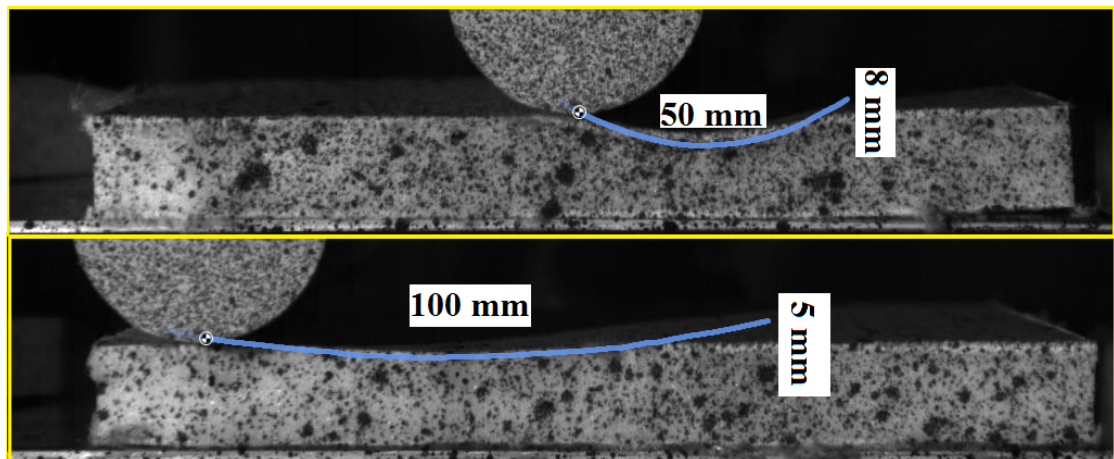


**Figure 5.12.** Parabolic trajectory of the cylindrical impactor: (Top) Traj2 and (Bottom) Traj3

the middle. A third trajectory (Traj3) was chosen with the width of the parabola is 100 mm (starting from 25 mm to the right of the centre of the plate) and a depth of 5 mm. A smaller value of depth was chosen to avoid any shear failure in the core or debonding in the sandwich.

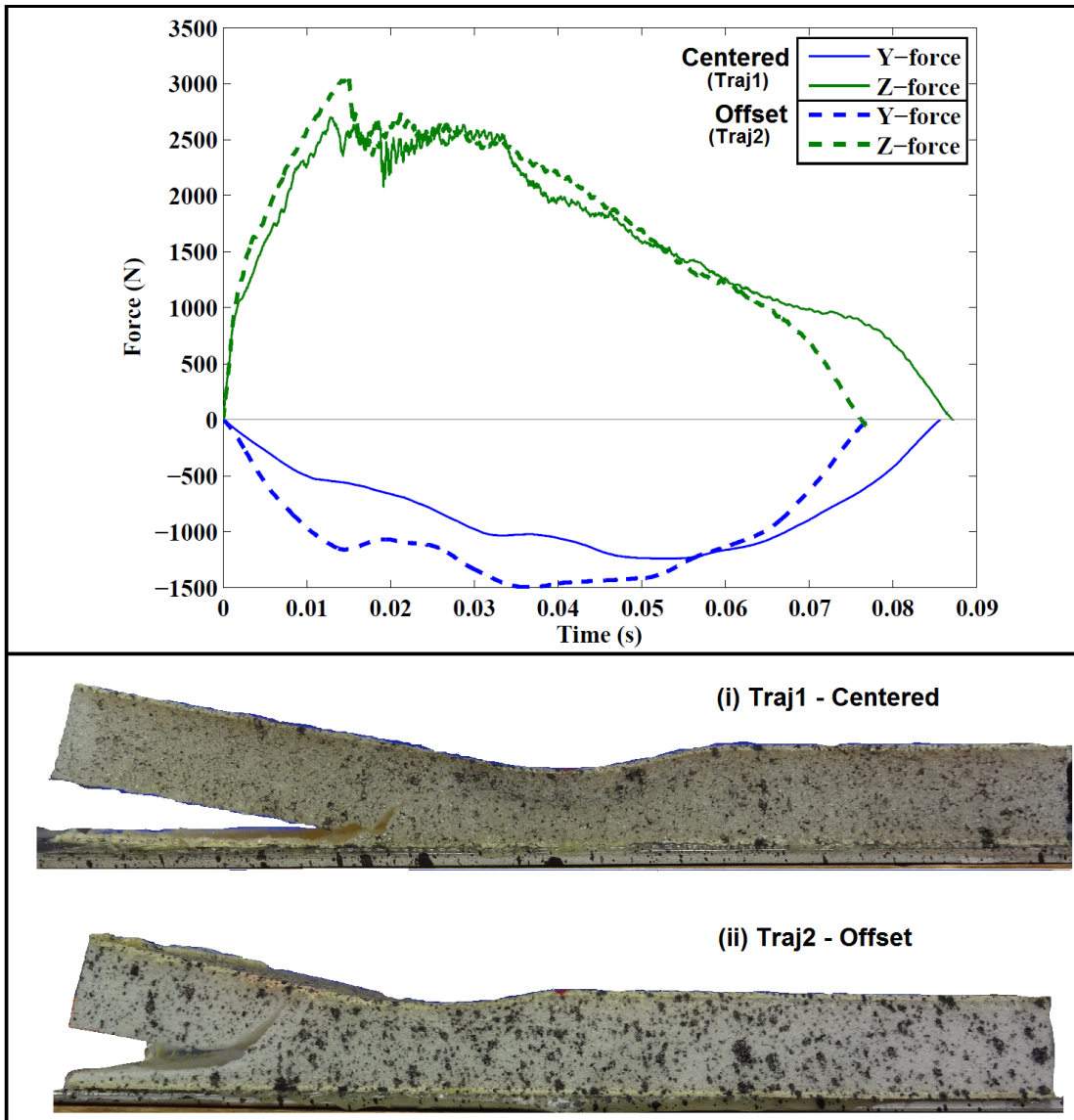


**Figure 5.13.** Effect of location of impact for KR sandwich plate and cylindrical impactor

Figure 5.13 shows the comparison of the force response for the parabolic impact of KR sandwich plate with a cylindrical impactor for two trajectories (Traj1 and Traj2) that correspond to the same opening and depth of the parabola but

at different locations in the plate. It can be seen that the overall response is very similar for the two cases. Visual examination of the samples show similar failure behaviour with debonding of the bottom facesheet - core interface and shear failure of the core. The sample with the offset trajectory has a shorter contact duration but this is because of the parameters input to the Hexapod and is not a reflection of the behaviour of the sandwich plates. It is proposed that the edge effects are not very prominent in the tri-dimensional impact behaviour of sandwich plates.

## 5.4 Development of FE model of parabolic impact of sandwich panels

A numerical model was developed using the finite element software, LS-Dyna similar to the model described in the previous chapter. The sandwich plate was modelled with solid elements for the core and shell elements for the thin facesheets. A preliminary model of a sandwich plate with metallic facesheets was developed to simulate the parabolic impact of the aluminium - Divinycell sandwich with cylindrical impactor. This model is compared with the results presented by Guérard et al. [120] and provides the opportunity to verify the capability of the LS-Dyna model to simulate tri-dimensional impacts. It is particularly important to observe the macroscopic behaviour of the foam core which is modelled as an isotropic material with uniaxial compression properties. Finally, the parabolic impact of sandwich panels with 0.8 mm thick facesheets of Kevlar fibre reinforced epoxy and a 20 mm thick Rohacell foam core presented in the previous section was simulated using a similar LS-Dyna model and the results are presented.

### 5.4.1 Validation of LS-Dyna model for Aluminium- Divinycell sandwich

An LS-Dyna model, shown in the Figure 5.14 LS-Dyna model of Aluminium - Divinycell sandwich and cylindrical impactor figure.5.14, was created to simulate the parabolic impact of the Aluminium - Divinycell sandwich. Two types of sandwich plates were modelled, with 0.5 mm thick facesheet and 1 mm thick facesheet. The aluminium facesheets were modelled using Belytschko-Tsai shell elements and the foam core was modelled using constant stress brick elements. The material model chosen for the foam core was the same as the one used for Rohacell foam in the previous chapter, i.e., MAT CRUSHABLE FOAM. The aluminium alloy facesheet was modelled with a PLASTIC KINEMATIC material law. The steel cylindrical

impactor was given displacement input in the Y and Z direction by defining a curve to BOUNDARY PRESCRIBED MOTION keyword. This is in contrast to the normal impact simulation where an initial velocity input is given to the impactor. The rotation motion of the cylindrical impactor were constrained. The simulation was initiated just before the contact to reduce the run-time, with the impactor placed 0.1 mm above the facesheet. The total duration of the simulation is 90 milliseconds corresponding to the impact duration observed in the experiment.

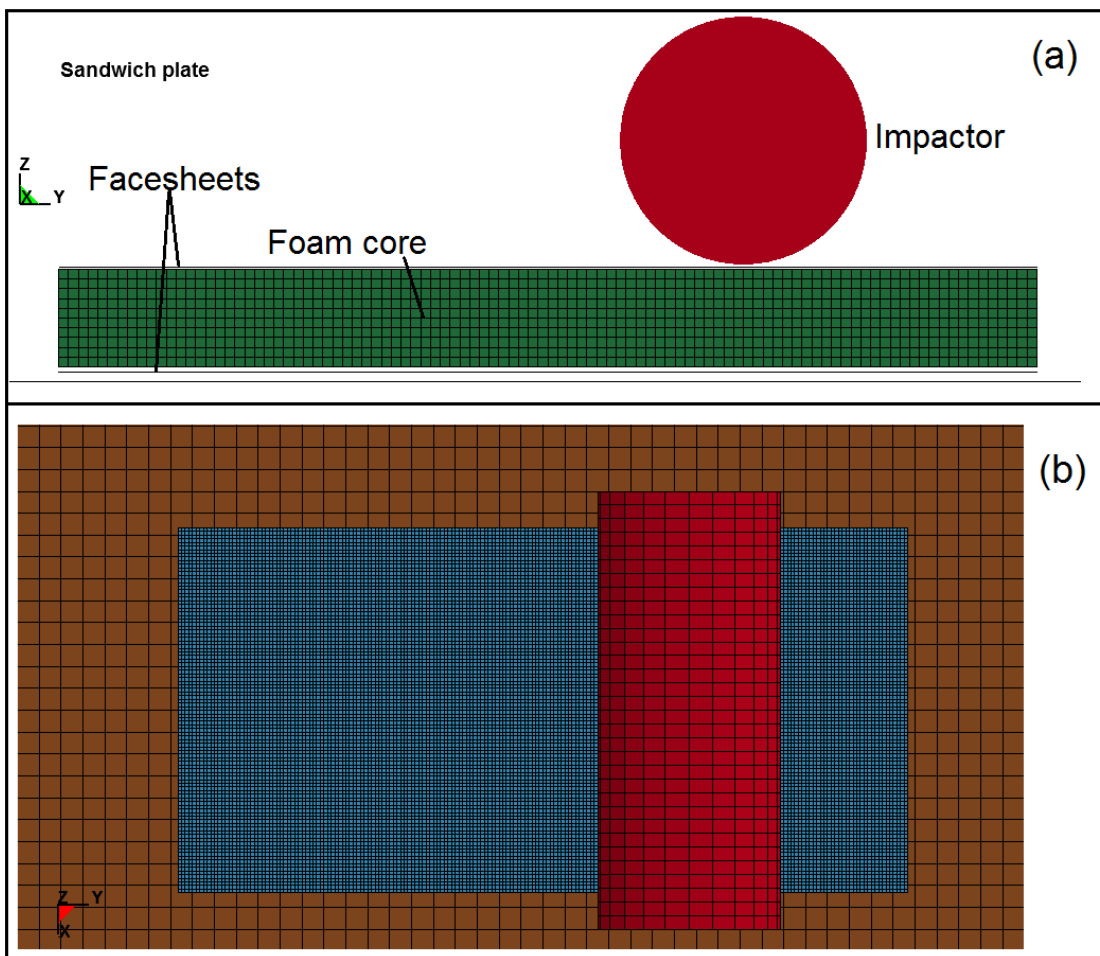


**Figure 5.14.** LS-Dyna model of Aluminium - Divinycell sandwich and cylindrical impactor

The LS-Dyna model is validated by comparing the force- time histories with experimental data obtained by Guérard et al. [120]. A comparison of the forces obtained from the LS-Dyna model and the experiments for the sample with 0.5-mm-thick facesheet are shown in Figure 5.15 Comparison of Force- time curves for

0.5 mm Aluminium - Divinycell sandwich model with experiment figure.5.15. The experimental force values are in solid lines and the FE results are in dash lines. It can be seen that the maximum vertical force (Z-force) from the experiment compares well with the simulation but the maximum horizontal force (Y-force) obtained from the simulation is much lower than the experiment. Guérard et al. [120] reported that the peak of the Z-force (2544 N) occurs before the maximum penetration depth whereas the peak of Y-force (1850 N) occurs slightly after which was attributed to the formation of a small wrinkle in front of the impactor during the test which generates a resistant horizontal force. The Y-force is higher in the experiment compared to the LS-Dyna model for the same reason. There is no wrinkling in the simulation and hence the value of Y-force is lower.

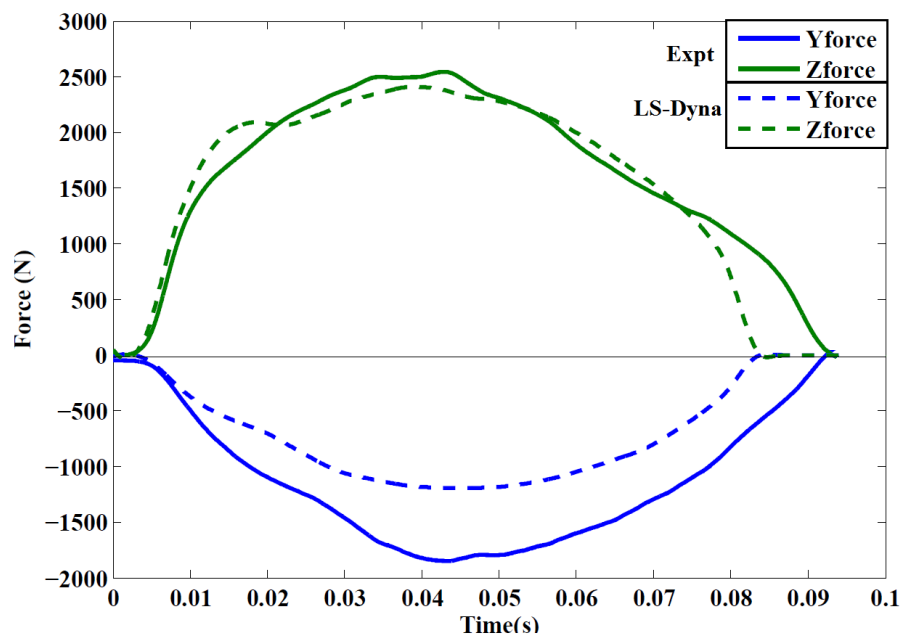


**Figure 5.15.** Comparison of Force- time curves for 0.5 mm Aluminium - Divinycell sandwich model with experiment

For the sample with 1 mm thick facesheet, shown in Figure 5.16 Comparison of Force- time curves for 1 mm Aluminium - Divinycell sandwich model with experiment figure.5.16, the maximum vertical force and maximum horizontal force obtained from the simulation are comparable to the experiment. It can be observed that the Z-force is slightly higher for thicker aluminium facesheet with a peak of 2780 N, whereas the Y-force, with a peak of 1670 N is lower for the thick facesheet. This is explained

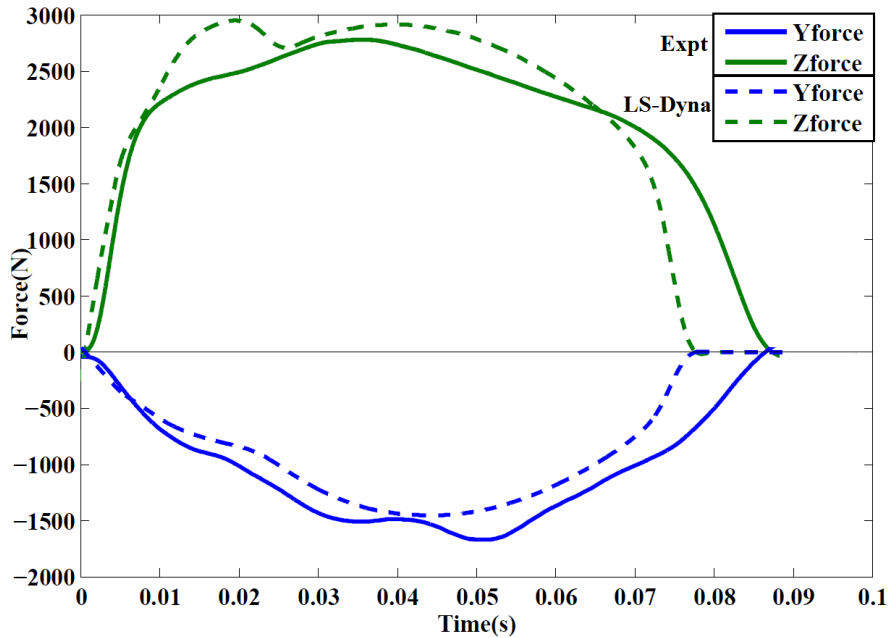


**Figure 5.16.** Comparison of Force- time curves for 1 mm Aluminium - Divinycell sandwich model with experiment

by the fact that there is no observable wrinkling with the 1 mm thick facesheet. The contact duration is shorter for the LS-Dyna model in both cases. One of the possible causes for this phenomenon is the permanent deformation observed in the foam material ahead of the point of contact. However, the overall characteristics of the response of the sandwich plate to parabolic impact was simulated and it can be concluded from these simulations that an LS-Dyna model can be used for the numerical modelling of tri-dimensional impacts.

### 5.5 Results of LS-Dyna simulation for parabolic impact of Kevlar Rohacell sandwich

The response of the Kevlar Rohacell sandwich plate to the tri-dimensional impact loading was examined using the model developed in LS-Dyna. The model developed in the previous chapter for the normal impact of the sandwich structure, with solid elements for the core and shell elements for the thin facesheets are used again for the parabolic impact case. This serves to validate if the model developed for normal impact case can be used for other loading conditions. 3 layers of plain woven fabric with the ply orientation  $[0/90]_3$  used for the facesheets were modelled with the

keyword *\*PART COMPOSITE* and the core and impactor are modelled with underintegrated constant stress hexahedral brick elements. The sandwich panels with the Kevlar fibre reinforced epoxy skins had a nominal thickness of 21.6 mm, with a 20 mm thick Rohacell foam core and 0.8 mm thick facesheets on either side of the core. The dimensions of the plates were 200 mm x 100 mm. The geometry of the sandwich plate and the different impactors are shown in Figure 5.17. LS-Dyna model of Kevlar Rohacell sandwich plate with different impactor geometries figure.5.17.

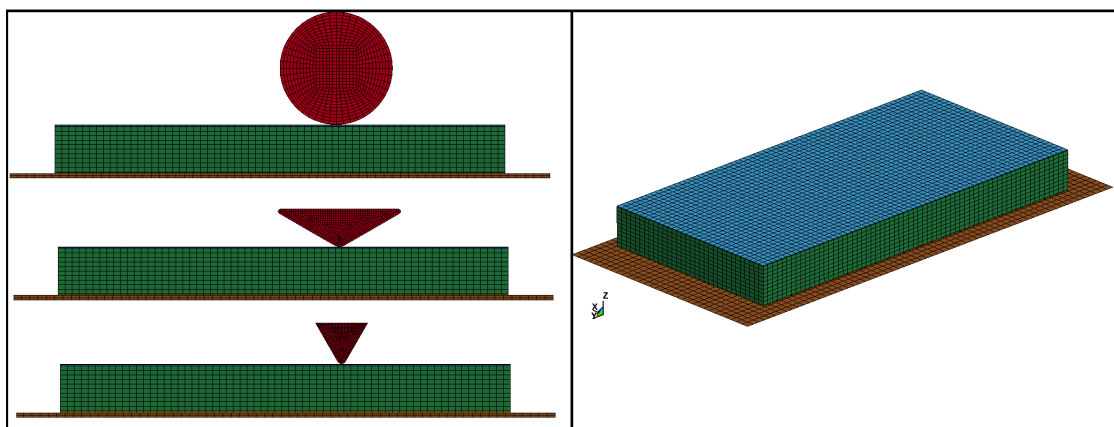


**Figure 5.17.** LS-Dyna model of Kevlar Rohacell sandwich plate with different impactor geometries

A fixed boundary condition is input to the aluminium support plate and a TIEBREAK contact with OPTION 1 is used to model a perfectly bonded contact between the sandwich plate and the support plate. The impactor in the LS-Dyna model is placed 0.1 mm above the sandwich plate and is given a displacement input in the y- direction and z- direction using a DEFINE CURVE keyword. In the case of the low velocity impacts with normal trajectory, an initial velocity is defined to the impactor but a displacement loading is used for the case of parabolic impact. It is possible to define different trajectories of the impactor using this option. A trajectory was chosen with the width of the parabola is 100 mm (starting from 25 mm to the right of the centre of the plate) and a depth of 5 mm (Traj3). This case was chosen for comparison with the experiment as the sandwich plate did not exhibit any shear failure in the core or debonding in the sandwich.

A comparison of the horizontal and vertical components of the force for the parabolic impact of KR sandwich plate with a cylindrical impactor and Traj3 is

shown in Figure 5.18 Comparison of Y-force and Z-force from experiment and LS-Dyna for Traj3figure.5.18. The dashed lines represent the experimental curves and the solid lines are for the LS-Dyna model. It should be noted that the magnitude of the forces are plotted for the comparison and the Y- force which is in the negative axis in the previous figures are shown in the positive axis along with the vertical force component. There is reasonable comparison between the FE model and the experiment. The horizontal component of the force (Y- force) is underestimated by the model but the peak of the Z- force is simulated closely.

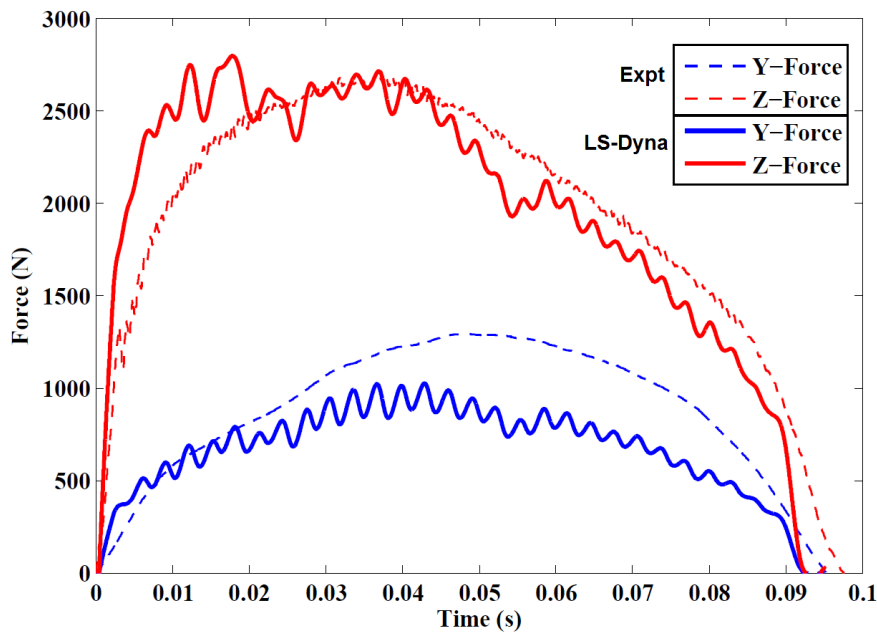


**Figure 5.18.** Comparison of Y-force and Z-force from experiment and LS-Dyna for Traj3

The progression of core effective strain for KR sandwich plate with cylindrical impactor and Traj3 is shown in Figure 5.19 Progression of core strain for KR sandwich plate with cylindrical impactor and Traj3figure.5.19. It can be seen that initially when the impactor comes into contact with the sandwich plate, the strain is limited to a small region of the sandwich plate at Time = 4.5 milliseconds and this region grows with increasing contact duration. The strain contour for contact time of 22.5, 45, and 90 milliseconds are also shown in the figure. It can be seen that there is a strain component that is ahead of the impactor as the core elements undergo deformation.

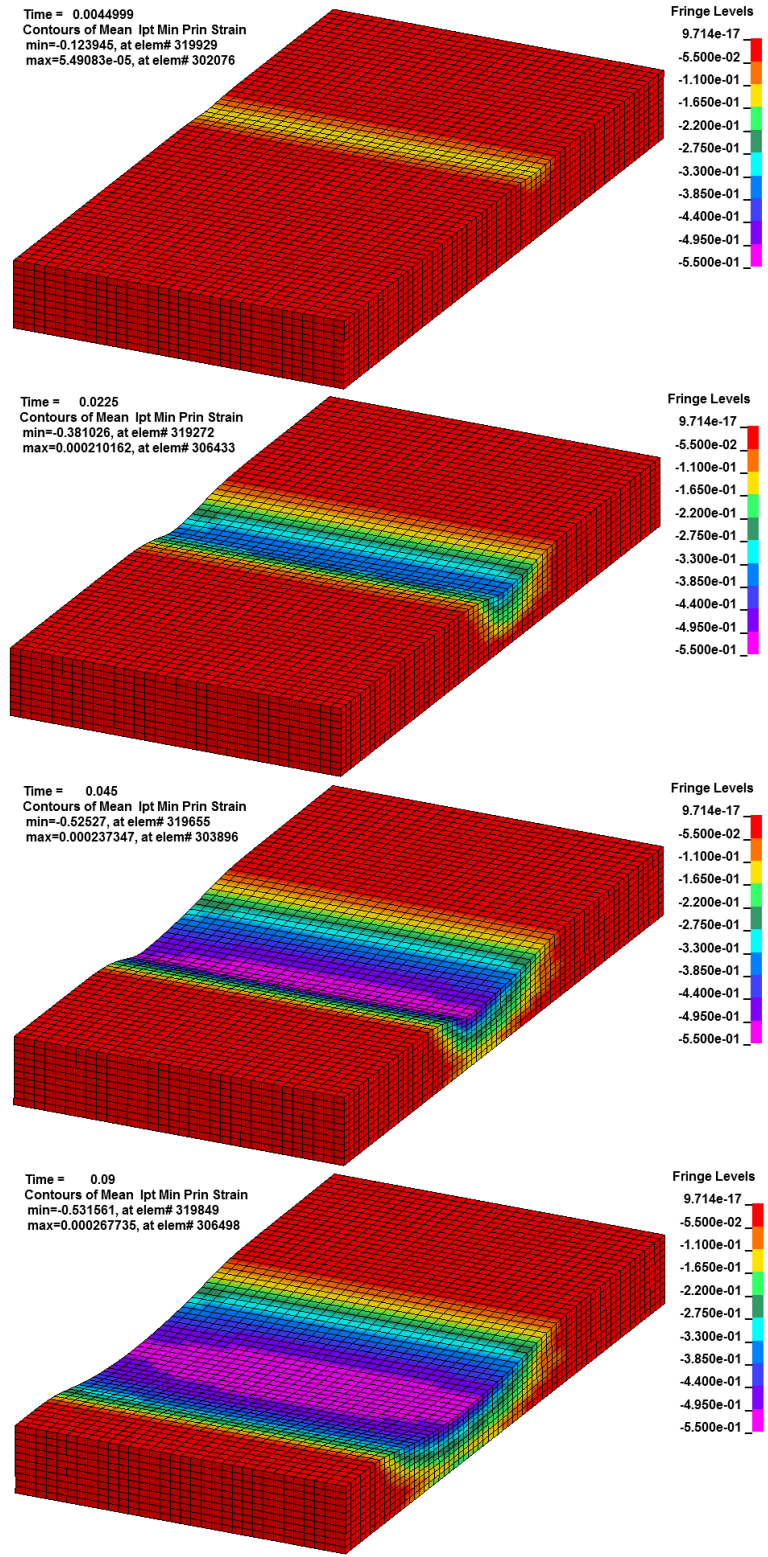


**Figure 5.19.** Progression of core strain for KR sandwich plate with cylindrical impactor and Traj3

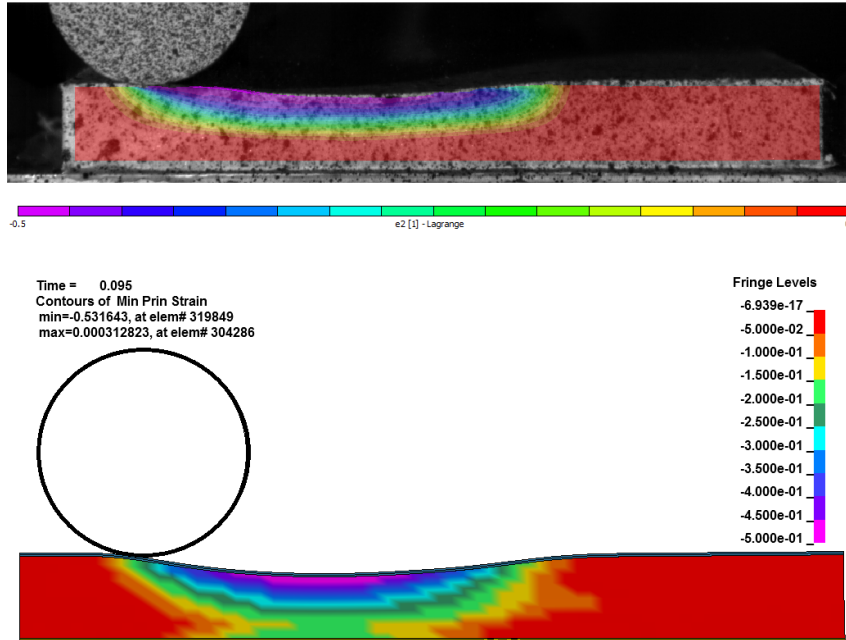


**Figure 5.20.** Comparison of Minimum principal strain history from Digital Image Correlation and LS-Dyna for Traj3

A comparison of the minimum principal strain contour at the end of the impact is shown in Figure 5.20. The experimental strain history is obtained from the Digital Image Correlation software Vic2D (Correlated Solutions). A speckled surface was created on the foam core facing the high speed camera using a spray can. A region of interest was selected in the high speed camera images that correspond to the speckled surface of the foam core and image correlation software was used to obtain the strain history (principal and effective strains) from these speckle images. The contours of the minimum principal strain from the LS-Dyna model are plot from the *d3plot* results file using LS-Prepost. It can be seen that the minimum strain value of  $-0.5$  in the Rohacell core close to the point of contact is reproduced in the FE model. The experimental strain contour shows that a smaller thickness of the core undergoes deformation, while the FE results suggests that the deformation in the core is through the entire thickness of the core.

A comparison of the force- time histories in the horizontal and vertical directions for the parabolic trajectory with 50 mm opening and 8 mm depth (Traj1) centred on the plate are shown in the Figures 5.21. Comparison of y-force and z-force

for KR sandwich from experiment and LS-Dyna for cylindrical impactor figure.5.21, 5.22 Comparison of Y-force and Z-force for KR sandwich from experiment and LS-Dyna for 120° wedge impactor figure.5.22 and 5.23 Comparison of Y-force and Z-force for KR sandwich from experiment and LS-Dyna for 60° wedge impactor figure.5.23 for Kevlar Rohacell sandwich with neat resin. It can be seen that the overall response of the sandwich panel obtained from the FE model is comparable to the experiment even though there are some marked differences between the two. The difference in the magnitude of the forces, for instance, are much larger than for the simulation of the Traj3 case, as the LS-Dyna model did not capture the different failure phenomena observed in the experiment. For instance, the drop in the Z-force observed for samples tested with the wedge shaped impactor correspond to the debonding failure between the sandwich and the support plate. This failure was not modelled and a perfect bonding was assumed for the LS-Dyna model. The force- history for the sandwich panel without this failure mode (for Traj3) had a good correlation with experimental data.

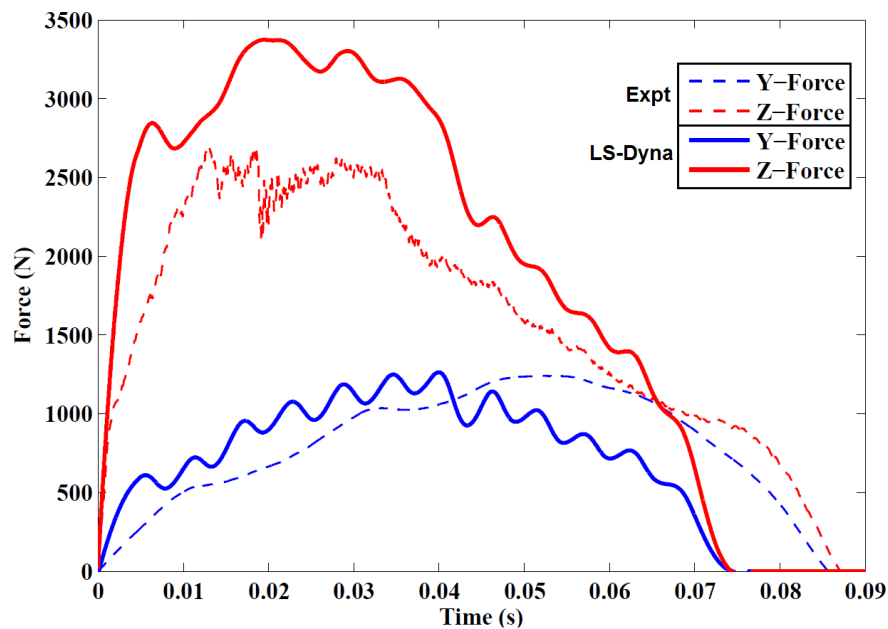


**Figure 5.21.** Comparison of y-force and z-force for KR sandwich from experiment and LS-Dyna for cylindrical impactor

The contact duration is one of the most significant differences between the experiment and simulation. The duration of contact for the case of cylindrical impactor

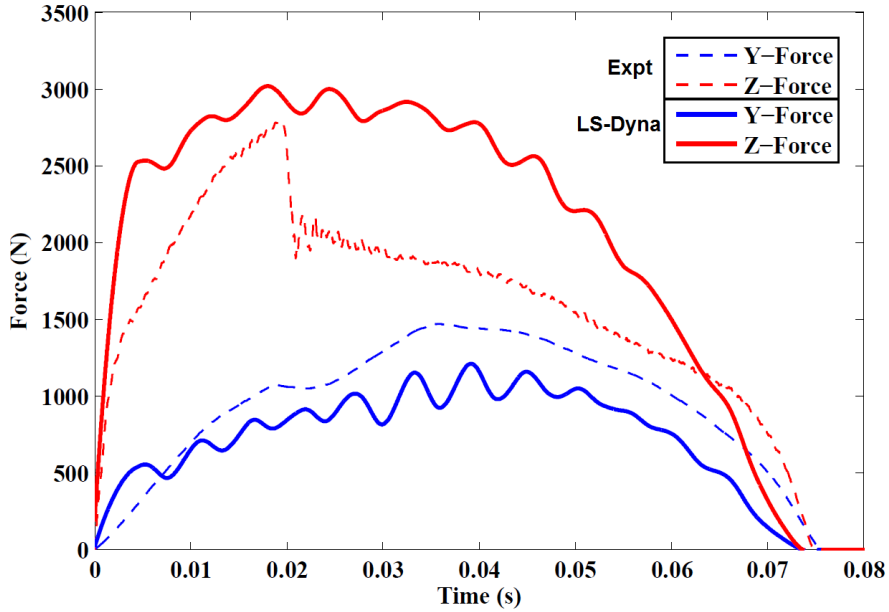


Figure 5.22. Comparison of Y-force and Z-force for KR sandwich from experiment and LS-Dyna for 120° wedge impactor

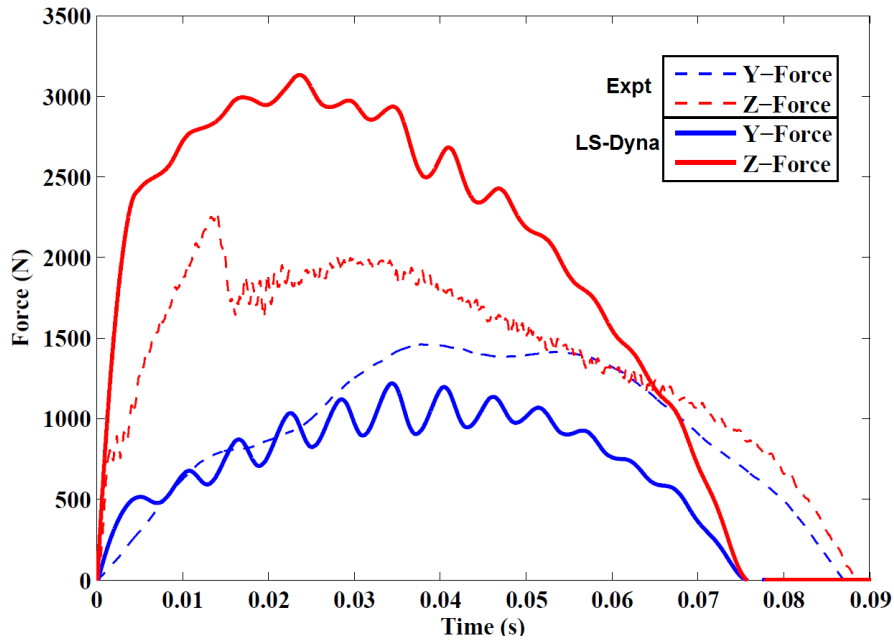
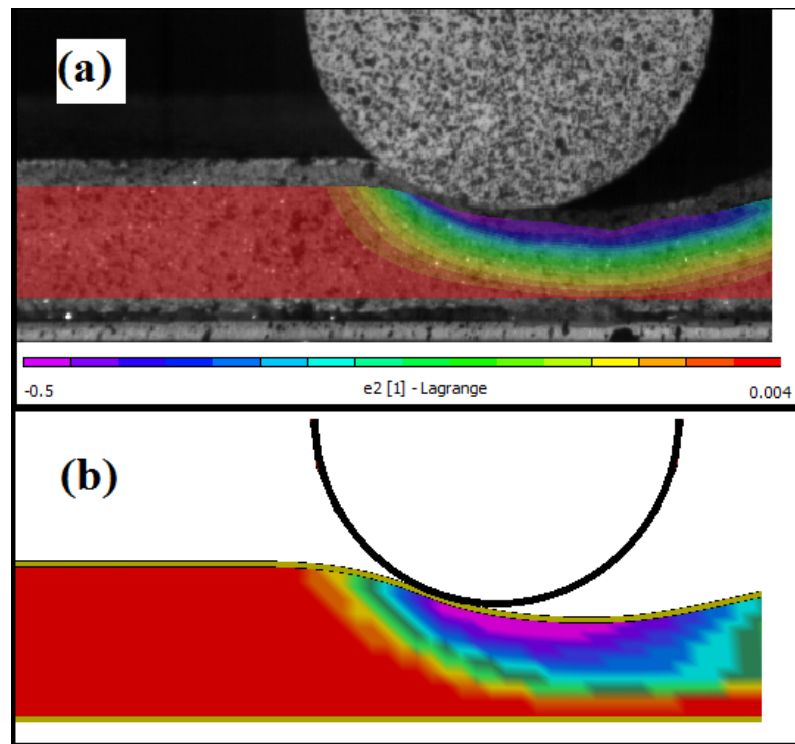


Figure 5.23. Comparison of Y-force and Z-force for KR sandwich from experiment and LS-Dyna for 60° wedge impactor

and 60° wedge impactor in the Hexapod experiment are approximately 86 milliseconds while the duration is only 75 milliseconds in the simulation. It is supposed that the shear strain in the foam core is the cause of this discrepancy. There is also a larger region in the foam core just ahead of the impactor with permanent deformation in the LS-Dyna simulation.

A comparison of the strain contour of the KR sandwich for cylindrical impactor with Traj1 is shown in Figure 5.24. Comparison of minimum principal strain for KR sandwich from DIC and LS-Dyna for cylindrical impactor figure.5.24. The strain contours shows the minimum principal strain obtained from the DIC software and LS-Dyna simulation show very good correlation. There is large localised strain immediately below the impactor and there is permanent plastic deformation in both the top facesheet and the core. This is different to the normal impact case, where there is elastic recovery of the top facesheet and core crushing in the foam, which results in debonding between the core and facesheet.



**Figure 5.24.** Comparison of minimum principal strain for KR sandwich from DIC and LS-Dyna for cylindrical impactor

A similar comparison is attempted for KNR sandwich for the case of impact with cylindrical impactor and Traj1 in Figure 5.25 Comparison of Y-force and Z-force for KNR sandwich from experiment and LS-Dyna for cylindrical impactor figure.5.25. It can be seen that the LS-Dyna model continues to over-estimate the vertical force values but there is reasonable comparison with the experiment. The problem with shortened contact duration also persists. As noted earlier, there is very good correlation of the z- force, y- force and contact duration for the case of Traj3 impact on KR sandwich panel but for the cases with different modes of failure, there is only reasonable comparison with experimental data.

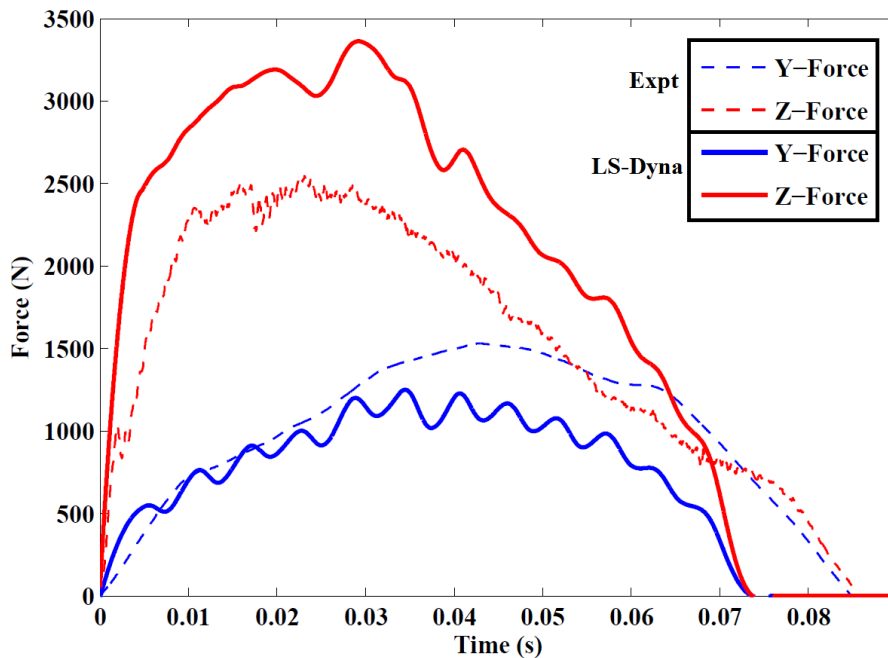


**Figure 5.25.** Comparison of Y-force and Z-force for KNR sandwich from experiment and LS-Dyna for cylindrical impactor

A comparison of the force history of the KR sandwich and KNR sandwich obtained from the LS-Dyna simulation for a cylindrical impactor and Traj1 is shown in Figure 5.26 Comparison of LS-Dyna force history of KR and KNR sandwich panels for cylindrical impactor figure.5.26. The magnitude of the horizontal and vertical components of the force and the shape of the curve are quite similar for the sandwich panels with and without nano-reinforcement. This is similar to the experimental results for the KR and KNR sandwich panels shown in Figure 5.7(a) KR sandwich samples after impact by cylindrical impactor, (b) Force -time curve for impact by

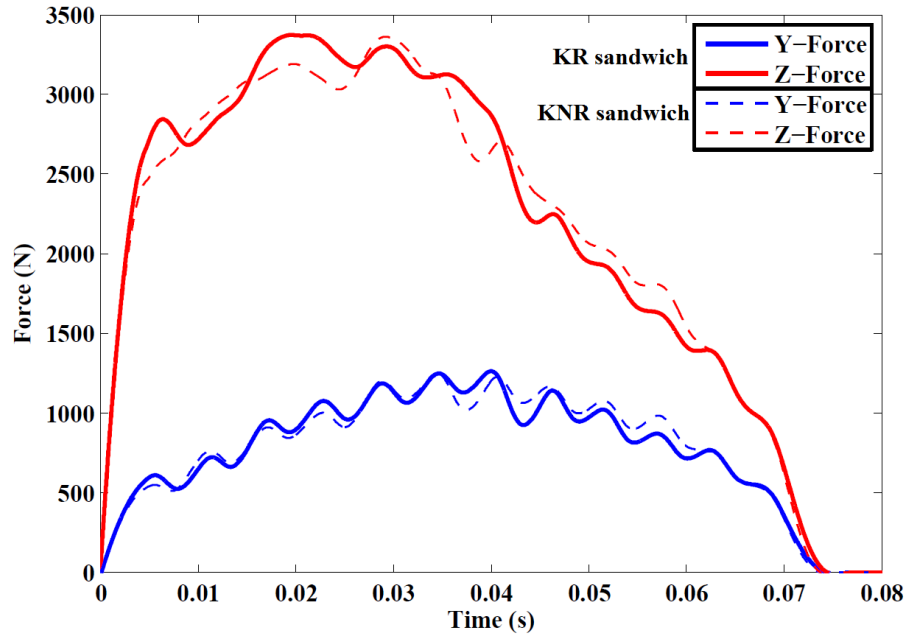


**Figure 5.26.** Comparison of LS-Dyna force history of KR and KNR sandwich panels for cylindrical impactor

cylindrical impactor and (c) KNR sandwich samples after impact by cylindrical impactorfigure.5.7.

One of the main reasons for the average quality of the comparison of simulation results and experiments is the assumption of perfect bonding between the sandwich plate and the aluminium support plate in the LS-Dyna model. In reality, there is debonding between the sandwich and the support plate during the impact as can be observed in the figures in previous section. The bonding of the sandwich plate to the aluminium sheet is necessitated by the clamping mechanism and attempts will be made to modify the fixture to avoid the failure of the adhesive layer. The study of the effect of the bonding strength between the sandwich plate and the support plate and the possibility of modelling this debonding failure is also proposed for future work. The modelling of the debonding is expected to appreciably improve the accuracy of the LS-Dyna model of parabolic impact. It is also recommended that tests are conducted on multiple samples for at least one configuration to verify the assumption of repeatability of the behaviour of the sandwich panels subjected to parabolic impact.

A limitation of the present FE model is the modelling of the shear behaviour of

the foam core. The Crushable foam model used for the Rohacell foam uses uniaxial compression load curves for different strain rates. In the present material model available in LS-Dyna, this law does not include hydrostatic curves for calculating the volumetric part of the stress and strain. The model is primarily focussed on compression loading of the foam and multi-axial loading conditions are not reproduced accurately.

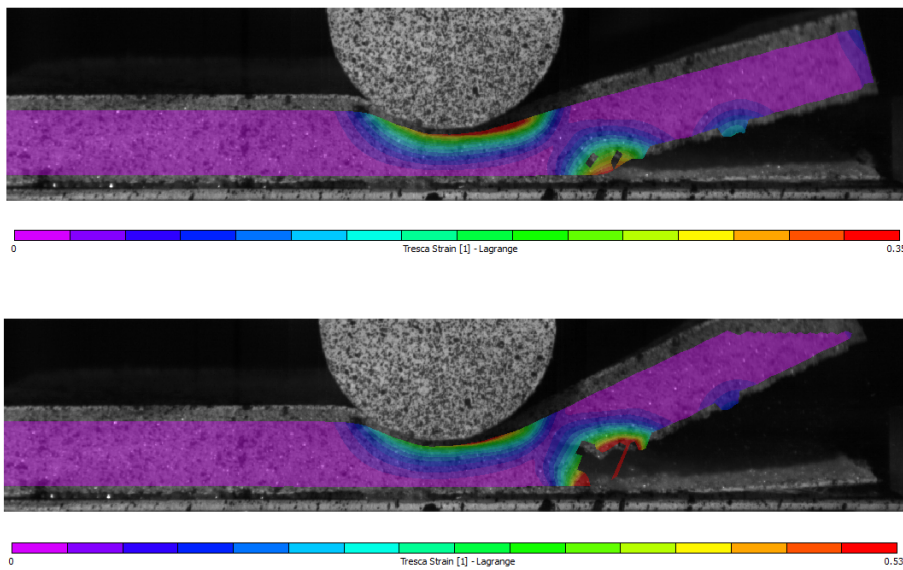


**Figure 5.27.** Tresca strain for KR sandwich plate and cylindrical impactor with Traj1

An example of the shear strain obtained from DIC for KR sandwich plate with a parabolic impact defined by Traj1, i.e., 50 mm opening and 8 mm depth and a cylindrical impactor is shown in Figure 5.27. It can be seen that the shear strain on the lower surface of the core is generated at the edge of the debonding region and a shear crack is seen when the strain exceeds 0.5. The failure modes observed in the experiment are also a combination of several modes with debonding between the core and the bottom facesheet occurring in some samples followed by shear failure in the core, whereas other samples show a debonding failure between the entire sandwich plate and the support plate and no shear failure.

Mostafa et al. [109] have shown that a Crushable foam plasticity material model in ABAQUS can be used to model the shear behaviour of polymer foams, though the plasticity model fails to capture the brittle failure of the foam in tension. Serifi

et al. [107] noted that the modelling of shear and tensile behaviour of foams in LS-Dyna using material models such as Crushable Foam and Fu Chang foam (MAT83) have certain limitations. A comparison of the shear response of EPP foam with LS-Dyna model using MAT83, it was observed that the shear stiffness in the simulation was lower than the experimental curves and that shear rupture was not captured in the model. Other material models such as the constitutive law proposed by Deshpande and Fleck which models the foam core as an isotropic porous solid with a principal stress- yield surface under compression and a quadratic- yield surface elsewhere in the stress space [100] may produce better comparison with experiments. Arezoo et al. [28] concluded that physically based, multi-scale modelling approach incorporating stochastic aspects of the foam microstructure can provide detailed predictions of all aspects of the mechanical response of foams but such a model doesn't exist presently and the development of a comprehensive material law for foams is left as a topic for a future study.

## 5.6 Summary

A new method to conduct low-velocity tri-dimensional impact tests on sandwich panels using a Hexapod with parabolic trajectory of the impactor was presented in the chapter. Initial tests conducted by Guérard et al. [120] on sandwich panels made with Aluminium facesheets and PVC foam core were described and an LS-Dyna model was developed to reproduce the response of the samples in terms of macroscopic force and digital image correlation. Good correlation was achieved with the LS-Dyna model for the parabolic impact of Aluminium- Divinycell sandwich. The Hexapod was also used to conduct parabolic impact tests on Kevlar Rohacell sandwich plates with and without block copolymer nanoparticles. The effect of impactor shape was studied by comparing the response of the sandwich plate for impact with different impactor geometries, namely; cylindrical impactor, wedge impactors with angle of  $120^\circ$  and  $60^\circ$ . Two additional trajectories were defined to study the effect of location of impact, especially to observe if there were edge effects. The LS-Dyna model developed in the previous chapter for the simulation of the low velocity impact of the Kevlar Rohacell sandwich plates were used to simulate the parabolic impacts. This serves to validate if the model developed for normal impact case can be used for other loading conditions. The results of the FE model show good correlation with experimental curves but the model was not able to capture

the complex failure modes such as debonding and shear of foam core. The LS-Dyna model provides reasonable results for the parabolic impact but more work is required to improve the model. Digital Image Correlation was used to characterise surface shear strain field and compared with the FE simulations. Some limitations of the FE model have been identified and are recommended for future work. The chapter presents the development of the Hexapod for tri-dimensional impact testing and the application of this setup for parabolic impact testing of Kevlar Rohacell sandwich plates. There are no standard testing methods available for this kind of impact and more experimental work is needed to establish clear protocols. Tests that allow the bending deflection of the sandwich panels have been proposed. It will avoid the problems associated with the bonding/debonding of the bottom facesheet to the aluminium plate. A post-mortem analysis of the tested specimen will also provide us insight on the phenomena that occurs during the parabolic impact.

## Chapter 6

# Conclusion and Recommendations

### 6.1 Conclusions

The objective of this thesis was to investigate the effect of including block copolymer nanoparticles in the matrix on the low velocity impact behaviour of sandwich composites based on Kevlar and Glass fibre reinforced epoxy and a closed cell PMI foam, Rohacell<sup>®</sup>. A 10% M52N Nanostrength<sup>®</sup> triblock copolymer was chosen for the study. An extensive review of the state of the art research on the topic of impact behaviour of sandwich structures was conducted. The experimental methods for impact testing and the different failure modes in sandwich panels were summarised. The toughening of the matrix of the FRP facesheets has long been identified as a viable means of improving impact resistance of composites and it was identified that of the different nano-reinforcements currently being investigated such as nanoclay, carbon nanotubes and block copolymer, the block copolymer was the most promising material to enhance the mechanical properties of sandwich composites. The main advantage of block copolymers is that they dispersed uniformly and do not suffer from problems of agglomeration of other nanoparticle reinforcements. The process of mixing the nanoparticles to the epoxy resin using a mechanical stirrer at elevated temperature was described.

The sandwich composites with Rohacell foam core bonded on either sides with Kevlar or Glass laminate facesheets with neat resin and nano-modified resin were manufactured using a wet lay-up method and cured in a hot press. A drop tower was used to conduct low-velocity impact tests on the two types of sandwich plates at different initial energies. The effect of the nano-reinforcements on the sandwich plates under low-velocity impact was first studied at the macroscopic level based on the force- displacement curves and visual examination of the samples after impact. While the KR sandwich plate failed by perforation, no perforation was detected in the top facesheet for the sandwich plate with nano-reinforcements for the same impact energy. Perforation of top facesheet was observed in KR sandwich plates for impact at 12 J whereas KNR sandwich plates did not have perforation even at 16 J

impact. A comparison of the Kevlar sandwich panels in terms of the energy absorbed by the panel was undertaken. The KNR sandwich plates required higher energy to fail and also did not exhibit perforation failure of the facesheets unlike the sandwich plates without the nano-reinforcements. The damage in the foam core was also not localised in the impact zone but was spread across a significant part of the structure in the nano-reinforced sandwich panels. Different damage parameters were defined to compare the two types of sandwich panels. Optical microscopy was undertaken to observe the failure mechanisms in the Kevlar facesheet. It was observed that the damage phenomena in the facesheets of the KNR sandwich plate consist mainly of matrix cracking and it was proposed that this may explain the improvement in impact resistance. It can be concluded that the M52N elastomeric nanoparticles significantly improve the resistance of Kevlar FRP sandwich structures under low velocity impact. Sandwich panels with Glass FRP facesheets, on the other hand, showed no significant improvement with the addition of the nanoparticles in the resin. The force- displacement curves and the failure in top facesheet were nearly identical for samples with and without Nanostrength. There were some improvements in the energy dissipated in the sandwich panels but they were not significant. Some possible reasons for this behaviour were posited and have been identified for future work.

A numerical model was developed using explicit FE software LS-Dyna to simulate the low velocity normal impact response of sandwich composite based on Kevlar fibre reinforced epoxy facesheets and Rohacell foam core. A constitutive law based on Continuum Damage Mechanics available in the material library as Laminated Composite Fabric model (MAT58) was used for the simulation of the composite plate. The input parameters to the material model were obtained by a combination of mechanical tests and parametric studies. A Crushable foam model (MAT63) was used for the foam core. The macroscopic properties of the Kevlar-epoxy facesheets with 10% M52N Nanostrength triblock copolymer was also studied to develop FE models of the sandwich plate with nanoparticles. The simulated force versus displacement responses along with the predicted failure modes are in good agreement with that of the experimental measurements. The LS-Dyna model was able to model the fibre failure in the facesheets and the core crushing observed in the foam core. However, the elastic recovery in sandwich plates with nanoparticles was not replicated. The inaccuracy in the modelling of the unloading phase of the impact

in the case of KNR sandwich was more pronounced than the case with neat resin, which is attributed to the inability of the FE model to reproduce the matrix damage modes prevalent in the sandwich with nano-modified resin. However, the peak force and maximum displacement were captured reasonably well in the simulation. The validated FE model can thus be used for studying the impact problem for other conditions reducing the need for experimental tests.

The standard test method for impact testing are for normal incidence impact but normal impacts rarely occur in real engineering situations. Instead, real structures are more frequently loaded at some oblique angle or with complex trajectory. Normal incidence impact tests are easy to carry out using a drop tower, but the response of sandwich panels to impact with a horizontal force component has not been studied extensively. A new method to conduct low-velocity tri-dimensional impact tests on sandwich panels using a Hexapod was developed and this setup was used to test Kevlar Rohacell sandwich panels for impact loading with parabolic trajectory. The parabolic impact testing of Kevlar Rohacell sandwich plates with and without nanoparticles in the epoxy matrix was conducted for different impactor shapes, namely; cylindrical impactor, wedge impactors with angle of  $120^\circ$  and  $60^\circ$  and the response of the sandwich plate was compared. The effect of location of impact was studied especially to observe if there were edge effects by defining two additional trajectories. The LS-Dyna model developed for the simulation of the low velocity normal impact of the Kevlar Rohacell sandwich plates were used to simulate the parabolic impacts. The results of the FE model show good correlation with experimental curves but the model was not able to capture the complex failure modes like debonding and shear of foam core. Digital Image Correlation was used to characterise surface shear strain field and compared with the FE simulations. The LS-Dyna model provides reasonable results for the parabolic impact but more work is required to improve the model.

## 6.2 Significant contributions

The results of the current work have important implications in the composite industry as it is impossible to avoid sandwich structures from being subjected to impact loading. When such a situation occurs, there will be a damage to the structure and hence reduction in the mechanical properties. Sandwich panels with nano-modified resin will not only be able to carry higher loads but also to minimise the damage

to the structure in the event of impact loading, at least in the case of sandwich panels with Kevlar facesheets. The reduction in damage size ameliorates the loss in mechanical properties due to the impact loading. It can be concluded that the development of sandwich panels with nano block copolymer reinforcements are a promising field of study with potential applications in many industries.

The main contribution of the thesis is the systematic study of the effect of block copolymer nanoparticles embedded in the epoxy matrix on the impact resistance of sandwich panels with FRP facesheets. Though toughening of the matrix has been an active area of research for decades, the advent of nanotechnology has ushered in a new era of high performance composites. The field is in its early stages but great progress has been made in fabrication of composites with various nano-reinforcements. Block copolymers have a marked advantage over other nanoparticles being studied in that they self-assemble in the nanometer scale and do not suffer from agglomeration. Therefore, the manufacturing process for composite laminates and sandwich panels with these nano-reinforcements do not need to be altered appreciably from the existing methods. This is the main reason that industries such as Thales and Arkema have shown in using block copolymers in their products.

The Finite Element model developed in this thesis shows that a macroscopic model with a phenomenological constitutive law is capable of simulating the low velocity impact response of composite laminates and sandwich panels. This will assist the product designer to optimise the structure for maximum impact resistance with fewer experiments. This will reduce both the time and the cost of developing new and stronger products.

The parabolic impact testing with Hexapod is another novel and significant contribution of the thesis. Existing test methods are confined to normal impact testing and this new device will be useful to study the response of sandwich structures to loading that resembles real engineering situations.

### **6.3 Recommendations**

Since this is one of the first research investigations undertaken on the effect of nano-block copolymers on impact resistance of sandwich panels, it is by no means complete and has opened up several questions and possible directions for future research in this area. Some recommendations for future work are:

- Drop tower tests on sandwich panels with Glass FRP facesheets with and without Nanostrength seem to suggest that the block copolymer reinforcements do not improve the impact resistance of these sandwich panels. It was our expectation that the toughening of the resin matrix with the nanoparticles would have similar effect independent of the fibre reinforcements. The addition of the nano block copolymers did not alter the macroscopic failure modes observed in the Glass fibre laminates or in the sandwich panels where such laminates were used as facesheets. The laminates, however show a clear improvement in terms of peak force and energy absorbed which are not apparent for the sandwich panels. The cause of this phenomenon is not clear but several reasons have been hypothesised. It is possible that the glass fibres fail before a threshold stress for delamination initiation and this results in the Glass fibre reinforced composite facesheet having no time for the improvement of the resin by the addition of the nanoparticles. On the other hand, the aramid fibres in Kevlar have a greater strain to failure, which could provide an opportunity for the improvement in the ductility of the matrix to have an effect. The fibre- matrix adhesion of Kevlar is notoriously weak when compared to Glass- epoxy and it is possible that the addition of the Nanostrength improved this adhesion and thus provided enhanced impact resistance. A strong composite interphase, which is the region between the fibre and the matrix, promotes the involvement of the fibre and thus increases the composite strength. It is particularly important to study the fibre- matrix interface and compare the interlaminar strength of the composite laminate with the nano-reinforcements. DCB tests for the Mode I fracture toughness have been investigated but the results so far are not conclusive. It is recommended that the effect of block copolymer nanoparticles on facesheets reinforced with different fibres be investigated in greater detail, with particular emphasis on the fibre- matrix interface.
- The composite laminate with nanoparticles in the resin matrix was modelled using a macroscopic phenomenological model. There is good potential to study the behaviour of these composites using multi-scale modelling techniques and it is proposed for subsequent investigations.
- It is recommended that more work be done in the future, on modelling of the debonding of the core and facesheets using Mixed Mode contact laws. The study of Mode I fracture toughness was undertaken using DCB tests but other

modes were not studied. The modelling of the contact in the present study was also limited to Tiebreak contacts, which can be improved with Cohesive elements.

- One of the limitations of the present FE model is the modelling of the shear behaviour of the foam core. The Crushable foam model used for the Rohacell foam uses uniaxial compression load curves for different strain rates. In the present material model available in LS-Dyna, this law does not include hydrostatic curves for calculating the volumetric part of the stress and strain. The model is primarily focussed on compression loading of the foam and multi-axial loading conditions such as in the parabolic impact study are not reproduced accurately. Other material models such as Deshpande and Fleck model have been suggested for the modelling of the foam. Implementation of a more accurate material model for the foam core is prescribed for further investigation.
- There are no standard testing methods available for tri-dimensional impact and more experimental work is needed to establish clear protocols. Tests that allow the bending deflection of the sandwich panels have been proposed. It will avoid the problems associated with the bonding/debonding of the bottom facesheet to the aluminium plate. A post-mortem analysis of the tested specimen will also provide us insight on the phenomena that occurs during the parabolic impact. This mode of test simulate the real world situations that sandwich plates can encounter and are an invaluable addition to the scientific knowledge on impact behaviour of sandwich panels.
- The study of the effect of the bonding strength between the sandwich plate and the support plate and the possibility of modelling this debonding failure is also proposed for future work. The modelling of the debonding is expected to appreciably improve the accuracy of the LS-Dyna model of parabolic impact.
- It is also proposed that the study of the effect of block copolymer nanoparticles on the high velocity or ballistic response of sandwich panels be considered for the future.

## References

- [1] L.A. Carlsson and G.A. Kardomateas. *Structural and failure mechanics of sandwich composites*, volume 121. Springer Science, 2011.
- [2] A.F. Avila, M.G.R. Carvalho, E.C. Dias, and D.T.L. da Cruz. Nano-structured sandwich composites response to low-velocity impact. *Composite Structures*, 92(3):745 – 751, 2010.
- [3] L. Sun, R.F. Gibson, F. Gordaninejad, and J. Suhr. Energy absorption capability of nanocomposites: A review. *Composites Science and Technology*, 69(14):2392 – 2409, 2009. The Sixteenth International Conference on Composite Materials with Regular Papers.
- [4] R. Barsotti. Nanostrength block copolymers for epoxy toughening. Technical report, Arkema Inc., September 2008.
- [5] S. Denneulin. *Étude du comportement dynamique de matériaux composites sous sollicitations de chocs- Application à un casque aéronautique*. PhD thesis, École Nationale Supérieure d’Arts et Métiers, France, 2011.
- [6] R.A.W. Mines, C.M. Worrall, and A.G. Gibson. The static and impact behaviour of polymer composite sandwich beams. *Composites*, 25(2):95 – 110, 1994.
- [7] Md.A. Bhuiyan, M.V. Hosur, and S. Jeelani. Low-velocity impact response of sandwich composites with nanophased foam core and biaxial braided face sheets. *Composites Part B: Engineering*, 40(6):561 – 571, 2009.
- [8] M.L. Bernard and P.A. Lagace. Impact resistance of composite sandwich plates. *Journal of Reinforced Plastics and Composites*, 8(5):432–445, 1989.
- [9] M.O.W. Richardson and M.J. Wisheart. Review of low-velocity impact properties of composite materials. *Composites Part A: Applied Science and Manufacturing*, 27(12):1123 – 1131, 1996.
- [10] C. Soutis. Carbon fiber reinforced plastics in aircraft construction. *Materials Science and Engineering: A*, 412(1-2):171 – 176, 2005. International Conference on Recent Advances in Composite Materials.

- 
- [11] W.K. Shih and B.Z. Jang. Instrumented impact testing of composite sandwich panels. *Journal of Reinforced Plastics and Composites*, 8(3):270–298, 1989.
- [12] A.J. Kinloch, K. Masania, A.C. Taylor, S. Sprenger, and D. Egan. The fracture of glass-fibre-reinforced epoxy composites using nanoparticle-modified matrices. *Journal of Materials Science*, 43(3):1151–1154, 2008.
- [13] L. Liu and H.D. Wagner. Rubbery and glassy epoxy resins reinforced with carbon nanotubes. *Composites Science and Technology*, 65(11-12):1861 – 1868, 2005.
- [14] F. Xia and X. Wu. Work on low-velocity impact properties of foam sandwich composites with various face sheets. *Journal of Reinforced Plastics and Composites*, 29(7):1045–1054, 2010.
- [15] J. Gustin, M. Mahinfalah, G.N. Jazar, and M.R. Aagaah. Low-velocity impact of sandwich composite plates. *Experimental Mechanics*, 44(6):574–583, 2004.
- [16] W.J. Cantwell, C. Dirat, and P. Davies. A comparative study of the mechanical properties of sandwich materials for nautical construction. *SAMPE Journal*, 30(4):45 – 51, 1994.
- [17] W.J. Cantwell and J. Morton. The impact resistance of composite materials: a review. *Composites*, 22(5):347 – 362, 1991.
- [18] B. Alcock, N.O. Cabrera, N.-M. Barkoula, and T. Peijs. Low velocity impact performance of recyclable all-polypropylene composites. *Composites Science and Technology*, 66(11-12):1724 – 1737, 2006.
- [19] M. W. Wardle. 2.06 - aramid fiber reinforced plastics properties. In Anthony Kelly and Carl Zweben, editors, *Comprehensive Composite Materials*, pages 199 – 229. Pergamon, Oxford, 2000.
- [20] P.N.B. Reis, J.A.M. Ferreira, Z.Y. Zhang, T. Benameur, and M.O.W. Richardson. Impact response of kevlar composites with nanoclay enhanced epoxy matrix. *Composites Part B: Engineering*, 46:7 – 14, 2013.
- [21] J. Gustin, A. Joneson, M. Mahinfalah, and J. Stone. Low velocity impact of combination kevlar/carbon fiber sandwich composites. *Composite Structures*, 69(4):396 – 406, 2005.
- [22] E. Sevkat, B. Liaw, F. Delale, and B.B. Raju. Drop-weight impact of plain-woven hybrid glass-graphite/toughened epoxy composites. *Composites Part A: Applied*

- Science and Manufacturing*, 40(8):1090 – 1110, 2009. Special Issue: 15th French National Conference on Composites - JNC15.
- [23] I.K. Varma and V.B. Gupta. 2.01 - thermosetting resin properties. In Anthony Kelly and Carl Zweben, editors, *Comprehensive Composite Materials*, pages 1 – 56. Pergamon, Oxford, 2000.
- [24] Andrey Shipsha. *Failure of sandwich structures with sub-interface damage*. PhD thesis, Royal Institute of Technology, Sweden, 2001.
- [25] Q.M. Li, R.A.W. Mines, and R.S. Birch. The crush behaviour of rohacell-51wf structural foam. *International Journal of Solids and Structures*, 37(43):6321 – 6341, 2000.
- [26] J. R. Vinson. Experimental and numerical study on the low-velocity impact behavior of foam-core sandwich panels. *Appl. Mech. Rev.*, 54(3):201 – 214, 2001.
- [27] Md. Akil Hazizan and W. J. Cantwell. The low velocity impact response of foam-based sandwich structures. *Composites Part B: Engineering*, 33(3):193 – 204, 2002.
- [28] S. Arezoo, V.L. Tagarielli, N. Petrinic, and J.M. Reed. The mechanical response of rohacell foams at different length scales. *Journal of Materials Science*, 46(21):6863–6870, 2011.
- [29] I. Ivanez, C. Santiuste, E. Barbero, and S. Sanchez-Saez. Numerical modelling of foam-cored sandwich plates under high-velocity impact. *Composite Structures*, 93(9):2392 – 2399, 2011.
- [30] H. Mahfuz, T. Thomas, V. Rangari, and S. Jeelani. On the dynamic response of sandwich composites and their core materials. *Composites Science and Technology*, 66(14):2465 – 2472, 2006. Special Issue in Honour of Professor C.T. Sun.
- [31] V. Rizov, A. Shipsha, and D. Zenkert. Indentation study of foam core sandwich composite panels. *Composite Structures*, 69(1):95 – 102, 2005.
- [32] T. Anderson and E. Madenci. Experimental investigation of low-velocity impact characteristics of sandwich composites. *Composite Structures*, 50(3):239 – 247, 2000.
- [33] E.A. Flores-Johnson and Q.M. Li. Experimental study of the indentation of sandwich panels with carbon fibre-reinforced polymer face sheets and polymeric foam core. *Composites Part B: Engineering*, 42(5):1212 – 1219, 2011.

- 
- [34] S. Abrate. Impact on laminated composite materials. *Appl. Mech. Rev.*, 44(4):155 – 190, 1991.
- [35] W. Goldsmith and J.L. Sackman. An experimental study of energy absorption in impact on sandwich plates. *International Journal of Impact Engineering*, 12(2):241 – 262, 1992.
- [36] K. T. Ramesh. High rates and impact experiments. In Jr. Sharpe, William N., editor, *Springer Handbook of Experimental Solid Mechanics*, pages 929–960. Springer US, 2008.
- [37] R.A.W. Mines, C.M. Worrall, and A.G. Gibson. Low velocity perforation behaviour of polymer composite sandwich panels. *International Journal of Impact Engineering*, 21(10):855 – 879, 1998.
- [38] A. M. Roach, K. E. Evans, and N. Jones. The penetration energy of sandwich panel elements under static and dynamic loading. part i. *Composite Structures*, 42(2):119 – 134, 1998.
- [39] P.R. Hampson and M. Moatamedi. A review of composite structures subjected to dynamic loading. *International Journal of Crashworthiness*, 12(4):411–428, 2007.
- [40] J.H. Park, S.K. Ha, K.W. Kang, C.W. Kim, and H.S. Kim. Impact damage resistance of sandwich structure subjected to low velocity impact. *Journal of Materials Processing Technology*, 201:425 – 430, 2008.
- [41] S. Denneulin, P. Viot, F. Léonardi, and J.L. Lataillade. The influence of acrylate triblock copolymer embedded in matrix on composite structures’ responses to low-velocity impacts. *Composite Structures*, 94(4):1471 – 1481, 2012.
- [42] S. Zhu and G.B. Chai. Damage and failure mode maps of composite sandwich panel subjected to quasi-static indentation and low velocity impact. *Composite Structures*, 101:204 – 214, 2013.
- [43] C. Atas and C. Sevim. On the impact response of sandwich composites with cores of balsa wood and pvc foam. *Composite Structures*, 93(1):40–48, 2010.
- [44] G. Caprino and R. Teti. Impact and post-impact behavior of foam core sandwich structures. *Composite Structures*, 29(1):47 – 55, 1994.
- [45] M.V. Hosur, A.A. Mohammed, S. Zainuddin, and S. Jeelani. Processing of nanoclay filled sandwich composites and their response to low-velocity impact loading. *Composite Structures*, 82(1):101 – 116, 2008.

- 
- [46] G.J. Dvorak and A.P. Suvorov. Protection of sandwich plates from low-velocity impact. *Journal of Composite Materials*, 40(15):1317–1331, 2006.
- [47] C. Borsellino, L. Calabrese, and A. Valenza. Experimental and numerical evaluation of sandwich composite structures. *Composites Science and Technology*, 64(10-11):1709 – 1715, 2004.
- [48] JK Kim, D.B. MacKay, and YW Mai. Drop-weight impact damage tolerance of {CFRP} with rubber-modified epoxy matrix. *Composites*, 24(6):485 – 494, 1993.
- [49] T.C. Triantafillou and L.J. Gibson. Failure mode maps for foam core sandwich beams. *Materials Science and Engineering*, 95:37 – 53, 1987.
- [50] S. Goswami and W. Becker. The effect of facesheet/core delamination in sandwich structures under transverse loading. *Composite Structures*, 54(4):515 – 521, 2001.
- [51] J. Wang, A. M. Waas, and H. Wang. Experimental and numerical study on the low-velocity impact behavior of foam-core sandwich panels. *Composite Structures*, 96:298 – 311, 2013.
- [52] W. Zhong and B.Z. Jang. Material design approaches for improving impact resistance of composites. *Key Engineering Materials*, 141:169 – 186, 1998.
- [53] K. Dransfield, C. Baillie, and Y.W. Mai. Improving the delamination resistance of {CFRP} by stitching a review. *Composites Science and Technology*, 50(3):305 – 317, 1994.
- [54] D.D. Cartié and N. A. Fleck. The effect of pin reinforcement upon the through-thickness compressive strength of foam-cored sandwich panels. *Composites Science and Technology*, 63(16):2401 – 2409, 2003. Porous Materials.
- [55] A. Nanayakkara, S. Feih, and A.P. Mouritz. Experimental impact damage study of a z-pinned foam core sandwich composite. *Journal of Sandwich Structures and Materials*, 14(4):469–486, 2012.
- [56] A Mostafa, K Shankar, and EV Morozov. In-plane shear behaviour of composite sandwich panel incorporated with shear keys methodology at different orientations: finite element study. *Journal of Composite Materials*, 48(24):2945–2959, 2014.
- [57] J. Njuguna, S. Michalowski, K. Pieliowski, K. Kayvantash, and A. C. Walton. Fabrication, characterization and low-velocity impact testing of hybrid sandwich composites with polyurethane/layered silicate foam cores. *Polymer Composites*, 32(1):6–13, 2011.

- [58] R. Bagheri, B.T. Marouf, and R.A. Pearson. Rubber-toughened epoxies: A critical review. *Polymer Reviews*, 49:201 – 225, 2009.
- [59] A. Garg and Y.W. Mai. Failure mechanisms in toughened epoxy resins - a review. *Composites Science and Technology*, 31(1):179 – 223, 1988.
- [60] N.A. Siddiqui, R.S.C. Woo, JK Kim, C.K.Y. Leung, and A. Munir. Mode I inter-laminar fracture behavior and mechanical properties of CFRPs with nanoclay-filled epoxy matrix. *Composites Part A: Applied Science and Manufacturing*, 38(2):449 – 460, 2007.
- [61] W. D. Bascom, R. L. Cottingham, R. L. Jones, and P. Peyser. The fracture of epoxy- and elastomer-modified epoxy polymers in bulk and as adhesives. *Journal of Applied Polymer Science*, 19(9):2545–2562, 1975.
- [62] J. He, D. Raghavan, D. Hoffman, and D. Hunston. The influence of elastomer concentration on toughness in dispersions containing preformed acrylic elastomeric particles in an epoxy matrix. *Polymer*, 40(8):1923 – 1933, 1999.
- [63] M. Zeng, X. Sun, X. Yao, G. Ji, N. Chen, B. Wang, and C. Qi. Effects of SiO<sub>2</sub> nanoparticles on the performance of carboxyl-randomized liquid butadieneacrylonitrile rubber modified epoxy nanocomposites. *Journal of Applied Polymer Science*, 106(2):1347–1352, 2007.
- [64] K Imielinska and R Wojtyra. Advanced epoxy composites of improved impact tolerance. *Kompozyty (Composites)*, 4(9):61–67, 2004.
- [65] B.B. Johnsen, A.J. Kinloch, R.D. Mohammed, A.C. Taylor, and S. Sprenger. Toughening mechanisms of nanoparticle-modified epoxy polymers. *Polymer*, 48(2):530 – 541, 2007.
- [66] J. Njuguna, K. Pielichowski, and A.J. Alcock. Epoxy-based fibre reinforced nanocomposites. *Advanced Engineering Materials*, 9(10):835–847, 2007.
- [67] F.H. Gojny, M.H.G. Wichmann, B. Fiedler, W. Bauhofer, and K. Schulte. Influence of nano-modification on the mechanical and electrical properties of conventional fibre-reinforced composites. *Composites Part A: Applied Science and Manufacturing*, 36(11):1525 – 1535, 2005.
- [68] P. Karapappas, A. Vavouliotis, P. Tsotra, and V. Kostopoulos. Enhanced fracture properties of carbon reinforced composites by the addition of multi-wall carbon nanotubes. *Journal of Composite Materials*, 43(9):977 – 985, 2009.

- [69] K. Iqbal, S.U. Khan, A. Munir, and J.K. Kim. Impact damage resistance of CFRP with nanoclay-filled epoxy matrix. *Composites Science and Technology*, 69(11-12):1949 – 1957, 2009. Experimental Techniques and Design in Composite Materials (ETDCM8) with Regular Papers.
- [70] F. Aymerich, A.D. Via, and M. Quaresimin. Energy absorption capability of nanomodified glass/epoxy laminates. *Procedia Engineering*, 10:780 – 785, 2011. 11th International Conference on the Mechanical Behavior of Materials (ICM11).
- [71] C.M. Manjunatha, A.C. Taylor, A.J. Kinloch, and S. Sprenger. The tensile fatigue behaviour of a silica nanoparticle-modified glass fibre reinforced epoxy composite. *Composites Science and Technology*, 70(1):193 – 199, 2010.
- [72] M.H.G. Wichmann, J. Sumfleth, F.H. Gojny, M. Quaresimin, B. Fiedler, and K. Schulte. Glass-fibre-reinforced composites with enhanced mechanical and electrical properties - benefits and limitations of a nanoparticle modified matrix. *Engineering Fracture Mechanics*, 73(16):2346 – 2359, 2006. Fracture of Polymers, Composites and Adhesives.
- [73] H. Kishi, Y. Kunimitsu, J. Imade, S. Oshita, Y. Morishita, and M. Asada. Nanophase structures and mechanical properties of epoxy/acryl triblock copolymer alloys. *Polymer*, 52(3):760 – 768, 2011.
- [74] S. Ritzenthaler, F. Court, L. David, E. Girard-Reydet, L. Leibler, and J. P. Pascault. ABC triblock copolymers/epoxy - diamine blends. 1. keys to achieve nanostructured thermosets. *Macromolecules*, 35(16):6245–6254, 2002.
- [75] V. Rebizant, A-S Venet, F. Tournilhac, E. Girard-Reydet, C. Navarro, J.P. Pascault, and L. Leibler. Chemistry and mechanical properties of epoxy-based thermosets reinforced by reactive and nonreactive SBMX block copolymers. *Macromolecules*, 37(21):8017–8027, 2004.
- [76] R. M. Boumbimba, C. Froustey, P. Viot, J.M. Olive, F. Léonardi, P. Gerard, and R. Inoubli. Preparation and mechanical characterisation of laminate composites made of glass fibre/epoxy resin filled with tri bloc copolymers. *Composite Structures*, 116:414 – 422, 2014.
- [77] J. Kalantar and L.T. Drzal. The bonding mechanism of aramid fibres to epoxy matrices. *Journal of Materials Science*, 25(10):4186–4193, 1990.

- [78] M.C. Andrews, D.J. Bannister, and R.J. Young. The interfacial properties of aramid/epoxy model composites. *Journal of Materials Science*, 31(15):3893–3913, 1996.
- [79] Y.W. Mai and F. Castino. Fracture toughness of kevlar-epoxy composites with controlled interfacial bonding. *Journal of Materials Science*, 19(5):1638–1655, 1984.
- [80] J. Mackerle. Finite element analyses of sandwich structures: a bibliography (19802001). *Engineering Computations*, 19(2):206 – 245, 2002.
- [81] R.C. Batra, G. Gopinath, and J.Q. Zheng. Damage and failure in low energy impact of fiber-reinforced polymeric composite laminates. *Composite Structures*, 94(2):540 – 547, 2012.
- [82] C. Bouvet, S. Rivallant, and J.J. Barrau. Low velocity impact modeling in composite laminates capturing permanent indentation. *Composites Science and Technology*, 72(16):1977 – 1988, 2012.
- [83] A. Rajaneesh, I. Sridhar, and S. Rajendran. Impact modeling of foam cored sandwich plates with ductile or brittle faceplates. *Composite Structures*, 94(5):1745 – 1754, 2012.
- [84] J.A. Nemes and K.E. Simmonds. Low-velocity impact response of foam-core sandwich composites. *Journal of Composite Materials*, 26(4):500–519, 1992.
- [85] D. Feng and F. Aymerich. Damage prediction in composite sandwich panels subjected to low-velocity impact. *Composites Part A: Applied Science and Manufacturing*, 52:12 – 22, 2013.
- [86] F. Collombet, X. Lalbin, J. Bonini, V. Martin, and J.L. Lataillade. Damage criteria for the study of impacted composite laminates. *Composites Science and Technology*, 58(5):679 – 686, 1998.
- [87] Y. Shi, T. Swait, and C. Soutis. Modelling damage evolution in composite laminates subjected to low velocity impact. *Composite Structures*, 94(9):2902 – 2913, 2012.
- [88] A.K. Noor, W.S. Burton, and C.W. Bert. Computational models for sandwich panels and shells. *Appl. Mech. Rev.*, 49:155–199, 1996.
- [89] M. May, M. Nossek, N. Petrinic, S. Hiermaier, and K. Thoma. Adaptive multi-scale modeling of high velocity impact on composite panels. *Composites Part A: Applied Science and Manufacturing*, 58:56 – 64, 2014.

- 
- [90] M.Q. Nguyen, S.S. Jacombs, R.S. Thomson, D. Hachenberg, and M.L. Scott. Simulation of impact on sandwich structures. *Composite Structures*, 67(2):217 – 227, 2005.
- [91] B. Wade, P. Feraboli, and M. Osborne. Simulating laminated composites using ls-dyna material model mat54 part i: [0] and [90] ply single-element investigation. In *FAA JAMS Technical review meeting*, 2012.
- [92] S. Heimbs, P. Middendorf, and M. Maier. Honeycomb sandwich material modeling for dynamic simulations of aircraft interior components. In *9th International LS-DYNA Users Conference*, 2006.
- [93] Y. Zhang, P. Zhu, and X. Lai. Finite element analysis of low-velocity impact damage in composite laminated plates. *Materials and Design*, 27(6):513 – 519, 2006.
- [94] X. Xiao, M.E. Botkin, and N.L. Johnson. Axial crush simulation of braided carbon tubes using {MAT58} in ls-dyna. *Thin-Walled Structures*, 47(67):740 – 749, 2009.
- [95] K. Schweizerhof, K. Weimar, Th. Munz, and Th. Rottner. Crashworthiness analysis with enhanced material models in ls-dyna - merits and limits. In *LS-DYNA World Conference*, 1998.
- [96] B.A. Gama and J.W. Gillespie Jr. Finite element modeling of impact, damage evolution and penetration of thick-section composites. *International Journal of Impact Engineering*, 38(4):181 – 197, 2011.
- [97] S. Basu, A.M. Waas, and D.R. Ambur. Prediction of progressive failure in multidirectional composite laminated panels. *International Journal of Solids and Structures*, 44(9):2648 – 2676, 2007.
- [98] R. Brooks, K.A. Brown, N.A. Warrior, and P.P. Kulandaivel. Predictive modeling of the impact response of thermoplastic composite sandwich structures. *Journal of Sandwich Structures and Materials*, 12(4):449–476, 2010.
- [99] K. V. Williams and R. Vaziri. Application of a damage mechanics model for predicting the impact response of composite materials. *Computers and Structures*, 79(10):997 – 1011, 2001.
- [100] J. Hallquist. *LS-Dyna Theory Manual*, 2006.
- [101] A. Matzenmiller, J. Lubliner, and R.L. Taylor. A constitutive model for anisotropic damage in fiber-composites. *Mechanics of Materials*, 20(2):125 – 152, 1995.

- 
- [102] Livermore Software Technology Corporation. Modeling of composites in ls-dyna, 2009.
- [103] X.L. Fan, T.J. Wang, and Q. Sun. Damage evolution of sandwich composite structure using a progressive failure analysis methodology. *Procedia Engineering*, 10:530 – 535, 2011. 11th International Conference on the Mechanical Behavior of Materials (ICM11).
- [104] P.F. Deslauriers, D.S. Cronin, and A. Duquette. Numerical modeling of woven carbon composite failure. In *8th International LS-DYNA Users Conference*, 2004.
- [105] M. Polanco, S. Kellas, and K. Jackson. Evaluation of material models within ls-dyna for a kevlar/epoxy composite honeycomb, 2009.
- [106] B. Croop and H. Lobo. Selecting material models for the simulation of foams in ls-dyna. In *7th European LS-DYNA Conference*, 2009.
- [107] E. Serifi, A. Hirth, S. Matthaei, and H. Mullerschön. Modelling of foams using mat83 - preparation and evaluation of experimental data. In *4th European LS-DYNA Conference*, 2003.
- [108] K. Jackson, E.L. Fasanella, M.S. Annett, and M.A. Polanco. Material model evaluation of a composite honeycomb energy absorber. In *12th International LS-Dyna users conference*, 2012.
- [109] A. Mostafa, K. Shankar, and E.V. Morozov. Insight into the shear behaviour of composite sandwich panels with foam core. *Materials & Design*, 50:92 – 101, 2013.
- [110] F. Dogan, H. Hadavinia, T. Donchev, and P.S. Bhonge. Delamination of impacted composite structures by cohesive zone interface elements and tiebreak contact. *Central European Journal of Engineering*, 2(4):612–626, 2012.
- [111] D.J. Elder, R.S. Thomson, M.Q. Nguyen, and M.L. Scott. Review of delamination predictive methods for low speed impact of composite laminates. *Composite Structures*, 66(14):677 – 683, 2004. Twelfth International Conference on Composite Structures.
- [112] M. Meo and E. Thieulot. Delamination modelling in a double cantilever beam. *Composite Structures*, 71(34):429 – 434, 2005. Fifth International Conference on Composite Science and Technology ICCST/5 Fifth International Conference on Composite Science and Technology.

- 
- [113] M. Loikkanen, G. Praveen, and D. Powell. Simulation of ballistic impact on composite panels. In *10th International LS-DYNA Users Conference*, 2008.
- [114] D. C. Fleming. Modelling composite crushing initiation using a cohesive element formulation. *International Journal of Crashworthiness*, 16(5):475–485, 2011.
- [115] S. Bala. Contact modelling in ls-dyna, 2001.
- [116] R. Bouix, P. Viot, and J.L. Lataillade. Polypropylene foam behaviour under dynamic loadings: Strain rate, density and microstructure effects. *International Journal of Impact Engineering*, 36(2):329 – 342, 2009.
- [117] N.B. Salem, M.K. Budzik, J. Jumel, M.E.R. Shanahan, and F. Lavelle. Investigation of the crack front process zone in the double cantilever beam test with backface strain monitoring technique. *Engineering Fracture Mechanics*, 98:272 – 283, 2013.
- [118] J. Zhou, M.Z. Hassan, Z. Guan, and W.J. Cantwell. The low velocity impact response of foam-based sandwich panels. *Composites Science and Technology*, 72(14):1781 – 1790, 2012.
- [119] G.B. Chai and S. Zhu. A review of low- velocity impact on sandwich structures. *Proceedings of the Institution of Mechanical Engineers, Part L: Journal of Materials Design and Applications*, 225(4):207–230, 2011.
- [120] S. Guérard, J-L. Barou, L. Mahéo, and P. Viot. Development of a new experimental device for tridimensional impacts - results on foam-core sandwich panels. In *4th International conference on impact loading of lightweight structures*, 2014.

## Comportement de matériaux sandwich sous sollicitations dynamiques de chocs : Effet de l'ajout de nanoparticules à la matrice thermodurcissable

**Résumé:** Les structures sandwich à peau composite renforcée de fibres plastiques et des cœurs en matériaux polymère représentent aujourd'hui une classe importante des matériaux structuraux légers dans de nombreux domaines de l'ingénierie tels que l'aéronautique et l'aérospatiale, l'automobile et les structures marines. Toutefois, ces structures sont susceptibles d'être soumises à un impact. L'endommagement par impact dans le cas de structures sandwich peut être dû, notamment, à des chutes d'outils ou des vols de débris sur piste d'atterrissage. Une des solutions proposées est alors la modification des résines thermodurcissables avec l'ajout de particules organiques et inorganiques de taille nanométrique. L'objectif de cette thèse est donc d'étudier l'effet d'une matrice renforcée par des copolymères tribloc sur les performances à l'impact basse vitesse de panneaux sandwich. L'effet de l'ajout de 10% M52N Nanostrength<sup>®</sup> nano-particules sur les performances à l'impact de panneaux sandwich à peaux en composites stratifiés Fibres/Epoxy a été étudié expérimentalement et numériquement. Deux types composites tissés ont été utilisées pour constituer les peaux des panneaux sandwich : Kevlar/Epoxy et Verre/Epoxy. Ce travail portera sur deux types de chargement d'impact différents; des impacts à faible vitesse dont l'angle d'incidence est normal à la surface de l'échantillon et des impacts à trajectoire parabolique. Un modèle LS-Dyna a été développé pour la simulation de l'impact normal sur plaque de composites stratifiés et sur plaques sandwich Kevlar/Epoxy - Rohacell<sup>®</sup> mousse. Une loi de comportement basée sur la mécanique de l'endommagement, Laminated Composite Fabric (MAT58) a été utilisée pour représenter le comportement des plaques composite. Le modèle Crushable Foam (MAT63) a été utilisé pour le cœur du sandwich en mousse Rohacell<sup>®</sup>. L'effort de contact, le déplacement de l'impacteur et les modes de ruptures obtenus numériquement ont montré une bonne correspondance avec les résultats expérimentaux. Le modèle macroscopique avec une loi de comportement phénoménologique est capable de simuler la réponse macroscopique de composites stratifiés et plaques sandwich soumis à des impacts de faible vitesse.

**Mots clés:** panneaux sandwich, copolymères tribloc, impacts à faible vitesse, tour de chute, LS-Dyna

### Impact behaviour of sandwich composites with nanoparticle modified facesheets

**Abstract:** Sandwich panels with Fibre Reinforced Polymers (FRP) composites facesheets and polymer foam core are lightweight structures with widespread applications in aerospace, offshore and marine industries. However, sandwich structures are susceptible to impact damage. Researchers have tried to improve the impact resistance of sandwich composites by various methods including toughening the matrix with nano-reinforcements such as carbon nanotubes and nanoclay. Current research has shown that acrylate triblock copolymers which self-assemble in the nano-scale do not agglomerate and are therefore a promising candidate for improving the impact performance of composites. The objective of this thesis is to investigate the effectiveness of these block copolymers in improving the impact resistance of sandwich structures with FRP facesheets. Normal impact tests are conducted using drop tower on sandwich composites made of Kevlar and Glass fibre reinforced epoxy facesheets and Rohacell<sup>®</sup> foam core. The response of the sandwich panels for parabolic impact was studied using a modified Stewart platform (Hexapod). The macroscopic behaviour and the microscopic phenomena involved in dissipating impact energy are identified and compared for sandwich plates with and without the nanoparticles. The results from drop tower impact tests show that the addition of 10% M52N Nanostrength<sup>®</sup> substantially improves the impact resistance of the Kevlar- Rohacell sandwich plates. Numerical simulation of the low velocity impact of sandwich plate is conducted using Finite Element Analysis (FEA) software LS-Dyna. Laminated Composite Fabric model (MAT58), a material model based on Continuum Damage Mechanics (CDM) and Hashin failure criteria is used for the facesheets and a Crushable foam model (MAT63) is used for the foam core. The FE models show good correlation with the experimental results.

**Keywords:** sandwich panels, block copolymer nanoparticles, low velocity impact, drop tower, LS-Dyna

